University of Strathclyde

Institute of Pharmacy and Biomedical Sciences

Solid and Hollow Gold Nanoparticles as Radiosensitisers in Combination with X-ray Radiation and Targeted Radiopharmaceuticals

Nicola Louise McGinely

A thesis presented in the fulfilment of the requirements for the degree of Doctor of Philosophy

2015

Declaration

This thesis is the result of the author's original research. It has been composed by the author and has not been previously submitted for examination which has led to the award of a degree.

The copyright of this thesis belongs to the author under the terms of the United Kingdom Copyright Acts as qualified by University of Strathclyde Regulation 3.50. Due acknowledgement must always be made of the use of any material contained in, or derived from, this thesis.

Signed:

Date:

Acknowledgements

Firstly, I would like to thank the BBSRC and the Institute of pharmacy and biomedical sciences (SIPBS) department at the University of Strathclyde for supporting this project both financially and academically.

I would like to thank my supervisor Dr Marie Boyd for providing me with the opportunity to complete this project in her laboratory, and for her enthusiasm towards the project throughout the 4 years. I would also like to extend sincere thanks to Professor Duncan Graham, Dr Karen Faulds and the nanoparticle expertise of the Graham laboratory at the University of Strathclyde. The collaboration with the Graham lab was invaluable in extending the scope and understanding of the project, and Duncan and Karen's continued support and guidance with all things nanoparticle was vital throughout the study.

Completion of this thesis would not have possible without the scientific knowledge, practical laboratory skills and the advice of the other members of the Boyd group both past and present, as well as other colleagues. Particular thanks must be given to Tony for his teachings in statistical analysis and his extensive thesis corrections. Thanks also to Mathias for his patience and lengthly training to help me to understand the linear quadratic model and spheroid analysis. Finally, thank you to Alex for his understanding and help to finally achieve the ICP-MS results.

My colleagues within the Boyd group were my primary resource of scientific answers; however the completion of this PhD would not have been possible without the unconditional support of my fellow PhD students, who were always there to offer a shoulder to laugh, cry or drunkenly fall on. The daily presence of Felicity Lumb, Jenny Crowe, Rhona Galloway, Kara Bell, Josie Fullerton, Megan Holden and the rest of the fifth floor who understood the difficult times which come with undertaking a PhD was vital. Together we supported each other with the provision of tea, chocolate, and wine, allowing us to retain the majority of our sanity throughout the process and have a truly memorable 4 years. In particular I owe a massive thank you to Miss Rhona Galloway. From work colleague to best friend in rapid time, together we supported each other through the epic highs and tremendous lows that accompanied not just the PhD but the

last 4 years of our lives and I couldn't have completed this process without having Rhona by my side through it all.

I also would like to thank my friends outside of SIPBS who, despite not always understanding my PhD distress, never stopped supporting and encouraging me throughout it.

I extend a special thank you to Dr Annette Sorensen, who has gone above and beyond to provide so much scientific, technical and emotional support throughout this project and ensure its completion. I not only couldn't have completed this study without her input but I would not have developed into the scientist I am today and for that I will be eternally grateful.

Finally, I would like to thank my incredible husband Gavin Wilkie and my loving family. I owe so much to Gavin for his unwavering support and encouragement throughout this process and for inspiring me with his incredible work ethic, to dig deeper and keep going. Gavin has been my best friend and biggest supporter through this process and I would like to thank him for always being there to listen to me, for believing in my when I didn't believe in myself, for always making me smile through the darkest days, for bringing so much happiness into my life and for continually providing the answer to "what is another word for…".

I have been incredibly lucky throughout this process to have had the continued support of my loving family, including my fantastic in-laws Alistair and Lynda, and my amazing parents Duncan and Linda who have always been there to listen and sympathise with my science woes and for all of their help when we decided to plan a wedding in the middle of my PhD.

I am truly the definition of my parents, they have raised me to be ambitious and have taught me that I can achieve anything through hard work, and everything I have achieved is because of their unwavering love and support. I am eternally grateful for everything they have done for me throughout my life and I would not be the person I am today without their wonderful influence.

Abstract

Radiotherapy is currently employed in the treatment of 50% of cancer patients. Cancer's heterogeneous nature mean optimal use of radiotherapy will be through combination and targeted therapies. Studies investigating the radiosensitising potential of solid gold nanoparticles have reported successful radiosensitisation only in combination with low kV radiation sources, but not with high kV or MV radiation. HGNs have been employed in photothermal ablation therapy, little work has been performed to investigate their potential as radiosensitisers, despite the superior physical properties, compared to solid AuNPs.

The aims of this study were to investigate the radiosensitising potential of solid AuNPs and HGNs in combination with kV external beam radiation (XBR) and high kV β and γ radiation from ^{131}I, from [^{131}I]-MIBG. The study then aimed to investigate the effect of solid gold nanoparticles (AuNPs), hollow gold nanoparticles (HGNs), XBR and [^{131}I]-MIBG alone and in combination on the growth of 3D MTS models.

Radiosensitisation was measured by a decrease in clonogenic cell survival and quantified using the linear quadratic model. Association of radiosensitisation with changes in the cell cycle, dynamics of DNA double strand break (DSB) formation and repair and apoptotic cell death was assessed. The growth of spheroids was examined by assessing changes in spheroid volume.

Significant radiosensitisation was observed in UVW/NAT and SK-N-BE cells, when solid AuNPs and HGNs were combined with [^{131}I]-MIBG which was associated with an increase in DNA DSB formation. Solid AuNPs in combination with XBR induced minimal radiosensitisation, compared to significant radiosensitisation observed with HGNs. Solid AuNPs and HGNs alone and in combination with XBR and [^{131}I]-MIBG had no significant effect on the growth of multicellular tumour spheroids (MTS), whereas exposure to XBR and [^{131}I]-MIBG induced a dose dependant decrease in spheroid growth.

Table of Contents

List of Figures

List of Tables

Abbreviations

[^{131}I]MIBG	^{131}Iodine-labelled meta-iodobenzylguanidine
2D	two-dimensional
3D	three-dimensional
3DRT	Three-dimensional radiotherapy
λ_{max}	Maximum wavelength of absorption
3DRT	Three-dimensional radiotherapy
^{o}C	celsius
µg	Microgram
µl	Microlitre
µm	Micometre
µM	Micromole
au/AU	Arbitrary units
Au	Gold
AuNPs	Gold nanoparticles
Ag	Silver
AgNPs	Silver nanoparticles
ANOVA	Analysis of variance
ATP	Adenosine triphosphate
ATCC	American type culture collection
ASCR	Autologous stem cell rescue
bNAT	bovine nor-adrenaline trasporter
BSA	bovine serum albumin
CA	Carrier added
C.I	Confidence interval
cm	Centimetre
cm^2	centimetre squared

CNS	Central nervous system
Co	Cobalt
CO_2	Carbon dioxide
cpm/10^5c	Counts per minute per 10^5 cells
CR	complete response
CTAB	hexadecyltrimethylammonium bromide
D	Dose
DDA	Discrete dipole approximation
DEF	Dose enhancement factor
DEF_{50}	Dose enhancement factor at 50% cytotoxicity level
dH_2O	distilled water
DLT	dose limiting toxicities
DLS	Dynamic light scattering
DMEM	Dulbecco's modified eagles medium
DNA	Deoxyribonucleic acid
DNA DSB	Double-strand DNA break
dsDNA	Double stranded DNA
DT	doubling time
DTT	Dithiothreitol
ECM	Extra-cellular matrix
EDTA	Ethylene-diamine-tetra-acetic acid
EGFR	epidermal growth factor receptor
EPR	Enahnced permeation and retention
FACS	Fluorescence-activated cell sorting
FCS	Foetal calf serum
G	gauge
Gy	Gray
h	hours

HCl	Hydrochloric acid
HEPES	4-(2-hydroxyethyl)-1-piperazineethanesulfonic acid
HGNs	Hollow gold nanoparticles
Hz	Hertz
i.p.	Intraperitioneal
IC_{10}	Inhibitory concentration (10%)
IC_{25}	Inhibitory concentration (25%)
IC_{50}	Inhibitory concentration (50%)
IC_{75}	Inhibitory concentration (75%)
IC_{90}	Inhibitory concentration (90%)
ICP-MS	Inductively coupled plasma – mass spectroscopy
ICP-AES spectroscopy	Inductively coupled plasma - atomic emission
IMRT	Intensity-modulated radiotherapy
INSS	International neuroblastoma staging system
INRG	International neuroblastoma risk group
IR	Ionising radiation
I.V	intravenous
kBq	Kilobequerel
kDa	Kilodalton
KI	Potassium iodide
kV	kilovoltage
keV	kilo-electron volts
kVp	Peak kilovoltage
IMRT	Intensity-modulated radiotherapy
L	litre
LET	Linear energy transfer
LINAC	Linear accelerator
LEM	Local effect model

m	Coefficient of sigmoidicity of dose-effect curve
M	molar
mA	milliamps
mAb	Monoclonal antibody
MDEF	Macroscopic dose enhancement factors
MBq	Megabequerel
mCi	millicurie
mm	millimetres
MEM	Minimum essential medium
meV	milli-electron volts
mV	milli-voltage
mg	milligram
$MgCl_2$	Magnesiun Chloride
MIBG	Metaiodobenzylguanidine
mins	Minutes
mL	Millilitre
MLC	Multi-leaf collimator
mM	millimole
mm	millimetre
MRI	Magnetic resonance imaging
mRNA	Messenger ribonucleic acid
MTS	multicellular tumour spheroid
MV	mega-voltage
NCA	No-carrier added
NaCl	Sodium Chloride
$NaHAuCl_4$	Sodium tetrachloroauric acid
$NaC_6H_7O_7$	Monosodium citrate
NAT	Noradrenaline transporter

Nb	Neuroblastoma
Ng	nanogram
NHEJ	Non-homologous end joining
NIR	near infra-red
nm	nanometre
nM	nanomolar
NP	Nanoparticle
PA	photoacoustic
PARP	Poly-(ADP-Ribose) Polymerase
PBS	Phosphate buffered saline
PEG	poly(ethylene glycol)
PCR	Polymerase chain reaction
PDT	Photodynamic therapy
PI	Propidium iodide
PF	Paraformaldehyde
PR	Partial response
PTA	Photothermal abalation
·OH	hydroxyl radical
RAI	Radioactive iodine
RES	Reticuloendolithial system
RME	Receptor mediated endocytosis
rpm	Revolutions per minute
ROS	Reactive oxygen species
RT	Reverse transcription
s.c.	subcutaneous
SCGE	Single cell gel electrophoresis
SE	Standard error
SERS	Surface enhanced Raman spectroscopy

SF	Surviving fraction
SNS	sympathetic nervous system
SPR	Surface plasmon resonance
DNA SSB	Single-strand DNA break
s	seconds
sd	standard deviation
T_2	Time required for a doubling of tumour volume
T_{10}	Time required for a ten-fold increase of tumour volume
TEM	Transmission electron microscopy
TPT	Topotecan
TPPMS	triphenylphosphine monosulfate
Tris	(Hydroxymethyl)aminomethane
TRT	Targeted radionuclide therapy
UV-Vis	Ultra violet – visible
V	Volt
VEGF	Vascular endothelial growth factor
VHEE	Very high energy electrons
W	watts
WHO	World Health Organisation
XBR	External beam radiation
Z	Elemental atomic number
Z_{eff}	effective atomic number

Chapter 1

The use of Gold Nanoparticles as radiosensitisers for the Enhancement of External Beam and Targeted Radiotherapy

Chapter 1: Introduction

1.1 The incidence and development of cancer

With over 200 different types, cancer is now recognised as the cause of one in four of all deaths within the UK (Cancer Research UK, 2015). According to the most recent statistics available from Cancer Research UK, 331,000 people were diagnosed with cancer in 2011, which equates to approximately 910 people a day, and 1 person every two minutes (Cancer Research UK, 2015). The most common cancers are breast, lung and bowel cancer, which together account for 54% of all diagnosed cancers each year, however there has been a large increase in the incidence of lifestyle linked cancers including kidney, liver and skin cancer. Despite an increase in the incidence of cancer, the survival rates have doubled over the past decade, with approximately 50% of people diagnosed with cancer surviving for more than 10 years (Cancer Research UK, 2015). However, despite the advances in cancer therapy which have led to the increase in survival rates, cancer still claimed the lives of 162,000 people in 2012 alone, demonstrating that significant improvements in cancer therapy are still needed to further reduce the number of deaths (Cancer Research UK, 2015).

Cancer is described as a malignant neoplasm which develops as a result of specific alterations to the DNA of normal cells. Mutations to the DNA modify the cells, causing excessive, uncontrolled growth into a neoplasm (Longo and Harrison, 2012). Within normal cells, there is a programmed balance between cell proliferation and cell death which is controlled by tumour promoter genes, termed oncogenes and tumour suppressor genes such as p53. Mutations within these genes can cause an overexpression of oncogenes, or a suppression of tumour suppressor genes which will result in uncontrolled cell proliferation (Weinberg, 2006). The primary tumour formed relies on the presence of a vascular supply in order to provide it with the necessary nutrients to sustain its uncontrolled growth. Utilising this vascular supply, cells from the primary tumour can undergo metastasis by entering into the circulation to migrate through the body and form metastatic secondary tumours (Pories et al., 2008). Once a tumour has metastasised throughout the body, treatment becomes more difficult as a result of the heterogeneity of the cells in the primary tumour and metastatic tumours (Weinberg, 2006).

1.2 Current treatment modalities for cancer

There are 3 primary treatment methods employed in cancer therapy namely; removal of the tumour by surgery or treatment of the tumour by either chemotherapy or radiotherapy. These treatment methods are most commonly employed in combination, in an attempt to achieve maximum destruction of the tumour.

Surgery plays a key role in both the diagnosis and treatment of cancer, and is typically used in combination with either chemotherapy and/or radiotherapy. Through diagnostic biopsies and pathological examination, the presence and stage of the cancer can be determined. Following this, the surgery performed can either be; curative– when the tumour resides can be fully removed (Cassidy et al., 2015), cytoreductive– if removal of the entire tumour without excessive damage to the surrounding tissues and organs is not possible (Missailidis, 2007), or palliative - which is used to ease the patients discomfort by treating problems caused either by the tumour itself or by side effects (Wichmann et al., 2013).

Chemotherapeutic agents elicit their response by creating a therapeutic differential between the rapidly proliferating cells of a tumour and normal non-dividing cells, with the specific cytotoxic action determined by the type of chemotherapeutic agent. Several classes of chemotherapeutic agents are typically employed in chemotherapy regimens including; alkylating agents, of which cisplatin is the most readily employed. Alkylating agents exert their efficacy by binding to target DNA and alkylating the nucleophilic groups, which distorts the cells DNA, and prevents replication and transcription of the cell, eventually leading to cell apoptosis (Harrap and Hill, 1969; Kartalou and Essigmann, 2001). Plant alkaloids, such as Vinca alkaloids, derived from Madagascar Periwinkle are another class of chemotherapeutic agents and are used to block cell division through interference in microtubule function (Moudi et al., 2013; Rowinsky, 2003). A third class are anthracyclines, such as Doxorubicin are employed to disrupt the normal function of the enzymes involved in DNA replication, leading to prevention of cell division and eventual cell apoptosis.

Despite the undeniable success in initiating cell death, chemotherapeutic agents do not fully discriminate between the rapidly dividing cells of a tumour, and cells which rapidly divide under normal conditions, such as those within the bone marrow, the

digestive tract, blood cells and hair follicles. The non-specific targeting of chemotherapeutic agents to all rapidly dividing cells therefore leads to side effects including, hairloss, neurotoxicity, nausea and immunotoxicity. These side effects consequently limit the effectiveness of the chemotherapeutic agents as the dose of drug which can be safely administered to the patient is often lower than the amount required to deliver lethality to the tumour. Additionally the administration of sub-lethal doses to the tumour allows the development of acquired drug resistance which further decreases the effectiveness of these drugs (Wheate et al., 2010).

1.3 External Beam Radiotherapy (XBR)

Radiotherapy is employed in the treatment of approximately 50% of all cancer patients, either alone or in combination with surgery or chemotherapy. XBR is typically delivered in the form of X-ray photons using a linear accelerator (LINAC) which utilises electricity to generate a stream of fast moving sub-atomic particles to create ionising radiation (IR). The IR generated can elicit cellular damage to both nuclear DNA and macromolecular structures through direct interaction with cellular DNA, or indirectly. Indirect DNA damage occurs when IR generates reactive oxygen species (ROS) through ionisation of water molecules within the cellular environment (Baskar et al., 2012; Kassis and Adelstein, 2005; Stockham et al., 2014).

Reactive oxygen species are radicals, ions or molecules that have a single unpaired electron in their outermost shell of electrons and as a result of this are highly reactive. ROS can be categorized into two groups: free oxygen radicals and non-radical ROS. Free oxygen radicals include superoxide ($O_2^{\bullet-}$), hydroxyl radical ($^{\bullet}OH$) and nitric oxide ($NO^{\bullet}$). Non-radical ROS include hydrogen peroxide (H_2O_2), singlet oxygen ($^1O_2$) and organic hydroperoxides (ROOH). Among them, superoxide, hydrogen peroxide and hydroxyl radicals are primarily involved in the biological effects following exposure to IR.

Following exposure to IR, ROS are produced primarily through the hydrolysis of intracellular water to generate hydroxyl radicals. Their presence increases the oxidative stress within cells and this increased oxidative stress can mediate signalling

events throughout the cell to impact the cell cycle progression, apoptosis, energy metabolism and cell motility (Liou and Storz, 2010).

Additionally, ROS generated by IR result in indirect DNA damage which contributes substantially to the resulting biological effect of external beam irradiation. The ROS such as hydroxyl radicals interact indirectly with DNA to create mutations and lesions in DNA bases along with deletions, insertions and rearrangements which all contribute to gross chromosomal aberrations. In addition to damage to DNA double strand helix itself, the ROS can oxidise lipids and amino acids in proteins and oxidatively deactivate enzymes.

Conventional XBR consisted of a single 2-dimensional (2D) beam delivered to the patient from several different directions using a LINAC, however as a result of the inadequate precision of the radiation to the tumour site this technique has largely been replaced in recent years by the use of 3-dimensional radiation therapy (3DRT) (Baskar et al., 2012). 3DRT allows each beam to be shaped around the target profile using a multi-leaf collimator (MLC), allowing radiation to conform to the exact tumour volume, greatly reducing any surrounding tissue toxicity and permitting substantially higher radiation doses to be delivered (Bucci et al., 2005).

Further advances to radiotherapy have been introduced by intensity-modulated radiotherapy (IMRT) which allows conformation of the radiation dose to concave tumour volumes. IMRT permits the treatment of tumours which reside around a vulnerable organs or blood vessels, such as the spinal cord, and is now used routinely in the treatment of head and neck tumours as well as prostate and brain cancer (Nagata, 2014; Tribius and Bergelt, 2011). As the intensity of the radiation beams can be modulated using advanced computer software it allows the highest intensity radiation to be delivered to the gross tumour, with lower intensity radiation to the outer tumour edges, which limits the damage to surrounding normal tissue, and goes some way to alleviate unequal dose deposition of radiation (Baskar et al., 2012).

Despite the advances in radiotherapy through the introduction of both 3DRT and IMRT, several key limitations of the treatment modality still exist. The limited control available in radiotherapy with regard to the size and specific shape of organs, as well

as the changes they may undergo throughout the course of treatment can result in unequal dose distribution of radiation throughout the tumour. This was highlighted in the study performed by Majewski *et al*, (2007) which demonstrated that 70% of patients with bladder cancer showed an increase in bladder volume across the course of radiotherapy which led to underdosing of the bladder, rectum and intestines with patients receiving <95% of the prescribed dose (Majewski et al., 2009). Additionally, toxicity to normal tissue surrounding the tumour remains a significant limitation of radiotherapy, as even with significant improvements in the precision of radiotherapy beams, direct targeting of tumour cells is not possible (Goldberg and Lehnert, 2002). Furthermore, the damage to normal tissue and unirradiated cells has been linked to the development of long-term toxicity effects later in life. For example, Brenner *et al*, (2014) used historical data from patients who received breast radiotherapy between 1958 and 2001 to estimate the risk of major coronary events induced by modern breast radiotherapy. Results of the study demonstrated that the estimated lifetime risk of a major coronary events following breast radiotherapy are in the range 0.05-3.5%, where supine positioning during left-sided breast radiotherapy carries the greatest risk (Brenner DJ et al., 2014)

As a result of these limitations the dose of radiotherapy which can be safely administered to patients in order to minimise toxicity to normal cells, and reduce late onset effects is typically too low to provide curative results if used alone. A method of direct radiation targeting which has been investigated is the use of radionuclides conjugated to tumour seeking moieties such as monoclonal antibodies or cell surface receptors to develop targeted radionuclide therapy (TRT). One such example of TRT known as [^{131}I]-MIBG is investigated in this study and is expanded in section 1.4.

1.4 [^{131}I]-MIBG Therapy

1.4.1 Targeted radionuclide therapy (TRT)

Targeted radionuclide therapy (TRT) has been investigated to overcome the limitations of conventional external beam radiotherapy. TRT involves the conjugation

of cytotoxic radionuclides to tumour seeking molecules to allow selective delivery of radiation to the primary tumour site and disseminated tumour cells, thus significantly reducing the damage caused to normal tissue (Hamoudeh et al., 2008). In TRT, a variety of tumour seeking moieties can be employed, allowing the treatment of many different types of cancer. Additionally, a range of different radionuclides can be employed which allow specific targeting of different tumour scenarios based on the isotopes individual characteristics.

The most common class of radionuclides currently employed in cancer therapy are (β)-emitters, such as ^{131}I and ^{90}Y, typically employed in the treatment of large, localised tumours, due to their low linear energy transfer (LET), which describes the rate at which the energy released from the ionising radiation is transferred to tissues, and their long path-length (Ersahin et al., 2011). (β)-emitting radionuclides induce damage within cells through interaction with atoms and water molecules within the cells. Through this interaction, the (β)-emitting radionuclides will lose their energy, and generate ionised atoms and free radical species which can interact with cellular DNA and macromolecules (Hamoudeh et al., 2008).

Conversely, (α)-emitting radionuclides, such as ^{233}Ra and ^{213}At, have a much shorter path-length compared to (β)-emitters (50-80 μm in tissue), and deposit their cytotoxic effects within a much smaller tissue range. The higher LET of (α)-emitters however, mean they may induce a greater degree of clustered DNA damage lesions which could lead to more double strand breaks in DNA and profound chromosomal damage compared with (β)-emitters (Hamoudeh et al., 2008). (α)-emitting radionuclides are therefore more suited to the treatment of smaller tumour clusters or metastasised tumour sites, where their shorter tissue range permits more precise tumour targeting and sparing of normal tissue damage (Nestor, 2010).

The third class of radionuclides which are employed in cancer therapy are Auger electron emitting radionuclides such as, ^{125}I and ^{111}In. Auger electron radionuclides have a high LET and a much shorter path-range (in the nm scale) meaning the cytotoxic effect will be deposited in the vicinity surrounding the radionuclide. Auger electron radionuclides are therefore typically employed for the eradication of single tumour

cells, very small tumour clusters and in some cases disseminated tumours (Sharkey and Goldenberg, 2005).

Various tumour seeking moieties have been investigated for use in TRT such as, monoclonal antibodies, peptides such as somatastatin analogues, and small molecules such as meta-iodobenzylguanidine (MIBG).

The use of radiolabelled peptides, such as the somatostatin receptor targeting peptides in TRT has demonstrated some potential for the treatment of gastroenteropancreatic neuroendocrine tumours due to their overexpression of the somatostatin receptor (Nicolas et al., 2011). Despite the promising anti-tumour effects observed with radiolabeled somatostatin peptides however, the presence of some subtypes of somatostatin receptor on the kidneys, and the involvement of the kidneys in clearing the radiolabeled molecules leads to substantial renal toxicity (Nicolas et al., 2011).

Monoclonal antibodies (mAbs) have also been utilised in TRT, however effective treatment of solid tumours is limited due to poor penetration of antibodies into the central portions of large tumours (Chamarthy et al., 2011). Two approved radiolabelled monoclonal antibodies, Bexxar (^{131}I labelled tositumomab) and Zevalin (^{90}Y labelled ibritumomab), which target the CD20 receptor, expressed on normal and malignant B lymphocytes, are now routinely employed in the treatment of non-Hodgkin's Lymphoma (Goldsmith, 2010). Despite the significant anti-tumour effects observed with Bexxar and Zevalin, as the CD20 receptor is expressed on normal B lymphocytes patients receiving treatment are susceptible to infection (Chamarthy et al., 2011).

The use of small molecules, such as radioactive iodine (RAI) using the isotope, ^{131}I have been utilised successfully for the treatment of differentiated thyroid cancer (DTC). This treatment exploits the strong affinity of normal thyroid cells, and to a lesser extent cancerous thyroid cells to uptake and retain circulating iodine due to the overexpression of the sodium iodide symporter (NIS), a transmembrane glycoprotein which is also expressed in the kidneys, ovaries and breast tissue (Zarnegar et al., 2002). Circulation of RAI within the body will firstly ablate any residual thyroid function which remains after surgery to remove the primary tumour and therefore remove any competition for the uptake of radioiodine between normal thyroid cells and cancerous

cells The radioactive iodine will then selectively treat the cancerous cells (Worden, 2014). Exploitation of this natural uptake mechanism therefore allows selective treatment for DTC and other NIS expressing tumours. This concept has been extended to investigate treatment of other cancers through the use of radiolabelled tumour specific small molecules such as, meta-iodobenzyleguanidine (MIBG) conjugated to ^{131}I, which has been investigated extensively in this present study.

1.4.2 Overview of [^{131}I]-MIBG

One example of targeted radionuclidetherapy utilised in the clinic is the use of meta-iodobenzyleguanidine (MIBG) conjugated to ^{131}I, termed [^{131}I]-MIBG. MIBG is a structural analogue of the adrenergic neurone blockers guanethidine and bretylium, (Figure 1-1) and is taken up selectively by the noradrenaline transporter (NAT). The NAT is expressed in tumours of the neural crest, such as neuroblastoma tumours, and allows [^{131}I]-MIBG to be selectively concentrated within neuroadrenergic tissue (Mairs et al., 1994). Conjugation of the β-emitter, ^{131}I to MIBG allows the delivery of cytotoxic radiation specifically to NAT expressing tumour cells, reducing normal tissue toxicity. The long path length of decay (0.80 mm) of ^{131}I makes it an optimal choice for targeted radiotherapy as the radioactive β-emission can span across several cells to alleviate unequal dosing and uptake of [^{131}I]-MIBG as a result of the heterogeneous expression of the NAT throughout tumour cells. In addition, the extended half-life of ^{131}I (8.02 days) allows chronic irradiation of cells resulting in cumulative DNA damage and a greater biological effect compared to the rapid irradiation by XBR. In this study the human neuroblastoma cell line, SK-N-BE which naturally expresses the NAT, was used as a model together with a NAT gene transfected human glioblastoma model, UVW/NAT to investigate the effects of [^{131}I]-MIBG treatment.

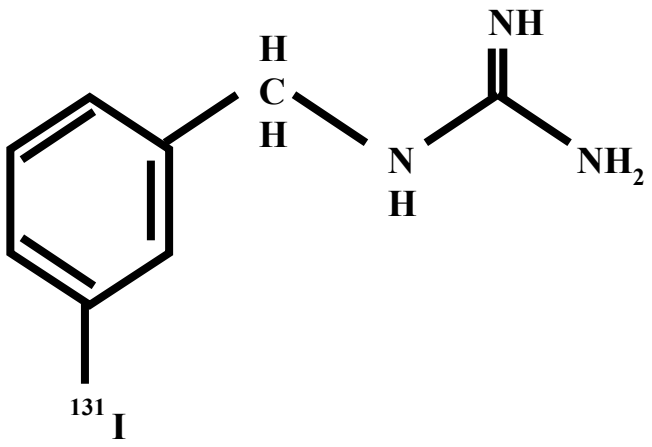

Figure 1-1: The chemical structure of [^{131}I]-meta-iodobenzylguanidine ([^{131}I]-MIBG).

Meta-iodobenzylguanidine is a structural analogue of the adrenergic neurone blockers guanethidine and bretylium and is taken up selectively by the noradrenaline transporter (NAT). Conjugated to ^{131}I it allows delivery of radiation selectively to tumour cells expressing the NAT

Treatment of neuroblastoma using [^{131}I]-MIBG has been investigated in many clinical trials for the past 30 years. Initial trials utilising [^{131}I]-MIBG as a mono-therapy demonstrated promising results, with an early pre-clinical trial carried out by Klingebiel *et al* (1990), reporting an objective response rate of 66%, including 2 complete responses (CR), 6 partial responses (PR) and a median survival of 369 days after [^{131}I]-MIBG therapy (T et al., 1990). Similarly, a phase II trial carried out in Holland reported an objective response rate of 53%, including 7 CR and progressive disease in 9 patients of 53 patients with relapsed or refractory neuroblastoma who received 100-200mCi [^{131}I]-MIBG (Hoefnagel et al., 1991). A more recent phase II study performed in France however, reported no objective response in any of the 26 patients treated, despite observed of pain reduction in 50% of patients, which may have been due to a lack of uptake of [^{131}I]-MIBG by the patients (Kayano and Kinuya, 2015).

Based on the conflicting results for the use of [^{131}I]-MIBG as a mono-therapy, more recent studies have demonstrated that a higher therapeutic gain could be achieved from combination of [^{131}I]-MIBG with compounds which radiosensitise cells to [^{131}I]-MIBG therapy, or prevent effective DNA damage repair in cells, with results of such studies expanded on in section 1.5.

1.5 Combination therapies to improve the efficacy of TRT and XBR

It is unlikely that any XBR or TRT protocol currently in clinical use will cause tumour sterilisation as a mono-therapy due to the surrounding tissue toxicity and unequal dose distribution associated with XBR, and the normal tissue toxicity and variable results achieved with current TRT approaches. It is therefore hypothesised that combination of XBR or TRT with radiosensitising compounds may help to overcome these limitations and improve the efficacy of current radiotherapy modalities (Higgins et al., 2015; Wardman, 2007). The primary aim of a radiosensitiser is to deliver a greater cytotoxic effect using the same radiation dose, thus allowing lower doses of radiation to be used, the toxicity to normal tissue to be alleviated and a greater radiobiological effect to be delivered. Radiosensitising compounds can enhance the effects of radiation

either through direct interaction with the ionising radiation to potentiate the radiation effects throughout the cell, or increase the dose deposition of radiation within the target area. Alternatively, radiosensitising compounds can interfere with the DNA repair pathways within cells, preventing effective repair of radiation induced DNA damage, and permitting the formation of cumulative damage which could demonstrate a greater lethality.

Initial studies which evaluated the use of chemotherapeutic agents such as, cisplatin and taxol as radiosensitisers demonstrated significant benefit from their combination with XBR for the treatment of a variety of tumour types including, head and neck squamous cell carcinoma (HNSCC), cervical cancer and non-small cell lung cancer. Despite these advances however, the literature reports that the optimum dosage and scheduling of chemotherapeutic agents for combination with radiotherapy have yet to be established (Caffo, 2001; Candelaria et al., 2006; Strojan et al., 2015).

More recent work demonstrated a therapeutic benefit from the use of molecularly targeted approaches to radiosensitisation. For example, work performed by Mueller *et al*, (2013) demonstrated in the metastatic neuroblastoma cell line $NB1691^{luc}$ both *in vitro* and *in vivo* that combination of the poly-(ADP-Ribose) Polymerase (PARP) inhibitor MK-4827 with XBR resulted in significant increase in the number of DNA DSBs observed 24 hours after XBR exposure, compared to cells treated with XBR alone. *In vivo* administration of MK-4827 1 hour prior to XBR resulted in significantly prolonged survival of mice, compared to treatment of either agent alone (Mueller et al., 2013).

Another class of molecularly targeted molecules which have been investigated are Topomerase I inhibitors, involved in DNA repair. Work by Kohara *et al*, (2002) investigated the combination *in vitro* of the topomerase I inhibitor, 7-ethyl-10-[4-(1-piperidyl)-1piperidyl] with 125 kV irradiation in human small cell lung cancer cells, SBC-3 and cisplatin-resistant subline (SBC3/CDDP). Results of the study demonstrated significant reduction in the growth of cisplatin-resistant cells, compared to radiation alone (Kohara et al., 2002).

The combination of Topomerase I and PARP inhibitors with targeted radiotherapy using [^{131}I]-MIBG has also been investigated in our laboratory. The study by McCluskey *et al,* (2008) demonstrated a decrease in cell survival and increase in DNA fragmentation in the neuroblastoma cell line, SK-N-BE and the NAT transfected glioma cell line, UVW/NAT following administration of [^{131}I]-MIBG in combination with the topomerase I inhibitor, Topotecan, compared to [^{131}I]-MIBG alone (McCluskey et al., 2008). The positive findings in this study have subsequently lead to further clinical investigation of [^{131}I]-MIBG and Topotecan in Neuroblastoma (MATIN) with 70 patients in 5 institutions across Europe currently enrolled in the trial (Gaze et al., 2005).

The successful results observed following the combination of Topotecan with [^{131}I]-MIBG were extended in the recent study by McCluskey *et al*, (2012) which demonstrated that the therapeutic benefit could be further enhanced by combination of Topotecan and [^{131}I]-MIBG with the PARP inhibitor, PJ34 both *in vitro* and *in vivo* in the neuroblastoma model, SK-N-BE and NAT transfected glioma model, UVW/NAT. Results of this study demonstrated that significant reduction in cell survival was achieved when PJ34 was administered simultaneously with Topotecan and [^{131}I]-MIBG in both cell lines. The reduction in cell survival was associated with an increase in the arrest of cells in G2/M phase of the cell cycle and an increase in phosphorylated γ-H2AX. *In vivo,* simultaneous administration of PJ34 with Topotecan and [^{131}I]-MIBG resulted in significant delay in tumour growth in both SK-N-BE and UVW/NAT models, compared to Topotecan and [^{131}I]-MIBG alone (McCluskey et al., 2012).

The combination of [^{131}I]-MIBG with chemotherapeutic agents has also shown encouraging results. For example, a recent phase I/II clinical trial of 32 patients with advanced neuroblastoma performed by DuBois *et al,* (2015) demonstrated [^{131}I]-MIBG in combination with the chemotherapeutic agents vincristine and irinotecan resulted in no dose-limiting toxicity compared to either agent alone (DuBois et al., 2015). Similarly, studies by Mastrangalo *et al,* (2001, 2011) combined [^{131}I]-MIBG with various chemotherapy schedules utilising cisplatin, VP16 and vincristine, in patients presenting with extensively treated, resistant neuroblastoma. Results of the

studies demonstrated high major response in the majority of patients (Mastrangelo et al., 2011, 2001). Results of these studies indicate the effectiveness of combining [^{131}I]-MIBG with other agents to improve the radiation efficacy, through disruption of effective DNA repair for example.

1.6 Gold Nanoparticles as radiosensitisers

Another combination strategy which has gained substantial investigation over the last decade is the use of gold nanoparticles (AuNPs) as potential radiosensitisers of XBR. To date, many studies have demonstrated that the combination of AuNPs with kV XBR results in an increase in the effective radiation dose within the target area, leading to an increase in the radiation induced biological effects, compared to XBR exposure alone

Early studies performed by Regulla *et al,* (1998) demonstrated the radiosensitising potential of gold when dose enhancement factors (DEFs) of up to 50 were achieved following irradiation of monolayers of mouse embryo fibroblasts in the presence and absence of thin gold foil (Regulla et al., 1998). The subsequent development of gold nanoparticles (AuNPs) has greatly accelerated the investigation into the radiosensitising potential of gold as the use of AuNPs circumvented many of the limitations associated with the delivery and distribution of gold. To date, several groups have demonstrated successful radiosensitisation by AuNPs in combination with XBR; however the results of these studies show great variation with respect to the magnitude of dose enhancement achieved. Additionally, as a result of the variables between each of the studies, with respect to the cell lines investigated, size and surface functionalisation of the AuNPs and the energy of radiation used, it is very difficult to draw accurate comparisons between the studies. The results of recent studies and the factors which could influence the radiosensitisation observed will be discussed in more detail in sections 1.6.2 and 1.6.5.

1.6.1 The rationale behind the radiation enhancement effect of AuNPs

The application of AuNPs as radiation sensitisers is based on their ability to increase dose deposition within the target volume due to differences in the photon mass absorption coefficient of AuNPs, compared to soft tissue (Figure 1-2). The photon mass absorption coefficient is defined as a measurement of how strongly a substance can absorb photons of electromagnetic radiation per unit of mass. The high atomic number (Z) of gold (Z=79), compared to soft tissue causes an increase in the photoelectric absorption of radiation within the target area, which means that when AuNPs are present in tumour cells they will absorb a greater amount of radiation and lead to an increase in the radiation dose within the target area.

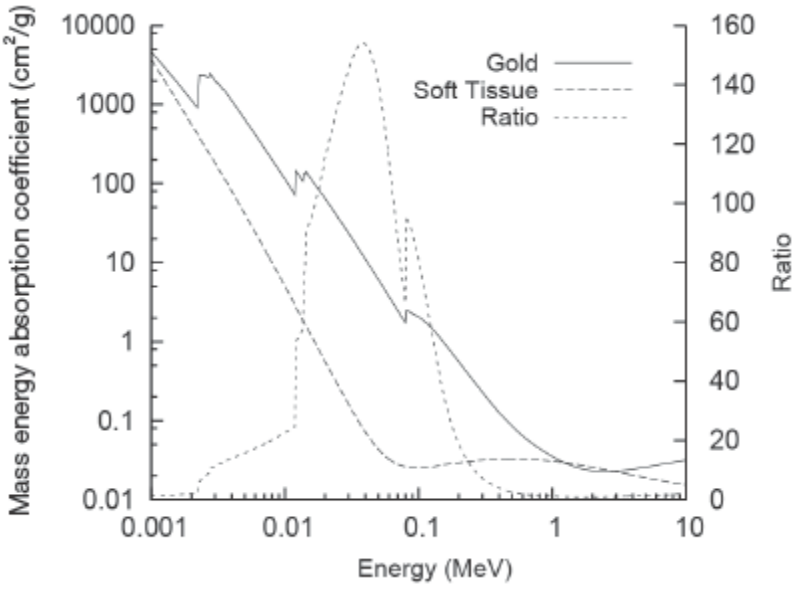

Figure 1-2: The photon mass absorption coefficients for gold and soft tissue, with the ratio of mass energy absorption coefficients given as a function of photon energy.

The data demonstrates that the mass absorption (amount of radiation absorbed) by soft tissue is lower than for AuNPs. When AuNPs are present within the target area therefore, they will absorb a greater amount of radiation causing an increase in the radiation delivered to the target area. Data taken from Butterworth (Butterworth et al., 2013).

In soft tissue, following exposure to ionising radiation, the energetic photon of radiation is scattered by a weakly bound outer shell electron which will be ejected and the photon will retain the majority of its original energy. The ejected electron and the photon will be scattered across long distances, and slow gradually, causing only sparse ionisation effects throughout the cell. This is known as Compton scattering and is the predominant ionisation process which will occur in soft tissue following exposure to radiation (Butterworth et al., 2012).

The presence of AuNPs within the target area, however, results in the photoelectric effect dominating ionisation events. In this process, the photons transfer all their energy to inner shell electrons within the AuNPs and as the inner shell electrons require much more energy to be removed, the electrons are ejected with greater energy which is deposited in the vicinity surrounding the AuNPs. Ejection of an inner shell electron leaves a vacancy within the shell which is filled when outer shell electrons move down into the inner shell. This movement results in the ejection of further energy usually in the form of secondary auger electrons. The ionisation process following interaction of radiation in the presence and absence of AuNPs are depicted in Figure 1-3.

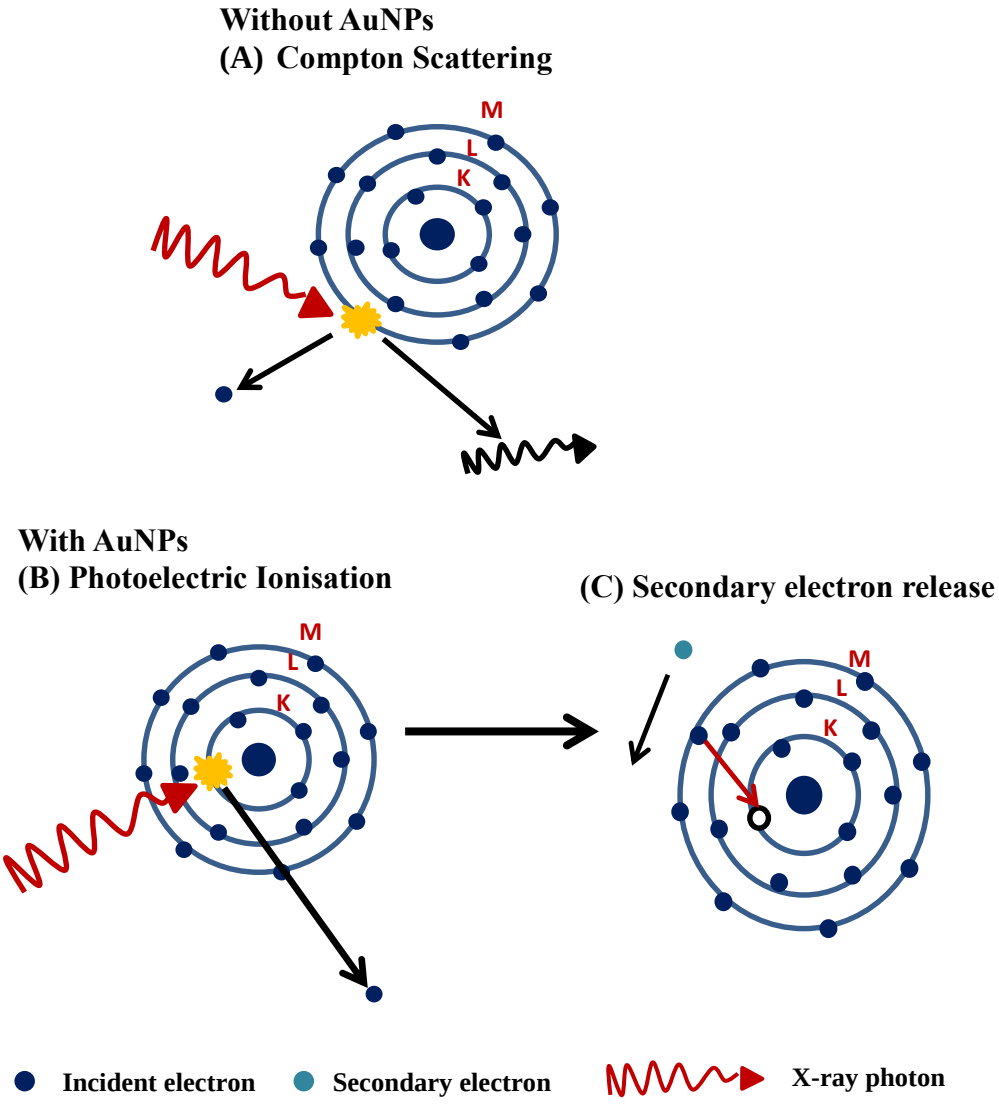

Figure 1-3: Schematic representation of ionisation processes in the presence and absence of AuNPs with X-ray photons.

Without AuNPs, Compton scattering (A) dominates and leads to scattering of the incident photon by a weakly bound outer electron. With AuNPs photoelectric ionisation (B) dominates and results in the complete absorption of the incident photon and release of an inner shell electron. This is followed by secondary electron release as an outer electron fills the vacancy left by the inner shell electron ejection.

The relative probability of photoelectric ionisation depends on the energy match between the photon energy of the radiation and the binding energy of the electrons. Several studies have estimated the effective atomic number (Z_{eff}) of soft tissue, where the Z_{eff} is proposed to be equivalent to the atomic number for mixtures of different materials in order to estimate the interactions of such materials with radiation. As average soft tissues are composed of low atomic number elements, typically carbon (C), hydrogen (H), oxygen (O) and nitrogen (N) the calculated Z_{eff} is estimated as 7.5 (Kurudirek, 2014; Singh and Badiger, 2014). Due to the low Z_{eff}, the binding energy of inner shell electrons in soft tissue is very low and has been reported to be in the order of 1 kV or less. As the photon energy of typical XBR is in the region of 225 kV the energy match between the electron binding energy in soft tissue and photon energy is very poor, meaning the probability of photoelectric ionisation is low and the photoelectric effect is therefore responsible for only a small contribution to the overall dose absorption in soft tissue. The electron binding energy increases with increasing atomic number, showing a dependence of approximately Z^4 with respect to atomic number (Coulter et al., 2013; Mesbahi, 2010).

The probability of photoelectric ionisation can also change with changes to the photon energy, where the maximum probability is observed when the photon energy is just above the binding energy of electron residing in each shell. This is demonstrated for AuNPs by the sharp increase in the mass absorption coefficient (Figure 1-2) which occurs when the photon energy lies just above that of the binding energies for electrons in the inner (K), middle (L) and outer (M) electron shells respectively, where the binding energies for K, L and M shell electrons are 79 keV, 13 keV and 3 keV respectively (Butterworth et al., 2012). Similarly, increases in photon energy to energies greatly above the electron binding energy of inner shell electrons will cause a steep decline in the probability of photoelectric ionisation and this rationale predicts, at beam energies much greater than the absorption maxima of gold ~ 79 keV, the photoelectric effect will not dominate the ionisation process (Butterworth et al., 2013).

Based on these predations, several studies have performed Monte Carlo simulations in order to predict the dose enhancement effect that will be achieved with AuNPs. Results presented by Lin *et al*, (2014) demonstrated that the dose enhancement when AuNPs

were combined with 150 and 250 kV photons was 2 times greater than for 6 MV photons and 8 times greater than for 10-150 MV proton exposure. The decrease in AuNP induced ionisation following an increase in radiation energy was therefore consistent with the prediction that at radiation energies significantly greater than the inner shell binding energy photoelectric ionisation will not occur.

The study by Lin *et al*, (2014) also examined the relative range of the secondary electrons produced following photoelectric ionisation of AuNPs by each radiation source. Results demonstrated that the electrons produced following ionisation of AuNPs by kV radiation had sufficient energy to travel from the AuNP surface, localised within intracellular lysosomes, to the cell nucleus. The secondary electrons produced from AuNPs ionised by MV photon or proton radiation however, had much lower energy as a result of Compton scattering and travelled only short distances to deposit their energy close to the AuNP surface (Lin et al., 2014).

Similarly, Cho *et al*, (2005) demonstrated that following combination of AuNPs with either 140 kV photons, 4 MV photons or 6 MV photons, significantly greater dose enhancement resulted with 140 kV photons (Cho, 2005).

It is clear from the studies discussed, that the energy of the radiation source is one of the major factors influencing the degree of dose enhancement observed from AuNPs in combination with radiation. As the use of kV radiation is limited clinically to the treatment of superficial skin tumours due to the short tissue penetration of kV photons, the ability of AuNPs to generate a dose enhancement with MV radiation sources must be further investigated.

1.6.2 Radiosensitisation by gold nanoparticles at kV energies

The first example of the use of AuNPs to radiosensitise tumour cells to XBR was demonstrated by Hainfield *et al*, (2004) who showed that 86% of mice bearing subcutaneous EMT-6 mammary carcinomas survived longer than 1 year when 1.9 nm AuNPs were intravenously administered prior to exposure of the tumour to 30 Gy of 250 kVp X-rays, compared to 20% survival for irradiation alone and 0% for AuNPs

alone (Hainfeld et al., 2004). Since then there have been numerous other publications investigating the radiosensitising effects of AuNPs both *in vitro* and *in vivo.* Table 1-1 gives an overview of some of the *in vitro* studies performed from 2008-2014, which have investigated the radiosensitising potential of AuNPs. Included in the table are details of the cell lines used, AuNP diameter, surface coating and concentration, and the radiation source and energies used in each study.

Table 1-1: An overview of *in vitro* studies utilising AuNPs as radiosensitisers

Study (author/year)	AuNP Size (nm)	AuNP concentration	Surface coating	Cell lines	Radiation energy	AuNP enhancement
Yasui et al, 2014	106nm	15-50ug/mL	PEG	SCCVII V79 A549	200kV x-rays	DEF_{10} 1.51 1.25 1.28
Wang et al, 2013	13nm	5nM	Glu	A549	6MV x-rays	DEF_{50} None given
Zhang et al, 2012	4.8nm 12.1nm 27.3nm 46.6nm	0.1mM	PEG	HeLa	662keV γ-rays	DEF_{50} 1.46 2.07 1.86 1.52
Geng et al, 2011	14nm	5nM	Glu	SK-OV-3	90kV x-rays 6MV photons	DEF_{50} 1.3 1.2
Jain et al, 2011	1.9nm (commercial)	12μM	Thiol	DU145 MDA-MB-231 L123	160kV 6MV 15MV	DEF_{50}/cell line 0.92, 1.41, 1.05 1.13, 1.29, 1.08 1.16 (MDA only)
Chithrani et al, 2010	14nm	1nM	Citrate	HeLa	220kVp	DEF_{50} 1.20
Kong et al, 2008	10.8nm	3.85nM 15nM 15nM	AET Glu Glu	MCF7 MCF-10A MCF7	200kV	DEF_{50} 1.37 1.00 1.63
Chang et al, 2008	13nm	10nM	Citrate	B16F10	6MV electrons	DEF_{50} 1.02

The studies summarised in Table 1-1 highlight the potential of AuNPs to radiosensitise cells to radiation at both kV and MV energies, with many studies reporting DEFs at the lethal dose greater than 1, indicating that the cell survival observed for AuNPs in combination with XBR was lower than for XBR alone. However the summary also highlights the substantial variation in the results achieved in different studies, and the great number of variables which change between each study.

The studies by Jain *et al*, (2011) and Kong *et al*, (2008) demonstrate cell line specific radiosensitisation. For example, Jain *et al*, (2011) reported DEFs of 0.92, 1.05 and 1.41 when 1.9 nm thiol capped AuNPs at 12 μM were combined with 160 kV X-rays in the human prostate cell line DU145, the normal human lung cell line L132 and human breast cancer cell line MDA-MB-231, indicating that radiosensitisation was achieved in MDA-MB-231 cells only (Jain et al., 2011). Similarly, Kong *et al*, (2008), reported radiosensitisation in MCF7 cells when 10.8 nm glucose capped AuNPs at 15 nM were combined with 200 kV photons (DEF=1.63), but no radiosensitisation in the human breast cancer cell line, MCF-10A (DEF=1.00) (Kong et al., 2008).

The dose enhancement observed could also be significantly affected by the amount of AuNPs present in the target area, dictated by the uptake of AuNPs by cells. Several studies have demonstrated how the AuNP uptake can be influenced by changes to AuNP characteristics such as size and surface functionalization. For example, Chithrani *et al*, (2006), reported up to 3 times higher uptake in HeLa cells for 50 nm AuNPs compared to 14 nm or 74 nm respectively (Chithrani et al., 2006). Geng *et al*, (2011) also reported 31% higher uptake of glucose coated AuNPs in the ovarian cancer cell line SK-OV-3, compared to unfunctionalised AuNPs (Geng et al., 2011).

The numerous variables which differ in each of the studies outlined in Table 1-1 with respect to AuNP size, surface functionalization, concentration, cell lines examined or radiation energy and source employed, and the factors which haven't been detailed such as the AuNP uptake and cell line radiosensitivity make it difficult to accurately compare the degree of radiosensitisation achieved in each study or draw any definitive conclusions about the optimum radiation source or AuNP formulation which would deliver maximum increase in the effective radiation dose. It is clear however, that further investigation is required to determine the extent to which the variables and

factors detailed impact the ability of AuNPs to radiosensitise cells in combination with kV and MV radiation.

1.6.3 Radiosensitisation by gold nanoparticles at MV energies

The majority of tumours treated with XBR are done so using 3DRT or IMRT which employ a LINAC to deliver radiation in the form of X-rays, which range in energy from 4-25 MV. Only superficial skin tumours are treated using kV X-rays due to their shorter tissue penetration, therefore in order to expand the clinical feasibility of AuNPs as radiosensitisers, their combination with MV radiation sources has been investigated. Several groups have used Monte Carlo simulations to predict the dose enhancement which should result through photoelectric ionisation when AuNPs are combined with different radiation sources across the kV to MV energy range. These studies hypothesise that a radiation dose enhancement effect will only result when the gold concentration within the target area is in the region 0.1-1%, and the photon energy is just above the binding energy of electrons within each energy shell, therefore, with MV photon energies, no dose enhancement is expected as a result of photoelectric ionisation of the AuNPs (Butterworth et al., 2012).

Despite these predictions, several studies have reported DEFs greater than 1.0 when AuNPs are combined with MV radiation and at gold concentrations as low as 0.05% (Table 1-1). The study performed by Jain *et al*, (2011), reported DEFs at the 50% toxicity levels of 1.29 and 1.16 when 1.9 nm commercial AuNPs were combined with 6 MV and 15 MV photons respectively in the human breast cancer cell line, MDA-MB-231 (Jain et al., 2011). Similarly, the study by Geng *et al*, (2011) reported a DEF at the 50% toxicity level of 1.2 when 14 nm AuNPs were exposed to 6 MV photons in SK-OV-3 cells (Geng et al., 2011). In contrast to these results however, the study by Chang *et al*, (2008) reported a DEF at the 50% toxicity levels of 1.02 from the combination of 50 nm AuNPs with 6 MV electrons in B16F10 cells indicating no dose enhancement, compared to cells exposed to radiation alone. The results of the studies therefore demonstrate the same variability in the magnitude of radiosensitisation observed from the combination of AuNPs with kV radiation sources.

In each study which has examined the radiosensitisation of AuNPs with both kV and MV radiation sources however, the observed DEFs at MV energies is lower than when the same AuNPs are combined with kV energy, which is consistent to some extent with the hypothesis presented that at MV energies the dose enhancement will be lower as photoelectric ionisations will not dominate and ionisations are likely to result from Compton scattering alone. However, as radiosensitisation has been observed in some studies where the simulations predict no enhancement at all, other processes must occur following the interaction of AuNPs with MV radiation and these have been investigated further and are discussed in section 1.6.4.

1.6.4 Prediction of the mechanism of dose enhancement by AuNPs at MV energies

1.6.4.1 The presence of low energy photons and secondary electrons contribute to AuNP dose enhancement

Initial studies investigating the observed dose enhancement following combination of AuNPs with MV radiation considered only the average physical dose enhancement which would be expected to result from AuNPs in combination with MV photons (Cho, 2005). However, more recent studies such as those performed by Butterworth *et al,* (2013) and McMahon *et al,* (2011) have studied the localised effect of secondary electron production around the individual AuNPs (Butterworth et al., 2013; McMahon et al., 2011).

At MV photon energies, Compton scattering will be the primary method of photon absorption for both AuNPs and soft tissue and as this process demonstrates only a weak dependence on atomic number, the dose deposition in the presence of AuNPs is likely to be comparable to soft tissue. The study by Butterworth *et al*, (2013) however, postulates that the method of ionisation by Compton scattering for AuNPs and soft tissue may be very different. In soft tissue, Compton scattering will result in sparse ionisation events as the ejected electrons and photons are scattered across long ranges, whereas with AuNPs, ionisation may result in the production of a cascade of Auger secondary electrons following ejection of inner shell electrons and the filling of vacancies by outer shell electrons with the subsequent release of energy. As Auger

electrons are very low energy, typically <5 keV they will have very short range and will therefore deposit their energy in the vicinity of the nanoparticle. This could therefore lead to extremely high dose deposition localised around the AuNPs (Butterworth et al., 2012).

Furthermore, the study by McMahon *et al,* (2011) assessed the energy deposition around individual AuNPs following irradiation with MV photons and investigated the beam profile for 6 MV photons. Results of this study demonstrated that the presence of AuNPs within an irradiated volume led to a heterogeneous distribution of dose surrounding the AuNPs, where large numbers of secondary electrons were localised around the AuNPs, consistent with the mechanism postulated by Butterworth *et al,* (2012). Additionally the results showed that the beam profile for 6 MV photons consisted of low energy photons and electrons which are scattered by the primary beam (Figure 1-4) (McMahon et al., 2011). It is possible therefore, that the small proportion of low energy photons and secondary electrons scattered from the primary MV beam allow ionisation of AuNPs through the photoelectric effect, which together with the high volume of secondary electrons surrounding the AuNPs contribute to the dose enhancement observed.

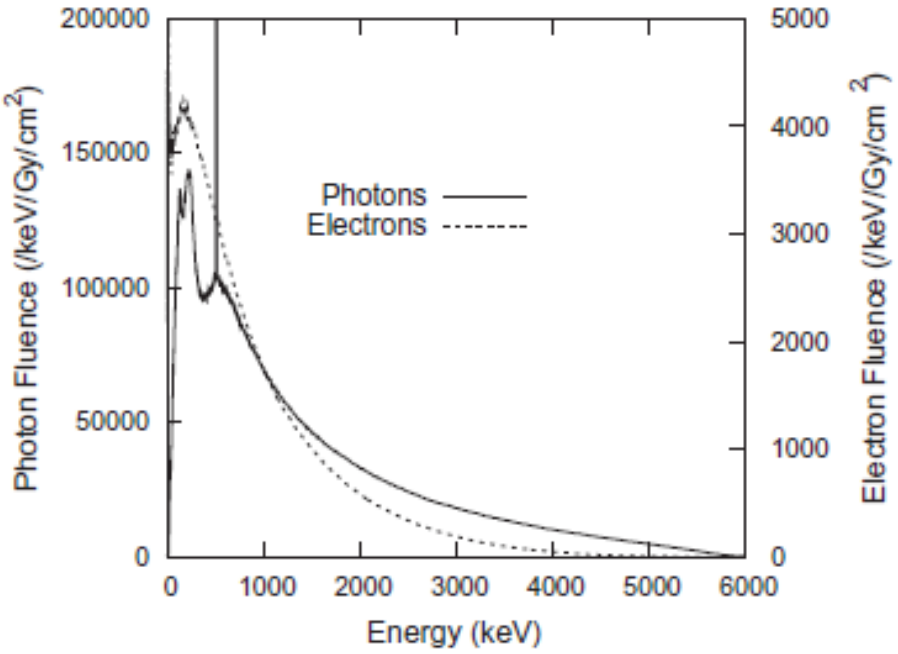

Figure 1-4: Photon and electron spectra resulting from 6 MV LINAC irradiation.

Spectra measured at a depth of 5 cm in a cylindrical water volume. The spectra show the presence of low energy photons and secondary electrons scattered from the primary photon peak. Data taken from McMahon *et al*, 2011 (McMahon et al., 2011).

1.6.4.2 The role of reactive oxygen species in the dose enhancement by AuNPs

Approximately 50-70% of DNA damage by X-ray irradiation is a result of oxidative stress, with the hydrolysis of intracellular water resulting in the formation of hydroxyl radicals (·OH), which can either interact with DNA or oxidise lipids and proteins in the cell to initiate apoptotic or necrotic cell death (Riley, 1994). Several studies have suggested that the production of reactive oxygen species (ROS) and subsequent oxidative stress in cells can enhance the radiosensitisation by AuNPs. This has been supported by studies such as those by Pan *et al*, (2007), reporting increased ROS from exposure of cells to 1.4 nm AuNPs (Pan et al., 2007). To date however, very little mechanistic data is available detailing the induction of ROS by AuNPs, and the role ROS play in AuNP radiosensitisation. The recent study by Sicard-Roselli *et al*, (2014) aimed to calculate a G-value for the ·OH production by AuNPs following exposure to ionising radiation, where the G-value (mol J^{-1}) is the number of moles of ·OH produced per Joule of radiation. The study postulates three possible mechanisms of ·OH production (Figure 1-5), namely, pathway A in which the radiation energy is absorbed by the AuNP, resulting in the release of secondary electrons which interact with intracellular water to generate ·OH. Pathway B describes the direct interaction of radiation with intracellular water to generate ·OH, with no interaction from AuNPs and pathway C describes direct interaction of radiation with intracellular water to generate ·OH and other excited species, which subsequently interact directly with AuNPs to result in increased ·OH levels. Work by Sicard-Roselli used coumarin trapping assays to successfully quantify the G value for ·OH production across varying AuNP concentrations and radiation dose rates, and found the presence of AuNPs resulted in enhanced levels of ·OH production compared to radiation alone. The results were consistent with the rationale of AuNP radiosensitisation in which ionisations within the AuNP will generate secondary electrons for which the most likely fate will be interaction with intracellular water to create ROS, namely ·OH. Through quantification of the yield of ·OH produced however, and comparison of this to the level of ·OH produced via each of the postulated pathways, Sicard-Roselli was able to deduce that the mechanism of ·OH production was via pathway C, indicating that not only do ionisations within the AuNPs result in ROS production, but that the ·OH also likely interact directly with the AuNPs to generate even greater amounts of ·OH.

Furthermore, research has shown that structured water layers at the AuNP-water interface occur through charges on the AuNP surface aligning the dipoles of water, with these layers stabilised through additional hydrogen bonding (Carrasco et al., 2012). Subsequent injection of energy into this AuNP-water system could result in breaking of the hydrogen bonding, resulting in the formation of more ·OH, which in turn would cause further hydrolysis of intracellular water, creating a cascade of ·OH production. It is suggested through this research that radiolysis and ·OH production is much more efficient and favourable in the presence of AuNPs, and leads to the enhanced ·OH production observed (Sicard-Roselli et al., 2014).

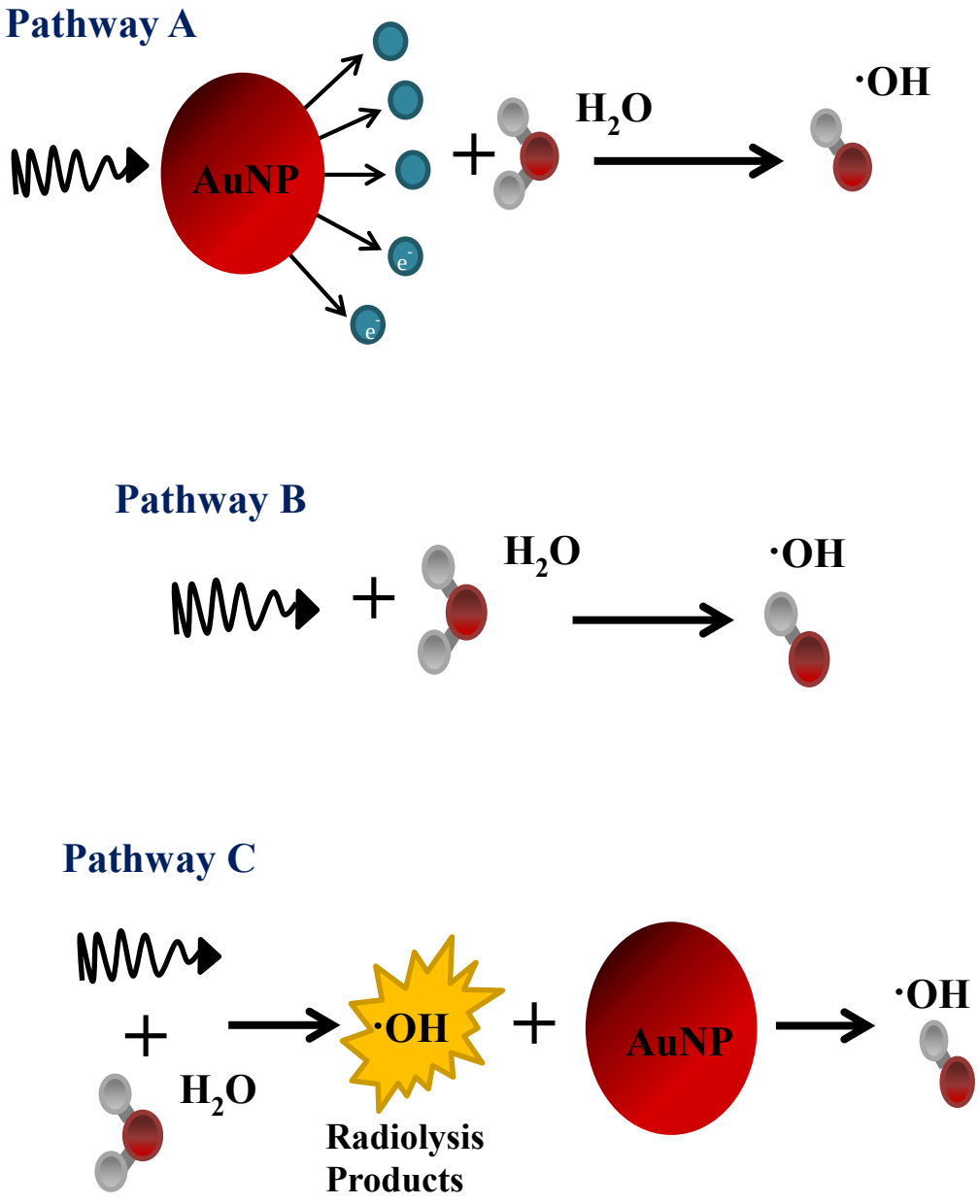

Figure 1-5: Schematic diagram adapted from the pathways A-C postulated by Sicard-Roselli et al, 2014 to form hydroxyl radical ˙OH species following irradiation in the presence of AuNPs (Sicard-Roselli et al., 2014).

The data taken together, therefore suggests that AuNPs can produce radiosensitisation at MV energies as a result of localised dose deposition in the nanoparticle vicinity through Compton scattering, the presence of low energy photons and electrons, and increased ·OH production leading to greater oxidative stress in cells. The successful radiosensitisation at MV energies allow AuNPs to be considered clinically relevant, however the inconsistencies in the observed radiosensitisation discussed earlier between AuNPs of different size and surface functionalisation, and the observation that radiosensitisation is cell line specific mean a great deal of research is still required to develop the optimum AuNP formulation suitable for clinical applications.

1.6.4.3 AuNPs in combination with radioisotopes

In addition to the suggested radiosensitisation achieved by the combination of AuNPs with MV photon beams, research has been performed to assess the radiosensitisation potential of AuNPs in combination with more novel radiation sources such as MeV proton beams and radioisotopes in low dose rate brachytherapy. For example, Kim *et al*, (2010, 2012) reported significant reduction in tumour volume (37-62%), in mice bearing CT26 colon tumours injected subcutaneously into the leg, following intravenous injection of 300 mg/kg AuNPs of either 2 nm or 13 nm and irradiation by 41.7 meV proton beam, compared to animals treated with protons alone (Kim et al., 2012; Kim et al., 2010). Ngwa *et al*, (2013) combined 50 nm AuNPs with continuous low energy ^{125}I containing brachytherapy seeds in cervical cancer HeLa cells *in vitro*. Radiation damage was assessed through measurement of residual γ-H2AX foci within the cell nucleus 24 hours post irradiation, with significantly higher foci numbers observed in cells exposed to AuNPs compared to control cells, and residual dose enhancement factors from 1.7-2.3 observed based on the dose rate of irradiation used (Ngwa et al., 2013). These studies demonstrate that AuNPs can also radiosensitise cells through chronic exposure to low dose rate radiation from β and γ radiation, as well as kV and MV photons as previously discussed. The combination of AuNPs with radioisotopes either through direct conjugation or in brachytherapy is another avenue which must be further investigated to assess the full potential of AuNPs to enhance the efficacy of current radiotherapy modalities.

1.6.5 Unique properties and limitations of gold nanoparticles as radiosensitisers

1.6.5.1 Origin of enhanced radiation absorption by the surface plasmon resonance (SPR) effect

The absorption of radiation photons by AuNPs relies on a number of unique physical properties of the AuNPs such as the size, intracellular concentration and surface functionalisation.

The absorption capability of AuNPs is due to the presence of free d-electrons, which reside in the conduction band of AuNPs and can move freely throughout the material (Faraday, 1857). When AuNPs are exposed to visible light of a wavelength greater than the AuNP size, the electric field of the incoming light causes the free d-electrons to oscillate strongly in resonance with the frequency of the visible light at the surface of the particle, allowing absorption of the light. This phenomenon is known as surface plasmon resonance (SPR) and is specific to nanoparticles of heavy metal elements, particularly Au and Ag (Huang et al., 2007; Link and El-Sayed, 1999). The resonance conditions and subsequent absorption properties will depend on the absorption and scattering spectroscopy on the AuNP surface, which can be altered by changes to the size and shape of the AuNP, and the dielectric constant of the surrounding medium (Eustis and El-Sayed, 2006; Kelly et al., 2002). In order to ensure the absorption properties of the AuNPs investigated in the present study remained consistent, citrate stabilised 20 nm AuNPs were used throughout to assess the radiosensitisation in combination with XBR and [^{131}I]-MIBG and the effects of AuNP size and surface functionalisation were not investigated at this time.

1.6.5.2 Cytotoxicity of AuNPs

AuNPs were traditionally considered chemically inert, however to be utilised successfully as a radiosensitiser or delivery vehicle in cancer therapy, the AuNPs should have little to no toxic effects as a single agent. Consequently, in recent years the inherent toxicity of AuNPs has been extensively investigated with varying outcome.

Early studies, such as those performed by Connor *et* al, (2005), reported incubation of cells with 4, 12 and 18 nm AuNPs functionalised with either citrate, biotin or glucose caused no toxicity in the human leukaemia cell line, K562 (Connor et al., 2005). Similarly, a study performed by Shukla *et al*, (2005) found no cellular toxicity with increasing concentrations of 35 nM AuNPs up to 100 µM in RAW264.7 macrophage cells, together with a decrease in the reactive oxygen species (ROS) and nitrite production following AuNP exposure (Shukla et al., 2005). In contrast, results by Patra *et al*, (2007) demonstrated that incubation of A459 human carcinoma lung cells with citrate capped 33 nm AuNPs induced significant concentration dependant toxicity from 10 nM to 120 nM (Patra et al., 2007).

Again, as with the comparison of the observed DEFs, discussed in section 1.6.2, due to the number of variables which differ in each study investigating AuNP toxicity, with respect to the AuNP diameter, concentration, surface functionalisation and cell line examined, it is not possible to accurately determine the cause of the cell toxicity or establish any definitive trends in cytotoxicity following AuNP exposure.

Several studies have demonstrated the effect of AuNP diameter on cell toxicity. For example, Pan et al, (2007) reported significant concentration dependant reduction in cell viability; with a calculated IC_{50} dose of 46 µM following incubation of HeLa cells with 1.4 nmtriphenylphoshine monosulfate (TPPMS) functionalised AuNPs. Comparatively, 15 nM AuNPs induced no toxicity at any of the concentrations investigated and had an extrapolated IC_{50} dose of 6300 µM (Pan et al., 2007). Similarly, the study performed by Coradeghini *et al*, (2013) demonstrated significant concentration dependant reduction in the colony formation of Balb/3T3 cells incubated with 5 nm AuNPs with no toxic effects observed following incubation with 15 nm AuNPs (Coradeghini et al., 2013).

The greater toxicity observed with small AuNPs, typically <5 nm, compared to larger AuNPs has been attributed to several factors including their increased surface area relative to their total mass, which could lead to increased interaction with intracellular molecules and result in adverse cellular effects (Shang et al., 2014). AuNPs smaller than 2 nm have also been reported to exhibit a greater degree of chemical reactivity which is not observed for larger AuNPs and could contribute to increased cell toxicity

(Alkilany and Murphy, 2010). Despite the literature supporting the hypothesis that smaller AuNPs exhibit greater cell toxicity than larger AuNPs, based on the significant number of variables present in each study it is very difficult to hypothesise the mechanism by which AuNPs cause the toxicity observed in some studies. For use as a radiosensitiser and ensure clinical feasibility of AuNPs, they should induce minimal inherent toxicity which would allow them to be safely administered to patients prior to radiotherapy.

1.6.5.3 Intracellular uptake and accumulation of AuNPs

As discussed in section 1.6.2, the amount of AuNPs within the cell at the time of radiation exposure could significantly affect the dose enhancement observed and the increase in radiation efficacy. Understanding the mechanism of uptake of AuNPs by cells, and the factors which affect it is therefore crucial to predicting the potential of AuNPs as successful radiosensitisers.

Several studies have confirmed that intracellular uptake of AuNPs occurs via receptor mediated endocytosis (RME) (Figure 1-5), with a number of factors demonstrating an effect on the cellular uptake of AuNPs, namely the AuNP diameter and surface functionalisation (Chithrani and Chan, 2007; Coulter et al., 2012; Z. Liu et al., 2014).

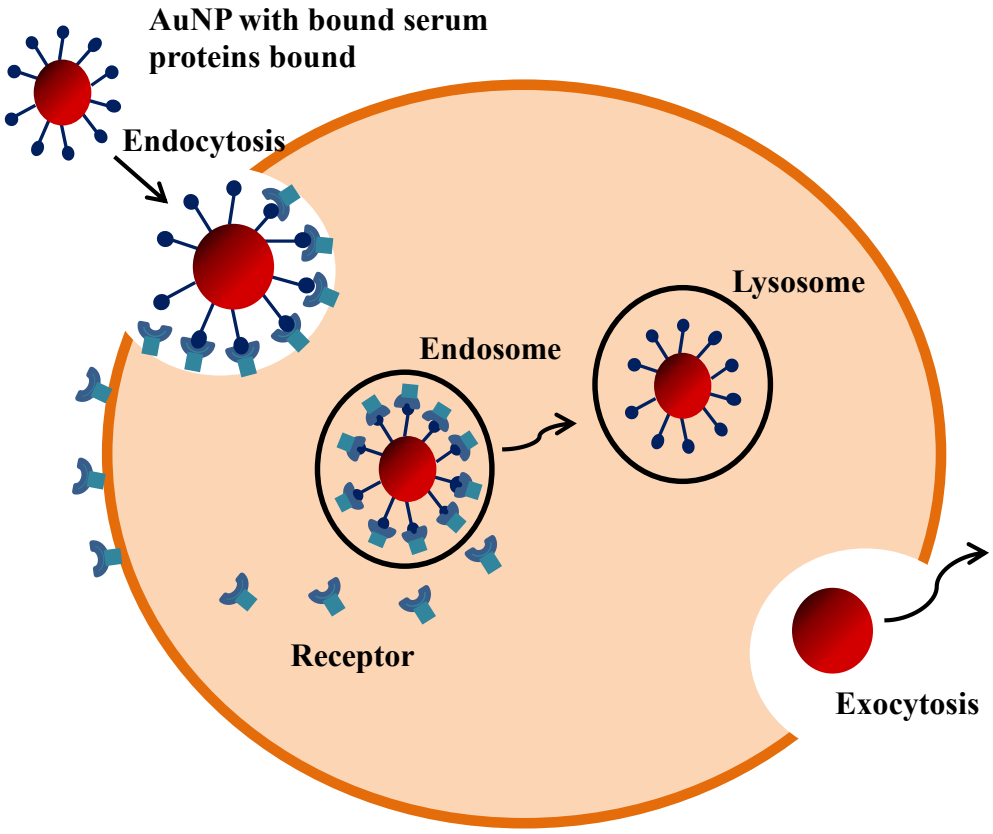

Figure 1-6: Schematic diagram showing receptor mediated endocytosis (RME) of AuNPs with serum proteins bound to the surface.

Data adapted from Tran et al (Tran and Webster, 2013).

Chithrani *et al*, (2006) investigated the effect of AuNP diameter on intracellular uptake and demonstrated that the number of 50 nm AuNPs within the cell was 2 and 3 fold higher than the number of 14 nm or 74 nm AuNPs respectively (Chithrani et al., 2006). A similar study by Jiang *et al*, (2008) found greater uptake of 40 nm AuNPs, compared to 2 nm AuNPs (Jiang et al., 2008).

The dependence on cellular uptake of AuNP diameter has been rationalised to some degree by the "wrapping effect" proposed and mathematically modelled by Gao *et al*, (2005), where the term wrapping relates to the enclosing and internalisation of macromolecules bound to the surface receptors during RME. Following the binding of a ligand to a surface receptor, it is proposed that this will result in the diffusion of further receptors across the membrane to the binding site and it is hypothesised that the "wrapping effect" is dependent on both the ligand-receptor interaction and the free energy generated by this, and the receptor diffusion kinetics. Gao *et al*, (2005) mathematically modelled these properties to propose a nanoparticle diameter range of 27-30 nm would result in the shortest wrapping time and therefore have the fastest rate of RME (Alkilany and Murphy, 2010; Gao et al., 2005). Like the inherent cytotoxicity of AuNPs, it is clear that cellular uptake of AuNPs also varies greatly based on the AuNP diameter, surface functionalisation and cell growth medium conditions. In order to accurately predict potential radiosensitisation from AuNPs in combination with radiation the uptake and accumulation of AuNPs must be quantified.

1.6.5.4 Selective accumulation of AuNPs *in vivo* by the enhanced permeation and retention effect

It has been demonstrated that *in vivo,* bare AuNPs have the ability to preferentially accumulate within tumour cells, allowing them to be utilised for selective delivery or targeted therapy approaches for cancer. The selective accumulation arises due to the enhanced permeation and retention (EPR) effect (Figure 1-6), which is a process by which macromolecules such as, nanoparticles and liposomes, with molecular size above 45 kDa accumulate at concentrations, 10-fold higher within tumour cells, compared to normal tissue (Maeda et al., 2003). It has been described that tumour cells have up-regulated levels of normal vasculature permeability factors, namely

bradykinin and nitric oxide (NO), and a higher dependence on vascular endolithial growth factors to sustain the great nutritional demand present as a result of their rapid and uncontrolled proliferation and this subsequently permits enhanced permeation of macromolecules into cells (Maeda et al., 2000). In addition to enhanced permeability, tumours also possess a suppressed lymphatic system with poor lymphatic drainage and clearance compared to normal healthy tissue. The enhanced permeability and poor clearance facilitates increased extravasation of macromolecules into the tumour, and increased retention, giving rise to the EPR effect which can be readily exploited as the basis for selective targeting of macromolecular compounds to the tumour site (Iyer et al., 2006; Prabhakar et al., 2013).

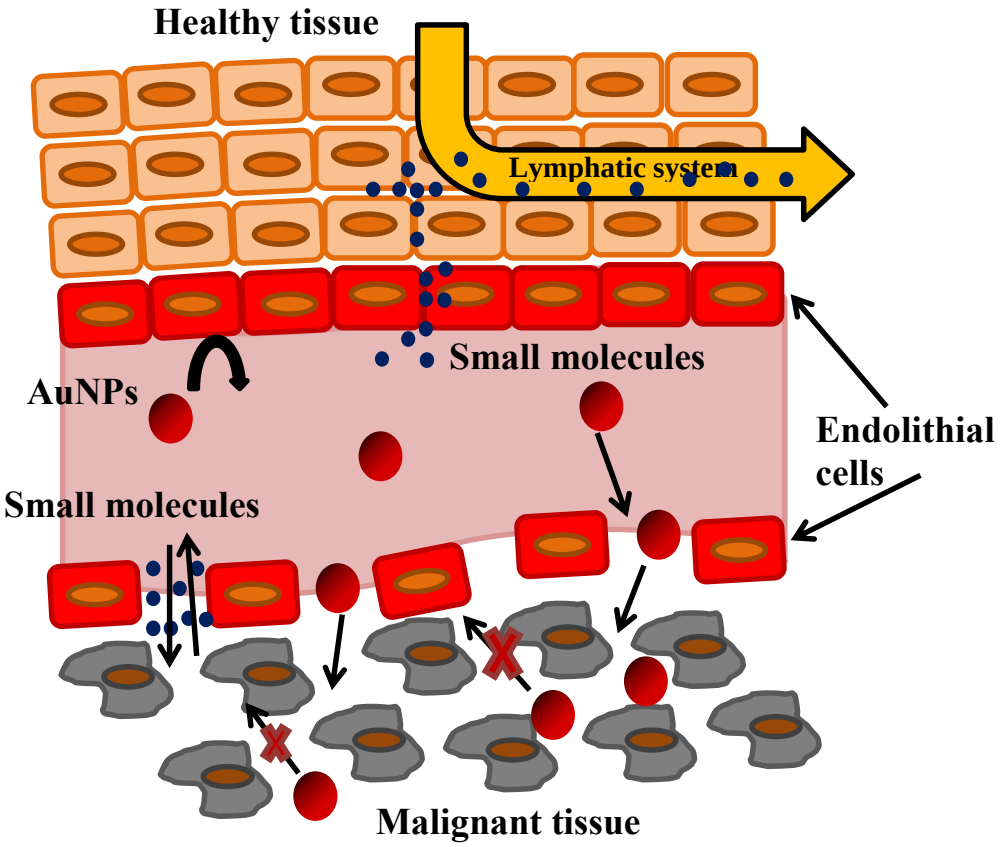

Figure 1-7: Schematic diagram showing the enhanced permeation and retention (EPR) effect in malignant tissue.

Schematic demonstrates the increased uptake and subsequent retention of macromolecules within malignant tissue as a result of the poor vasculature and suppressed lymphatic system, compared to normal tissue. Small molecules can enter both normal and malignant tissue through passive diffusion and are readily cleared by the lymphatic system. Data adapted from Stockhofe et al (Stockhofe et al., 2014).

Many studies to date have investigated the uptake, accumulation and biodistribution of AuNPs *in vivo*. All studies demonstrated that, in the absence of tumours, bare AuNPs accumulate significantly in the liver and spleen, and to a lesser extent in the lung and kidneys (Morais et al., 2012; Terentyuk et al., 2009). This accumulation has been attributed to the adsorption of blood proteins to the AuNP surface which allow them to be easily taken up by the reticuloendolithial system (RES) and quickly cleared from the blood circulation (Dreaden et al., 2012). The quick blood clearance observed with bare AuNPs is a significant limitation for the use of AuNPs as targeting or therapeutic modalities and many studies have aimed to enhance the circulation time of AuNPs through surface functionalisation with polyethylene glycol (PEG) (Niidome et al., 2006). Whilst the EPR effect allows passive accumulation of AuNPs within tumour cells, several studies have functionalised AuNPs with tumour targeting moieties such as monoclonal antibodies directed as surface receptors overexpressed selectively in cancer cells (Meyers et al., 2014).

The EPR effect for AuNPs has successfully been exploited in a clinical trial with AuNPs conjugated to the recombinant human tumour necrosis factor alpha (rhTNF), a cell signalling protein which has demonstrated dramatic anti-tumour effects (Libutti et al., 2010). This clinical trial utilises the AuNP formulation, CYT-6091, a 27 nm AuNP functionalised with (PEG) and rhTNF, to investigate if delivering rhTNF using untargeted AuNPs via the EPR effect can circumvent the dose limiting side effects observed for rhTNF. Results of the study demonstrated that the dose of AuNP bound rhTNF was three times higher than the maximum tolerated dose of free rhTNF, with no major dose limiting toxicity, indicating specific accumulation of AuNPs in tumour tissue, confirmed by post treatment biopsies (Libutti et al., 2010).

This study demonstrates the potential of AuNPs to act as delivery vehicles in cancer therapy through the EPR effect, however the EPR effect is also advantageous to the use of AuNPs as potential radiosensitisers, as the selective accumulation of AuNPs within tumour cells will lead to an increase in radiation dose deposition within the target area and reduce dosing of normal tissue.

1.6.6 Rationale for AuNPs in combination with ^{131}I

To date, several studies have described successful combination of AuNPs with radionuclides either to enhance the efficacy of low dose-rate brachytherapy or through direct conjugation of a radioisotope to the nanoparticle. For example, a dosimetric study performed by Cho *et al,* (2009), investigated the macroscopic dose enhancement factors (MDEF) which would be produced when a tumour loaded with AuNPs was combined with ^{169}Yb, which decays via electron capture at 93 keV and ^{192}Ir, which decays with β electron emission at 1.4 MV. Results demonstrated that, combination of AuNPs with ^{169}Yb delivered 70% higher dose enhancement compared to combination with ^{192}Ir, which was concurrent with the previously discussed hypothesis that significantly higher dose enhancement would occur at lower energies, closer to the absorption edge of Au (Cho et al., 2009).

Another method of combining AuNPs with radioisotopes was investigated by Kao *et al,* (2013) who developed radioimmuno-AuNPs. In this study, AuNPs were conjugated to the CD225 monoclonal antibody, which binds specifically to the extracellular domain of the human epidermal growth factor receptor (EGFR), and then conjugated to ^{131}I. ^{131}I induced significant reduction in cell viability in the human lung cancer cell line, A549, compared to AuNPs conjugated to CD225 alone, and allowed tumour imaging in an A549 carcinoma mouse model by microSPECT/CT (Kao et al., 2013). Despite these positive results, there is limited literature detailing the effects of AuNPs in combination with radioisotopes, where the primary focus of previous studies has been to assess the ability of AuNPs to enhance tumour imaging and not to investigate their potential for tumour therapy. This gap in the literature is therefore a major focus of the work performed in this present study.

Based on the recent advances in AuNP research which have demonstrated their ability to offer a greater than expected radiosensitisation with MV photon beams, proton beams and radioisotopes, it was hypothesised that the presence of AuNPs could radiosensitise cells to ^{131}I. Throughout the present study, ^{131}I conjugated to MIBG was utilised to evaluate the potential of AuNPs to radiosensitise cells to ^{131}I.

As briefly discussed in section 1.6.4, McMahon *et al,* (2011) mapped the photon and electron spectra following 6 MV LINAC irradiation and demonstrated that while the majority of particles remain in the primary beam peak; low-energy photons and electrons with energies less than 200 kV make up approximately 13% of the spectrum. The study further demonstrated that only 5% of the observed ionisations which occur in a 2 nm AuNPs following exposure to 6 MV radiation resulted from Compton scattering (McMahon et al., 2011). This study supports the hypothesis that despite the energy of the incident radiation not being in the optimal range for AuNP absorption (3-79 keV), a dose enhancement in combination with radiation may still occur due to the presence of small quantities of low-energy particles.

Following emission from ^{131}I (Figure 1-7), the low LET β and γ radiation will travel through the cells, continually depositing energy, up to their maximum path range (0.8 mm), which is equivalent to a few cell diameters. The probability of the β and γ emissions from ^{131}I causing photoelectric ionisations within the AuNPs, at their maximum energies of 606 keV and 364 keV is very low due to the poor energy match between the radiation and electron binding energies of Au. However the probability of interactions with AuNPs will increase as the β and γ emissions lose energy as they traverse through the cell population, and at some point throughout the lifetime of the emission, its energy will lie in the optimum range to induce ionisations in the AuNPs.

Additionally, the long half-life of the β emissions from ^{131}I (8.02 days) mean that both the cells and AuNPs experience chronic radiation exposure, which could allow more ionisations within the AuNPs, and generation of a greater dose enhancement, compared to the rapid delivery of XBR.

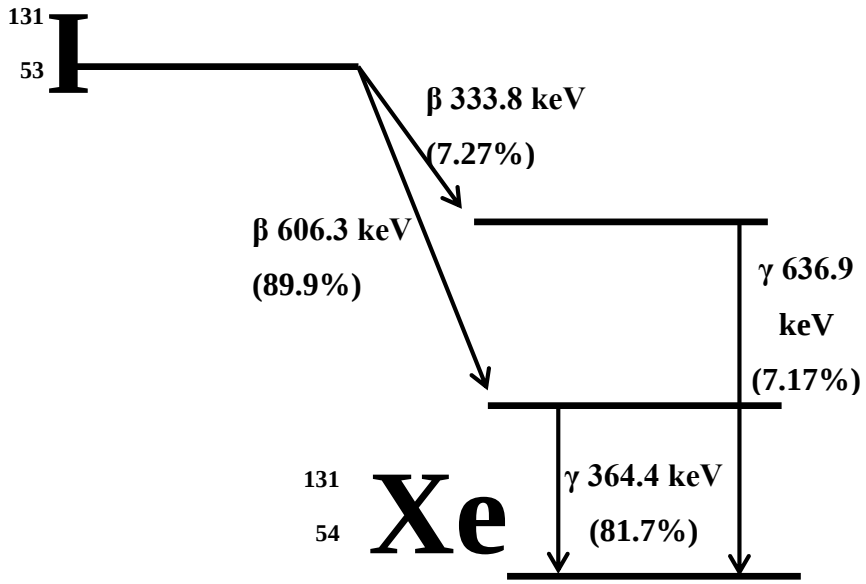

Figure 1-8: Simplified radioactive decay of ^{131}I.

Primary emission from ^{131}I is via release of β electrons at 606 keV to form ^{131}Xe isotopes with 89% abundance. Primary γ emission of 364 keV has 81.7% abundance.

1.7 Hollow Gold Nanoparticles (HGNs)

1.7.1 Physical characteristics and optical properties of HGNs

The dose enhancement of radiation which results from the unique absorption properties of AuNPs, and allows them to be utilised as radiosensitisers for cancer therapy could be further enhanced by using hollow gold nanoparticles (HGNs). HGNs are gold nanoshells, with an average diameter between 30-80 nm and a hollow centre, typically synthesised using a sacrificial template such as Ag or Co nanoparticles (Schwartzberg et al., 2006). Like solid AuNPs, HGNs display significant absorption properties via the SPR effect as discussed in section 1.6.5.1. The wavelength of maximum absorption for HGNs however can be significantly tuned across a wide range, through changes to the particle diameter, shell thickness, inner core diameter or environmental changes such as the dielectric constant of the surrounding medium, allowing absorption of energy with wavelengths anywhere between ~520-820 nm,. Comparatively, the wavelength of maximum absorption for solid AuNPs can be red-shifted only slightly (Li et al., 2013; Sun and Xia, 2002).

In addition to the greater tune-ability of the SPR effect, HGNs also display much higher SPR absorption due to the presence of two surfaces as a result of the hollow centre. Gutrath *et al,* (2012) investigated the differences in photoacoustic signal, namely the conversion of light absorption into sound waves, produced by solid AuNPs, gold nanorods (AuNRs) and HGNs. Results of the study demonstrated that the maximum photoacousitic (PA) intensity, which gives an indication of the strength of absorption, and the maximum energy conversion was measured in HGN samples (Gutrath et al., 2012). This study demonstrated that HGNs, compared to solid AuNPs, had substantially greater absorption of electromagnetic radiation at their respective wavelengths of maximum absorption, and that HGNs could convert the light absorbed into sound waves much more efficiently. Although this study measured the absorption and conversion of electromagnetic radiation, it is reasonable to extrapolate that in combination with ionising radiation, HGNs could be hypothesised to display the same increase in absorption and conversion of the ionising radiation, compared to solid AuNPs. This greater absorption could therefore lead to an increase in the ionisations

within HGNs and the greater conversion ability lead to the production of more secondary electrons.

In addition to the enhanced absorption of HGNs compared to solid AuNPs, the study performed by Jackson *et al*, (2003) demonstrated an enhancement in the localised electromagnetic field both surrounding nanoshells and in the far field (Jackson et al., 2003). The enhancement in the localised electromagnetic field, and the ability of hollow nanoparticles to induce absorption and scattering effects in regions further away from their surface, could lead to larger regions of localised dose enhancement.

Furthermore, it has also been demonstrated by Hao *et al*, (2004) computationally, that the presence of pinholes on the surface of HGNs concentrated the electromagnetic field from the SPR effect, and resulted in localised hot spots across the HGN surface which were 3-4 times higher than that for seamless HGNs (Hao et al., 2004).

Taken together, the unique physical and optical advantages offered by HGNs compared to solid AuNPs could lead to an increase in the radiosensitisation and subsequent dose enhancement observed in their combination with ionising radiation.

1.7.2 Current uses of HGNs

Despite the enhanced absorption properties of HGNs, compared to solid AuNPs very few studies to date have assessed their capability for use as radiosensitisers in cancer therapy. HGNs have been investigated primarily for use in photothermal ablation (PTA) therapy due to their wide SPR range and heat generation in this wavelength range. Recent studies have successfully utilised HGNs for PTA therapy in combination with monoclonal antibodies (anti-EGFR HGNs) to enhance direct targeting of HGNs to tumour cells specifically, allowing selective PTA therapy Melancon *et al*, (2008). Additionally, HGNs have been successfully conjugated to chemotherapeutic agents such as, Doxorubicin, where the hollow core of the particles allowed two surfaces for doxorubicin attachment which lead to a substantially greater payload of doxorubicin than is achievable for solid AuNPs. The resulting nanoparticles were able to induce

PTA of cancer cells through irradiation with NIR light and induce toxicity from the presence of doxorubicin (You et al., 2010).

As to date, HGNs have only been investigated in combination with non-ionising electromagnetic radiation sources, such as NIR lasers which provide excitation of the electrons but not removal a major focus of this present study was to investigate the radiosensitisation potential of HGNs combination with ionising radiation.

In summary, as a result of the increased absorption of HGNs, and their ability to utilise absorbed radiation more effectively, together with the presence of two surfaces in the HGNs, it is hypothesised that an increase in the number of ionisations within the HGNs may result and lead to greater secondary electron production. Additionally, the presence of pinholes on the HGN surface may allow diffusion of the secondary electrons produced within the HGN core out of the HGNs, where they could interact with cellular water and generate hydroxyl radicals or induce subsequent ionisations within the HGNs, resulting in a cascade of secondary electron production around the HGNs. The presence of two surfaces could also enhance the development of structured water-nanoparticles layers, hypothesised by Sicard-Roselli (2014), and discussed in section 1.6.4.2. This could lead to a further increase in the number of hydroxyl radical species formed following radiation exposure, increasing the dose enhancement observed and resulting in a greater biological effect. Finally, the greater electromagnetic field created around HGNs, and at regions further away from the HGN surface, could lead to a significant increase in the absorption and scattering of ionising radiation by the HGNs, which could potentiate the radiation effects further throughout the cells and lead to greater radiobiological effect. Taken together, it was hypothesised that the physical properties of HGNs discussed could allow them to act as successful radiosensitisers in combination with ionising radiation both in the form of XBR at kV energies and with the MV isotope ^{131}I.

1.8 Multicellular tumour spheroids (MTS)

1.8.1 Rationale for MTS use

In the development of new therapies for cancer treatment, the first stage is to investigate the efficacy of any treatment modalities *in vitro* using 2D cell culture models. There are vast differences however, in cell morphology, physiology and behaviour between 2D monolayer cultured cancer cells and those found in patient tumours. For examples the cell-cell interactions or extracellular matrix (ECM) present in malignant tumours are not present in 2D cells, and significant differences in gene expression levels and signalling have been found between 3D tumours and 2D cells (Hirschhaeuser et al., 2010). The use of 3D multicellular tumour spheroid (MTS) models has been suggested as an appropriate bridge between 2D monolayer cell culture and *in vivo* animal studies as they provide a more representative model to assess the efficacy of therapeutics (Haycock, 2011; Mehta et al., 2012).

The physiology of 3D MTS will depend primarily on the spheroid size. When initially formed, spheroids will consist of a mass of proliferating cells. As the cells divide and the spheroids grow larger, concentration gradients will develop for the delivery of oxygen, nutrients and drugs to the cells residing at the centre of the tumour, and for the removal of CO_2 and waste products from those cells out of the spheroid. As a result of these gradients, cells throughout the spheroid volume will become quiescent and necrotic based on their proximity to the centre and their nutrient availability. Spheroids with a diameters >350 µm consist of an outer layer of proliferating cells, which resemble the actively proliferating cells residing on the outer layer of tumours lying close to capillaries *in vivo*, and inner most cells which are hypoxic and/or quiescent from lack of oxygen and nutrient availability, and with further increase in the spheroid size a core of necrotic cells will form (Figure 1-8) (Mehta et al., 2012).

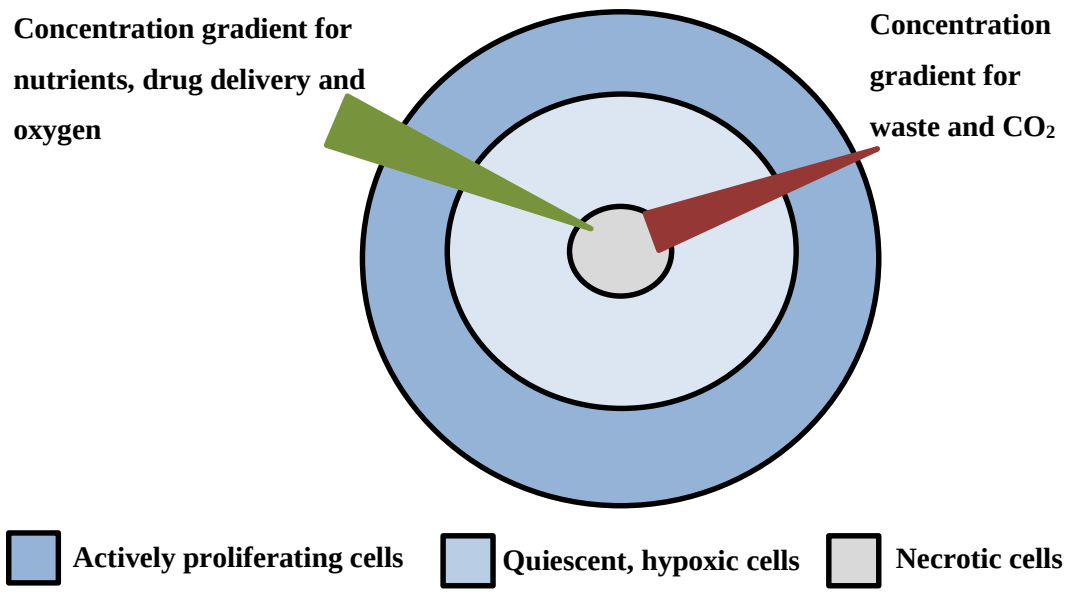

Figure 1-9: Physiological cell structure of a 3D MTS with an approximate diameter of 400-500 µm.

Schematic details the presence of necrotic cells at the spheroid core as a result of the concentration gradients for the delivery of oxygen and nutrients and removal of CO_2 and waste products which lead to a severe lack of oxygen and nutrients and a build-up of waste products at the spheroid core. Subsequent layer consists of hypoxic and quiescent cells due to insufficient oxygen delivery with proliferating cells making up outer edge of spheroid allowing continual growth.

1.8.2 The effect of spheroid physiology on treatment efficacy

As a result of the concentration gradients, and the heterogeneity with respect to cell proliferation status and gene expression within 3D MTS, studies have demonstrated increased resistance to both chemotherapeutic agents and radiotherapy compared to 2D monolayer cells. For example, Li *et al*, (2010) found that MCF10A cells grown as 3D spheroids were more resistant to doxorubicin than in their 2D form (Li et al., 2010) . Similarly, Chen *et al*, (2011) demonstrated that MCF-7 cells grown as 3D spheroids were more resistant to tamoxifen than their 2D counterparts (Chen et al., 2011). The indirect effect of ionising radiation on cellular DNA results from the hydrolysis of water molecules to create reactive oxygen species (ROS) which can interact with cellular DNA to create DNA single strand breaks. This process relies on the presence of oxygen within the cellular environment and it therefore follows that hypoxic cells will be more resistant to the effects of ionising radiation than normoxic cells, with resistance increasing as oxygen levels fall (Harrison et al., 2002; Janssen et al., 2005). This has been supported with studies showing radiation resistance increases with increasing spheroid size (West, 1989).

Conversely, following decay, radiopharmaceuticals exert their damaging effects through the cross-fire of radiation throughout the cell population. In 2D monolayer cell cultures, the effects of the cross-fire of radiation are largely lost; with only the direct neighbouring cells of those containing the radiopharmaceutical exposed to radiation. In 3D MTS models however, cross-fire effects of radiation can extend to all cells surrounding the cell containing the radiopharmaceutical, meaning a great deal more cells will be targeted. This has been demonstrated in the study performed by Boyd *et al*, (1999) which reported that treatment of UVW/NAT cells with [^{131}I]-MIBG was twice as effective in 3D MTS, compared to 2D monolayers as a result of increased radiation cross-fire through 3D MTS (Boyd et al., 1999). The study by Gaze *et al*, (1992) also demonstrated that smaller spheroids were more resistant to treatment with [^{131}I]-MIBG than larger ones, where 250 µm spheroids absorbed only 20% of the administered [^{131}I]-MIBG, compared to 30% absorption in 400 µm spheroids, indicating substantially more of the radiation is lost in smaller spheroids (Gaze et al., 1992).

1.8.3 MTS with gold nanoparticles

To date, the majority of studies utilising 3D MTS models with AuNPs have investigated the penetration of AuNPs within spheroids, typically with respect to AuNP size. Generally investigations have demonstrated that smaller AuNPs can penetrate further through MTS, for example, the study by Huang *et al,* (2012) found 2 nm and 6 nm AuNPs distributed completely through spheroids (Huang et al., 2012). In comparison, AuNPs > 100 nm were seen to localise around the peripheral edge of MTS with limited uptake throughout the spheroids (Huo et al., 2013). Liu *et al,* (2014) also reported limited uptake and distribution of 100nm transferrin conjugated AuNPs following 48 hour incubation (T. Liu et al., 2014).

The study by Lee *et al,* (2009) is one of the only studies which has investigated the toxicity of AuNPs within 3D MTS models, compared to 2D cells. In this study, the viability and membrane integrity of human hepatocarcinoma (hepG2) liver cells grown as 3D MTS was assessed following 24 hour exposure to both citrate and CTAB stabilised 5.5 nm AuNPs. Results showed CTAB coated AuNPs induced significantly less toxicity in 3D spheroids compared to 2D monolayers (Lee et al., 2009).

The differences discussed in the response of 3D MTS to radiation both as XBR and radiopharmaceuticals, and the cytotoxicity of AuNPs as single agents compared to 2D monolayer cultured cells, make it vital to gain a more accurate idea of the radiosensitisation potential of AuNPs in 3D MTS, in combination with both XBR and radiopharmaceuticals such as [^{131}I]-MIBG. The examination of AuNPs in combination with XBR and [^{131}I]-MIBG within 3D MTS models is a necessary step to examine the dose enhancement potential prior to planning any *in* vivo studies. Due to the hypoxic conditions within 3D MTS, which are more representative of the different oxygen concentrations present in tumour cells, it is likely that the radiosensitisation observed in 2D monolayer cells with AuNPs in combination with XBR (section 1.6.2) may be overestimated, and a reduction in the DEF at the 50% toxicity level may be observed in 3D models. The radiosensitisation which is reported in studies such as that by Ngwa *et al,* (2013) however, for AuNPs in combination with radiopharmaceuticals, is likely to be enhanced within 3D MTS models as a result of their aggregated structure, which allows more damaging effects from the cross-fire of radiation. Based on this evidence

it was therefore hypothesised that assessment of the effect of AuNPs and their radiosensitising potential using 3D MTS models will provide a better understanding of the potential use of AuNPs in combination with different radiation qualities.

1.9 Aims of the study

1.9.1 Project Rationale

The overall aims of this study were to investigate and compare the potential of both solid AuNPs and HGNs as radiosensitisers combined with the radioisotope, ^{131}I when administered in the form of [^{131}I]-MIBG and comparison of this radiosensitisation with that occurring from combination with other radiation qualities in cancer cell lines.

The specific aims of this study were;

I. To characterise the effect of solid and hollow AuNPs within different cancer cell lines and evaluate differences in uptake, cellular localisation, and cyctoxicity of AuNPs as single agents.

II. To assess the radiosensitisation of AuNPs and HGNs in combination with kVp X-ray photons and ^{131}I in the form of [^{131}I]-MIBG using the linear quadratic model and determine alterations to the dynamics and magnitude of DNA damage and repair, and cell cycle progression.

III. Evaluation of the radiosensitisation observed for solid and hollow AuNPs in combination with kVp X-ray photons and ^{131}I in the form of [^{131}I]-MIBG within 3D MTS models.

Chapter 2

Radiosensitisation achieved with commercially available gold nanoparticles

Chapter 2: Radiosensitisation achieved with commercially available gold nanoparticles

2.1 Introduction

As detailed in section 1.6, AuNPs have received wide spread interest in the past decade in biomedical research for use in imaging applications, as drug delivery vehicles and as radiosensitisers, as a result of their unique optical and physical properties. Some previous studies, (Table 1-1) have demonstrated the capacity of AuNPs to radiosensitise a variety of cancer cell lines, however this is not a universal phenomenon with not all cell lines or AuNPs demonstrating radiosensitisation. Additionally in studies demonstrating radiosensitisation the degree of radiation dose enhancement observed at the 50% toxicity level varies greatly between studies. Given the different parameters between the studies, in the cell lines investigated, as well as the AuNP diameter, concentration and surface functionalisation, and the energy of the radiation used across the various studies it is difficult to directly compare the results of the studies and derive any meaningful conclusions.

In this preliminary investigation we aimed to determine if commercial AuNPs available from BBI International radiosensitised the nor-adrenaline transporter transfected glioma cell line UVW/NAT to XBR radiation from a 225 kVp X-ray beam. Initially the cytotoxicity of AuNPs as single agents was evaluated as a function of both concentration and diameter with a view to determine the diameter and concentration of AuNPs which displayed the lowest inherent toxicity and would be optimum for use in combination with X-ray photons to assess radiosensitisation.

2.2 Aims

The initial aim of this chapter was to assess the inherent toxicity of commercially sourced AuNPs in UVW/NAT cells as a function of AuNP diameter and concentration. Secondly, the radiosensitisation potential of commercially sourced AuNPs in combination with XBR was assessed. Finally, preliminary studies utilising reflectance

confocal microscopy were performed in an attempt to assess the localisation of 40 nm AuNPs within the cell.

2.3 Materials and Methods

2.3.1 Cells and culture conditions

The human glioblastoma cell line UVW/NAT used in this study was obtained from the Institute of Cancer Sciences, Wolfson Wohl Building, Glasgow. This cell line was derived from the human glioblastoma line, UVW by plasmid-mediated transfection of bovine NAT (bNAT) cDNA (Invitrogen, Paisley UK), (Boyd et al., 1999), to render the cells able to uptake [^{131}I]-MIBG which was investigated in subsequent studies.

Cells were maintained in MEM cell growth medium, supplemented with 10% (v/v) FCS (LabTech Int. Ltd, East Sussex, UK) and 5% (v/v) of each of penicillin streptomycin (10000 µg/mL), fungazone (250 µg/mL) and L-glutamine (200 mM) (Life Technologies, Paisley UK), at 37ºC in a 5% CO_2 atmosphere. To maintain stable transfection of the NAT cDNA, cell growth medium also contained the plasmid selection agent Geneticin, at 10 µg/mL which is toxic to cells which do not express the NAT gene-containing plasmid. Geneticin was prepared by addition of 10mL sterile water to 1 g geneticin (Life Technologies, Paisley UK), and filtration through 10µm syringe driven filter. The 10% resulting solution was stored in the dark to avoid degradation by light and stored at 4^0C. To maintain healthy cell cultures, cells were passaged when they reached approximately 70-80% confluence. Cells were passaged by removal of the existing cell growth medium, washing with PBS and detachment using 0.05% Trypsin EDTA (Life Technologies, Paisley, UK). Once fully detached, culture medium was added to neutralise the trypsin, and the cell suspension seeded into 75 cm^3 culture flasks containing fresh growth medium.

2.3.2 Commercial gold nanoparticles

The commercial AuNPs used in this study were purchased from BBI International (Cardiff, UK) and were 5, 10, 20 and 40 nm in diameter. The AuNPs were citrate stabilised and supplied in a stock solution in dH_2O at concentrations ranging between 0.15-83 nM for AuNPs with diameters of 5 nm, 10 nm, 20 nm and 40 nm respectively with AuNPs diluted to the required concentration using culture medium.

2.3.3 Treatment of cells with AuNPs and XBR

For treatment, UVW/NAT cells were seeded into 25 cm^2 culture flasks and incubated at 37^oC in a 5% CO_2 atmosphere for 48 hours to ensure all treatments were carried out with cells in the exponential growth phase.

To assess the cytotoxic effect in cells as a result of AuNP diameter, AuNPs at each diameter from 5-40nm were measured at a concentration of 0.05 nM. The incubation time for UVW/NAT cells with AuNPs was selected as 24 hours based on previous studies (Geng et al., 2011; Jain et al., 2011). To determine the cytotoxic effect of increasing AuNP concentration 5 nm AuNPs were examined across the concentration range from 0-20 nM.

For XBR treatment, following incubation cell growth medium was removed and replaced with fresh growth medium (5 mL) prior to irradiation. All XBR irradiation of cells was performed using a cell irradiation cabinet (XRAD 225) with a 225 kVp X-ray beam and a dose rate of 2.2 Gy/min and 13.00 mA current. For all experiments examining the effect of XBR as a single agent cells were treated with XBR within a dose range from 0-6 Gy.

For all combination experiments cells were incubated with AuNPs in the concentration range 0-20 nM for 24 hours and then exposed to XBR across the dose range 0-2 Gy.

2.3.4 Clonogenic survival assay

In this study, clonogenic survival assays (Rae et al., 2013) were used to assess the effect of AuNPs alone with respect to diameter and concentration, and in combination with XBR (Kimling et al., 2006; Söderstjerna et al., 2014). While clonogenic cells will undergo unlimited proliferation, damaged cells will be capable of a finite number of cell divisions and be unable to form colonies.

Clonogenic assays were performed 24 hours after treatment with AuNPs and XBR alone or in combination. After treatment, cell growth medium was removed and cells washed in PBS and detached by addition of 0.05% trypsin EDTA. Once detached, fresh growth medium was added, and cells were disaggregated using a 21 g needle and counted using a haemocytometer. 250 cells from each treatment group were seeded into 60 mm dishes (Fischer Scientific, Loughborough, UK) in triplicate for each experimental treatment (McCluskey et al., 2013).

Dishes were then incubated at 37^{o}C in a 5% CO_2 atmosphere for 7-10 days to allow colonies of sufficient size to form in the untreated control samples (>50 cells). Colonies were visualised for quantification using Giemsa's stain. Briefly, colonies were washed with PBS, fixed in 100% methanol for 10 mins and stained using 10% Giemsa's stain solution (BDH Laboratory Supplies). The number of colonies was then counted by eye and the fraction of cells surviving (SF) a given treatment was calculated by normalising the number of colonies to that of the untreated control sample. In each experiment analysis was carried out in triplicate for each experimental group and results reported as the mean cell survival fraction (mean ± sd) of 3 independent experiments with respect to control cells where SF = number of colonies formed in treated cells/number of colonies formed in untreated control cells.

2.3.5 Confocal reflectance microscopy

To confirm the intra-cellular presence of AuNPs, reflectance microscopy studies using a Leica SP5 scanning system coupled to a Leica DM6000 upright microscope were carried out. Cells were seeded onto 13 mm coverslips (Fischer Scientific,

Leicestershire, UK) at a density of $1x10^5$/ 3mL and incubated for 48 hours in MEM growth medium as described in section 2.3.1. Cell growth medium was then removed and replaced with cell growth medium containing AuNPs and cells incubated at 37ºC in a 5% CO_2 atmosphere for a further 24 hours. Cells were then washed with PBS, fixed in formalin (10%, Sigma Aldrich, Dorset), stained with 0.05% crystal violet and mounted onto slides using hydromount (Fischer Scientific, Leicestershire). Images were taken in confocal reflection mode with a 488 nm laser, focused through a 20x/0.7 N.A. objective lens at a rate of 1Hz and processed using ImageJ v1.48i software (National Institutes of Health, USA).

2.3.6 Statistical Analysis

2.3.6.1 Analysis of variance (ANOVA)

All experiments were carried out 3 times, with results reported as the mean clonogenic survival fraction normalised to untreated control cells for treatment with AuNPs and XBR alone or normalised to AuNP treatment alone for combination treatments (mean ± sd). To determine if the effects of AuNP diameter or concentration on the clonogenic survival were statistically significant compared to untreated control cells one-way ANOVA analysis with Bonferroni post-tests were used. To determine if the effect of AuNPs in combination with XBR on the clonogenic survival was statistically significant compared to the effects of XBR, two-way ANOVA analysis with Bonferroni post-tests was used. In each case P-values lower than 0.05 were considered statistically different. All statistical tests were carried out using GraphPad Prism software, version 6.0, 2014 (CA).

2.3.6.2 Linear quadratic analysis

To assess mathematically whether the presence of AuNPs sensitised UVW/NAT cells to XBR, the experimental clonogenic survival data for cells exposed to XBR alone and in combination with AuNPs was fitted to the linear quadratic model which describes the relationship between radiation dose and cell survival. Other models commonly employed to assess the interaction of two agents in combination include the

isobologram method and combination index analysis, however both of these methods are used to assess the interaction of two agents which are both cytotoxic as single agents. In this study incubation of UVW/NAT cells with AuNPs alone demonstrated no significant toxicity, and across the entire concentration range investigated for AuNPs alone 50% cell kill was not reached and therefore neither of these methods could be employed in this study.

The linear quadratic model contains two key components of cell kill. The linear component, defined by the α coefficient, (equation 1) describes the initial slope of the survival curve in the low dose area, and the cell death which results from the α component increases linearly with radiation dose. As the administered radiation dose increases, the cell death resulting from the quadratic component, defined by the β coefficient increases in proportion to the square of the dose (equation 1).

The close relationship between radiation cell kill and the linear quadratic equation is not fully understood. It is suggested however that the linear component, defined by the α coefficient represents cell death caused by single particle ionisation events, and that the quadratic component, defined by the β coefficient describes damage in cells as a consequence of accumulation of sub-lethal lesions occurring from two independent ionisation events at higher radiation doses. However, the contribution of single and multiple ionisation events to the relationship is still to be fully understood (Barendsen, 1994; Brenner, 2008; P. Franken et al., 2012).

The linear quadratic model is defined by equation 1;

$SF = \exp(-\alpha D - \beta D^2)$ Equation 1

where; SF denotes the fraction of colonies which survive a given dose D of radiation.

GraphPadPrism software, version 6.01, 2014 (CA) was used to fit the experimental clonogenic survival fractions to the linear quadratic model (equation 1), and to obtain the values for the α and β coefficients (Hall and Giaccia, 2006).

The radiation dose required to induce 50% clonogenic cell kill (IC_{50}) was calculated using equation 2 for cells exposed to XBR alone from 0-2 Gy and in combination with AuNPs at 5 nM, 10 nM and 20 nM respectively.

$$IC_{50} = [-\alpha + \sqrt{(\alpha^2 - 48\ln 0.5)}] / 2\beta \qquad \text{Equation 2}$$

Following calculation of the IC_{50} for XBR alone and with each AuNP concentration, the dose enhancement factor at 50% clonogenic cell kill (DEF_{50}) was calculated using equation 3. The DEF is defined as the ratio of effect observed following exposure of cells to radiation in combination with AuNPs to that of radiation alone at a given survival fraction (Roeske et al., 2007). Therefore, if the effect of AuNPs in combination with XBR results in the same amount of clonogenic cell kill as XBR alone the DEF equals 1. A DEF > 1 indicates that AuNPs act as a radiosensitisers and increase the effect compared to radiation alone, whilst a DEF < 1 suggests the AuNPs are acting as a radioprotector.

$$DEF_{50} = IC_{50} \text{ radiation alone} / IC_{50} \text{ radiation + AuNPs} \qquad \text{Equation 3}$$

2.4 Results

2.4.1 The effect of AuNP diameter on the clonogenic survival of UVW/NAT cells

The effect of AuNP diameter on clonogenic survival was assessed at 0.05 nM for 5 nm, 10 nm, 20 nm and 40 nm AuNPs.

Incubation of UVW/NAT cells with AuNPs at 5 nm, 10 nm and 20 nm resulted in no significant reduction in clonogenic survival, compared to untreated control cells (Figure 2-1). Incubation of cells with 40nm AuNPs however, significantly reduced the clonogenic cell survival, compared to untreated control cells to 0.38±0.02 ($p<0.0001$).

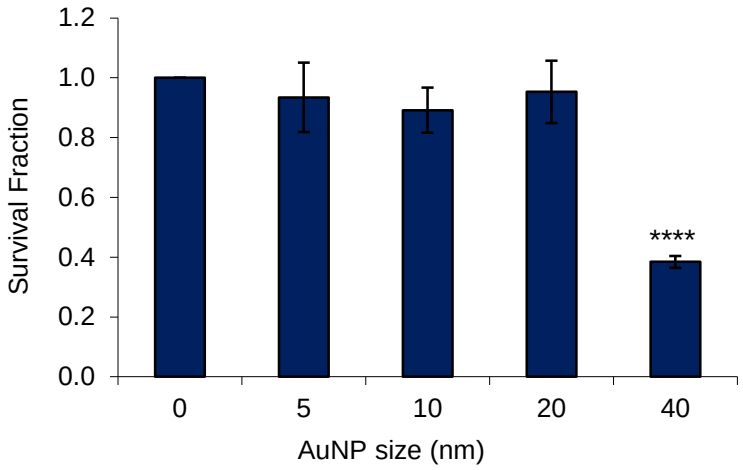

Figure 2-1: Clonogenic survival of UVW/NAT cells treated with commercially sourced AuNPs across the AuNP diameter range 0-40 nm.

UVW/NAT cells were incubated for 24 hours with AuNPs, with diameters of 5 nm, 10 nm, 20 nm and 40 nm at a concentration of 0.05 nM. Results are presented as the mean survival fraction of 3 independent experiments (mean ± sd). Statistical significance was assessed using one-way ANOVA with Bonferroni post-tests at 95% C.I. Four (****) symbols indicate $p<0.0001$.

2.4.2 The effect of increasing AuNP concentration on the clonogenic survival of UVW/NAT cells

The effect of increasing AuNP concentration on the clonogenic cell survival, of UVW/NAT cells was assessed following incubation with 5 nm AuNPs across the concentration range 0-20 nM (Figure 2-2). The greatest reduction in clonogenic survival was observed following incubation of UVW/NAT cells with AuNPs at 20 nM where the cell survival fraction was 0.9±0.05, however this reduction was not significantly different compared to untreated control cells ($p>0.05$).

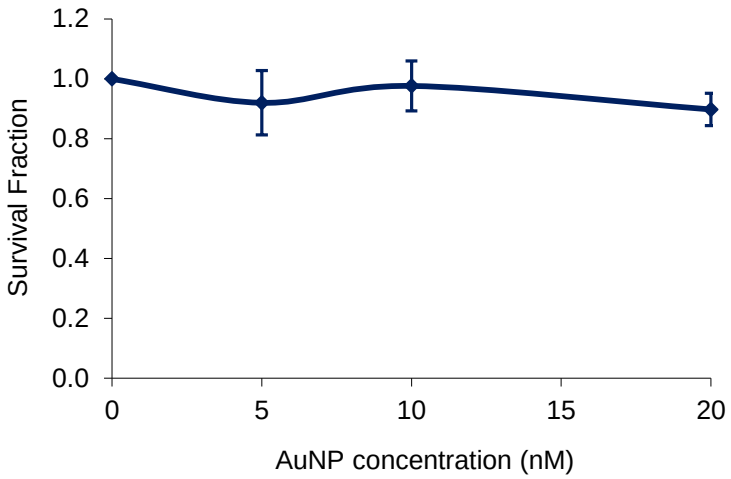

Figure 2-2: Clonogenic survival of UVW/NAT cells treated with commercially sourced AuNPs across the concentration range 0-20 nM.

UVW/NAT cells were incubated for 24 hours with 5 nm AuNPs, in the concentration range 0-20 nM. Results are presented as the mean survival fraction of 3 independent experiments (mean ± sd). Statistical significance was assessed using one-way ANOVA with Bonferroni post-tests at 95% C.I.

2.4.3 The effect of XBR on the clonogenic survival of UVW/NAT cells

Before assessing the effect of AuNPs in combination with XBR, the effect of increasing XBR dose on the clonogenic survival of UVW/NAT cells was measured across the dose range 0-6 Gy to determine the optimum dose range of XBR to be used in subsequent combination studies (Figure 2-3). The experimental clonogenic survival fraction data was fitted to the linear quadratic model and values for the α and β coefficients, and the dose required to reduce clonogenic survival by 50% (IC_{50}) calculated.

Dose dependent reduction in the clonogenic survival of UVW/NAT cells was observed following exposure to XBR. The dose of XBR which resulted in 50% clonogenic cell kill was 2.89 Gy. Based on this data the XBR dose range from 0-2 Gy was employed in subsequent XBR and AuNP combination studies.

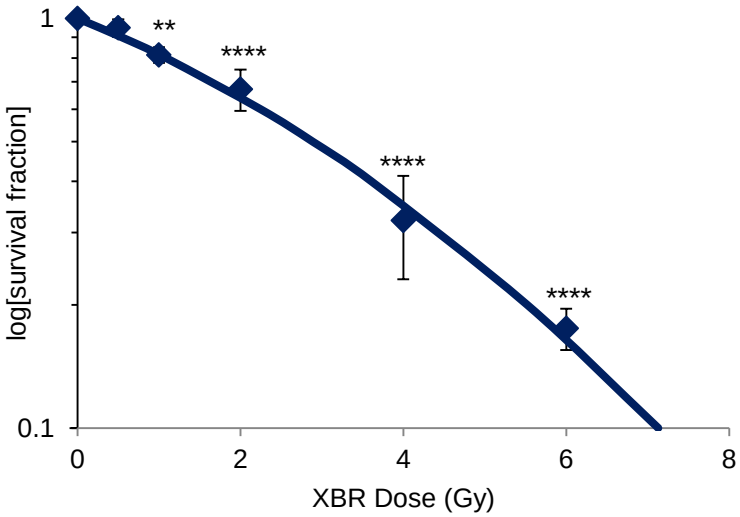

UVW/NAT			
α (Gy^{-1})	**β (Gy^{-1})**	**R^2**	**IC_{50}**
0.1828	0.01964	0.98	2.89Gy

Figure 2-3: Clonogenic survival of UVW/NAT cells exposed to XBR from 0-6 Gy fitted to the linear quadratic model.

UVW/NAT cells were exposed to 0-6 Gy of XBR and clonogenic survival assays performed 24 hours after irradiation. Results are presented as the mean survival fraction of 3 independent experiments (mean ± sd). Statistical significance of the clonogenic survival following XBR exposure at each dose, compared to untreated control cells was assessed using one-way ANOVA with Bonferroni post-tests at 95% C.I. Two (**) and four (****) symbols indicate $p<0.01$ and 0.0001 respectively. Experimental survival fractions were fitted to the linear quadratic model using GraphPad Prism v.6.0 and the α and β coefficient values, the R^2 and IC_{50} values determined.

2.4.4 The effect of AuNPs in combination with XBR on the clonogenic survival of UVW/NAT cells

Based on the results obtained in sections 2.4.1, 2.4.2 and 2.4.3 for the effects of AuNP diameter and concentration, and XBR exposure alone on the clonogenic survival of UVW/NAT cells, the AuNP concentration range 0-20 nM was employed with 5 nM AuNPs in combination with XBR across the dose range 0-2 Gy.

UVW/NAT cells treated with 5 nM AuNPs in combination with XBR demonstrated a statistically significant decrease in clonogenic cell survival at all AuNP and XBR combinations, compared to XBR exposure alone, with the exception of 5 nM AuNPs in combination with 1 Gy XBR (Figure 2-4). In cells exposed to 2 Gy XBR alone the cell survival fraction was 0.67±0.08, compared to 0.49±0.08 ($p<0.001$), 0.28±0.07 ($p<0.0001$) and 0.39±0.05 ($p<0.001$) in cells incubated with AuNPs at concentrations of 5 nM, 10 nM and 20 nM respectively for 24 hours prior to 2 Gy XBR exposure.

The clonogenic survival data from Figure 2-4(A) was fitted to the linear quadratic model (Figure 2-4(C)) and values for α, β, IC_{50} and DEF_{50} calculated (Figure 2-4(D)). In UVW/NAT cells, treatment with AuNPs across the concentration range 0-20 nM for 24 hours before irradiation with XBR resulted in a dose dependant decrease in the radiation dose required to kill 50% of the cell population (IC_{50}). The IC_{50} values decreased from 2.89 Gy for XBR alone to 2.23 Gy, 0.88 Gy and 0.80 Gy respectively for XBR in the presence of AuNPs at 5 nM, 10 nM and 20 nM. The calculated α values for the combination of AuNPs at 5 nM, 10 nM and 20 nM with XBR were 0.16 Gy^{-1}±0.05 for XBR exposure alone and 0.33 Gy^{-1}±0.08, 0.93 Gy^{-1}±0.08 and 1.17 Gy^{-1}±0.10 with AuNPs at 5 nM, 10 nM and 20 nM respectively. The concentration dependant increase in α value suggests that the presence of AuNPs results in an increase in the toxicity at low radiation doses, as discussed in section 2.3.6.2 (Barendsen, 1994). The DEFs calculated at the 50% toxicity level (DEF_{50}) were 1.40, 3.55 and 3.89 for XBR in combination with AuNPs at 5 nM, 10 nM and 20 nM, indicating that in UVW/NAT cells the presence of AuNPs with XBR induced a concentration dependant increase in the effects of radiation.

(A)

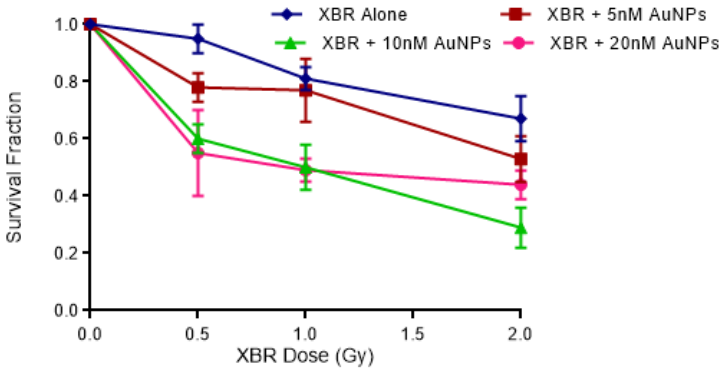

(B)

AuNP Concentration (nM)	0.5Gy	1.0Gy	2.0Gy
5	**	ns	***
10	****	****	****
20	****	****	***

Figure 2-4 continued overleaf

(C)

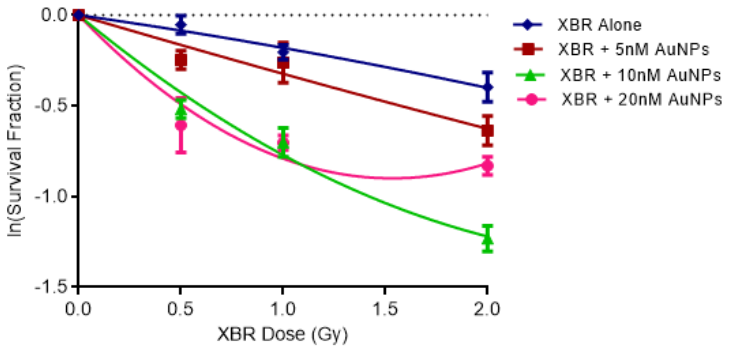

(D)

	0nM	5nM	10nM	20nM
α (Gy^{-1})	0.16±0.048	0.33±0.08	0.93±0.08	1.17±0.10
β (Gy^{-1})	0.02±0.02	-0.01±0.04	-0.16±0.04	-0.38±0.05
R^2	0.92	0.90	0.97	0.91
IC_{50} (Gy)	2.89	2.23	0.88	0.80
DEF_{50}	1.00	1.40	3.55	3.89

Figure 2-4: Clonogenic survival of UVW/NAT cells exposed to 5 nm AuNPs in combination with XBR.

UVW/NAT cells were incubated with 5 nM AuNPs from 0-20 nM for 24 hours. Following this cells were exposed to 0-2 Gy XBR and clonogenic survival assays performed 24 hours after irradiation. Clonogenic survival results are presented as the average survival fraction of 3 independent experiments (mean ± sd), compared to untreated control cells (A). Statistical significance of cell survival fraction for AuNPs in combination with XBR, compared to XBR alone was assessed using two-way ANOVA with Bonferroni post-tests at 95% C.I. Two (**), three (***) and four (****) symbols indicate $p<0.01$, $p<0.001$ and $p<0.0001$ and ns indicates no significance (B) Clonogenic survival data presented in (A) was fitted to the linear quadratic model using GraphPad Prism version 6.0.1 (C) and values calculated for the α and β coefficients and the IC_{50} and DEF_{50} for XBR in combination with 5 nM AuNPs at each AuNP concentration (D).

2.4.5 Localisation of AuNPs within the Cell Environment

Preliminary studies were performed to evaluate the location of commercially sourced AuNPs within UVW/NAT cells using confocal reflectance microscopy (Figure 2-5). As the degree of reflectance from the AuNP surface increases with increasing AuNP diameter, 40 nm AuNPs were selected for evaluation by confocal microscopy. Images of cells incubated with and without 40 nm AuNPs were captured in bright field (A-1, B-1) and reflectance mode (A-2, B-2) to capture the reflectance of the AuNPs and then overlaid to demonstrate the location of the reflectance of AuNPs around the cells (A-3, B-3).

Enhanced reflectance was observed in UVW/NAT cells incubated with 40nm AuNPs, compared to untreated control cells. In cells incubated with AuNPs the observed reflectance (shown in green) was concentrated on and around the cells, with very little reflectance signal observed in background areas containing formalin fixative only, which suggested successful uptake of the AuNPs by UVW/NAT cells. In untreated control cells however, a much lower reflectance signal was observed, and the reflectance observed was evenly distributed across the coverslips, and demonstrated no localisation of reflectance around areas containing cells.

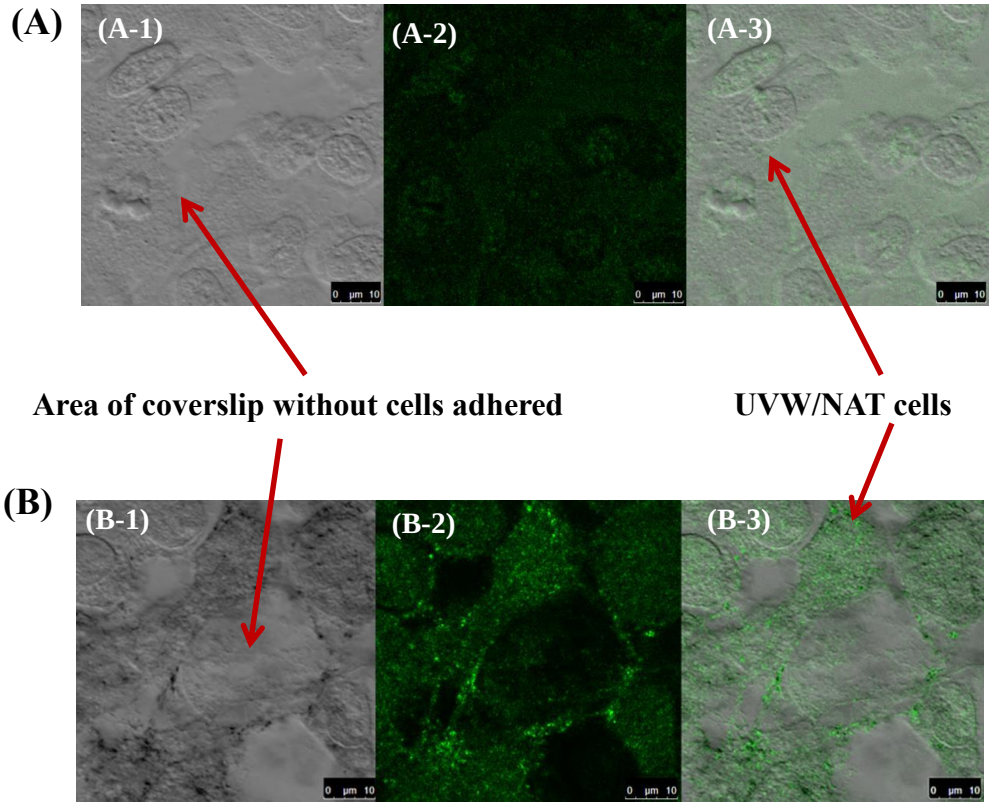

Figure 2-5: Localisation of 40nm commercially sourced AuNPs within UVW/NAT cells assessed by confocal reflectance microscopy.

Reflectance images were captured using a Lecia SP5 confocal microscope in UVW/NAT cells incubated with and without 40 nm AuNPs for 24 hours. Cells were captured in bright field (A-1, B-1) and reflectance mode to visualise reflectance from the presence of AuNPs (A-2, B-2, green). An overlay of these images (A-3, B-3) for both untreated control cells (A), and cells incubated with 40 nm AuNPs (B) is presented.

2.5 Discussion

The aim of this study was to firstly evaluate the effect of commercially sourced AuNPs across the diameter range, from 0-40 nm diameter and concentration range, from 0-20 nM alone on the clonogenic survival of UVW/NAT cells.

In this study a significant reduction in clonogenic survival ($p<0.0001$) was observed in UVW/NAT cells following 24 hour incubation with 40 nm diameter AuNPs at 0.05 nM (Figure 2-1). The results of previous studies performed to evaluate the cytotoxicity of AuNPs with respect to diameter have demonstrated considerable variation, discussed in section 1.6.5.2. For example, in the study carried out by Pan et al, (2007), incubation of HeLa cells with 1.4 nm diameter AuNPs resulted in significant reduction in cell viability, whereas incubation with 15 nm diameter AuNPs with the same surface functionalisation caused no significant toxicity, indicating that AuNPs with smaller diameters induced greater toxicity which was in contrast to the results observed in the present study (Pan et al., 2007).

A further study, by Mironava *et al*, (2014) however, demonstrated a significantly higher rate of apoptosis following incubation with 45 nm diameter AuNPs, compared to 13nm AuNPs, indicating that larger AuNPs could induce greater toxicity, which is consistent with the results of this present study. Additionally, the study by Mironava *et al*, (2014) demonstrated that 45 nm AuNPs penetrated cells via clathrin-mediated endocytosis, whereas 13 nm AuNPs were taken up primarily by phagocytosis, which could contribute to the differences in toxicity observed (Mironava et al., 2014). It can be hypothesised therefore, that the UVW/NAT cells employed in this study may utilise different uptake mechanisms for the internalisation of the commercial AuNPs, depending on the AuNP diameter, and this could lead to the greater toxicity observed following incubation with 40 nm AuNPs compared to AuNPs of 5 nm, 10 nm and 20 nm respectively.

To further investigate the effect of AuNP diameter on cell toxicity, the mechanism of uptake of the AuNPs across the diameter range could be investigated, along with a wider range of AuNP diameters to determine if the mode of AuNP uptake differed with AuNP diameter, and if this correlated with differences in cell toxicity. For the purpose of this present study however, the aim was to utilise AuNPs which

demonstrated no toxicity as single agents and investigate their radiosensitising, therefore the toxicity was not further investigated at this stage.

Following evaluation of the toxicity of AuNPs alone as a function of increased diameter and concentration the radiosensitisation potential of the AuNPs in combination with XBR was investigated.

The combination of AuNPs across the concentration range 0-20 nM with 0-2 Gy XBR resulted in statistically significant decrease in the clonogenic survival of UVW/NAT cells, compared to XBR exposure alone (Figure 2-4), with dose enhancement factors at the 50% cytotoxicity level (DEF_{50}) of 1.40, 3.55 and 3.89 for AuNPs at 5 nM, 10 nM and 20 nM respectively.

The observed radiosensitisation was in good agreement with the results of previous studies, such as those performed by Wang *et al*, (2013) and Zhang *et al*, (2012), outlined in Table 1-1. It is hypothesised that in cells containing AuNPs, the photoelectric effect will dominate the ionisation processes due to the differences in the photon mass absorption coefficient of AuNPs compared to soft tissue. Photoelectric ionisations will lead to an increase in the deposition of radiation within the target area, as discussed in section 1.6.2 (Coulter et al., 2013). Comparatively, in cells which do not contain AuNPs, Compton scattering is the predominant ionisation process following exposure to radiation and results in only sparse ionisation effects throughout the cell (Butterworth et al., 2012).

The clonogenic survival data for AuNPs in combination with XBR was fitted to the linear quadratic model (equation 1) which is a common method employed to assess the effect of a radiation modifier on the radiation survival curves, as discussed in section 2.3.6.2. The linear quadratic model consists of two key components of cell kill, the linear component, defined by the α coefficient, describes the initial slope of the survival curve in the low dose area, and the quadratic component, defined by the β coefficient, where the cell death, increases in proportion to the square of the dose. The close relationship between radiation cell kill and the linear quadratic model however is not fully understood. It has been suggested, that the α coefficient represents cell death as a result of single particle ionisation events and an increase in the observed

α value is indicative of increased toxicity at lower radiation doses. The β coefficient is suggested to represent cell death due to the accumulation of sub-lethal lesions which result from two or more independent ionisation events which occur at higher radiation doses and a decrease in the β coefficient has been hypothesised to indicate an increase in the linearity of the radiation survival curves, indicative of increased toxicity (Barendsen, 1994; Brenner, 2008). The results of this study were consistent with the presented hypotheses, whereby an increase in the radiation induced toxicity in the presence of AuNPs was associated with an increase in the value of the α coefficient.

The manufacture process employed by BBI International in the synthesis of the AuNPs used throughout this study was unknown. It was known however, that industrially manufactured AuNPs commonly contain trace amounts of chemical additives and elemental stabilisers in order to afford bulk manufacture and enhance the particle shelf life, compared to AuNPs synthesised in house in small laboratory batches. It therefore cannot be confirmed whether the presence of unknown compounds within the AuNP suspensions contributed to the toxicity observed across the concentration and diameter range, or to the radiosensitisation observed in combination with XBR. In order to overcome the lack of knowledge and control regarding the AuNP synthesis, a collaboration was initiated with an established nanobiotechnology group, led by Professor Duncan Graham at the University of Strathclyde. This collaboration allowed the synthesis of custom made AuNPs across any size and shape range necessary, and afforded complete control of the surface chemistry. As a result of this, the scope of the project was expanded to allow the investigation of different particle shapes. The next chapter describes the optimisation and characterisation of the AuNPs synthesised in the Graham lab and the subsequent work outlined in this thesis employed the use of in house synthesised particles.

Chapter 3

Synthesis and Characterisation of 20 nm Gold Nanoparticles (AuNPs)

Chapter 3: Synthesis and Characterisation of 20 nm Gold Nanoparticles (AuNPs)

3.1 Introduction

As discussed in section 2.5, a substantial limitation when using commercially sourced AuNPs is the lack of control of the surface chemistry and formulation of the AuNPs. As discussed previously the surface chemistry of the AuNPs can affect both the inherent toxicity and the uptake of AuNPs within cells. To overcome this, a successful collaboration was initiated with the Graham Lab (University of Strathclyde) which allowed in house synthesis of AuNPs. Full knowledge of the AuNP synthesis and resulting surface chemistry allowed any cytotoxicity observed in cells following incubation with AuNPs to be attributed to the AuNPs only, rather than the presence of additives present in the AuNP suspension. Following synthesis of AuNPs, their physical properties and interaction with several cancer cell lines was evaluated.

3.2 Aims

The aim of this chapter was to first characterise in house AuNPs, synthesised via the Turkevich-Frens method in collaboration with the Graham Lab (University of Strathclyde). Following this the study aimed to confirm the diameter of the synthesised AuNPs and their stability within cell growth medium. The intracellular uptake, localisation and cytotoxicity of the synthesised AuNPs within the human glioma cell line UVW/NAT, human neuroblastoma cell line SK-N-BE and human melanoma cell line A375 were then evaluated using inductively coupled plasma-mass spectroscopy (ICP-MS), transmission electron microscopy (TEM) and clonogenic survival assays.

3.3 Materials and Methods

3.3.1 Synthesis of 20 nm AuNPs

All AuNPs were synthesised in the Graham Lab (University of Strathclyde) using the method outlined by Turkevich *et al* (1951, 1953) and later refined by Frens *et al,* (1973) as described by Brown *et al,* (2010) (Brown et al., 2010; Frens, 1973; Turkevich et al., 1953, 1951). Prior to synthesis all glassware was soaked in aqua regia for 4 hours to remove any impurities, and washed with distilled water until the pH of the water was neutral. The aqua regia was prepared by the addition of concentrated nitric acid (Sigma Aldrich, Dorset, UK) to concentrated hydrochloric acid (Sigma Aldrich, Dorset, UK) in a 3:1 ratio. The Turkevich-Frens synthesis method allowed the synthesis of mono-dispersed citrate stabilised AuNPs where the diameter of the AuNPs could be tuned by altering the sodium citrate concentration (Craig et al., 2012; Turkevich et al., 1953). In a typical synthesis, sodium tetrachloroaurate, $HAuCl_4$ (50 mg, 0.14 mM) (Sigma Aldrich, Dorset, UK) was dissolved in dH_2O (500 mL) and heated with continuous stirring. To synthesise 20 nm diameter AuNPs 0.075 g in 7.5 mL dH_2O of sodium citrate solution (Sigma Aldrich, Dorset, UK) was added, and the solution boiled for 15 mins. The solution was cooled to room temperature with stirring throughout. To concentrate AuNP samples, 20 mL aliquots were centrifuged at 6000 rpm for 3 hours, the supernatant was removed using a plastic syringe, and the AuNPs re-suspended in 5 mL dH_2O.

3.3.2 Size and zeta potential measurement of synthesised 20 nM AuNPs

Following synthesis the diameter and zeta potential of AuNPs were measured by dynamic light scattering (DLS) using a Malvern Zetasizer Nano Zs instrument, to ensure the synthesised AuNPs were the desired diameter, mono-dispersed and were stable in suspension. The zeta potential of AuNPs is the electrical charge between the dispersion medium and the surface chemistry of the particles. It gives an indication of the stability of AuNPs where the greater the magnitude of the zeta potential the greater the electrostatic repulsion between adjacent, similarly charged particles. A high zeta potential indicates that the AuNPs have a high repulsion and will therefore resist

aggregation. Zeta potentials ranging from 0 to ±30 are indicative of low stability, ±30 to ±40 moderate stability and above ±40 is indicative of good stability (O'Brien et al., 1990).

For measurement of the AuNP diameter a standard solution (nanosphere tm) of 20 nM particles (Thermo Scientific, Loughborough, UK) was used to calibrate the Malvern Zetasizer Nano Zs instrument. 1mL of the sample solution was loaded into a polystyrene cell and the particle diameter was measured simultaneously 3 times. For zeta potential measurements a zeta potential transfer standard at -42 mV +/- 4.2 mV was used to calibrate the instrument. Again 1mL of AuNP sample was loaded into a zeta dip cell and zeta potential measured simultaneously 3 times. Results are presented as the mean particle size or zeta potential (mean ± sd) of 3 independent experiments.

3.3.3 Stability of synthesised 20 nM AuNPs in cell culture medium

To ensure that the synthesised AuNPs would remain dispersed in solution and not aggregate when added to cell growth medium the stability of the AuNPs was measured following incubation in growth medium by UV-Visible spectrophotometry over a 24 hour period. Synthesised AuNPs were diluted to a concentration of 2 nM in MEM cell growth medium. MEM growth medium without phenol red (which absorbs UV-light and would interfere with stability measurements) was used and was supplemented with 5% (v/v) of each of penicillin-streptamyocin, L-glutamine and fungizone. AuNPs diluted to the same concentration using dH_2O and incubated at 37^oC in a 5% CO_2 were used as a positive control for stability. MEM growth medium was further supplemented with FCS at concentrations from 0-50% in order to establish the effect of increasing FCS concentration on the stability of AuNPs (Hauck et al., 2008; Wiogo et al., 2010). All UV-visible spectrophotometry measurements were carried out using a Varian Cary® 300 Bio UV-visible spectrophotometer across the wavelength range 200-800 nm. The absorbance of dH_2O was measured prior to measurement of the AuNP dH_2O samples and the absorbance of the growth medium without AuNPs was measured prior to each sample to account for any background absorbance from the growth medium alone. AuNP samples were diluted 1 in 3 using dH_2O to obtain

absorbance values between 0 and 1 AU (arbitrary units) and loaded into a 1 cm silica cuvette. Absorbance spectra for AuNPs in growth medium were compared to that for AuNPs in dH_2O to establish if incubation in growth medium caused any deviations from the typical absorption profile of AuNPs which would indicate changes to the size or shape of the AuNPs resulting from aggregation. Results are presented as the absorbance versus wavelength for AuNPs of different experimental treatments.

3.3.4 Cells and culture conditions

The human glioblastoma cell line UVW/NAT (Boyd et al., 1999) was cultured and maintained in MEM culture medium as described in section 2.3.1. Two additional human cell lines were introduced for this study, firstly the human melanoma cell line, A375 (Giard et al., 1973) which was cultured in DMEM medium supplemented with 10% (v/v) FCS and 5% (v/v) of each of penicillin streptomycin (10000 µg/mL), fungizone (250 µg/mL) and L-glutamine (200 mM). Secondly the human neuroblastoma cell line, SK-N-BE (Biedler et al., 1978) was cultured in DMEM medium supplemented with 15% (v/v) FCS and 5% (v/v) of each of penicillin streptomycin, fungizone and L-glutamine, non-essential amino acids (NEAA) and sodium pyruvate (Life Technologies, Paisley, UK). All cell lines were maintained at 37^{o}C in a 5% CO_2 atmosphere. To maintain healthy cell cultures, all cell lines were passaged when they reached approximately 70-80% confluence as detailed in section 2.3.1. Detachment of UVW/NAT and A375 cells was performed using 0.05% Trypsin EDTA and for SK-N-BE cells Accutase® (Sigma Aldrich, Dorset, UK) was used.

3.3.5 Intracellular localisation of synthesised 20 nm AuNPs

To confirm intracellular uptake of the 20 nm AuNPs and identify their intracellular localisation, transmission electron microscopy (TEM) was performed (Brown et al., 2010; Jain et al., 2011) in collaboration with the University of Glasgow. Uptake of AuNPs into the human glioblastoma cell line UVW/NAT, human melanoma cell line A375 and human neuroblastoma cell line SK-N-BE was examined. A total of $1.5x10^5$

cells were seeded into 25 cm^2 culture flasks and incubated at 37ºC in a 5% CO_2 atmosphere for 48 hours to ensure all treatments were carried out with cells in the exponential growth phase. Following incubation, growth medium was removed and replaced with medium containing AuNPs (2 nM), and cells incubated at 37ºC in a 5% CO_2 atmosphere for a further 24 hours. Cells were then washed with PBS and detached using either 0.05% trypsin EDTA for UVW/NAT and A375 cells or Accutase® (Sigma Aldrich, Dorset, UK) for SK-N-BE cells. Cells were pelleted by centrifugation at 1200 rpm for 10 mins and fixed using 4% gluteraldehyde in 0.1 M sodium cocodylate for 15 mins at room temperature. Following fixation, cells were re-pelleted and rinsed with 0.1 M sodium cocodylate before being placed in 1% osmium tetraoxide for 1 hour at room temperature. Cells were washed thrice in dH_2O for 5 mins and then placed in aqueous uranyl acetate for 1 hour in the dark. After rinsing with dH_2O, cells were put through a series of dehydrating ethanol solutions from 30%-100% and dried in absolute ethanol. Samples were washed thrice in propylene oxide for 5 mins before being embedded into 1:1 propylene oxide resin and left overnight. To set the resin the samples were heated in a 60ºC oven for 48 hours before sections were sliced and stained using 3% methanolic uranyl acetate and Reynolds lead citrate stains. Sections were imaged using an Olympus LEO 912AB TEM at 120 kV. Images of cells incubated with AuNPs were compared to control images in order to assess AuNP uptake and localisation.

3.3.6 Measurement of intracellular uptake of synthesised 20 nm AuNPs

Indicatively coupled plasma-mass spectroscopy (ICP-MS) was used to assess the uptake of 20 nm AuNPs by measurement of the Au concentration within UVW/NAT, A375 and SK-N-BE cells following incubation (De Jong et al., 2008). $1.5x10^5$ cells were seeded into 25 cm^2 culture flasks and incubated at 37ºC in 5% CO_2 for 48 hours. Following incubation, cell growth medium was removed and replaced with medium containing AuNPs (0.5-2.0 nM) and cells incubated at 37ºC in 5% CO_2 for a either 2, 6 or 24 hours to assess AuNP uptake over time. At each timepoint cells were washed with PBS, detached using either 0.05% trypsin EDTA (UVW/NAT and A375 cells) or Accutase® (SK-N-BE cells) and counted using a haemocytometer. Cells were pelleted

by centrifugation at 1200 rpm for 5 mins and digested in 500 µL aqua regia at 60ºC overnight before dilution in dH_2O to a final aqua regia concentration of 2%. ICP-MS measurements were performed using an Agilent 7700X instrument, with a micromist nebuliser and an octapole collision cell, which was calibrated using solutions prepared from a Qmx ICP gold standard (Qmx Laboratories, Essex, UK) prepared in 2% aqua regia to concentrations ranging from 0-1000 µg/L. The Au concentration (µg/mL) within samples was measured using the ^{197}Au isotope with the ^{175}Lu isotope used as an internal standard for all measurements. The instrument operating conditions used were 1,550W RF forward power, 0.85 L min-1 plasma carrier gas flow, 0.2 L min-1 makeup gas flow, 4.6mL min-1 helium gas flow in the collision cell and 0.1 revolutions per second (rps) for the nebulizer pump. Sample depth was 8 mm, sample period was 0.31 s and integration time was 0.1 s. To determine the number of AuNPs/cell a concentration curve (0-2 nM) was generated from the in house synthesised AuNP solution and the equations below used to calculate the average number of AuNPs present per cell.

The Au content (ng/L) was converted into a molar concentration using the equation of the line for the AuNP calibration curve (equation 4)

$y = 177.64x + 14.347$ Equation 4

Following this, the molar concentration (moles/litre) was converted into mole/mL and then the number of particles/mL calculated (equation 5)

Number of particles/mL = molar concentration * $6.022x10^{\wedge 23}$ Equation 5

where; $6.022x10^{\wedge 23}$ is Avagadro's number

The number of cells per mL was known and therefore the number of particles/cell was calculated (equation 6)

Number of particles/cell = Number of particles/mL / Number of cells/mL Equation 6

3.3.7 Clonogenic survival assay

Clonogenic survival assays were performed to assess the clonogenic survival of each cell line following 24 hour incubation with AuNPs across the concentration range 0-2 nM. Preliminary studies performed to assess the ability of each cell line to form suitable colonies showed that both UVW/NAT and A375 cells formed sufficient colonies when plated into petri-dishes, however SK-N-BE cells had a very poor plating efficiency and it was therefore not possible to assess their clonogenic survival using this assay. To circumvent this, clonogenic survival in SK-N-BE cells was assessed using the soft agar clonogenic assay protocol as outlined below.

All clonogenic survival assays in UVW/NAT and A375 cells were performed as described in section 2.3.4 with results presented as the mean cell survival fraction (mean ± sd) of 3 independent experiments.

3.3.7.1 Soft agar clonogenic survival assay

To assess the clonogenic survival of SK-N-BE cells following 24 hour incubation with AuNPs, soft agar clonogenic assays were performed (Kubetzko et al., 2004). The assay was carried out in 96-well agar coated plates, which were prepared by adding 50 µL of a 1% agar-medium solution into each well and allowing this to set at 4^{o}C for at least 1 hour. The agar-medium solution was prepared by dissolving 0.1 g agar (Sigma Aldrich, Dorset, UK) in 10 mL dH_2O and boiling until molten and completely dissolved. To this 10 mL of 2xDMEM cell growth medium (Life Technologies, Paisley, UK) containing 20% (v/v) FCS and 14% sodium bicarbonate (Sigma Aldrich, Dorset, UK) was added.

Following AuNP incubation, cells were washed with PBS, detached using Accutase® and disaggregated using a 21 g needle before being counted using a haemocytometer. To achieve a cell density of 2500 cells/5µL cells were centrifuged at 1200 rpm for 5 mins and resuspended in the appropriate volume of growth medium to achieve this density. Cells suspensions were disaggregated before being added to a 0.7% agarose-medium solution and seeding into 96 well plates. For each experimental treatment 8 replicates were seeded with 5 µL of cells added to 70 µL agarose for each sample

replicate. The 0.7% agarose-medium solution was prepared by dissolving 0.03 g agarose (Sigma Aldrich, Dorset, UK) in 4 mL dH_2O and boiling until completely dissolved and molten. To this, 4 mL of 2xDMEM medium containing 20% (v/v) FCS and 14% (v/v) sodium bicarbonate was added. Once seeded the cell agarose solution was allowed to set at 37^oC for 20 mins before 100 µL of DMEM cell growth medium containing 15% (v/v) FCS and 5% (v/v) of each of penicillin streptomycin, fungazone and L-Glutamine, NEAA and sodium pyruvate was added to each well. Plates were incubated at 37^oC in a 5% CO_2 atmosphere for 7 days and then stained with 10% AlamarBlue® (Life Technologies, Paisley, UK) in DMEM culture medium. Fluorescence intensity was quantified using a Spectra Max Gemini XS plate reader from 560-590 nm at 4 hours and 24 hours after AlamarBlue® addition and processed using SoftMax Pro software, version 4.3. Average fluorescence intensity measurements for each experimental treatment were converted to survival fraction by normalising the fluorescence intensity of treated cells with that of untreated control cells and results plotted as the mean cell survival fraction (mean ± sd) of 3 independent experiments.

3.3.8 Statistical Analysis

3.3.8.1 Analysis of variance (ANOVA)

All experiments were carried out 3 times with results reported as the (mean ± sd). Significant differences between the uptake of AuNPs in the 3 cell lines investigated, and the cell survival following AuNP incubation in each cell line were evaluated using two-way ANOVA analysis with Bonferroni post-testing. All tests were performed using GraphPad Prism version 6.0.1 (CA.) at the 95% C.I where p values below 0.05 were considered statistically different.

3.4 Results

3.4.1 Size and zeta potential measurement of synthesised AuNPs

In this study AuNPs with an average diameter of 20 nm were synthesised via the Turkevich-Frens method. Following synthesis the average diameter and zeta potential of the AuNPs were measured to confirm successful synthesis of mono-dispersed 20 nm diameter AuNPs and ensure their stability within suspension. The average diameter of in house synthesised AuNPs used throughout the study was 21.76±0.64 nm and the zeta potential -44.63±2.69 mV, as shown in Table 3-1.

Table 3-1: Average diameter and zeta potential of in house synthesised AuNPs measured using dynamic light scattering (DLS).

Average AuNP diameter (nm)	Average zeta potential (mV)
21.76 ± 0.46	-44.63 ± 2.69

3.4.2 Stability of in house synthesised 20 nm AuNPs within cell growth medium

The UV-visible absorption spectra of AuNPs was measured to determine the colloidal stability of the synthesised AuNPs incubated within cell growth medium throughout the 24 hour cell incubation period used in subsequent cell based experiments (section 3.4.3). The UV-visible absorption spectrum of cell growth medium alone supplemented with increased FCS concentration displayed no absorption peak at ~520 nm which was expected due to the absence of AuNPs within the sample (Figure 3-1(A)). AuNPs incubated in distilled water were used as a positive control and displayed an intense absorption peak at approximately 520 nm, which is the wavelength of maximum absorption (λ_{max}) for 20 nm AuNPs as a result of the plasmon excitation (Figure 3-1(B)). For AuNPs incubated in cell growth medium without FCS the UV-visible absorption spectrum showed no intense absorption peak at ~520 nm at any of the timepoints investigated which indicated that in the absence of FCS, the AuNPs aggregated almost immediately and were no longer detectable (Figure 3-1(C)). In the presence of 10-50% FCS in the growth medium, the AuNPs remained stable across

the time period measured with each UV-visible absorption spectrum measured demonstrating an absorption peak at ~520 nM (Figure 3-1(D-F)). The λ_{max} values remained consistent at each FCS concentration from 10-50%, indicating that despite increasing FCS; the AuNPs remained stable within the cell growth medium throughout the 24 hours incubation period (Figure 3-1(G)).

These data suggested that the synthesised AuNPs were stable within the cell growth medium and were therefore used in all subsequent cell based experiments, utilising an incubation time of 24 hours and where the cell growth medium used was supplemented with 10% FCS under normal conditions.

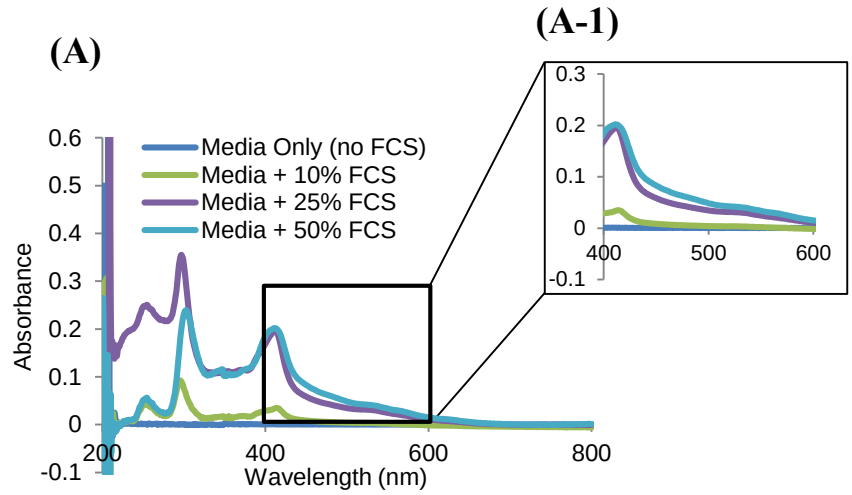
(A)
(A-1)
Media Only (no FCS)
Media + 10% FCS
Media + 25% FCS
Media + 50% FCS
Absorbance
Wavelength (nm)
0.6
0.5
0.4
0.3
0.2
0.1
0
-0.1
200
400
600
800
0.3
0.2
0.1
0
-0.1
400
500
600

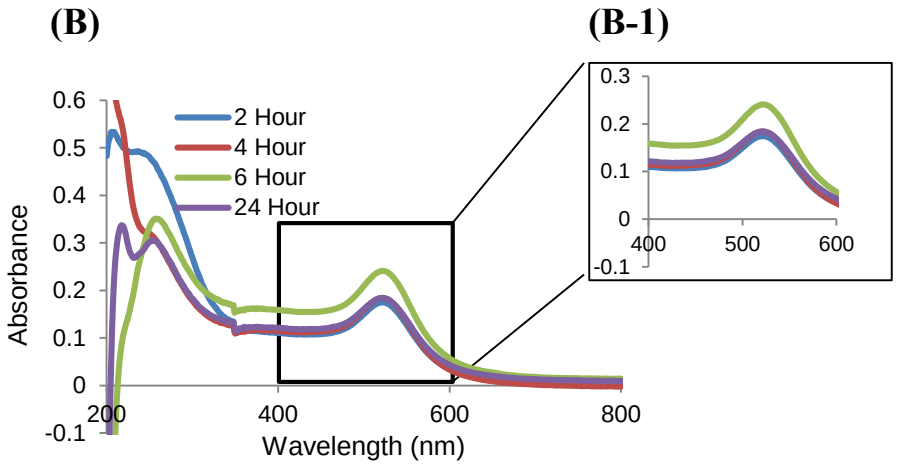
(B)
(B-1)
2 Hour
4 Hour
6 Hour
24 Hour
Absorbance
Wavelength (nm)
0.6
0.5
0.4
0.3
0.2
0.1
0
-0.1
200
400
600
800
0.3
0.2
0.1
0
-0.1
400
500
600

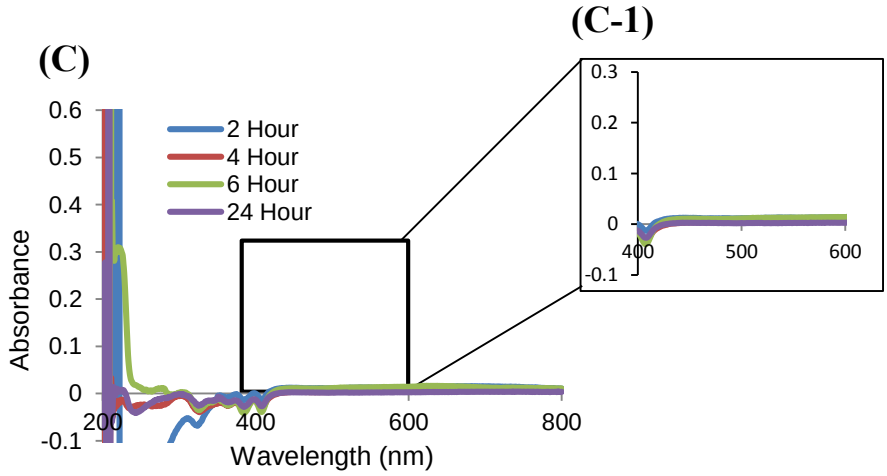
(C)
(C-1)
2 Hour
4 Hour
6 Hour
24 Hour
Absorbance
Wavelength (nm)
0.6
0.5
0.4
0.3
0.2
0.1
0
-0.1
200
400
600
800
0.3
0.2
0.1
0
-0.1
400
500
600

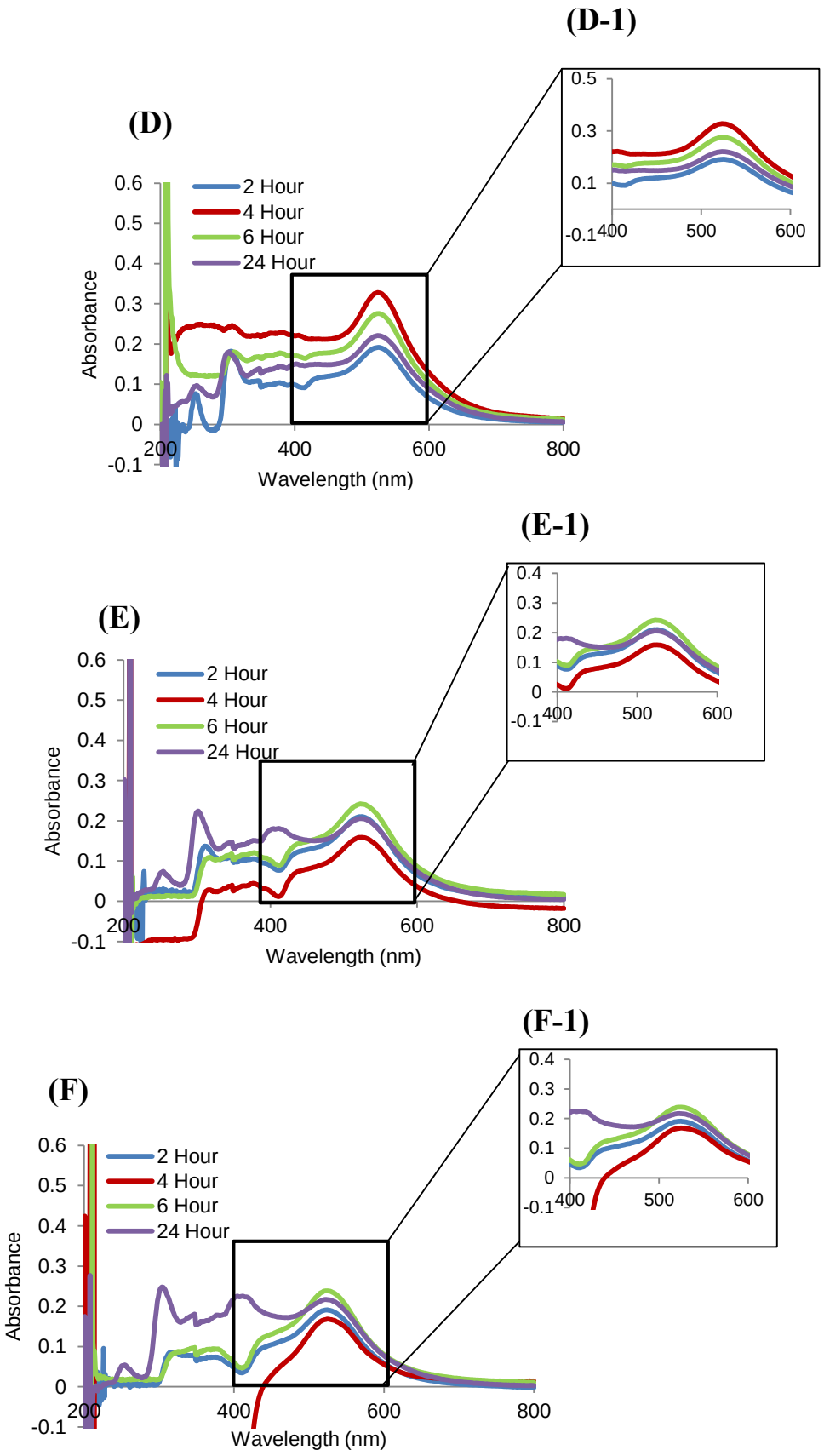
(D-1)
(D)
2 Hour
4 Hour
6 Hour
24 Hour
Absorbance
Wavelength (nm)
(E-1)
(E)
2 Hour
4 Hour
6 Hour
24 Hour
Absorbance
Wavelength (nm)
(F-1)
(F)
2 Hour
4 Hour
6 Hour
24 Hour
Absorbance
Wavelength (nm)

(G)

Incubation Time	SPR Peak Wavelength (nm)			
	FCS Concentration			
	dH_2O Control	10%	25%	50%
2 Hour	523	524	525	524
4 Hour	524	523	521	525
6 Hour	521	525	523	522
24 Hour	522	524	522	523

Figure 3-1: The UV-visible absorption spectra of synthesised 20 nM AuNPs in cell growth medium with increasing FCS concentration from 0-50% over a 24 hour period.

The UV-visible absorption spectra of growth medium alone (A) and synthesised 20 nm AuNPs at a concentration of 2 nM was measured in dH_2O (B) and cell growth medium either without FCS (C) or supplemented with 10% FCS (D), 25% FCS (E) or 50% FCS (F) at 2, 4, 6 and 24 hours. The cell growth medium was additionally supplemented with 5% of each of penicillin streptomyacin, L-glutamine and fungazone respectively. The absorbance between 400-600 nm has been highlighted for all samples to allow clearer visualisation of the absorption peak at the wavelength of maximum absorption (λmax) which occurs at approximately 520 nm for 20 nm AuNPs with the wavelength of maximum absorption (λmax) of 20 nm AuNPs under each culture condition listed (G)

3.4.3 Intracellular localisation of synthesised 20 nm AuNPs in UVW/NAT, SK-N-BE and A375 cells

The intracellular localisation of synthesised AuNPs was evaluated by TEM following 24 hour incubation of UVW/NAT, SK-N-BE and A375 cells with 2 nM AuNPs. In each cell line tested, AuNPs aggregated in the intracellular endosomes and lysosomes in the cell cytoplasm (Figure 3-2). Additionally AuNPs can be seen around the cell membrane, undergoing invagination which is supportive of uptake via receptor mediated endocytosis as discussed in section 1.6.5.3.

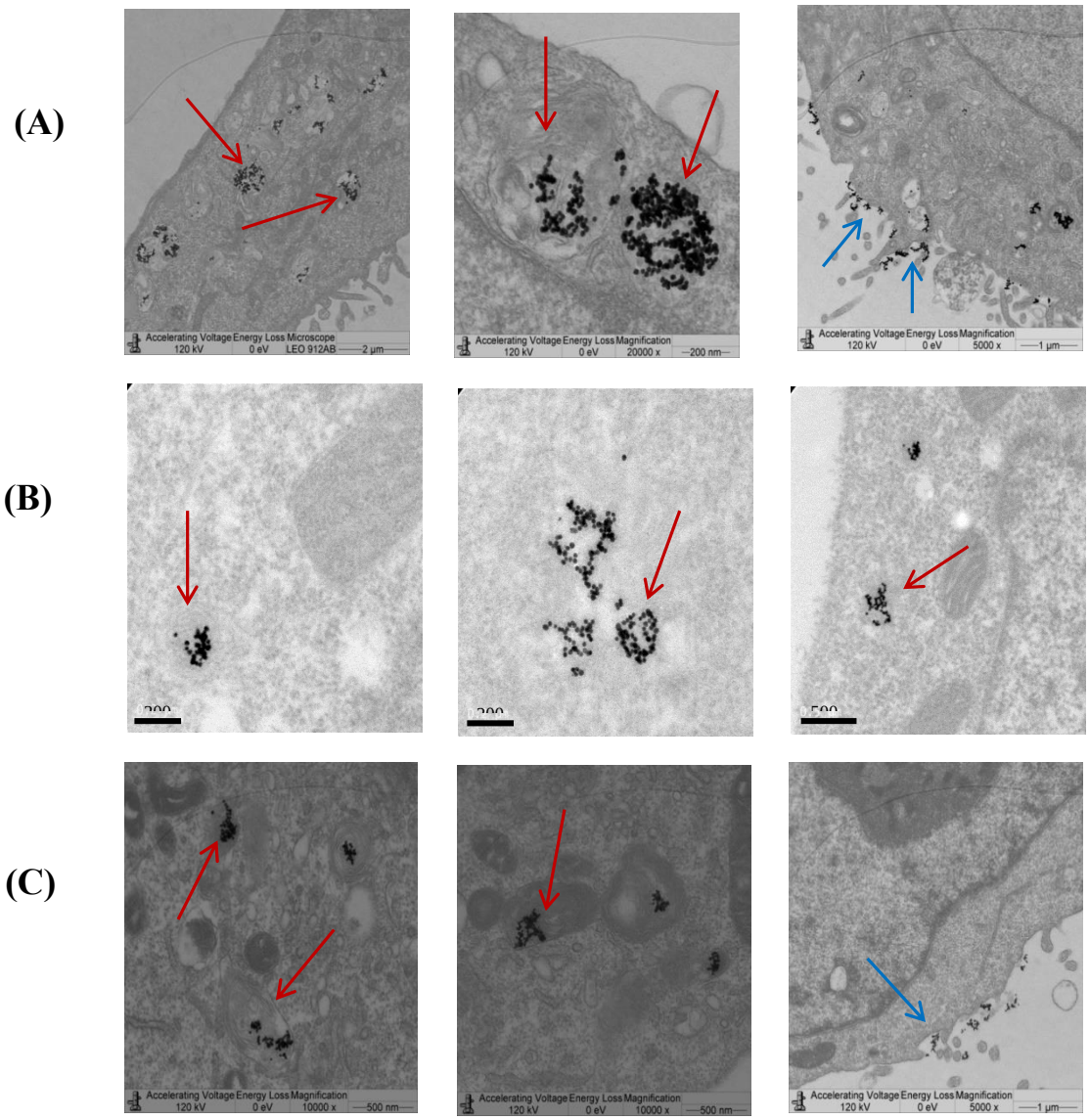

Figure 3-2: Intracellular localisation of 20 nm AuNPs in UVW/NAT, SK-N-BE and A375 cells evaluated by TEM.

UVW/NAT (A), SK-N-BE (B) and A375 (C) cells were incubated with AuNPs at a concentration of 2 nM for 24 hours and processed for TEM imaging. TEM images demonstrate localisation of AuNPs in the endosomes and lysosomes of cells indicated by the red arrows and localisation of AuNPs around the cell membrane undergoing invagination, indicated by the blue arrows. Representative images for each cell line were selected. Scale bars are shown on each image and range between 200-1000 nm and images captured at magnifications between 1000-20000x.

3.4.4 Intracellular uptake of synthesised 20 nm AuNPs in UVW/NAT, SK-N-BE and A375 cells

ICP-MS was used to measure the intracellular Au content after 2, 6 and 24 hour incubation with AuNPs (Figure 3-3).

In all cell lines investigated, a linear increase in the Au content/cell was evident over the 24 hour time period investigated when cells were exposed to AuNPs at a concentration of 0.5 nM and 2 nM. Following an increase in 2 nM AuNP exposure time from 2 to 24 hours the average Au content per cell (ng/L) increased significantly from 0.45±0.28 ng/L to 1.65±0.34 ng/L ($p<0.0001$) in UVW/NAT cells. Likewise in SK-N-BE cells the Au content per cell (ng/L) increased significantly from 0.05±0.02 ng/L following 2 hour incubation with AuNPs at 2 nM to 0.71±0.26 ng/L ($p<0.0001$) at 24 hours. In A375 cells an increase in the incubation time also resulted in an increase in the Au content per cell from 0.08±0.0039 ng/L to 0.22±0.1 ng/L however this increase was not statistically significant ($p>0.05$).

Increasing the AuNP concentration from 0.5 nM to 2 nM also increased the average Au content per cells, in all cell lines investigated. In UVW/NAT cells the 4-fold increase in AuNP concentration resulted in a significant increase in the Au content measured after both 6 hour ($p<0.001$) and 24 hour ($p<0.0001$) incubation where the measured Au content increased from 0.27±0.04 ng/L with 0.5 nM AuNPs to 1.65±0.34 ng/L ($p<0.0001$) with 2 nM AuNPs at 24 hours incubation. In SK-N-BE cells, significantly greater AuNP uptake resulted after 24 hour incubation, where the measured Au content was 0.71±0.26 ng/L when cells were treated with 2 nM AuNPs compared to 0.13±0.04 ng/L ($p<0.0001$) in cells incubated with 0.5 nM AuNPs. Finally in A375 cells, the increase in administered AuNP concentration significantly increased the Au concentration at both 6 hour ($p<0.01$) and 24 hour ($p<0.0001$) incubation. At 24 hours for example the measured Au content was 0.22±0.1 ng/L in cells exposed to 2 nM AuNPs compared to 0.04±0.02 ng/L ($p<0.0001$) when cells were treated with 0.5 nM AuNPs.

AuNP uptake differed significantly between the 3 cell lines examined. The highest uptake was found in UVW/NAT cells and the lowest in A375 cells. Following 24 hour incubation with 2 nM AuNPs the average Au content in UVW/NAT cells was

1.65±0.34 ng/L compared to 0.71±0.26 ng/L in SK-N-BE cells and 0.22±0.10 ng/L ($p<0.0001$) in A375 cells. The average Au content was also greatest in UVW/NAT cells following exposure to AuNPs at 0.5 nM however the difference in Au content between the 3 cell lines was not statistically significant at any time point at this AuNP concentration.

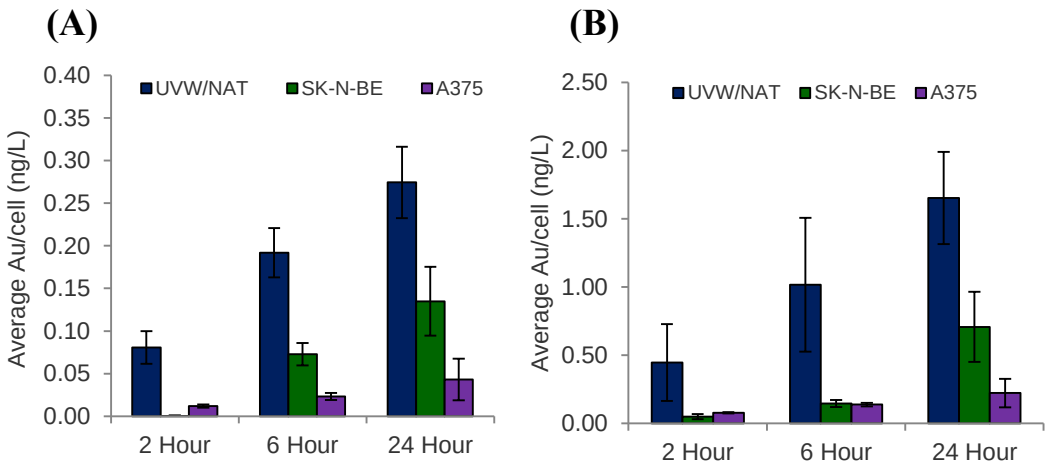

(C)

	UVW/NAT	SK-N-BE	A375
Incubation time (Hours)	2nM AuNP concentration		
2 vs. 6	***	ns	ns
2 vs. 24	****	****	ns
6 vs. 24	****	**	ns
	0.5nM vs. 2nM AuNP Concentration		
2 hour	ns	ns	ns
6 hour	***	ns	**
24 Hour	****	****	****
	UVW/NAT vs A375	**UVW/NAT vs. SK-N-BE**	**A375 vs. SK-N-BE**
	2nM AuNP Concentration		
2 hour	ns	ns	ns
6 hour	****	****	ns
24 Hour	****	****	**

Figure 3-3: Intracellular uptake of synthesised AuNPs in UVW/NAT, SK-N-BE and A375 cells at 2, 6 and 24 hours.

The mean Au content per cell was measured by ICP-MS in UVW/NAT. SK-N-BE and A375 cells incubated with AuNPs at 0.5 nM (A) or 2 nM (B). Results are displayed as the average Au content per cell in ng/L (mean ± sd) of 3 independent experiments. Statistically significant differences in AuNP uptake as an effect of AuNP concentration, incubation time and cell line were assessed using two-way ANOVA with Bonferroni post-tests (D). All statistical analysis was performed at the 95% C.I. Two (**), three (***) and four (****) symbols indicate $p<0.01$, $p<0.001$ and $p<0.0001$ and ns indicates no significance.

3.4.5 The cytotoxicity of synthesised 20 nm AuNPs in UVW/NAT, A375 and SK-N-BE cells

Clonogenic survival assays were performed to assess the cytotoxicity of synthesised AuNPs following 24 hour incubation in each cell line. The clonogenic survival fraction decreased in all cell lines following incubation with AuNPs, compared to untreated control cells (Figure 3-4). However, only A375 cells demonstrated a concentration dependant decrease in cell survival. In UVW/NAT and SK-N-BE cells no further decrease in the clonogenic survival was observed with an increase in AuNP concentration from 1 nM to 2 nM.

The greatest reduction in cell survival following AuNP exposure was observed in A375 cells. The clonogenic survival fractions were 0.86±0.04, 0.88±0.03 and 0.63±0.10 following incubation with AuNPs at 0.5 nM, 1 nM and 2 nM respectively and demonstrated concentration dependant toxicity at the higher AuNP concentrations. UVW/NAT and SK-N-BE cells did not demonstrate the same significant concentration responsive reduction in cell survival following AuNP incubation. The clonogenic survival fractions following incubation with AuNPs at 0.5 nM, 1 nM and 2 nM were 0.94±0.05, 0.84±0.10 and 0.80±0.08 in UVW/NAT cells and 0.95±0.07, 0.84±0.06 and 0.79±0.07 in SK-N-BE cells respectively. As a significant concentration dependant decrease in cell survival was not observed following AuNP incubation, with the exception of A375 cells, in all subsequent combination studies the AuNP concentration range of 0-2 nM was employed.

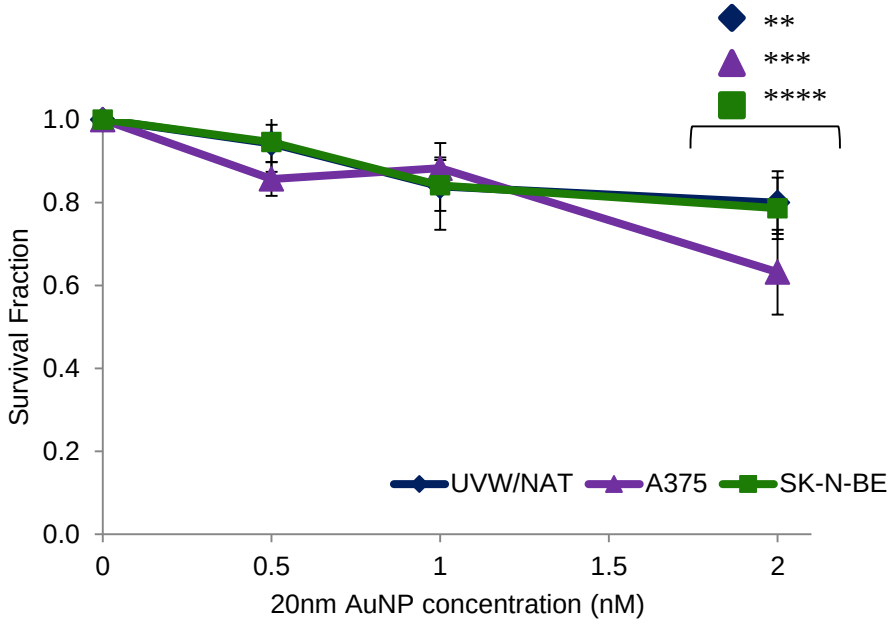

Figure 3-4: Clonogenic survival of UVW/NAT, A375 and SK-N-BE cells incubated with AuNPs across the concentration range 0-2 nM.

Each cell line tested was incubated with AuNPs across the concentration range 0-2 nM for 24 hours and cells plated for clonogenic survival assays. Results are presented as the mean survival fraction (mean ± sd) of 3 independent experiments, normalised to untreated control cells. Two-way ANOVA with Bonferroni post-tests was performed to assess the effect of AuNP incubation on the clonogenic survival in each cell line. All tests were performed at the 95% C.I. Two (**), three (***) and four (****) symbols indicate $p<0.01$, $p<0.001$ and $p<0.0001$ respectively.

3.5 Discussion

The aim of this study was to initially evaluate the stability of in house synthesised AuNPs within cell growth medium. Results of the study demonstrated that the synthesised AuNPs were stable following 24 hour incubation in MEM cell growth medium, provided the medium was supplemented with FCS (Figure 3-1). The dependence of the AuNP stability on the presence of FCS within cell growth medium was consistent with other studies. (Maleki et al.;Saptarshi et al., 2013). Results of previous studies have demonstrated almost instantaneous adsorption of serum proteins such as bovine serum albumin (BSA) onto the surface of citrate capped AuNPs, confirmed by a shift in the SPR peak of the AuNPs as a result of the increase in AuNP diameter (Chithrani et al., 2006). The adsorption of serum proteins onto the AuNP surface is hypothesised in other studies as the mechanism underpinning the stability of the AuNPs in cell growth medium. In this present study however no shift in the SPR peak of the AuNPs was observed following incubation of AuNPs in cell growth medium, suggesting that the substantial adsorption of serum proteins onto the AuNP surface, resulting in a measurable change to the AuNP diameter did not occur. Despite this, the consistency of the absorption peak indicated that incubation of the AuNPs in growth medium resulted in no aggregation of the AuNPs, confirming their stability within cell growth medium. In the absence of FCS, studies have demonstrated that the high concentration of charged ions and electrolytes such as, phosphate and magnesium within the cell growth media results in the citrate stabilisation of the AuNPs being stripped off and the collapse of the AuNP stability.

Following evaluation of the stability of AuNPs in cell growth medium their internalisation and localisation in each cell line was assessed. In each cell line investigated AuNPs were internalised and were localised in intracellular lysosomes and endosomes where they appeared aggregated (Figure 3-2) which was consistent with previous studies (Brown et al., 2010; Jain et al., 2011). The AuNPs will remain within the lysosomes and endosomes unless functionalised with an agent such as an endosomal disruption motif (EDM) or lysosomotropic agents such as, chloroqunie or sucrose (Joshi et al., 2012). Release of AuNPs from the lysosomes and endosomes into the cytoplasm could dramatically increase their effectiveness as radiosensitisers by

allowing the secondary electrons to damage more critical organelles throughout the cell.

The magnitude of AuNP uptake differed between each of the cell lines and was dependant on Au concentration and incubation time (Figure 3-3). The dependence of AuNP concentration on the uptake of AuNPs in the 3 cell lines investigated in this study has also been reported previously in a broad range of cancer cell lines (Coulter et al., 2012).

The differences in the magnitude of AuNP uptake observed between the 3 cell lines investigated in this study has been demonstrated in previous studies, and is attributed to a higher rate of endocytosis in the cell lines which demonstrate the greatest AuNP uptake (Coulter et al., 2012). It is therefore possible that the differences in AuNP uptake observed between the cell lines investigated in this study were due to differences in the rate of endocytosis, although this was not directly examined in this study.

The cytotoxicity of synthesised AuNPs was then evaluated in each cell line (Figure 3-4). The data indicated that in UVW/NAT and SK-N-BE cells there was little induction of significant cytotoxicity, which was only observed at the highest AuNP concentration of 2 nM and was not dose dependant. Previous studies have reported varying degrees of toxicity of AuNPs, ranging from no toxicity to significant dose dependant toxicity following AuNP incubation (Pan et al., 2009, 2007).

The differences in toxicity observed between the 3 cell lines examined was consistent with results presented in the study by Coulter *et al*, (2012) which demonstrated that exposure to 12 µM 1.9 nm AuNPs resulted in significant reduction in the clonogenic survival of MDA-MB-231 cells, where comparatively, no reduction in cell survival was observed in either DU145 or L132 cells respectively (Coulter et al., 2012). The study by Patra *et al*, (2007) also observed cell line selective toxicity where following 48 hour exposure to 33 nm citrate capped AuNPs significant toxicity in the A549 human lung cancer cell line but not in either BHK21 baby hamster cells or HepG2 human hepatocellular liver carcinoma cells was observed (Patra et al., 2007).

Although many studies use AuNPs of varying diameter and surface functionalisation it is consistently reported that the cytotoxicity induced by AuNPs results from the generation of ROS and oxidative stress within cells (Manke et al., 2013). For example in the studies by Pan *et al*, (2007, 2009) incubation of HeLa cells with 1.4 nm AuNPs caused significant reduction in cell viability, where the observed toxicity was associated with an increase in the intracellular ROS, which continued to increase throughout the entire AuNP exposure time of 48 hours. Measurement of the caspase 3/7 activity in cells exposed to 1.4 nm AuNPs demonstrated no significant increase in caspase 3/7 activity compared to untreated control HeLa cells indicating that the mode of cell death was via necrosis and not apoptosis. As the aim of this present study was to investigate the radiosensitising potential of AuNPs in combination with ionising radiation the toxicity observed was not further investigated at this stage.

This chapter demonstrated that the in house synthesised AuNPs were stable in cell growth medium, were internalised into each of the 3 cell lines investigated and displayed varying toxicity which was not concentration dependant. The aim of the subsequent chapters was to assess the radiosensitisation potential of the synthesised AuNPs in combination with kV X-ray photons (225 kV) and high energy β electrons emitted from ^{131}I in the form of the radiopharmaceutical [^{131}I]-MIBG.

Chapter 4

Investigation of the radiosensitisation potential of AuNPs in combination with External Beam Radiation (XBR)

Chapter 4: Investigation of the radiosensitisation potential of AuNPs in combination with External Beam Radiation (XBR)

4.1 Introduction

The previous chapter demonstrated the stability of AuNPs in cell growth medium. Furthermore, successful internalisation of the AuNPs was observed, with each of the 3 cell lines investigated demonstrating differential uptake of AuNPs. In each of the cell lines the AuNPs localised within the cytoplasmic endosomes/lysosomes. In this chapter the radiosensitisation potential of the synthesised AuNPs in combination with kVp X-ray XBR was assessed.

As previously discussed, the primary aim in combining AuNPs with XBR is to increase the radiation dose deposition in the target area, and thus induce an enhancement of the biological effects caused by radiation exposure. Radiosensitisation in this study was primarily evaluated by assessing the cell survival of UVW/NAT, SK-N-BE and A375 cells following exposure to XBR alone and then in combination with AuNPs. It was hypothesised that the radiosensitisation achieved by the combination of AuNPs with XBR is due to an increase in the dose of XBR within the target area, as outlined in section 1.6.1, and this will therefore lead to an increase in the radiation induced effects such as an arrest of cells in the G2/M phase of the cell cycle and the formation of DNA DSBs. The effect of AuNPs in combination with XBR on the magnitude and dynamics of DNA double stranded damage and repair, and the progression of cells through the cell cycle were therefore assessed and compared to the effect in cells exposed to XBR alone.

4.2 Aims

The primary aim of this chapter was to evaluate the radiosensitisation potential of AuNPs in combination with XBR by investigating the clonogenic cell survival of UVW/NAT, SK-N-BE and A375 cells incubated with AuNPs prior to XBR exposure. The second aim was to determine the mechanisms of any observed radiosensitisation

by analysis of the progression of cells through the cell cycle, and the DNA double stranded damage and repair kinetics.

4.3 Materials and Methods

4.3.1 Cells and culture conditions

The human glioblastoma cell line UVW/NAT, human neuroblastoma cell line SK-N-BE and human melanoma cell line A375 were employed in this study. All cells were cultured and maintained as detailed in sections 2.3.1 and 3.3.4.

4.3.2 Synthesis of 20 nm AuNPs

All AuNPs were synthesised in the Graham Lab (University of Strathclyde) (Brown et al., 2010) using the Turkevich-Frens method as described in section 3.3.1.

4.3.3 Treatment of cells with AuNPs and XBR

The concentration range of AuNPs employed in this study was 0-2 nM. All cells lines were incubated with AuNPs for 24 hours as described in section 2.3.3.

All irradiation of cells with XBR was performed using a cell irradiation cabinet (XRAD 225) with a 225 kVp X-ray beam and a dose rate of 2.2 Gy/min and 13.00 mA current, as described in section 2.3.3. To examine the effect of radiation dose, cells were treated with XBR within a dose range from 0-6 Gy in all experiments.

For all combination experiments cells were incubated with AuNPs in the concentration range 0-2 nM for 24 hours and then exposed to XBR across the dose range 0-4 Gy.

4.3.4 Clonogenic survival assay

Clonogenic survival assays were used to assess the clonogenic survival of each cell line examined following exposure to XBR alone, and in combination with AuNPs. For the assessment of UVW/NAT and A375 cell lines, clonogenic survival assays were performed as described in section 2.3.4. Due to the low plating efficiency of SK-N-BE cells however, soft agar clonogenic survival assays were performed as described in section 3.3.7.1. All results are presented as the average cell survival fraction (mean ± sd) of 3 independent experiments.

4.3.5 Cell doubling time

The time taken for the cell population of UVW/NAT, SK-N-BE and A375 cells to double during the exponential growth phase was determined. $1x10^5$, $1x10^4$ and $1x10^5$ cells for UVW/NAT, A375 and SK-N-BE respectively were seeded into each well of a 6 well plate in 3 mL of cell growth medium. After 24 hour incubation the cells in the first well were washed with PBS, detached with either 0.05% Trypsin EDTA (UVW/NAT and A375 cells) or Accutase® (SK-N-BE cells), disaggregated through a 21 g needle and counted using a haemocytometer. One subsequent well was counted every 24 hours for a further 5 days. The time required for the cell population to double in the exponential growth phase (DT) was calculated using equation 7.

Doubling Time (DT) = Time A (hours) – Time B (hours) Equation 7

Where; Time A = the time taken in hours for the cell population to reach $1x10^5$ cells and Time B is the time taken in hours for the cell population to double to $2x10^5$ cells.

4.3.6 Cell cycle analysis

The progression of cells through the cell cycle was determined in order to assess whether AuNPs alone, and in combination with XBR caused an abrogation to the normal cycling of cells (Pollack and Ciancio, 1990).

Following experimental therapy, cells were collected at 2, 6 and 24 hours after XBR exposure. Cells were washed with PBS, detached using 0.05% trypsin EDTA (UVW/NAT and A375 cells) or Accutase® (SK-N-BE cells) and pelleted by centrifugation at 1500 rpm, for 5 mins. The supernatant was removed and cells were washed with PBS and re-pelleted at 1500 rpm, for 5 mins. Cells were fixed in 70% ice-cold ethanol and incubated at 4°C for at least 1 hour. Fixed cells were pelleted by centrifugation at 2000 rpm for 10 mins, washed with PBS and resuspended in 300 µL PBS containing 10 µg/mL propidium iodide (Sigma Aldrich, Doreset, UK) to label DNA content and 50 ug/mL RNase (Sigma Aldrich, Doreset, UK). Cells were incubated on ice in the dark for at least 1 hour before the distribution of cells throughout the cell cycle was analysed by flow cytommetry, using BDCellDiva™ software version 6.1.3. A minimum of 10000 cells per sample were analysed and experiments were carried out in triplicate and results presented as the percentage of cells in each phase of the cell cycle (mean ± sd) of 3 independent experiments, unless otherwise stated.

4.3.7 γ-H2AX detection

The effects of XBR and AuNP exposure as single agents and in combination on the magnitude and dynamics of DNA double stranded damage and repair was assessed in each cell line by immunostaining of the H2AX histone protein in its phosphorylated form using the commercially available Ser-139 antibody (Banáth et al., 2004; Chattopadhyay et al., 2010). Cells were seeded onto 13 mm coverslips at a density of $1x10^4$ cells/coverslip and incubated for 48 hours. To establish the effect of XBR exposure on the formation and resolution of γ-H2AX foci, cells were cells were fixed at 0.5, 1, 2, 5 and 24 hours post irradiation. The outcome of these experiments were used to determine the timepoints at which any possible effects of AuNPs in combination with XBR on the magnitude and repair of DNA DSBs could be assessed. For all combination treatments cells were therefore fixed at 2 and 24 hours post irradiation. At each timepoint cells were washed thrice in PBS and fixed in 4% paraformaldehyde (PF) for 20 mins. Permeablised in 0.5% triton X-100 for 20 mins and blocked for non-specific antibody binding in 0.5% BSA in PBS containing 0.15%

triton X-100 for 20 mins. After a 5 min wash in PBS samples were incubated at 4ºC overnight with the mouse monoclonal anti-γ-H2AX (ser-139) antibody (dilution 250 in 0.5% BSA in PBS containing 0.15% triton X-100) (Millipore Ltd, Watford, UK). Following incubation, cells were washed thrice in PBS and incubated with a goat antimouse alexa-488 conjugated IgG antibody (Millipore Ltd, Watford, UK) for 1.5 hours at room temperature. Coverslips were then washed thrice in PBS, thrice in dH_2O and mounted onto glass slides using vectashield (Vector Labs, Peterborough, UK). Cells were imaged by laser scanning confocal microscopy using a Leica DM6000 upright microscope. All images were captured with a 63x objective lens and 10Z stack images with a 1 µm resolution were taken for each coverslip area and combined in a maximum projection using LasAF software. The number of γ-H2AX foci present within the nuclei of cells was quantified using Volocity image analysis software (Perkin Elmer, UK) (Savic et al., 2009) with a minimum of 100 cells analysed per treatment sample. Three independent experiments were carried out, unless otherwise stated, and results presented as the number of γ-H2AX foci/cell (mean ± sd). The number of foci in AuNP or XBR cells was compared to that of control cells to determine treatment efficacy and for combination treatments foci number was compared to XBR treated cell alone.

4.3.8 Caspase 3 apoptosis assays

Caspase 3 activity assays were performed to assess if exposure of UVW/NAT, A375 and SK-N-BE cells to AuNPs and XBR alone, and in combination induced cell apoptosis. Caspase 3 is activated in early apoptosis and is responsible for the proteolysis of critical molecules such as ADP-ribose and PARP to prevent DNA repair. The upstream cleavage site in PARP is DEVD (Asp-Glu-Val-Asp), DEVD-AMC is a synthetic tetrapeptide flourogenic substrate which contains the amino acid sequence for the PARP cleavage site and can therefore be used to quantify capsase 3 activity (Pan-Bartneck and Jahnen-Dechent, 2010). In the assay caspase 3 cleaves the tetrapeptide between the DEVD and AMC, releasing the flourogenic AMC which can then be quantified by spectrophotometry. Cells were seeded into 25 cm^2 culture flasks at a density of $1.5x10^5$ cells/flask and incubated for 48 hours. Following treatment with

AuNP and/or XBR cells were incubated for either 6 or 24 hours post irradiation and caspase 3 activity measured. Following incubation, cell growth medium was removed and cells washed with PBS, detached using 0.05% Trypsin EDTA (UVW/NAT and A375 cells) or Accutase® (SK-N-BE cells) and counted using a haemocytometer. For each sample, a density of 5000 cells was seeded into each well of a 96 well plate with 8 replicates of each sample performed. After seeding cells were lysed in a cell lysis buffer containing the flourogenic substrate DEVD-AMC for caspase 3 cleavage. The lysis buffer contained 150 mM Hepes, 450 mM sodium chloride, 150 mM potassium chloride, 30 mM magnesium chloride, 1.2mM EGTA, 1.5% nonidet P40 (Fluka, UK), 0.3% CHAPS and 30% sucrose in dH_2O. The pH of the solution was adjusted to 7.4. Immediately before the assay was performed 3 mM phenylmethanesulfonylfluoride, 30 mM Dithiothreitol and 10mM DEVD-AMC caspase substrate (BD Bioscience, Oxford, UK) was added to the lysis buffer. All reagents were purchased from Sigma Aldrich, Dorset, UK unless otherwise stated.

The fluorescence intensity of free AMC was read using a Spectra Max Gemini XS plate reader with an excitation wavelength of 360 nm and an emission wavelength of 460 nm following 1 hour incubation with caspase substrate solution and processed using SoftMax Pro software, version 4.3. The mean fluorescence intensity for each experimental treatment was compared to that for untreated control cells and data expressed as the mean fold increase in fluorescence intensity normalised to untreated control cells for treatment with AuNPs and XBR alone or normalised to AuNP treatment alone for combination treatments (mean ± sd) of 3 independent experiments. Furthermore, in each experiment, Staurosporine a drug known to induce apoptotic cell death through caspase dependant mechanism was used as a positive control for caspase 3 activity at a concentration of 50 μM. Cells were incubated with Staurosporine for 1 hour before caspase 3 activity was measured.

4.3.9 Statistical Analysis

4.3.9.1 Analysis of variance (ANOVA)

All experiments were carried out 3 times unless otherwise stated, with results reported as the (mean ± sd). Clonogenic survival data are presented as the cell survival fraction normalised to untreated control cells for treatment with AuNPs and XBR alone or normalised to AuNP treatment alone for combination treatments. Cell cycle data is presented as the percentage of cells within each phase of the cell cycle and γ-H2AX data as the number of foci/cell for each treatment group. Caspase 3 activity for each treatment group is presented as the fold change in activity compared to untreated control cells. Results were evaluated using two-way ANOVA analysis with Bonferroni post-tests to determine if the effects of combination therapy on the clonogenic survival, progression and accumulation of cells throughout the cell cycle, formation of γ-H2AX foci and caspase activity were statistically significant compared to the effects of XBR alone. P-values lower than 0.05 were considered statistically different.

4.3.9.2 Linear quadratic analysis

To evaluate the radiosensitisation potential of AuNPs in combination with XBR and determine if the intracellular presence of AuNPs enhanced the clonogenic cell kill, the experimental clonogenic survival data for UVW/NAT, SK-N-BE and A375 cells exposed to XBR alone and in combination with AuNPs was fitted to the linear quadratic model (equation 1) (Dale, 2004) using GraphPadPrism software, version 6.01, 2014 (CA) as described in section 2.3.6.2. The α and β values, IC_{25}, IC_{50}, IC_{75} and DEF_{50} were calculated for XBR alone and in combination with AuNPs for each cell line using equations 2 and 3 as described in sections 2.3.6.2.

4.4 Results

4.4.1 Determination of the effect of XBR dose on clonogenic survival of UVW/NAT, A375 and SK-N-BE cells using the linear quadratic model

The effect of XBR as a single agent on the clonogenic survival of UVW/NAT, SK-N-BE and A375 cells was firstly investigated to establish the cell line sensitivity to radiation, and to establish the radiation dose range to be used in combination with AuNPs. There was a dose response relationship between administered radiation dose and clonogenic cell survival in all cell lines, where the clonogenic cell survival reduced proportionally with increasing radiation dose (Figure 4-1). Two-way ANOVA analysis of the clonogenic survival data demonstrated that the cell survival fractions in A375 cells were significantly lower than both UVW/NAT and SK-N-BE cells following XBR exposure at doses above 1 Gy.

The clonogenic data was fitted to the linear quadratic model as described in section 2.3.6.2. The doses of XBR which killed 25%, 50% and 75% of the cell population ($IC_{25\text{-}75}$) were 1.32 Gy, 2.85 Gy and 4.98 Gy in UVW/NAT cells, 1.74 Gy, 3.40 Gy and 5.99 Gy in SK-N-BE cells and 0.74 Gy, 1.79 Gy and 3.65 Gy in A375 cells respectively. The data demonstrated that across all radiation doses evaluated, A375 cells had the greatest sensitivity towards XBR and SK-N-BE cells the least. The α values for each cell line were 0.19 Gy^{-1}±0.02, 0.163 Gy^{-1}±0.02 and 0.39 Gy^{-1}±0.03 for UVW/NAT, SK-N-BE and A375 cells respectively suggesting higher toxicity in response to XBR in A375 cells, compared to either UVW/NAT or SK-N-BE cells.

Based on the effect of XBR alone in each cell line the dose range from 0-4 Gy was used for subsequent AuNP combination studies as it allowed for decreases in survival fraction beyond that of radiation alone to be identified.

(A)

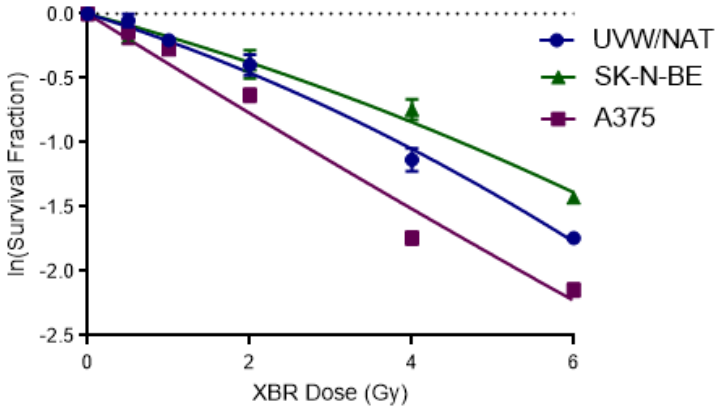

(B)

	UVW/NAT	SK-N-BE	A375
α (Gy^{-1})	0.19±0.02	0.16±0.02	0.39±0.03
β (Gy^{-1})	0.016±0.003	0.01±0.003	-0.004±0.01
R^2	0.99	0.97	0.97
IC_{25} (Gy)	1.32	1.74	0.74
IC_{50} (Gy)	2.85	3.40	1.79
IC_{75} (Gy)	4.98	5.99	3.65

(C)

XBR Dose (Gy)	UVW/NAT vs. A375	SK-N-BE vs. A375	UVW/NAT vs. SK-N-BE
0.5	**	ns	ns
1	ns	ns	ns
2	ns	***	***
4	****	***	****
6	ns	ns	**

Figure 4-1: Clonogenic survival of UVW/NAT, SK-N-BE and A375 cells exposed to increasing XBR doses from 0-6 Gy.

Cells were exposed to XBR from 0-6 Gy with clonogenic survival assays performed 24 hours after irradiation. Clonogenic survival data were then fitted to the linear quadratic model and the α, β and IC_{25}, IC_{50}, IC_{75} values for each cell line were calculated using GraphPad Prism software version 6.0.1 (B). Results are presented as the mean survival fraction of 3 independent experiments (mean ± sd) (A). Two-way ANOVA with Bonferroni post hoc testing for multiple comparisons was performed to establish if significant differences in the cell survival existed between the cell lines at a given XBR dose (C). All tests were performed at 95% C.I. Two (**), three (***) and four (****) symbols indicate $p<0.01$, $p<0.001$ and $p<0.0001$ respectively and ns indicates no significance.

4.4.2 Determination of the radiosensitising effect of AuNPs in combination with XBR using the linear quadratic model

For each of the cell lines examined, the effect of AuNPs on the radiation induced cell kill was assessed using clonogenic survival assays. Cells were incubated with AuNPs across the concentration range 0-2 nM for 24 hours, before irradiation with 0-4 Gy XBR and clonogenic assays were performed 24 hours after irradiation. The clonogenic survival of cells treated with AuNPs in combination with XBR was normalised to the effect of AuNP alone. Two-way ANOVA with Bonferroni post-hoc testing for multiple comparisons was carried out for each cell line to determine if the clonogenic survival fractions observed for cells treated with AuNPs in combination with XBR were significantly different from those observed following exposure to XBR alone. The clonogenic survival data for each cell line was then fitted to the linear quadratic model as previously described in section 2.3.6.2 using GraphPad Prism software version 6.0.1.

4.4.2.1 The effect of AuNPs in combination with XBR on clonogenic cell kill in UVW/NAT cells

In UVW/NAT cells incubated with AuNPs across the concentration range 0-2 nM for 24 hours prior to XBR exposure, no statistically significant decrease in clonogenic survival, compared to cells exposed to XBR alone was observed, with the exception of 2 nM AuNPs in combination with 0.5 Gy (Figure 4-2(A-B)). Combination of 2 nM AuNPs with 0.5 Gy, 1 Gy, 2 Gy and 4 Gy resulted in survival fractions of 0.66±0.11, 0.64±0.04, 0.46±0.09 and 0.28±0.05, compared to 0.95±0.05 ($p<0.01$), 0.81±0.04, 0.67±0.08 and 0.32±0.09 for 0.5 Gy, 1 Gy, 2 Gy and 4 Gy alone.

The clonogenic survival data from Figure 4-2(A) was fitted to the linear quadratic model (Figure 4-2(C)) and values for α, β, IC_{50} and DEF_{50} calculated (Figure 4-2(D)). Treatment of UVW/NAT cells with 2 nM AuNPs and XBR exposure resulted in a decrease in the dose of XBR required to kill 50% of the cell population (IC_{50}), compared to XBR alone. The IC_{50} decreased from 2.89 Gy for XBR alone to 2.57 Gy in the presence of 2 nM AuNPs. At 0.5 nM and 1 nM AuNPs the IC_{50} values in combination with XBR were 3.02 Gy and 3.33 Gy, compared to 2.89 Gy for XBR

alone, indicating no enhancement of the cytotoxicity of XBR. The calculated α values for the combination of AuNPs at 0.5 nM and 2 nM with XBR were 0.24 Gy^{-1}±0.02 and 0.30 Gy^{-1}±0.03 demonstrating an increase compared to XBR alone which was 0.13 Gy^{-1}±0.02. The increase in α value suggests that the presence of AuNPs at 0.5 nM and 2 nM results in an increase in the toxicity at low radiation doses, as discussed in section 2.3.6.2 (Barendsen, 1994). The α value for the combination of AuNPs at 1 nM with XBR was comparable to that for XBR alone, and suggested that there was no increase in toxicity. The DEFs calculated at the 50% toxicity level (DEF_{50}) were 0.96, 0.87 and 1.12 for XBR in combination with AuNPs at 0.5 nM, 1 nM and 2 nM, indicating that the combination of XBR with 2 nM AuNPs resulted in enhanced toxicity compared to XBR alone.

(A)

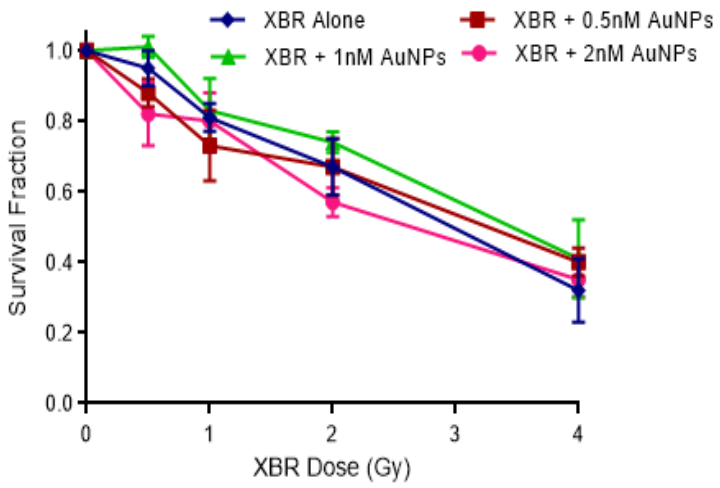

(B)

	0.5nM	1.0nM	2.0nM
0.5Gy	ns	ns	**
1.0Gy	ns	ns	ns
2.0Gy	ns	ns	ns
4.0Gy	ns	ns	ns

Figure 4-2 continued overleaf

(C)

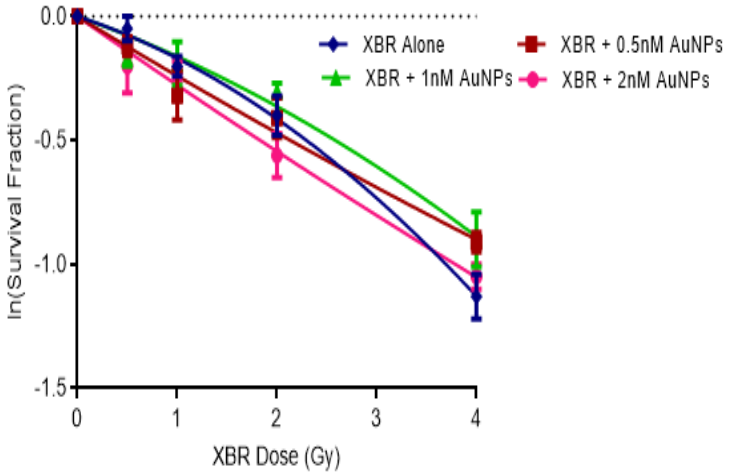

(D)

	0nM	0.5nM	1.0nM	2.0nM
α (Gy^{-1})	0.13±0.02	0.24±0.02	0.14±0.03	0.30±0.03
β (Gy^{-1})	0.03±0.01	-0.01±0.01	0.02±0.01	-0.004±0.01
R^2	0.98	0.94	0.93	0.96
IC_{50} (Gy)	2.89	3.02	3.33	2.57
DEF_{50}	1.00	0.96	0.87	1.12

Figure 4-2: Clonogenic survival of UVW/NAT cells exposed to AuNPs in combination with XBR.

UVW/NAT cells were incubated with AuNPs from 0-2 nM for 24 hours. Following this, cells were exposed to 0-4 Gy XBR with clonogenic survival assays performed 24 hours after irradiation. Clonogenic survival results are presented as the mean survival fraction of treated cells (mean ± sd), normalised to untreated control cells, of 5 independent experiments (A). Statistical significance of the cell survival fractions for AuNPs in combination with XBR, compared to XBR alone was assessed using two-way ANOVA with Bonferroni post-tests at 95% C.I. Two (**) symbols indicate $p<0.01$ and ns indicates no significance (B). Clonogenic survival data presented in (A) was fitted to the linear quadratic model using GraphPad Prism version 6.0.1 (C) and values calculated for the α and β coefficients and the IC_{50} and DEF_{50} for XBR in combination with AuNPs at each AuNP concentration (D).

4.4.2.2 The effect of AuNPs in combination with XBR on clonogenic cell kill in SK-N-BE cells

In SK-N-BE cells, treatment with AuNPs at 0.5 nM, 1 nM and 2 nM in combination with 0-4 Gy XBR resulted in no statistically significant decrease in clonogenic cell survival, compared to cells exposed to 4 Gy XBR alone, at any combination ($p<0.05$), (Figure 4-3(A-B)) indicating that the presence of AuNPs in combination with XBR induced no enhancement in the effects of radiation.

The clonogenic survival data from Figure 4-3(A) was fitted to the linear quadratic model (Figure 4-3(C)) and values for α, β, IC_{50} and DEF_{50} were calculated (Figure 4-3(D)). In SK-N-BE cells, the presence of AuNPs across the concentration range 0-2 nM in combination with XBR resulted in no change in the IC_{50} values, compared to cells exposed to XBR alone, indicating that the presence of AuNPs with XBR in SK-N-BE cells had no effect on the radiation dose required to kill 50% of the cell population, compared to XBR alone. Similarly, the α values for the combination of AuNPs at 0.5 nM, 1 nM and 2 nM with XBR were comparable to that of XBR alone, and indicated no enhancement of the effects of XBR through increased toxicity at lower radiation doses (Barendsen, 1994). The DEFs calculated at the 50% toxicity level (DEF_{50}) were 1.08, 0.95 and 0.93 for XBR in combination with AuNPs at 0.5 nM, 1 nM and 2 nM indicating again that the combination of AuNPs with XBR did not increased the clonogenic cell kill compared to XBR alone in SK-N-BE cells.

(A)

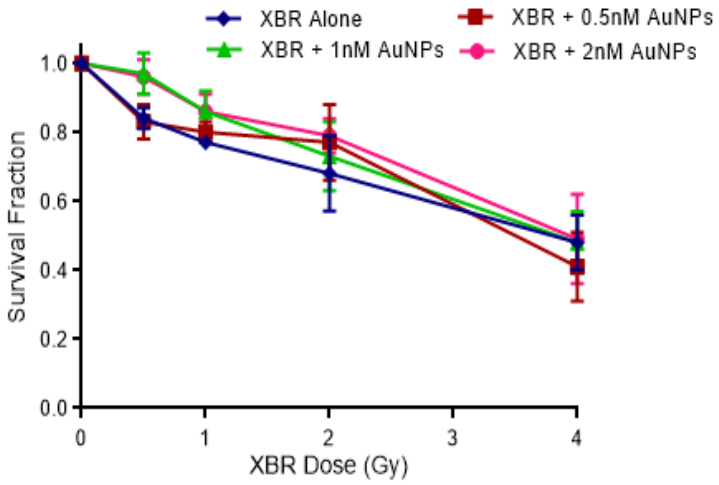

(B)

	0.5nM	1.0nM	2.0nM
0.5Gy	ns	ns	ns
1.0Gy	ns	ns	ns
2.0Gy	ns	ns	ns
4.0Gy	ns	ns	ns

Figure 4-3 continued overleaf

(C)

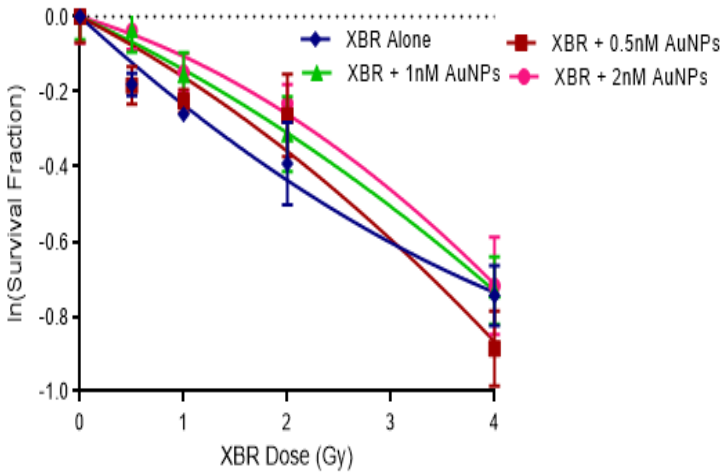

(D)

	0nM	0.5nM	1.0nM	2.0nM
α (Gy^{-1})	0.25±0.03	0.14±0.04	0.13±0.03	0.08±0.03
β (Gy^{-1})	-0.02±0.01	0.02±0.01	0.01±0.01	0.02±0.01
R^2	0.94	0.90	0.94	0.93
IC_{50} (Gy)	3.65	3.38	3.84	3.92
DEF_{50}	1.00	1.08	0.95	0.93

Figure 4-3: Clonogenic survival of SK-N-BE cells exposed to AuNPs in combination with XBR.

SK-N-BE cells were incubated with AuNPs from 0-2 nM for 24 hours. Following this cells were exposed to 0-4 Gy XBR with clonogenic survival assays performed 24 hours after irradiation. Clonogenic survival results are presented as the mean survival fraction of treated cells (mean ± sd), normalised to untreated control cells, of 4 independent experiments (A). Statistical significance of the cell survival fractions for AuNPs in combination with XBR, compared to XBR alone was assessed using two-way ANOVA with Bonferroni post-tests at 95% C.I, ns indicates no significance (B). Clonogenic survival data presented in (A) was fitted to the linear quadratic model using GraphPad Prism version 6.0.1 (C) and values calculated for the α and β coefficients and the IC_{50} and DEF_{50} for XBR in combination with AuNPs at each AuNP concentration (D).

4.4.2.3 The effect of AuNPs in combination with XBR on clonogenic cell kill in A375 cells

In A375 cells, the combination of AuNPs at 2 nM with all XBR doses resulted in a statistically significant decrease in clonogenic survival, compared to the effects of XBR alone, as well as the combination of 1 nM AuNPs with 1 Gy and 2 Gy XBR (Figure 4-4(A-B)). The clonogenic survival fractions were 0.29±0.07, 0.20±0.04 and 0.22±0.07 following treatment with 2 nM AuNPs in combination with 0.5 Gy, 1 Gy and 2 Gy XBR, compared to 0.87±0.09 ($p<0.0001$), 0.76±0.03 ($p<0.0001$) and 0.53±0.05 ($p<0.05$) respectively for 0.5 Gy, 1 Gy and 2 Gy alone. The clonogenic survival data indicated that the presence of 2 nM AuNPs during XBR exposure induced a significant enhancement in the radiation induced cell kill, compared to XBR alone. Due to time constraints data for A375 cells exposed to AuNPs in combination with 4 Gy was not obtained.

The clonogenic survival data from Figure 4-4(A) was fitted to the linear quadratic model (Figure 4-4(C)) and values for α, β, IC_{50} and DEF_{50} calculated (Figure 4-4 (D)). In A375 cells, the presence of AuNPs across the concentration range 0-2 nM in combination with XBR resulted in a dose dependant decrease in the radiation dose required to kill 50% of the cell population (IC_{50}). The IC_{50} values decreased from 2.16 Gy for XBR alone to 1.44 Gy, 1.22 Gy and 0.46 Gy respectively for XBR in the presence of AuNPs at 0.5 nM, 1 nM and 2 nM. The calculated α values for the combination of AuNPs at 0.5 nM, 1 nM and 2 nM with XBR were 0.58 Gy^{-1}±0.09, 0.53 Gy^{-1}±0.1 and 1.79 Gy^{-1}±0.06, compared to 0.25 Gy^{-1}±0.04 for XBR alone, demonstrating a concentration dependant increase with increasing AuNP concentration. The increase in α values suggested that the presence of AuNPs increased the toxicity at lower radiation doses as discussed in section 2.3.6.2 (Barendsen, 1994). The DEFs calculated at the 50% toxicity level (DEF_{50}) were 1.50, 1.77 and 4.68 for XBR in combination with AuNPs at 0.5 nM, 1 nM and 2 nM indicating that in A375 cells the presence of AuNPs in combination with XBR induced a concentration dependant increase in toxicity.

(A)

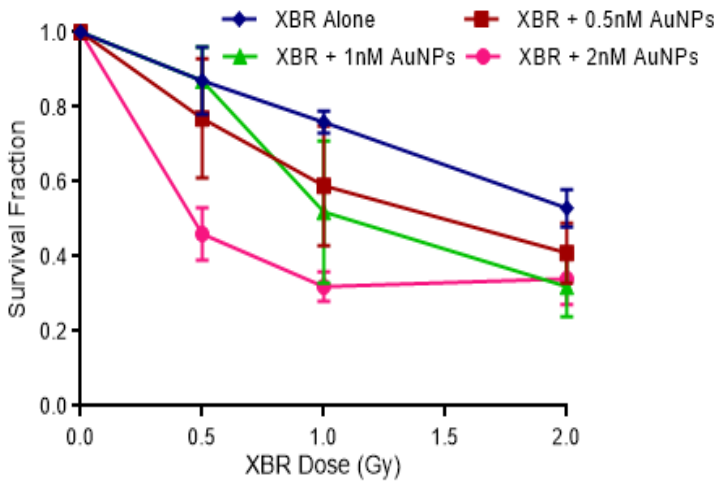

(B)

	0.5nM	1.0nM	2.0nM
0.5Gy	ns	ns	****
1.0Gy	ns	*	****
2.0Gy	ns	*	*

Figure 4-4 continued overleaf

(C)

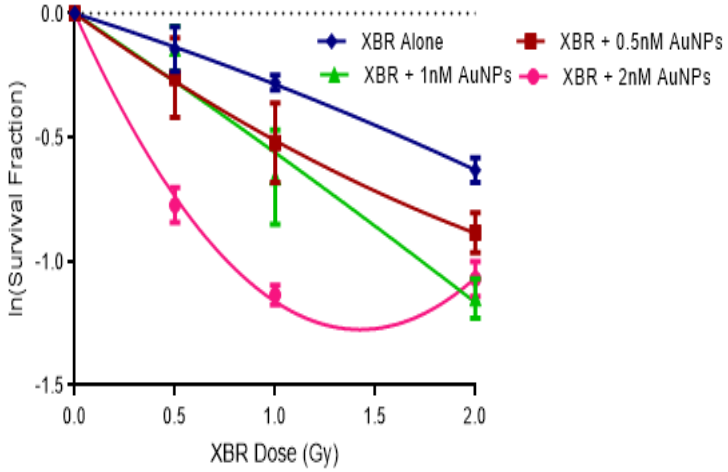

(D)

	0nM	0.5nM	1.0nM	2.0nM
α (Gy^{-1})	0.25±0.04	0.58±0.09	0.53±0.1	1.79±0.06
β (Gy^{-1})	0.03±0.02	-0.07±0.06	0.02±0.06	-0.62±0.03
R^2	0.96	0.90	0.92	0.97
IC_{50} (Gy)	2.16	1.44	1.22	0.46
DEF_{50}	1.00	1.50	1.77	4.68

Figure 4-4: Clonogenic survival of A375 cells exposed to AuNPs in combination with XBR.

A375 cells were incubated with AuNPs from 0-2 nM for 24 hours. Following this cells were exposed to 0-2 Gy XBR with clonogenic survival assays performed 24 hours after irradiation. Clonogenic survival results are presented as the mean survival fraction of treated cells (mean ± sd), normalised to untreated control cells, of 4 independent experiments (A). Statistical significance of the cell survival fractions for AuNPs in combination with XBR, compared to XBR alone was assessed using two-way ANOVA with Bonferroni post-tests at 95% C.I. One (*) and four (****) symbols indicate $p<0.05$ and $p<0.0001$, and ns indicates no significance (B) Clonogenic survival data presented in (A) was fitted to the linear quadratic model using GraphPad Prism version 6.0.1 (C) and values calculated for the α and β coefficients and the IC_{50} and DEF_{50} for XBR in combination with AuNPs at each AuNP concentration (D).

In summary, the clonogenic survival data demonstrated that the radiosensitisation potential of in house synthesised AuNPs was cell line dependant, with UVW/NAT and A375 cells displaying increased clonogenic cell kill in response to combination treatment, compared to XBR treatment alone with DEF_{50} values of 1.12 and 4.68. In SK-N-BE cells however, the DEF_{50} was 0.93 indicating no enhanced toxicity when XBR was combined with AuNPs, compared to XBR alone.

The uptake of 2 nM AuNPs following 24 hour incubation, the IC_{50} for XBR and the DEF_{50} for 2 nM AuNPs in combination with XBR are presented in Table 4-1 for each of the cell lines investigated to allow clear visualisation of the differences in dose enhancement between each of the cell lines, and the corresponding radiation sensitivity and intracellular Au content of the cell lines.

Based on these data, AuNPs at 2 nM were combined with 2 Gy XBR and compared to 2 Gy treatment alone to determine if the observed radiosensitisation was associated with changes in the progression of cells through the cell cycle, or the magnitude and resolution of DNA double stranded breaks or caspase mediated apoptosis.

Table 4-1: Uptake of 2 nM AuNPs, IC_{50} dose for XBR and DEF_{50} for 2 nM AuNPs with XBR in UVW/NAT, SK-N-BE and A375 cells respectively.

	UVW/NAT	SK-N-BE	A375
2nM AuNP uptake (ng/cell)	1.65±0.34	0.71±0.26	0.22±0.1
XBR IC_{50} (Gy)	2.89	3.65	2.16
DEF_{50} for 2nM AuNPs + XBR	1.12	0.93	4.68

4.4.3 The effect of AuNPs in combination with XBR on the cell cycle progression of UVW/NAT, SK-N-BE and A375 cells

The arrest of cells in the G2/M phase of the cell cycle is observed in virtually all cell lines following radiation exposure, and can be used as an indicator of the presence of radiation induced cellular damage (Maity et al., 1995). In this study measurement of the progression of cells through the cell cycle following treatment with 2 Gy XBR and 2 nM AuNPs as single agents and in combination was used to assess the effects of XBR and AuNPs alone, and then to evaluate whether the combination of AuNPs with XBR resulted in an increase in the G2/M arrest compared to XBR alone in UVW/NAT, SK-N-BE and A375 cells.

Despite the decrease in clonogenic survival in UVW/NAT, SK-N-BE and A375 cells following exposure to 2 nM AuNPs alone (Figure 3-4) treatment with AuNPs alone in each cell line had no effect on the normal progression of cells through the cell cycle, compared to untreated control cells at any timepoint ($p>0.05$) (Figure 4-5).

Exposure of UVW/NAT cells to 2 Gy XBR resulted in a significant accumulation of cells within the G2/M phase of the cell cycle at 24 hours post irradiation compared to untreated control cells (Figure 4-5(A)). The percentage of cells within G2/M increased from 25.1%±7.4 in untreated control cells to 38.0%±4.6 ($p<0.05$) in cells irradiated with 2 Gy XBR. Exposure of UVW/NAT cells to 2 Gy XBR alone induced no significant accumulation of cells in G2/M at 2 and 6 hours after irradiation ($p>0.05$), which was consistent with the calculated doubling time of the cells which was 29 hours.

In SK-N-BE cells, exposure to 2 Gy XBR resulted in an increase in the accumulation of cells within the G2/M phase of the cell cycle at 6 and 24 hours post irradiation compared to untreated control cells (Figure 4-5(B)) however this accumulation was not significantly different compared to untreated control cells at either timepoint. The doubling time of SK-N-BE cells was 19 hours i.e shorter than for UVW/NAT cells and therefore the accumulation of cells at the earlier time point of 6 hours was consistent with the shorter doubling time.

In A375 cells, exposure to 2 Gy XBR resulted in an increase in the accumulation of cells within the G2/M phase of the cell cycle at 2 and 6 hours post irradiation compared to untreated control cells (Figure 4-5(C)) however this increase was not significantly different compared to untreated control cells at either time point. At 24 hours after irradiation, no increase in the accumulation of cells in G2/M was observed following 2 Gy XBR exposure, compared to untreated control cells. The doubling time of A375 cells was calculated as 15 hours, which was lower than for both UVW/NAT and SK-N-BE cells, the earlier arrest of cells in G2/M at 2 and 6 hours after irradiation is therefore consistent with the shorter doubling time.

In UVW/NAT, SK-N-BE and A375 cells, treatment with 2 nM AuNPs in combination with 2 Gy XBR resulted in no increase in the accumulation of cells within G2/M, compared to XBR alone at any timepoint measured (Figure 4-5).

In each case the proportion of cells in G1 decreased as the proportion of cells in G2/M increased and no significant changes to the proportion of cells in the S phase of the cell cycle was observed following any treatment in any of the cell lines or timepoints measured.

In summary, analysis of the progression of cells through the cell cycle demonstrated that the combination of AuNPs at 2 nM with 2 Gy XBR did not result in a statistically significant increase in the proportion of cells which arrested in G2/M compared to XBR exposure alone.

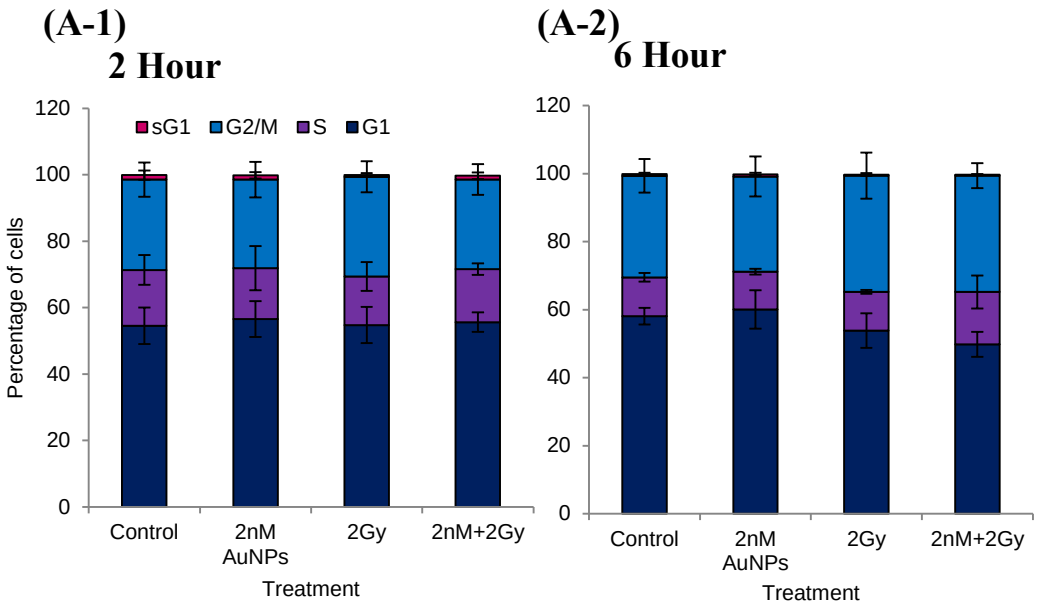

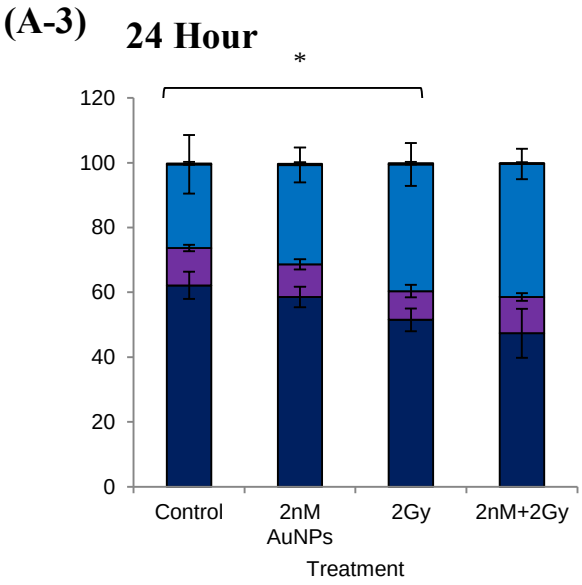

Figure 4-5 continued overleaf

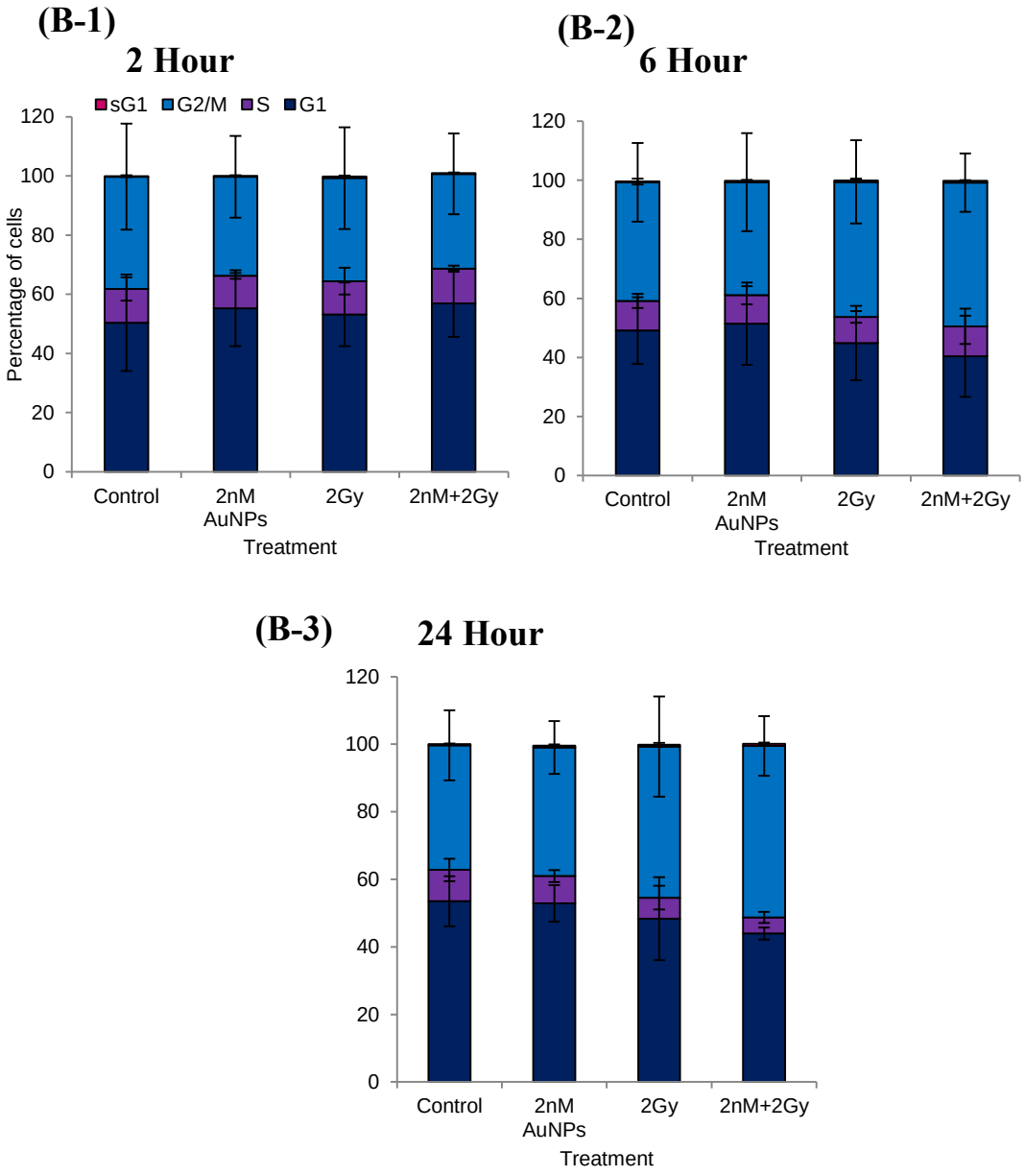

Figure 4-5 continued overleaf

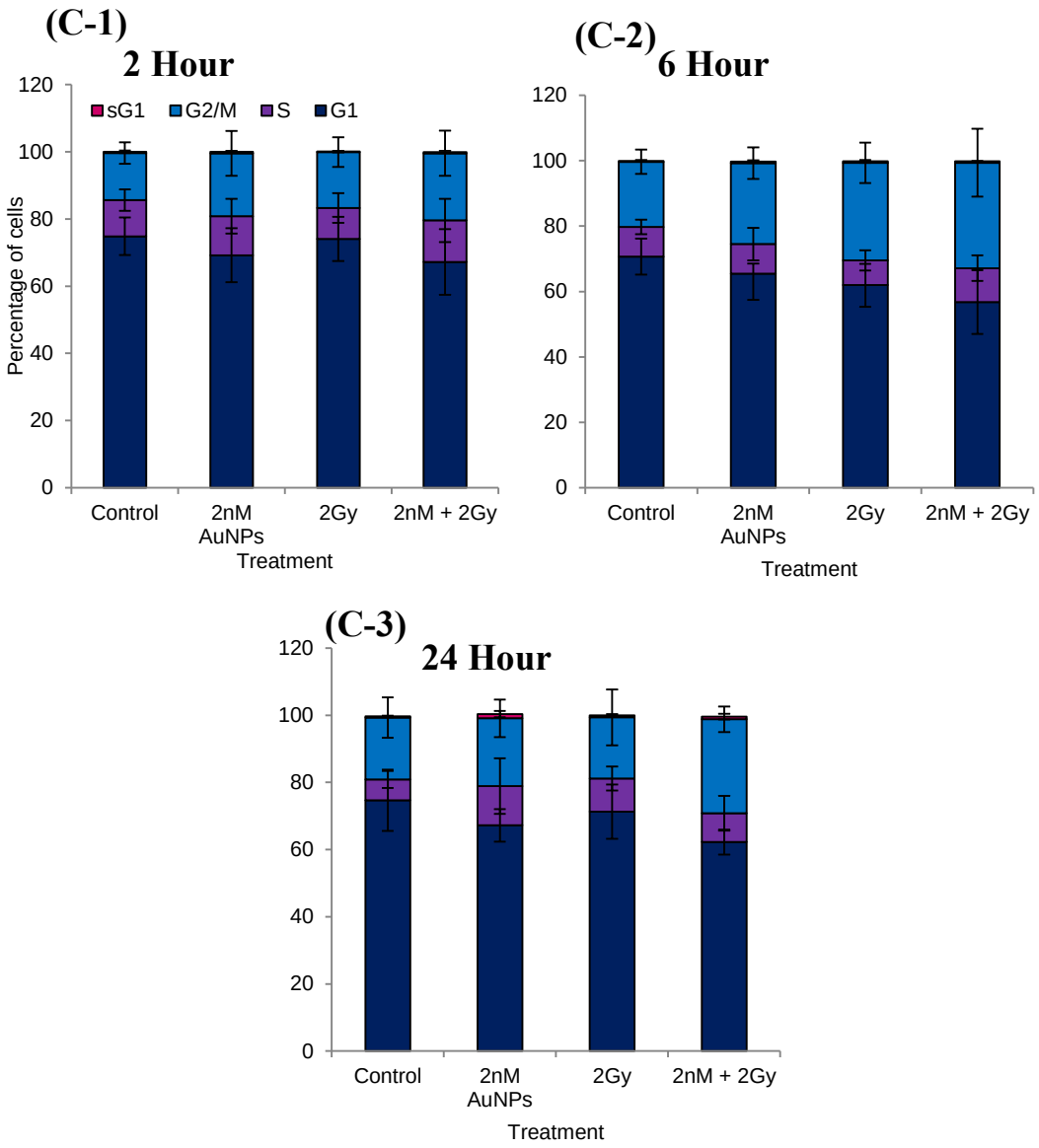

Figure 4-5: The effect of 2 nM AuNPs and 2 Gy XBR alone, and in combination on the distribution of UVW/NAT, SK-N-BE and A375 cells throughout each stage of the cell cycle.

UVW/NAT (A), SK-N-BE (B) and A375 (C) cells were incubated with 2 nM AuNPs for 24 hours prior to 2 Gy XBR irradiation. The DNA content of the cells was labelled with PI and the cell cycle profiles obtained by FACS analysis at 2 (A-1, B-1, C-1), 6 (A-2, B-2, C-2) and 24 (A-3, B-3, C-3) hours after irradiation. The proportion of cells in G0/G1, S, sG1 and G2/M were measured using BDCellDiva™ software. Two-way ANOVA was used to determine if statistically significant changes in the distribution of cells throughout the cell cycle resulted as an effect of AuNP and XBR exposure alone (compared to untreated control cells) or in combination (compared to the effects of XBR alone). All tests were performed at the 95% C.I of 3 independent experiments unless otherwise stated (A375 n=5). One (*) symbols indicate $p<0.05$.

4.4.4 The effect XBR exposure on the magnitude and dynamics of DNA double stranded damage and repair in UVW/NAT, SK-N-BE and A375 cells

Exposure of cells to ionising radiation results in various types of DNA damage, one of which is DNA DSBs. As DNA SSBs are more easily repaired and thus harder to accurately quantify, in this study the formation and repair of DNA DSBs was assessed to provide information regarding the effects of XBR and AuNPs alone and in combination. The formation of DNA DSBs results in rapid phosphorylation of the histone protein H2AX at the Ser-139 location (γ-H2AX), where the phosphorylation of H2AX has been shown to correlate with the number of DNA DSBs formed. The number of γ-H2AX foci therefore increases with increasing DNA DSBs formation, and decreases as the DNA DSBs are repaired over time (Short et al., 2007). In this study, assessment of the number of γ-H2AX foci using immunohistochemistry was used to provide a measure of the magnitude and dynamics of DNA damage and repair following XBR exposure.

Before combination studies, each cell line was characterised to establish the time points which would allow changes in DNA damage and repair from the combination of AuNPs with XBR to be assessed. The number of γ-H2AX foci was therefore determined in UVW/NAT, SK-N-BE and A375 cells at 0.5, 1, 2, 5 and 24 hours after XBR exposure with 1 Gy, 2 Gy and 4 Gy of XBR. The average number of γ-H2AX foci/cell at each radiation dose over time is presented in Figure 4-6.

In each cell line the number of γ-H2AX foci/cell increased from 0.5-2 hours after irradiation at all XBR doses. At 5 hours post irradiation the number of γ-H2AX foci had decreased in all cell lines compared to 2 hours post irradiation but still remained significantly elevated compared to untreated control cells (Figure 4-6). The number of γ-H2AX foci/cell in UVW/NAT, SK-N-BE and A375 cells decreased significantly from 39 foci/cell±1.25, 48 foci/cell±2.60 and 34 foci/cell±1.95 at 2 hours after exposure to 2 Gy XBR to 30 foci/cell±5.96 ($p<0.05$), 24 foci/cell±0.28 ($p<0.0001$) and 20 foci/cell±1.33 ($p<0.0001$) respectively 5 hours after XBR exposure. 24 hours after irradiation with 2 Gy, the number of γ-H2AX foci/cell had decreased further compared to 5 hours post irradiation. Foci numbers per cell 24 hours post irradiation were 17 foci/cell±1.04 ($p<0.001$), 15 foci/cell±0.97 ($p<0.01$) and 15 foci/cell±1.63 ($p<0.05$) in

UVW/NAT, SK-N-BE and A375 cells respectively. Despite this decrease, the number of γ-H2AX foci/cell 24 hours after irradiation in all cell lines examined remained significantly greater than in untreated control cells at all XBR doses with the exception of 1 Gy in UVW/NAT and A375 cells.

Additionally, the number of γ-H2AX foci increased with increasing XBR dose where the number of γ-H2AX foci/cell in UVW/NAT, SK-N-BE and A375 cells at 2 hours post irradiation increased from 38 foci/cell±3.94, 38 foci/cell±2.36 and 32 foci/cell±1.55 following 1 Gy XBR exposure to 39 foci/cell±1.25, 48 foci/cell±2.60 ($p<0.001$) and 34 foci/cell±1.95 following 2 Gy XBR exposure.

A375 cells displayed the greatest fold increase in γ-H2AX foci compared to untreated control cells at 2 hours after 1 Gy and 2 Gy XBR exposure and SK-N-BE cells the lowest. The average fold increase compared to untreated control cells in UVW/NAT, SK-N-BE and A375 cells were 9.4±2.85, 6.7±1.53 and 11.9±1.34 2 hours after 1 Gy exposure and 11.5±5.10, 8.4±1.87 and 12.9±0.13 2 hours after 2 Gy exposure respectively. This observation concurred with the clonogenic survival data (Figure 4-1) which demonstrated that A375 had the highest sensitivity towards XBR and SK-N-BE cells the least.

Based on the effect of XBR alone on the formation and resolution of γ-H2AX foci as a single agent, the effects of AuNPs in combination with XBR were investigated 2 and 24 hours after irradiation. These timepoints would allow any enhancement in the formation and resolution of γ-H2AX foci as an effect of AuNPs and XBR in combination, compared to XBR alone to be detected.

(A-1)

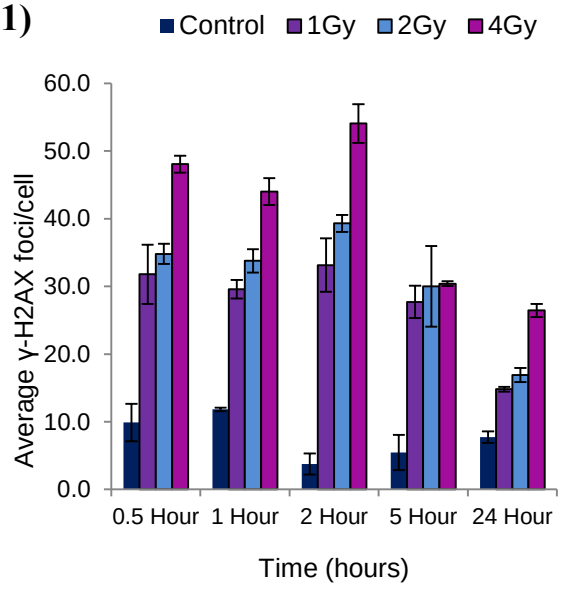

(A-2)

Time (hours)	1Gy	2Gy	4Gy
2.0 vs. 5.0	**	*	****
5.0 vs 24.0	*	***	ns

(B-1)

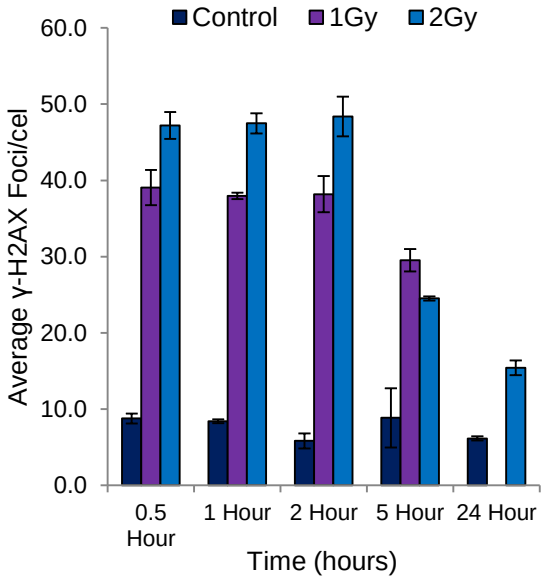

(B-2)

Time (hours)	1Gy	2Gy
2.0 vs. 5.0	**	****
5.0 vs 24.0	****	**

Figure 4-6 continued overleaf

(C-1)

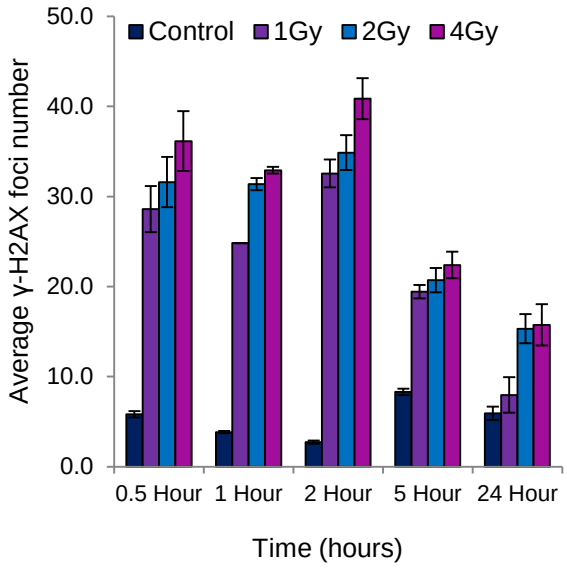

(C-2)

Time (hours)	1Gy	2Gy	4Gy
2.0 vs. 5.0	****	****	***
5.0 vs 24.0	***	*	**

Figure 4-6: The effect of XBR exposure on the formation and resolution of γ-H2AX foci in UVW/NAT, SK-N-BE and A375 cells.

Cells were exposed to 0-4 Gy XBR and the mean number of γ-H2AX foci/cell measured at 0.5, 1, 2, 5 and 24 hour after irradiation using immunohistochemistry. Results presented are the mean number of γ-H2AX foci/cell (mean ± sd) of 3 independent experiments in UVW/NAT (A-1), SK-N-BE (B-1) and A375 (C-1) cells respectively. Two-way ANOVA was used to determine statistically significant effects of radiation and time on the formation and resolution of γ-H2AX foci/cell for each XBR dose between 2 and 5 hours, and 5 and 24 hours post irradiation and is presented for UVW/NAT (A-2), SK-N-BE (B-2) and A375 cells (C-2). All tests were performed at the 95% C.I. One (*), two (**), three (***) and four (****) symbols indicate $p<0.05$, $p<0.01$, $p<0.001$ and $p<0.0001$ respectively and ns indicates no significance.

4.4.5 The effect of AuNPs in combination with XBR on the magnitude and dynamics of DNA double strand break and repair in UVW/NAT, SK-N-BE and A375 cells

The mean number of γ-H2AX foci/cell was measured in UVW/NAT, SK-N-BE and A375 cells following treatment with 2 nM AuNPs and 2 Gy XBR alone and in combination at 2 and 24 hours after irradiation (Figure 4-7).

In each of the cell lines investigated incubation with 2 nM AuNPs alone for 24 hours had no significant effect on the number of γ-H2AX foci/cell compared to untreated control cells at either timepoint measured.

In UVW/NAT cells the number of γ-H2AX foci/cell was 3 9foci/cell±1.25, 2 hours after 2 Gy XBR exposure, and increased significantly to 47 foci/cell±0.77 ($p<0.0001$) in cells exposed to XBR and AuNPs. Between 2 hours and 24 hours post XBR exposure the average number of foci/cell in cells exposed to XBR alone decreased by 57%±4 however, in the presence of AuNPs the number of γ-H2AX foci/cell had decreased by only 29%±2 ($p<0.0001$). This suggested that the presence of AuNPs in combination with XBR both increased the magnitude of DNA damage and reduced the resolution of DNA DSBs.

In SK-N-BE cells, there was no significant difference between the number of γ-H2AX foci/cell induced by the combination of AuNPs and 2 Gy XBR compared to 2 Gy alone, 2 hours after irradiation (38 foci/cell±3.70 vs. 42 foci/cell±8.01 $p>0.05$). Likewise, 24 hours after irradiation the average number of γ-H2AX foci/cell in cells exposed to XBR in combination with AuNPs was 17 foci/cell±1.77 compared to 15 foci/cell±0.78 ($p>0.05$) for cells exposed to 2 Gy alone. This suggested that the presence of AuNPs in combination with XBR in SK-N-BE cells caused no increase in the formation of DNA DSBs and also has no effect on the resolution of DNA DSBs compared to XBR alone.

In A375 cells, there was no significant difference between the number of γ-H2AX foci/cell induced by the combination of AuNPs and 2 Gy XBR compared to 2 Gy alone 2 hours after irradiation (35 foci/cell±1.95 vs. 34 foci/cell±1.69 $p>0.05$). However, 24 hours after irradiation the average number of foci/cell in cells exposed to XBR alone

had decreased by 56%±4 whilst in cells treated with AuNPs and XBR in combination, the average number of γ-H2AX foci/cell reduced by only 16%±8 ($p<0.0001$), suggesting that the presence of AuNPs reduced the resolution of DNA DSBs, compared to XBR alone.

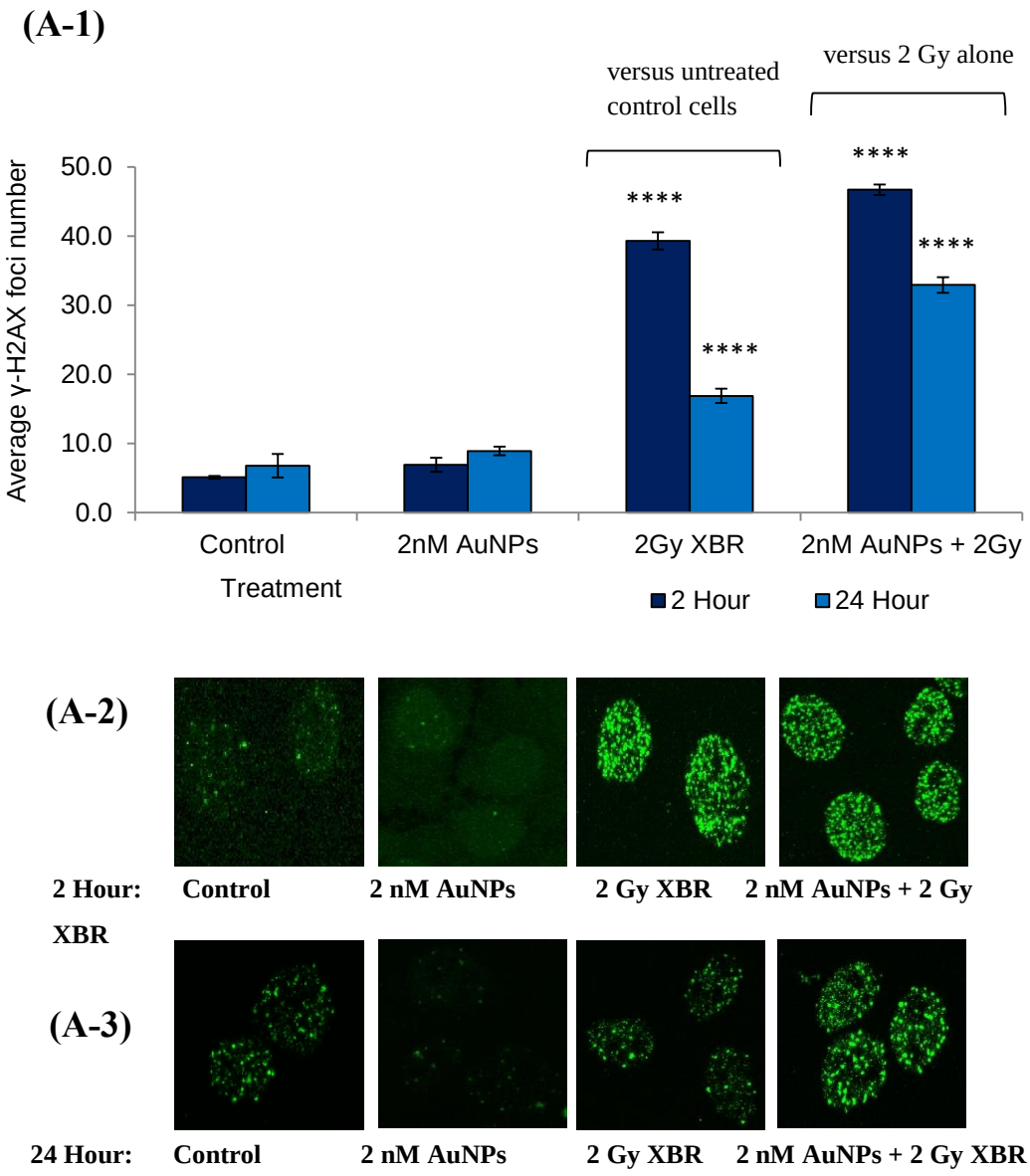

Figure 4-7 continued overleaf

(B-1)

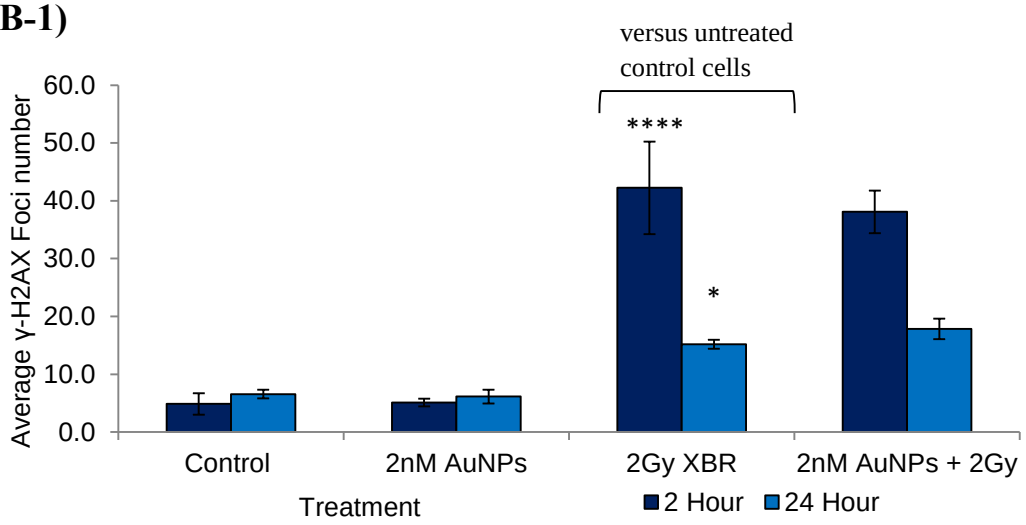

(B-2)

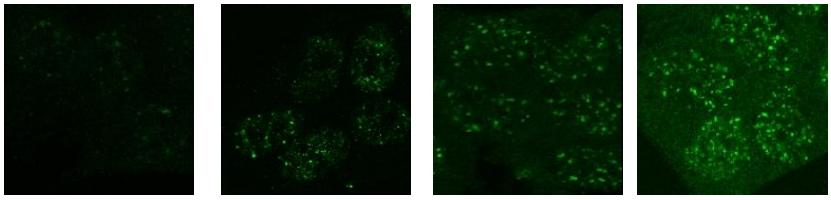

2 Hour: Control **2 nM AuNPs** **2 Gy XBR** **2 nM AuNPs + 2 Gy XBR**

(B-3)

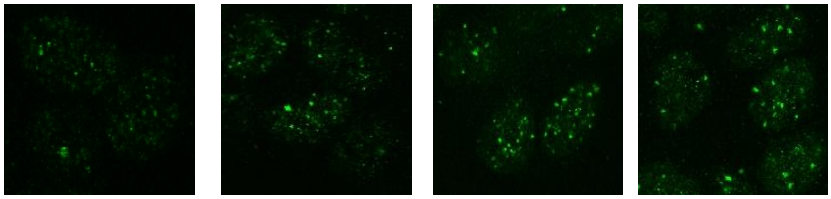

24 Hour: Control **2 nM AuNPs** **2 Gy XBR** **2 nM AuNPs + 2 Gy XBR**

Figure 4-7 continued overleaf

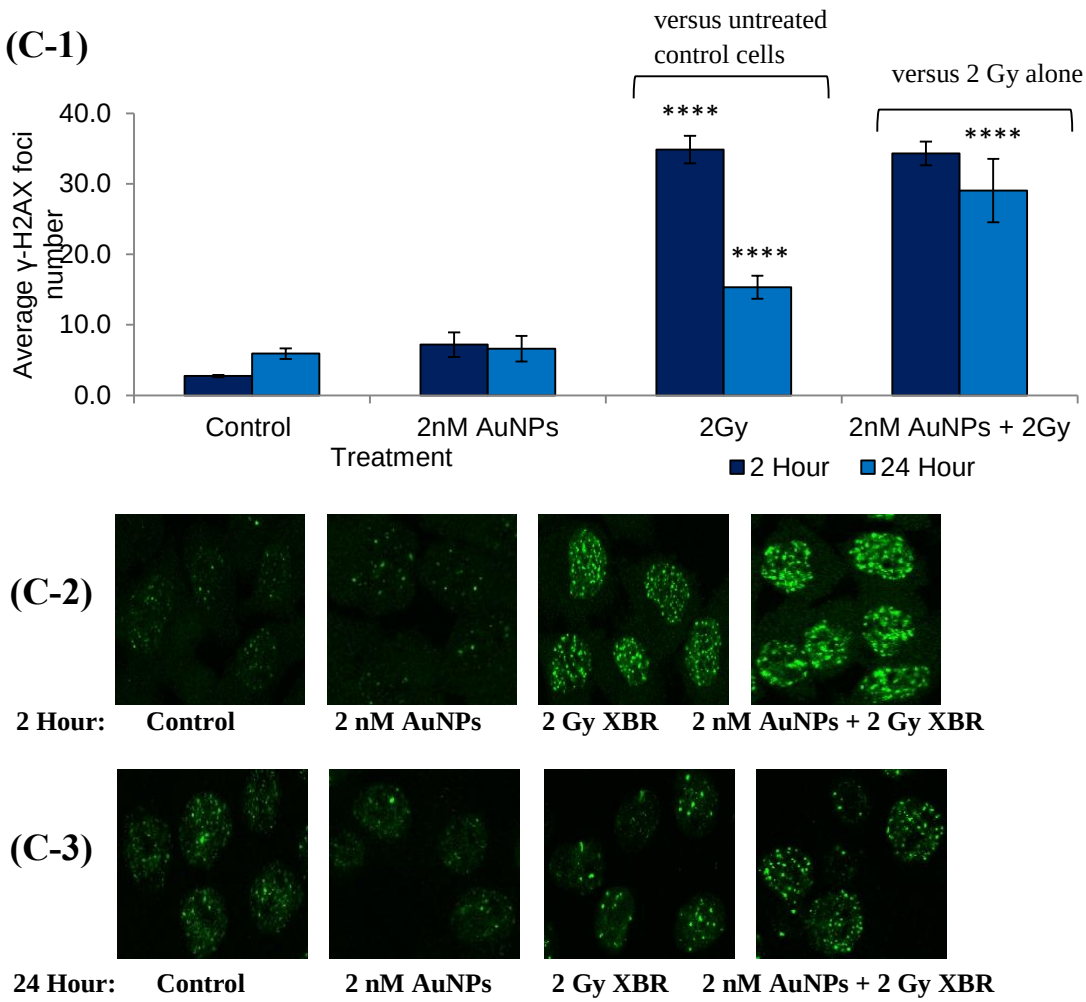

Figure 4-7: The effect of 2 nM AuNPs and 2 Gy XBR alone and in combination on the formation and resolution of γ-H2AX foci in UVW/NAT, SK-N-BE and A375 cells.

Each cell line was treated with 2 nM AuNPs for 24 hours prior to 2 Gy XBR exposure. The mean number of γ-H2AX foci/cell was assessed 2 and 24 hours after irradiation using immunohistochemistry. Results presented are the mean number of γ-H2AX foci/cell (mean ± sd) of 3 independent experiments for AuNPs and XBR alone and in combination in UVW/NAT (A), SK-N-BE (B) and A375 (C) cells respectively. Two-way ANOVA was used to determine if statistically significant changes in the number of γ-H2AX foci/cell resulted as an effect of 2 nM AuNPs and 2 Gy XBR alone (compared to untreated control cells) or in combination (compared to the effects of XBR alone). All tests were performed at the 95% C.I. One (*), three (***) and four (****) symbols indicate $p<0.05$, $p<0.001$ and $p<0.0001$ respectively. Representative images of γ-H2AX foci in each treatment group at 2 hours (A/B/C-2) and 24 hours (A/B/C-3) are presented.

In summary, the data demonstrated that in UVW/NAT cells the increased clonogenic cell kill observed from the combination of 2 nM AuNPs with 2 Gy XBR was associated with an increase in double stranded DNA damage and a decrease in the repair of DNA DSBs, compared to XBR alone. In A375 cells, however the increased clonogenic cell kill observed from the same combination is associated only with a decrease in the repair of DNA DSBs, with no increase in the number of γ-H2AX foci observed compared to XBR alone. In SK-N-BE cells the combination of AuNPs and XBR had no effect on the formation or repair of double stranded DNA damage compared to XBR alone which was consistent with the clonogenic survival data which demonstrated no increase in clonogenic cell kill from combination treatments.

4.4.6 The effect of XBR and AuNPs alone and in combination on the activity of caspase 3 in UVW/NAT, SK-N-BE and A375 cells

Caspase 3 activity assays were performed to assess if exposure of UVW/NAT, A375 and SK-N-BE cells to AuNPs and XBR alone, and in combination induced cell apoptosis. In this study, caspase 3 activity was measured in UVW/NAT, SK-N-BE and A375 cells at 6 and 24 hours post treatment with AuNPs from 0-2 nM, 2 Gy XBR and treatment with 2 nM AuNPs and 2 Gy XBR (Figure 4-8).

In all cell lines investigated, incubation with AuNPs for 6 or 24 hours at concentrations of 0.5 nM, 1 nM and 2 nM induced no significant increase in caspase 3 activity compared to untreated control cells. Similarly, exposure to 2 Gy XBR alone induced no significant increase in caspase 3 activity compared to untreated control cells in any of the cell lines examined. The combination of 2 nM AuNPs with 2 Gy XBR induced no significant increase in caspase 3 activity compared to XBR exposure alone in any of the cell lines examined. At 24 hours after treatment the average fold-increase in fluorescence intensity following exposure to 2 nM AuNPs and 2 Gy was 1.08±0.12, 1.68±0.53 and 1.00±0.04 compared to 0.98±0.04 ($p>0.05$), 1.22±0.03 ($p>0.05$) and 1.00±0.04 ($p>0.05$) for 2 Gy alone in UVW/NAT, SK-N-BE and A375 cells respectively. In summary, AuNPs and 2 Gy XBR as single treatments had no effect on caspase 3 activity compared to untreated control cells. The combination of 2 nM

AuNPs and 2 Gy XBR also had no effect on caspase 3 activity compared to 2 Gy XBR alone at any of the timepoints investigated. This suggested that the increased clonogenic cell kill observed from the combination of AuNPs and XBR in UVW/NAT and A375 cells was not a result of cell death by caspase mediated apoptosis.

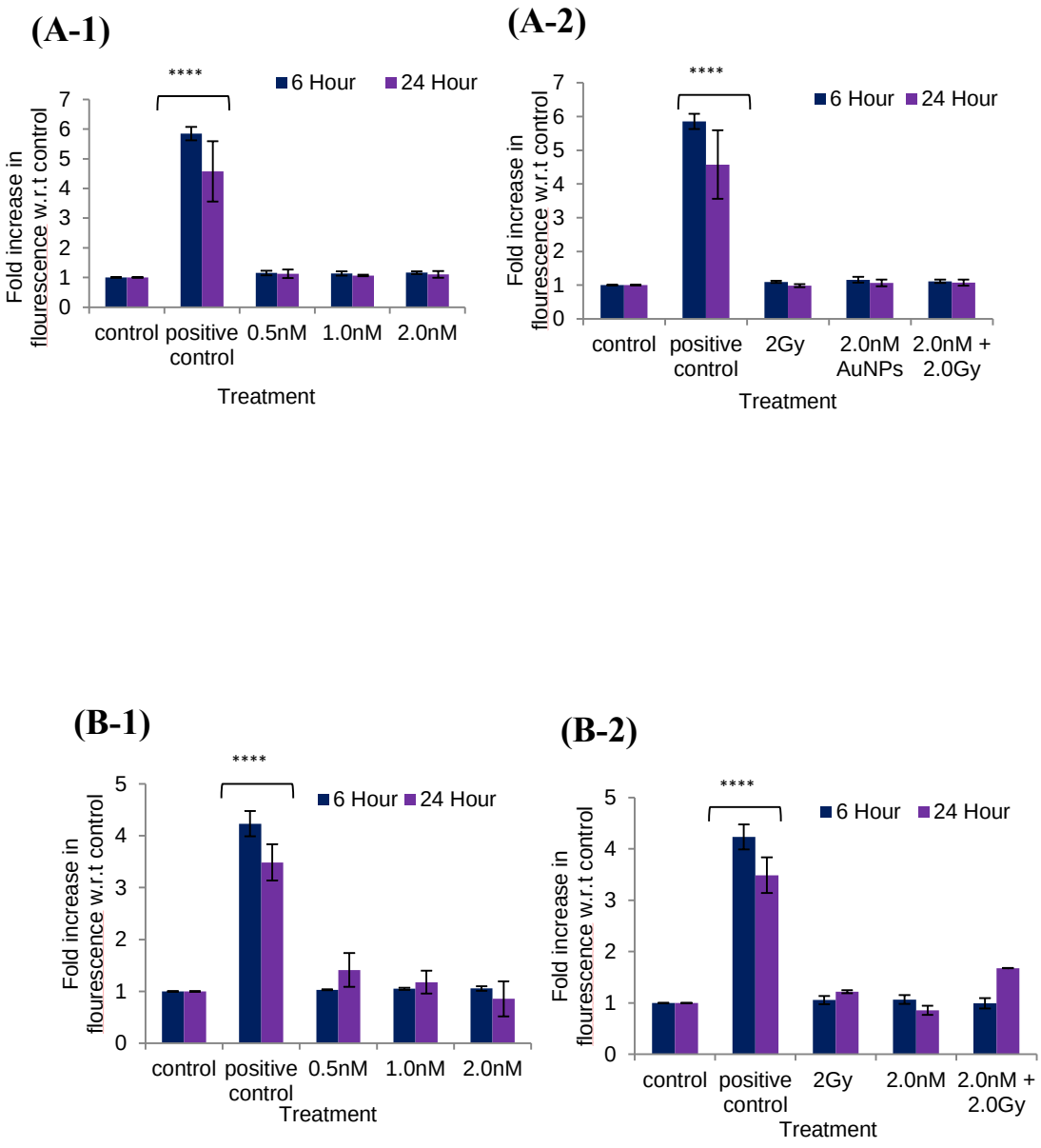

Figure 4-8 continued overleaf

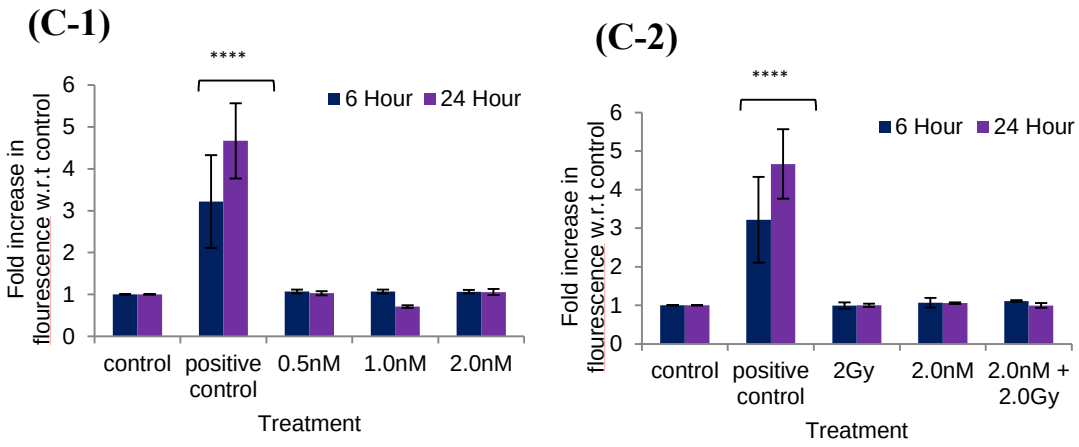

Figure 4-8: The effect of AuNPs and XBR alone and in combination on the activity of caspase 3 measured in UVW/NAT, SK-N-BE and A375 cells.

Cells were exposed to AuNPs from 0-2 nM alone or to AuNPs at 2 nM in combination with XBR at 2 Gy. The activity of caspase 3 was measured at 6 and 24 hours after irradiation in UVW/NAT (A), SK-N-BE (B) and A375 (C) cells. In all experiments Staurosporine (50µM) was used as a positive control for apoptosis associated with increased caspase 3 activity. The data is presented as the mean fold increase in fluorescence intensity (mean ± sd) of 3 independent experiments for AuNPs alone (A-1, B-1, C-1), compared to untreated control cells and AuNPs in combination with XBR (A-2, B-2 and C-2) compared to 2 Gy XBR alone for each cell line. Two-way ANOVA with Bonferroni post-hoc testing was used to determine if treatment with AuNPs alone induced significant caspase 3 activity compared to untreated controls and to determine if the combination of AuNPs with XBR induced significant caspase activity compared to XBR alone. All tests were performed at the 95% C.I. Four (****) symbols indicate $p<0.0001$.

4.5 Discussion

The aim of this study was to establish the radiosensitising potential of in house synthesised AuNPs to 225 kVp XBR. The data presented demonstrated that the radiosensitisation induced by AuNPs was cell line specific, with radiosensitisation observed in both the human glioma cell line, UVW/NAT (DEF_{50} 1.12) and the human melanoma cell line, A375 (DEF_{50} 4.68), but not in the human neuroblastoma cell line, SK-N-BE (DEF_{50} 0.93). Where radiosensitisation was observed, it was associated with a decrease in the resolution of γ-H2AX foci, but not necessarily with an increase in the number of DNA DSBs, compared to XBR exposure alone. In A375 cells 24 hours post irradiation, the number of γ-H2AX foci had decreased by 56%±5, in cells exposed to 2 Gy XBR. However in the presence of 2 nM AuNPs, γ-H2AX foci/cell decreased by only 16%±9, indicating that the presence of AuNPs significantly reduced the resolution of DNA DSBs. Similarly, in UVW/NAT cells the combination treatment resulted in less repair of DNA double strand breaks 24 hours after irradiation, with a decrease in foci number from 57%±4 in cells treated with 2 Gy alone to 29%±1 in combination treated cells.

In the previous chapter it was found that AuNPs as a single agent induced a decrease in the clonogenic capacity in the 3 cell lines investigated at the highest administered AuNP concentration (Figure 3-4). Data from the current chapter indicated that this decrease was not a result of either increased double stranded DNA damage (Figure 4-7), or cell death via caspase mediated apoptosis (Figure 4-8). Previous studies have reported that AuNPs induce toxicity by the generation of oxidative stress within the cell (Manke et al., 2013; Pan et al., 2009). In this present study the production of ROS was not measured however this could be performed in future studies using fluorescent DCFH-DA assays to measure intracellular ROS and determine if the presence of nanoparticles in combination with radiation significantly increased the ROS concentration (Aranda et al., 2013). Additionally, as it is hypothesised that the radiosensitisation results through a ROS mediated mechanism, ROS scavengers could be used to remove the ROS species generated following radiation exposure in the presence and absence of AuNPs. Analysis of the effect of diminished ROS on the clonogenic survival and DNA damage and repair in the presence and absence of AuNPs, compared to the results in this study would indicate whether ROS affected the

observed radiosensitisation and the effect on DNA damage and repair (Kim et al., 2005).

In some previous studies the observed toxicity was not associated with a significant increase in caspase 3/7 activity, indicating that the mode of cell death was not via apoptosis (Pan et al., 2009, 2007). However this was not true of all studies, where some have demonstrated that AuNP toxicity induced apoptotic cell death via p53 and caspase 3 and 9 assays (Selim and Hendi, 2012). Results of this present study demonstrated that the observed radiosensitisation was not a result of caspase 3 mediated apoptosis. Following on from this the reduction in cell survival could be further characterised by examining early and late cell apoptosis, together with necrotic cell death using dual staining with PI and Annexin V.

The rationale behind the radiosensitisation potential of AuNPs, discussed in section 1.6.1, is based on the ability of AuNPs to increase the dose deposition of radiation within the target volume due to differences in the photon mass absorption coefficient of AuNPs, compared to soft tissue (Figure 1-3). Photoelectric absorption of radiation by the AuNPs causes ionisations in the AuNPs, which ultimately leads to the ejection of secondary electrons which deposit their energy in the vicinity of the AuNPs (Figure 1-4) (Coulter et al., 2013). One possible mode of action is that the secondary electrons produced by the AuNPs interact directly with nuclear DNA, resulting in DNA DSBs, however this is unlikely due to the low energy of the secondary electrons. More likely however is the interaction of the secondary electrons with intracellular water to generate ROS which contribute to the formation of DNA SSBs and other DNA lesions. It has also been proposed by Sicard-Roselli *et al*, (2014), that ·OH species generated by radiolysis could interact directly with structured water layers which exist at the AuNP-water interface as a result of charges on the AuNP surface aligning the dipoles of water. The injection of energy into this AuNP-water system through the interaction of ·OH species could result in breaking of the hydrogen bonding which holds the layers together, and result in a cascade of ·OH production (Carrasco et al., 2012; Sicard-Roselli et al., 2014).

Based on the suggested mechanisms, it is most likely therefore that the interaction of radiation with DNA in the presence of AuNPs is enhanced by a free radical mediated

mechanism. Within target cells two mechanisms of DNA damage are therefore occurring, namely damage induced by radiation alone and subsequent damage induced by the interaction of radiation with AuNPs. ROS mainly elicit damage in the form of oxidised bases and DNA SSBs. Within normal cells, the majority of DNA SSBs are easily repaired, however genomic instability and aberrant repair processes in cancer cells can leave SSBs unrepaired which can lead to subsequent genomic instability and the conversion of SSBs into more complex damage which is more difficult to repair. In an experimental setting, this mechanism would not necessarily present as an increase in the number DNA DSBs, but possibly as a reduction in the repair of the DNA damage, due to an increase in the complexity of the DNA breaks which results in the failure of cells to resolve them. This is consistent with the results of this study where, the combination of AuNPs with XBR did not necessarily induce an increase in the absolute number of γ-H2AX foci/cell, but a decrease in the resolution of γ-H2AX foci/cell, compared to XBR alone.

This was consistent with the results presented by Taggart *et al*, (2014) where the number of 53BP1 foci in the human breast cancer MDA-MB-231cells, and human prostate cancer DU145 cells were significantly higher following treatment with 1.9nm AuNPs in combination with 2 Gy XBR, at 1 hour and 24 hours post irradiation, compared to 2 Gy XBR alone (Taggart et al., 2014). Although these previous studies utilised different cell lines and AuNPs with different diameters and surface functionalisation to this present study, their results support the general principle of AuNP-induced radiosensitisation through an increase in the complexity of DNA damage.

Other studies have demonstrated an increase in the absolute number of γ-H2AX foci in response to AuNPs combined with XBR, suggesting an increased in the number of DNA double stranded breaks. In this present study an increase in the number of γ-H2AX foci/cell was found in the UVW/NAT cell line, but not in A375 cells which demonstrated the greatest DEF. The study by Liu *et al*, (2010) demonstrated significantly higher numbers of γ-H2AX foci 1 hour post irradiation, in murine breast carcinoma EMT-6 cells treated with PEGylated-AuNPs in combination with 2 Gy, compared to cells exposed to 2 Gy alone (Liu et al., 2010). Similarly, in the study by

Chattopadhyay *et al*, (2013) both AuNPs functionalised with the human epidermal growth factor (Au-T) and unfunctionalised AuNPs (Au-P) in combination with 11 Gy XBR induced an increase in the number of γ-H2AX foci by 3.3-fold and 1.7-fold respectively 30 minutes post XBR exposure, compared to XBR exposure alone (Chattopadhyay et al., 2013). These studies demonstrate that the combination of AuNPs with XBR induced an increase in the formation of γ-H2AX foci, compared to XBR alone, suggesting that the presence of AuNPs increases the magnitude of double stranded DNA damage which was observed only in UVW/NAT cells in this study. Neither of the aforementioned studies however measured the later effects of XBR and AuNPs, therefore the effect of AuNPs on the repair of radiation induced double stranded DNA damage cannot be determined as in this present study.

In this study, the greatest radiosensitisation with AuNPs was observed in A375 cells (DEF_{50}=4.68, compared to 1.12 and 0.93 in UVW/NAT and SK-N-BE cells respectively). Theoretical studies have shown that the amount of Au within the target area will lead to an increase in the ionisations and secondary electron production, and therefore a greater increase in the effective radiation dose (Su et al., 2014). This was experimentally confirmed by Jain *et* al, (2011), who demonstrated cell line specific radiosensitisation which was directly related to the degree of AuNP uptake by each cell line (Jain et al., 2011). In this present study, variations in the observed radiosensitisation by AuNP could not be attributed to differences in intracellular uptake of the AuNPs by the 3 cell lines as A375 cells demonstrated the lowest uptake of AuNPs. The significantly higher radiosensitisation observed in A375 cells was therefore not a result of increased Au content within the target area. It is likely however, that other intrinsic radiobiological factors within the cells, such as the inherent radiosensitivity of different cell lines also contribute to the observed radiosensitisation.

It was demonstrated in this study that A375 cells were more sensitive to radiation as a single agent, compared to UVW/NAT and SK-N-BE cells (Figure 4-1). This was likely due to the less efficient repair of double stranded DNA damage, where A375 cells demonstrated a fold difference of 2.64±0.63 in the number of γ-H2AX foci 24 hours after treatment with 2 Gy XBR compared to untreated control cells, compared to fold

differences of 2.19±0.10 and 2.50±0.27 in UVW/NAT and SK-N-BE cells respectively.

Additionally, the cells capacity to neutralise intracellular ROS has been shown to influence the sensitivity of cells to radiation. Jayakumar *et al,* (2014) recently demonstrated that increased basal levels and radiation induced gene expression of the redox sensitive transcription factor (Nrf2) which controls the transcription of anti-oxidants such as superoxide dismutase (SOD) and glutathione is associated with radioresistance (Jayakumar et al., 2014). The intracellular levels of ROS and the anti-oxidant capability of cells in addition to affecting their sensitivity to radiation as a single agent could also influence the radiosensitisation observed from the combination of AuNPs with ionising radiation. One of the primary effects of the secondary electrons ejected following ionisations within the AuNPs is hydrolysis of intracellular water to generate ROS, therefore in cell lines which have a greater anti-oxidant capacity the generated ROS will have a lower efficacy and less radiosensitisation may be observed. The intracellular ROS levels of the cell lines used in this study, and their capacity to neutralise ROS through the expression of anti-oxidants such as superoxide dismutase (SOD) and glutathione was not measured during this study, however this would be an interesting follow up study to investigate if the greater sensitivity of A375 cells to XBR alone, and the greater radiosensitisation achieved, compared to UVW/NAT and SK-N-BE cells is due to higher basal and radiation induced levels of ROS in A375 cells, and a lower anti-oxidant capability of A375 cells.

Following on from this study there are several ways in which it was hypothesised that the radiosensitisation and radiation dose enhancement could be increased. The subsequent chapters investigated the combination of AuNPs with high energy β and γ radiation in the form of the radioisotope ^{131}I conjugated to meta-iodobenzyleguanidine (MIBG), and the potential of HGNs to act as radiosensitisers towards both kVp XBR and radiation from [^{131}I]-MIBG.

Chapter 5

Investigation of the radiosensitisation potential of AuNPs in combination with the radioisotope ^{131}I in the form of [^{131}I]-MIBG

Chapter 5: Investigation of the radiosensitisation potential of AuNPs in combination with the radioisotope ^{131}I in the form of [^{131}I]-MIBG

5.1 Introduction

As discussed in section 1.6.2, experimental studies which have examined the photon absorption in AuNPs (Figure 1-3), have demonstrated that AuNP radiosensitisation in a variety of cell lines results with photon beams across the energy range 6 kV to 6 MV (Coulter et al., 2013). Additionally, the potential of AuNPs to sensitise cells to radioisotopes has also been investigated, most commonly in an attempt to improve current low energy brachytherapy. Ngwa *et al*, (2012) reported a dose enhancement factor of 1.7-2.3 following 24 hour treatment of HeLa cells with AuNPs in combination with ^{125}I brachytherapy seeds which had photon energy of 28 keV. Due to the close energy match between the photon energy and the electron ejection energy within AuNPs the radiosensitisation observed in this experiment was likely to be a result of a dose enhancement occurring through photoelectric absorption.

There have been numerous studies assessing AuNPs as delivery vehicles for imaging purposes and as a potential tool for tumour therapy utilising a variety of radioisotopes such as, ^{125}I (Su et al., 2015), ^{131}I (Kao et al., 2013) and ^{111}In (Ng et al., 2014). However to date, no study has provided experimental evidence of AuNP radiosensitisation with higher energy targeted radionuclides such as ^{131}I. In the study by Kao et al, (2013), AuNPs were conjugated with the EGFR specific monoclonal antibody, CD225 in part to facilitate uptake of AuNPs but also to enable radioimmunotherapy via ^{131}I conjugation. A significant dose dependant reduction in the viability of a lung cancer cell line was evident. However, AuNP radiosensitisation could not be assessed in this study due to the inability of the lung cancer cell line to take up unconjugated ^{131}I, thus not allowing assessment of the isotope alone.

As previously discussed (section 1.6, section 4.5) the total physical enhancement in radiation dose delivered through AuNP and radiation interactions is dependent on photon energy. The probability of photoelectric ionisation of the AuNPs is most likely in the kilovoltage range of energy where the differential in mass absorption coefficient

between soft tissue and AuNPs is high. ^{131}I decays by β emission where 89% of the β particles have energy of 606.3 keV. Following this decay, intensive gamma rays are emitted, of which 81% have energy of 364.5 keV. At these energies, photon absorption and subsequent ionisation occurs predominately through Compton scattering which results in only sparse ionisation effects throughout the cell and therefore the probability of an enhancement in total dose delivered in the presence of AuNPs is low. It is possible that AuNP sensitisation to ^{131}I may occur as a result of photoelectric absorption with lower energy emissions, as suggested by (McMahon et al., 2011), or through an increase in $^{\cdot}$OH generation in the presence of AuNPs, proposed by (Sicard-Roselli et al., 2014) and discussed fully in section 1.6.4. It is likely however, that the DEFs from AuNP sensitisation of ^{131}I will be lower than those observed with lower energy kVp beams as experimental evidence has demonstrated that greater radiosensitisation results where the photoelectric effect is likely to dominate (Jain et al., 2011). Despite this, we hypothesised that AuNPs may sensitise cells to ^{131}I and that the mechanism might at least in part be due to photoelectric ionisation of AuNP by β particles and γ rays with the rationale behind this hypothesis is fully discussed in section 1.6.6.

5.2 Aims

The aims of this study were to establish the dose response of UVW/NAT, SK-N-BE and A375 cells to [^{131}I]-MIBG as a single agent, before assessing the radiosensitising potential of AuNPs in combination with [^{131}I]-MIBG by assessing the reduction in cell survival.

Following this, the effect of single and combination treatments of AuNPs and [^{131}I]-MIBG on the progression of cells through the cell cycle and the DNA damage and repair kinetics was assessed in both cell lines.

5.3 Materials and Methods

5.3.1 Cells and culture conditions

The human glioblastoma cell line UVW/NAT, human neuroblastoma cell line SK-N-BE and human melanoma cell line A375 were employed in this study. All cells were cultured and maintained as detailed in sections 2.3.1 and 3.3.4.

5.3.2 Transfection of A375 cells with the NAT gene

The human melanoma cell line A375 was transfected with the noradrenaline transporter gene by the method established by Boyd *et al* (Boyd et al., 1999).

Following transfection of A375 cells the uptake of [^{131}I]-MIBG by A375/NAT cells was assessed and compared to the uptake of [^{131}I]-MIBG by both UVW/NAT and SK-N-BE cells (data not shown). It was determined at this stage that the uptake of [^{131}I]-MIBG by A375/NAT cells was insufficient and this cell line was not employed in any further studies investigating the effects of [^{131}I]-MIBG.

5.3.3 Synthesised 20 nm AuNPs

All gold nanoparticles were synthesised in the Graham Lab (University of Strathclyde) (Brown et al., 2010) using the Turkevich-Frens method as described in section 3.3.1.

5.3.4 Treatment of cells with AuNPs and [^{131}I]-MIBG

The concentration range of synthesised AuNPs employed in this study was 0-2 nM. All cells lines were incubated with AuNPs for 24 hours as described in section 2.3.3.

For irradiation of cells with [^{131}I]-MIBG, cells were incubated with 0-6 MBq/mL [^{131}I]-MIBG for 2 hours as this duration had been shown in previous studies to deliver maximal uptake (Armour et al., 1997). Following this, excess [^{131}I]-MIBG was

removed by washing cells thrice with PBS and cells incubated for a further 24 hours in fresh growth medium.

For all combination experiments cells were incubated with AuNPs in the concentration range 0-2 nM for 24 hours and then exposed to [^{131}I]-MIBG across the dose range 0-3 MBq.

5.3.5 Clonogenic survival assay

Clonogenic survival assays were used to assess the clonogenic survival in each cell line following exposure to [^{131}I]-MIBG alone, and then to assess any radiosensitisation achieved with AuNPs in combination with [^{131}I]-MIBG For the assessment of UVW/NAT cells and SK-N-BE cells, clonogenic survival assays were performed as described in section 2.3.5 and 3.3.7. All results are presented as the mean cell survival fraction normalised with respect to untreated control cells for [^{131}I]-MIBG and AuNP alone and to AuNP alone in all combination treatments (mean ± sd) of 3 independent experiments.

5.3.6 Cell cycle analysis

The progression of cells through the cell cycle was determined to assess whether [^{131}I]-MIBG alone, and in combination with AuNPs caused an abrogation to the normal cycling of cells (Deitch et al., 1982; Pollack and Ciancio, 1990) and was performed as described in section 4.3.7. Three independent experiments were carried out and results presented as the percentage of cells in each phase of the cell cycle (mean ± sd).

5.3.7 γ-H2AX detection

The effect of [^{131}I]-MIBG alone and in combination with AuNPs on the magnitude and dynamics of DNA DSBs was determined as described in section 4.3.8. Results are

presented as the mean number of γ-H2AX foci/cell (mean ± sd) of 3 independent experiments.

5.3.8 Statistical Analysis

5.3.8.1 Analysis of variance (ANOVA)

All experiments were carried out 3 times, with results reported as the (mean ± sd). Clonogenic survival data are presented as the cell survival fraction normalised to untreated control cells for treatment with AuNPs and [^{131}I]-MIBG alone or normalised to AuNP treatment alone for combination treatments. Cell cycle data is presented as the percentage of cells within each phase of the cell cycle and γ-H2AX data as the number of γ-H2AX foci/cell for each treatment group. Results were evaluated using two-way ANOVA analysis with Bonferroni post-tests to determine if the effects of combination therapy on the clonogenic survival, progression and accumulation of cells throughout the cell cycle and the number of γ-H2AX foci/cell were statistically significant compared to the effects of [^{131}I]-MIBG alone. P-values lower than 0.05 were considered statistically different.

5.3.8.2 Linear quadratic analysis

To evaluate the radiosensitisation potential of AuNPs in combination with [^{131}I]-MIBG, the experimental clonogenic survival data for UVW/NAT and SK-N-BE cells was fitted to the linear quadratic model (equation 1) (Dale, 2004) using GraphPadPrism software, version 6.0.1, 2014 (CA) as described in section 2.3.6.2. The α and β values, IC_{50} and DEF at the 50% toxicity level were calculated for [^{131}I]-MIBG alone and in combination with AuNPs for each cell line using equations 2 and 3 as described in sections 2.3.6.2.

5.4 Results

5.4.1 Determining the effect of [^{131}I]-MIBG dose on the clonogenic survival of UVW/NAT and SK-N-BE cells using the linear quadratic model

The effect of [^{131}I]-MIBG exposure as a single agent on the clonogenic survival of UVW/NAT and SK-N-BE cells was investigated to determine the response of each cell line and to establish radiation dose range to be used in combination with AuNPs. There was a dose response relationship between administered radiation dose and clonogenic cell survival in each cell line, where the clonogenic cell survival reduced proportionally with increasing radiation dose (Figure 5-1).

The clonogenic data was fitted to the linear quadratic model as described in section 2.3.6.2. The doses of [^{131}I]-MIBG which killed 25%, 50% and 75% of the cell population (IC_{25-75}) were calculated in each cell line and were 1.26 MBq, 2.80 MBq and 5.03 MBq in UVW/NAT cells, and 2.00 MBq, 3.24 MBq and 4.69 MBq in SK-N-BE cells. The α values for each cell line, which describe the initial slope of the radiation survival curve, associated with lower doses of [^{131}I]-MIBG were 0.21 MBq^{-1}±0.04 and 0.03 MBq^{-1}±0.02 for UVW/NAT and SK-N-BE cells respectively. As the α value in UVW/NAT cells was higher than for SK-N-BE cells, it suggested that greater toxicity resulted in UVW/NAT cells following [^{131}I]-MIBG exposure, compared to SK-N-BE cells at lower [^{131}I]-MIBG doses.

Based on the effect of [^{131}I]-MIBG alone in each cell line the dose range from 0-3 MBq was used for subsequent AuNP combination studies as it allowed for decreases in survival fraction beyond that of radiation alone to be identified.

(A)

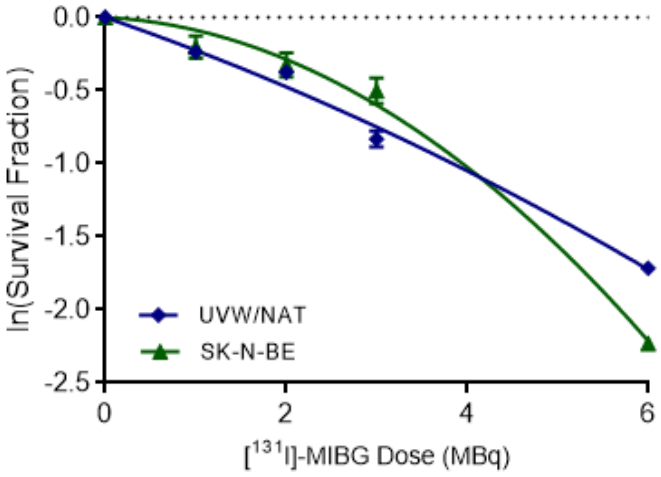

(B)

	UVW/NAT	SK-N-BE
α (MBq^{-1})	0.21±0.04	0.03±0.02
β (MBq^{-1})	0.01±0.008	0.06±0.004
R^2	0.94	0.98
IC_{25} (MBq)	1.26	2.00
IC_{50} (MBq)	2.80	3.24
IC_{75} (MBq)	5.03	4.69

Figure 5-1: Clonogenic survival of UVW/NAT and SK-N-BE cells exposed to increasing [^{131}I]-MIBG doses from 0-6 MBq.

Cells were exposed to [^{131}I]-MIBG from 0-6 MBq with clonogenic survival assays performed 24 hours after removal of [^{131}I]-MIBG. Clonogenic survival data were then fitted to the linear quadratic model and results are presented as the mean survival fraction (mean ± sd) of 3 independent experiments (A). The α, β and IC values for each cell line were calculated using GraphPad Prism software version 6.0.1 as detailed in section 2.3.6.2 (B)

5.4.2 Determination of the radiosensitising effect of AuNPs in combination with [^{131}I]-MIBG using the linear quadratic model

The effect of AuNPs on the radiation induced cell kill in UVW/NAT and SK-N-BE cells was assessed using clonogenic survival assays. Cells were incubated with AuNPs across the concentration range 0-2 nM for 24 hours, before irradiation with 0-3 MBq [^{131}I]-MIBG and clonogenic assays performed 24 hours after removal of [^{131}I]-MIBG. The mean clonogenic survival for cells treated with AuNPs in combination with [^{131}I]-MIBG were normalised to the effect of AuNP alone. Two-way ANOVA with Bonferroni post-hoc testing for multiple comparisons was carried out for each cell line to determine if the clonogenic survival fractions observed for cells treated with AuNPs in combination with [^{131}I]-MIBG were significantly different from those observed following exposure to [^{131}I]-MIBG alone. The clonogenic survival data for each cell line was then fitted to the linear quadratic model as previously described in section 2.3.6.2 using GraphPad Prism software version 6.0.1.

5.4.2.1 The effect of AuNPs in combination with [^{131}I]-MIBG on the clonogenic cell kill in UVW/NAT cells

In UVW/NAT cells incubated with AuNPs for 24 hours prior to [^{131}I]-MIBG exposure the clonogenic survival decreased significantly compared to cells exposed to [^{131}I]-MIBG alone at all AuNP concentration and [^{131}I]-MIBG dose combinations, with the exception of 0.5 nM AuNPs combined with 1 MBq (Figure 5-2(A-B)). Combination of 2 nM AuNPs with 1 MBq, 2 MBq and 3 MBq resulted in survival fractions of 0.37±0.08, 0.18±0.04 and 0.09±0.02 compared to 0.79±0.0 ($p<0.0001$), 0.69±0.02 ($p<0.0001$) and 0.44±0.05 ($p<0.001$) for 1 MBq, 2 MBq and 3 MBq alone.

The clonogenic survival data from Figure 5-2(A) was fitted to the linear quadratic model (Figure 5-2(C)) and values for α, β, IC_{50} and DEF_{50} calculated (Figure 5-2(D)). Incubation of UVW/NAT cells with AuNPs prior to [^{131}I]-MIBG exposure resulted in a concentration dependant decrease in the dose of [^{131}I]-MIBG required to kill 50% of the cell population (IC_{50}) where the IC_{50} values were 2.71 MBq for [^{131}I]-MIBG alone and 1.62 MBq, 1.08 MBq and 0.90 MBq in the presence of AuNPs at 0.5 nM, 1 nM and 2 nM respectively. The α values for the combination of 0.5 nM, 1 nM and 2 nM

AuNPs with [^{131}I]-MIBG were 0.14 MBq^{-1}±0.06, 0.72 MBq^{-1}±0.07 and 0.79 MBq^{-1}±0.03 compared to 0.12 MBq^{-1}±0.01 for [^{131}I]-MIBG alone. The concentration dependant increase in α value suggested that the presence of AuNPs resulted in an increase in the toxicity at lower [^{131}I]-MIBG doses compared to [^{131}I]-MIBG alone, as discussed in section 2.3.6.2. The DEFs calculated at the 50% toxicity level (DEF_{50}) were 1.68, 2.52 and 3.03 for [^{131}I]-MIBG in combination with 0.5 nM, 1 nM and 2 nM AuNPs and demonstrated that the presence of AuNPs resulted in a concentration dependant enhancement of clonogenic cell kill.

(A)

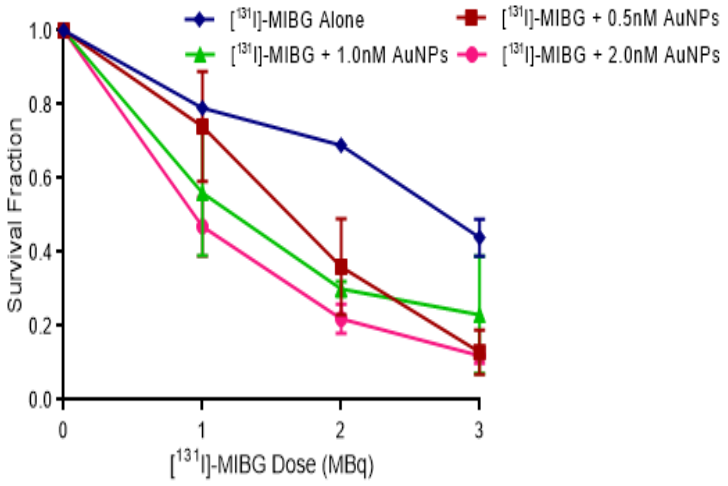

(B)

	0.5nM	1.0nM	2.0nM
1.0MBq	ns	*	****
2.0MBq	***	****	****
3.0MBq	***	*	***

Figure 5-2 continued overleaf

(C)

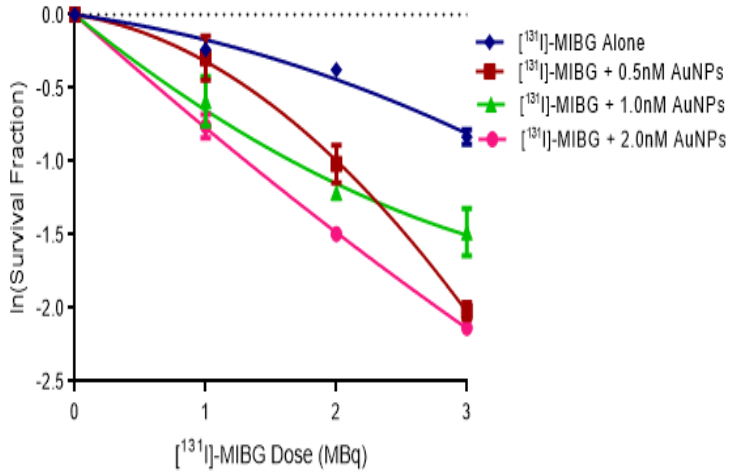

(D)

	0nM	0.5nM	1.0nM	2.0nM
α (MBq^{-1})	0.12±0.01	0.14±0.06	0.72±0.07	0.79±0.03
β (MBq^{-1})	0.05±0.04	0.17±0.02	-0.07±0.03	-0.02±0.01
R^2	0.97	0.99	0.97	1.00
IC_{50} (MBq)	2.71	1.62	1.08	0.90
DEF_{50}	1.00	1.68	2.52	3.03

Figure 5-2: Clonogenic survival of UVW/NAT cells exposed to AuNPs in combination with [^{131}I]-MIBG.

UVW/NAT cells were incubated with AuNPs from 0-2 nM for 24 hours. Following this, cells were exposed to [^{131}I]-MIBG from 0-3 MBq for 2 hours and clonogenic survival assays performed 24 hours after removal of [^{131}I]-MIBG. Clonogenic survival results are presented as the mean survival fraction (mean ± sd) of 3 independent experiments unless otherwise stated, normalised to AuNP alone treated cells (A). Statistical significant differences in cell survival fraction for AuNPs in combination with [^{131}I]-MIBG, compared to [^{131}I]-MIBG alone was assessed using two-way ANOVA with Bonferroni post-tests at 95% C.I. One (*), three (***) and four (****) symbols indicate $p<0.05$, $p<0.001$ and $p<0.0001$ and ns indicates no significance (B). Clonogenic survival data presented in (A) was fitted to the linear quadratic model using GraphPad Prism version 6.0.1 (C) and calculated values for the α and β coefficient and the IC_{50} and DEF_{50} for [^{131}I]-MIBG in combination with AuNPs at each AuNP concentration presented (D).

5.4.2.2 The effect of AuNPs in combination with [^{131}I]-MIBG on the clonogenic cell kill in SK-N-BE cells

In SK-N-BE cells incubated with AuNPs 24 hours prior to [^{131}I]-MIBG exposure, a statistically significant decrease in clonogenic survival, compared to the clonogenic survival of cells exposed to [^{131}I]-MIBG alone was observed at all AuNP concentrations and [^{131}I]-MIBG doses (Figure 5-3(A-B)). Combination of 2 nM AuNPs with 1 MBq, 2 MBq and 3 MBq resulted in survival fractions of 0.33±0.01, 0.19±0.06 and 0.16±0.09 compared to 0.82±0.08 ($p<0.0001$), 0.71±0.07 ($p<0.0001$) and 0.59±0.0.08 ($p<0.0001$) for 1 MBq, 2 MBq and 3 MBq alone.

The clonogenic survival data from Figure 5-3(A) was fitted to the linear quadratic model (Figure 5-3(C)) and values for α, β, IC_{50} and DEF_{50} calculated (Figure 5-3(D)). Incubation of SK-N-BE cells with AuNPs prior to [^{131}I]-MIBG exposure resulted in a decrease in the dose of [^{131}I]-MIBG required to kill 50% of the cell population (IC_{50}). The IC_{50} decreased from 4.56 MBq for [^{131}I]-MIBG alone to 0.83 MBq, 0.91 MBq and 0.75 MBq in the presence of AuNPs at 0.5 nM, 1 nM and 2 nM respectively. Unlike in UVW/NAT cells, the decrease in IC_{50} in SK-N-BE cells demonstrated no dependence on AuNP concentration. The calculated α values for the combination of AuNPs at 0.5 nM, 1 nM and 2 nM with [^{131}I]-MIBG were 0.93 MBq^{-1}±0.06, 0.88 MBq^{-1}±0.04 and 1.05 MBq^{-1}±0.04 compared to 0.19 MBq^{-1}±0.04 for [^{131}I]-MIBG alone and suggested that the presence of AuNPs enhanced the clonogenic cell kill at lower [^{131}I]-MIBG doses, although this was not dependant on AuNP concentration. The DEFs calculated at the 50% toxicity level (DEF_{50}) were 5.48, 5.03 and 6.08 for [^{131}I]-MIBG in combination with AuNPs at 0.5 nM, 1 nM and 2 nM, demonstrating that the presence of AuNPs in combination [^{131}I]-MIBG resulted in a greater than 5-fold enhancement in the [^{131}I]-MIBG dose, irrespective of AuNP concentration.

(A)

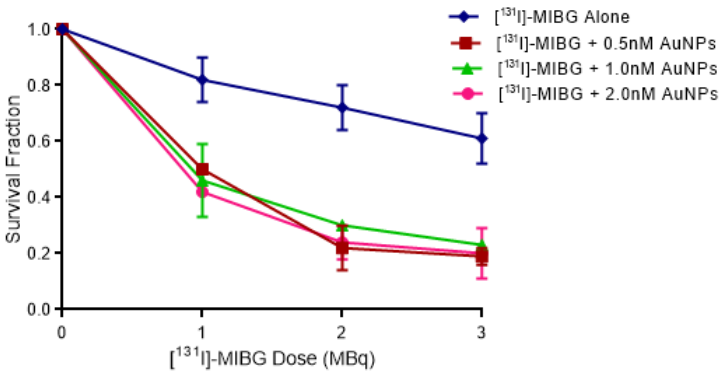

(B)

	0.5nM	1.0nM	2.0nM
1.0MBq	****	****	****
2.0MBq	****	****	****
3.0MBq	****	****	****

Figure 5-3 continued overleaf

(C)

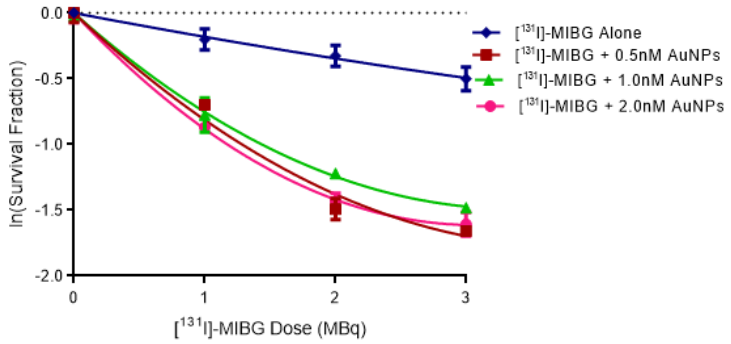

(D)

	0nM	0.5nM	1.0nM	2.0nM
α (MBq^{-1})	0.19±0.04	0.93±0.06	0.88±0.04	1.05±0.04
β (MBq^{-1})	-0.008±0.02	-0.12±0.02	-0.13±0.02	-0.17±0.01
R^2	0.90	0.97	0.98	0.99
IC_{50} (MBq)	4.56	0.83	0.91	0.75
DEF_{50}	1.00	5.48	5.03	6.08

Figure 5-3: Clonogenic survival of SK-N-BE cells exposed to AuNPs in combination with [^{131}I]-MIBG.

SK-N-BE cells were incubated with AuNPs from 0-2 nM for 24 hours. Following this cells were exposed to [^{131}I]-MIBG from 0-3 MBq for 2 hours and with clonogenic survival assays performed 24 hours removal of [^{131}I]-MIBG. Clonogenic survival results are presented as the mean survival fraction (mean ± sd) of 3 independent experiments unless otherwise stated, normalised to AuNP alone treated cells (A). Statistical significant differences in cell survival fraction for AuNPs in combination with [^{131}I]-MIBG, compared [^{131}I]-MIBG alone was assessed using two-way ANOVA with Bonferroni post-tests at 95% C.I. Four (****) symbols indicate $p<0.0001$ (B). Clonogenic survival data presented in (A) was fitted to the linear quadratic model using GraphPad Prism version 6.0.1 (C) and calculated values for the α and β coefficient and the IC_{50} and DEF_{50} for [^{131}I]-MIBG in combination with AuNPs at each AuNP concentration presented (D).

In summary, the clonogenic survival data demonstrated that significant radiosensitisation was observed in both UVW/NAT and SK-N-BE cells when in house synthesised AuNPs were combined with ^{131}I from [^{131}I]-MIBG. In SK-N-BE cells the presence of AuNPs resulted in a greater dose enhancement factor (DEF_{50}) of 6.08 compared to 3.03 in UVW/NAT cells.

The uptake of 2 nM AuNPs following 24 hour incubation, the IC_{50} for [^{131}I]-MIBG and the DEF_{50} for 2 nM AuNPs in combination with [^{131}I]-MIBG for both cell lines is presented in Table 5-1. To determine if radiosensitisation was associated with changes in the cell cycle progression and dynamics of DNA damage and repair, AuNPs at a concentration of 2 nM were combined with 2 MBq [^{131}I]-MIBG in subsequent studies.

Table 5-1: Uptake of 2 nM AuNPs, IC_{50} dose for [^{131}I]-MIBG and DEF_{50} for 2 nM AuNPs in combination with [^{131}I]-MIBG in UVW/NAT and SK-N-BE cells respectively.

	UVW/NAT	SK-N-BE
2nM AuNP uptake (ng/cell)	1.65±0.34	0.71±0.26
[^{131}I]-MIBG IC_{50} (MBq)	2.71	4.56
DEF_{50} for 2nM AuNPs + [^{131}I]-MIBG	3.03	6.08

5.4.3 The effect of AuNPs in combination with [^{131}I]-MIBG on the cell cycle progression of UVW/NAT and SK-N-BE cells

The effect of 2 MBq [^{131}I]-MIBG alone and in combination with 2 nM AuNPs on the progression of UVW/NAT and SK-N-BE cells through the cell cycle was determined at 2 and 24 hours after removal of [^{131}I]-MIBG.

Despite the decrease in clonogenic survival in UVW/NAT and SK-N-BE cells following exposure to 2 nM AuNPs alone (Figure 3-4) treatment with AuNPs alone in each cell line had no effect on the normal progression of cells through the cell cycle, compared to untreated control cells at either timepoint ($p>0.05$) (Figure 5-4).

Exposure of UVW/NAT cells to 2 MBq [^{131}I]-MIBG resulted in a statistically significant increase in the accumulation of cells within the G2/M phase of the cell cycle 24 hours after removal of [^{131}I]-MIBG, compared to untreated control cells (Figure 5-4(A)). The percentage of cells within G2/M increased from 30.6%±7.3 in untreated control cells to 60.1%±4.4 ($p<0.001$) in cells exposed to 2 MBq [^{131}I]-MIBG. No significant accumulation of cells in G2/M 2 hours after removal of [^{131}I]-MIBG ($p>0.05$) was observed.

Similarly, exposure of SK-N-BE cells to [^{131}I]-MIBG at 2 MBq resulted in a statistically significant accumulation of cells within the G2/M phase of the cell cycle 24 hours after removal of [^{131}I]-MIBG, compared to untreated control cells (Figure 5-4(B)). The percentage of cells within G2/M increased from 34.0%±4.7 in untreated control cells to 55.7%±1.2 ($p<0.001$) in cells exposed to 2 MBq [^{131}I]-MIBG. Exposure of SK-N-BE cells to 2 MBq [^{131}I]-MIBG alone induced no significant accumulation of cells in G2/M at 2 hours after removal of [^{131}I]-MIBG, compared to untreated control cells ($p>0.05$).

In both UVW/NAT and SK-N-BE cells, treatment with 2 nM AuNPs in combination with 2 MBq [^{131}I]-MIBG resulted in no significant increase in the accumulation of cells within G2/M, compared to 2 MBq [^{131}I]-MIBG alone at any timepoint measured (Figure 5-4). Throughout the course of the cell cycle experiments, in each case where an increase in the percentage of cells in G2/M was observed this was associated with a decrease in the percentage of cells G1. Furthermore, no significant changes to the

proportion of cells in the S phase of the cell cycle was observed following [^{131}I]-MIBG exposure alone or in combination with AuNPs, compared to untreated control cells or cells exposed to [^{131}I]-MIBG alone at any timepoint measured.

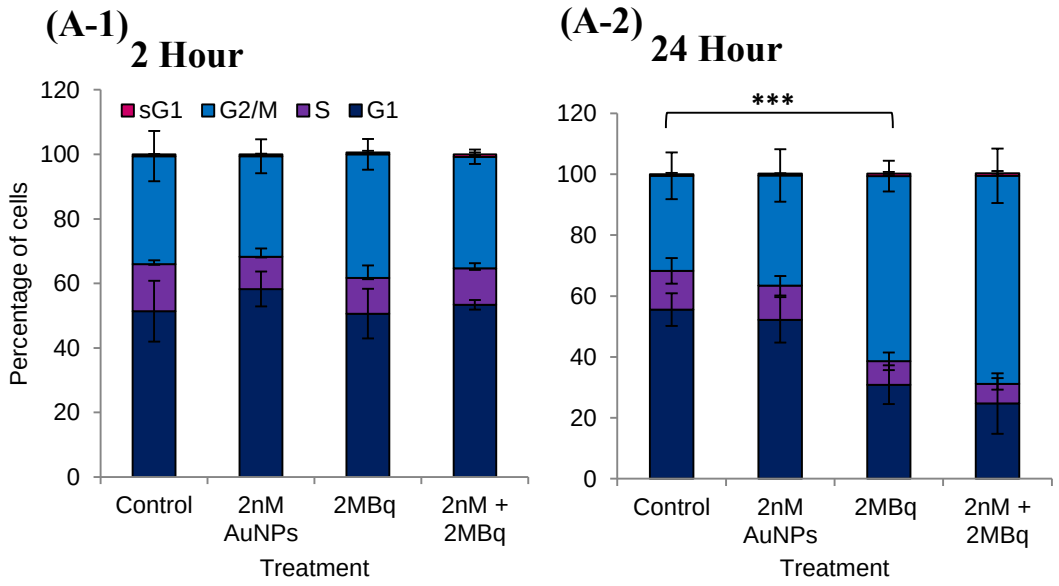

Figure 5-4 continued overleaf

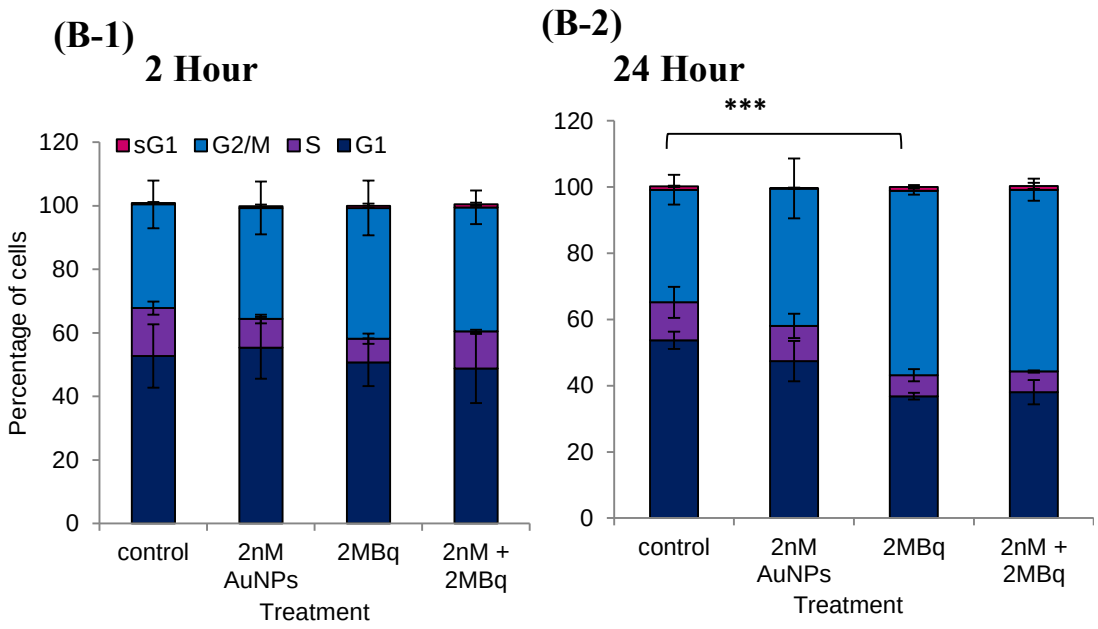

Figure 5-4: The effect of 2 MBq [^{131}I]-MIBG alone, and in combination with 2 nM AuNPs on the distribution of UVW/NAT and SK-N-BE cells throughout each stage of the cell cycle.

UVW/NAT (A) and SK-N-BE (B) cells were incubated with AuNPs at a concentration of 2 nM for 24 hours prior to exposure to 2 MBq [^{131}I]-MIBG. The DNA content of the cells was labelled with PI and the cell cycle profiles obtained by FACS analysis at 2 (A-1, B-1) and 24 (A-2, B-2) hours after removal of [^{131}I]-MIBG. The proportion of cells in G0/G1, S and G2/M were measured using BDCellDiva^{TM} software. Two-way ANOVA was used to determine if statistically significant changes in the distribution of cells throughout the cell cycle resulted as an effect of AuNP and [^{131}I]-MIBG exposure alone (compared to untreated control cells) or in combination (compared to the effects of [^{131}I]-MIBG alone). All tests were performed at the 95% C.I of 3 independent experiments unless otherwise stated (SK-N-BE n=4). Three (***) symbols indicate $p<0.001$.

5.4.4 The effect of AuNPs in combination with [^{131}I]-MIBG on the dynamics of DNA double strand break and repair in UVW/NAT and SK-N-BE cells

The number of γ-H2AX foci/cell was determined in UVW/NAT and SK-N-BE cells following treatment with 2 MBq [^{131}I]-MIBG alone and in combination with 2 nM AuNPs at 2 and 24 hours after removal of [^{131}I]-MIBG (Figure 5-5).

In both cell lines two-way ANOVA with Bonferroni post-hoc testing for multiple comparisons was used to assess whether 2 nM AuNPs or 2 MBq [^{131}I]-MIBG alone significantly increased the number of γ-H2AX foci/cell in cells compared to untreated controls, and whether treatment with 2 nM AuNPs in combination with 2 MBq [^{131}I]-MIBG significantly increased the number of γ-H2AX foci/cell in cells compared to treatment with 2 MBq [^{131}I]-MIBG alone.

As was found in the previous chapter, in both UVW/NAT and SK-N-BE cells treatment with AuNPs alone at 2 nM resulted in no significant increase in the formation γ-H2AX foci compared to untreated control cells at any of the timepoints investigated ($p>0.05$).

In UVW/NAT cells exposed to 2 MBq [^{131}I]-MIBG alone the number of γ-H2AX foci/cell was significantly higher 24 hours after removal of [^{131}I]-MIBG, compared to untreated control cells (Figure 5-5(A)). The number of γ-H2AX foci/cell increased from 10 foci/cell±5.29 in untreated control cells to 59 foci/cell±4.29 ($p<0.0001$) in cells exposed to 2 MBq [^{131}I]-MIBG at 24 hours after removal of [^{131}I]-MIBG. Although exposure of UVW/NAT cells to [^{131}I]-MIBG increased the number of γ-H2AX foci at 2 hours after removal of [^{131}I]-MIBG compared to untreated control cells, this difference was not statistically significant ($p>0.05$).

Combination treatment in UVW/NAT cells with 2 nM AuNPs and 2 MBq [^{131}I]-MIBG, however significantly increased the number of γ-H2AX foci/cell at 2 hours after removal of [^{131}I]-MIBG, compared to cells exposed to 2 MBq [^{131}I]-MIBG alone. The number of γ-H2AX foci increased by 94% from 17foci/cell±0.56 in cells exposed to 2 MBq [^{131}I]-MIBG alone to 33 foci/cell±3.26 ($p<0.01$) in cells treated with 2 nM AuNPs and 2 MBq [^{131}I]-MIBG. Although the number of γ-H2AX foci/cell following combination treatment was 22% higher (72 foci/cell±10.85) than for treatment with

[^{131}I]-MIBG alone (59 foci/cell±4.29) at 24 hours after removal of [^{131}I]-MIBG, this difference was not statistically significant ($p>0.05$).This suggested that the presence of AuNPs in combination with [^{131}I]-MIBG increased the magnitude of DNA damage.

In contrast to UVW/NAT cells, in SK-N-BE cells, exposure to 2 MBq [^{131}I]-MIBG alone induced a significant increase in the formation of γ-H2AX foci/cell at both 2 and 24 hours after removal of [^{131}I]-MIBG, compared to untreated control cells (Figure 5-5(B)). The number of γ-H2AX foci/cell increased from 3.71 foci/cell±0.84 and 6.57 foci/cell±0.75 in untreated control cells, to 22 foci/cell±1.24 ($p<0.0001$) and 32 foci/cell±6.88 ($p<0.0001$) in cells exposed to 2 MBq [^{131}I]-MIBG at 2 and 24 hours after removal of [^{131}I]-MIBG.

Treatment of SK-N-BE cells with 2 nM AuNPs in combination with 2 MBq [^{131}I]-MIBG induced a significant increase in the number of γ-H2AX foci/cell at 24 hours after removal of [^{131}I]-MIBG, compared to cells treated with 2 MBq [^{131}I]-MIBG alone. The number of γ-H2AX foci/cell increased by 66% from 32 foci/cell±6.88 in cells exposed to 2 MBq [^{131}I]-MIBG alone to 53foci/cell±4.13 ($p<0.0001$) in cells treated with 2 nM AuNPs and 2 MBq [^{131}I]-MIBG. However at 2 hours after removal of [^{131}I]-MIBG, the number of γ-H2AX foci in [^{131}I]-MIBG treated cells was comparable to that of combination treated cells (23foci/cell±1.24 compared to 27 foci/cell±0.19, $p>0.05$).

As with UVW/NAT cells, the significant increase in the number of γ-H2AX foci in combination treated samples, compared to [^{131}I]-MIBG treatment alone suggested an increase in the number of DNA DSBs in the presence of AuNPs.

(A-1)

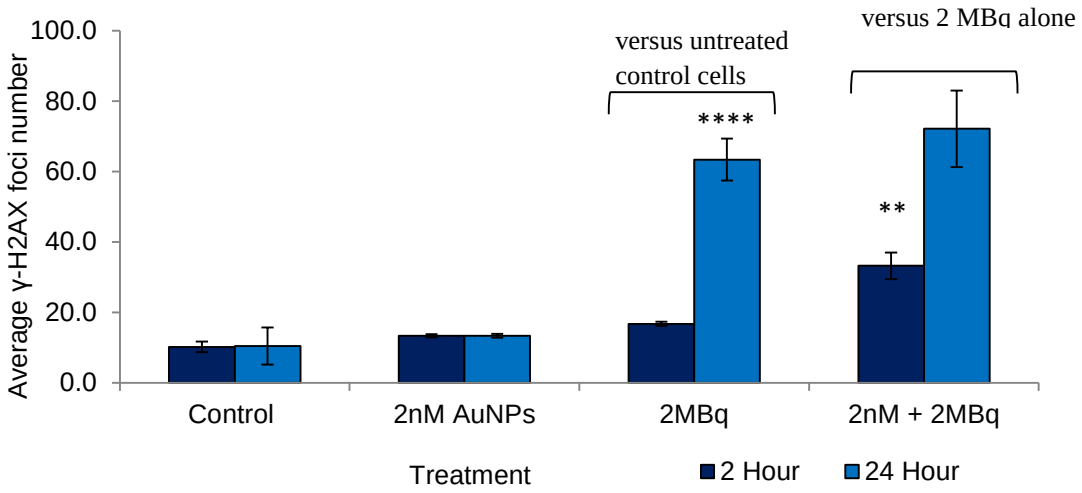

(A-2)

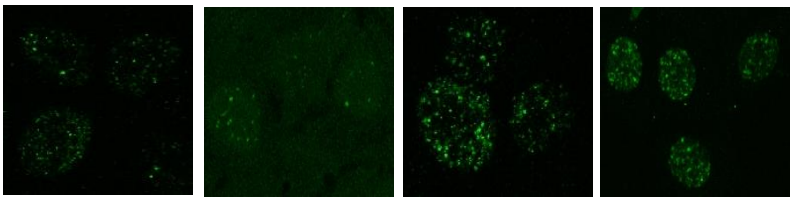

2 Hour: Control **2 nM AuNPs** **2 MBq [^{131}I]-MIBG** **2 nM AuNPs + 2 MBq [^{131}I]-MIBG**

(A-3)

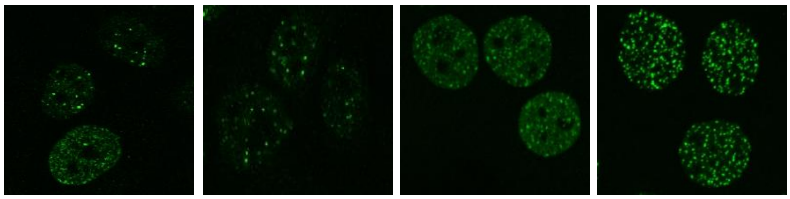

24 Hour: Control **2 nM AuNPs** **2 MBq [^{131}I]-MIBG** **2 nM AuNPs + 2 MBq [^{131}I]-MIBG**

Figure 5-5 continued overleaf

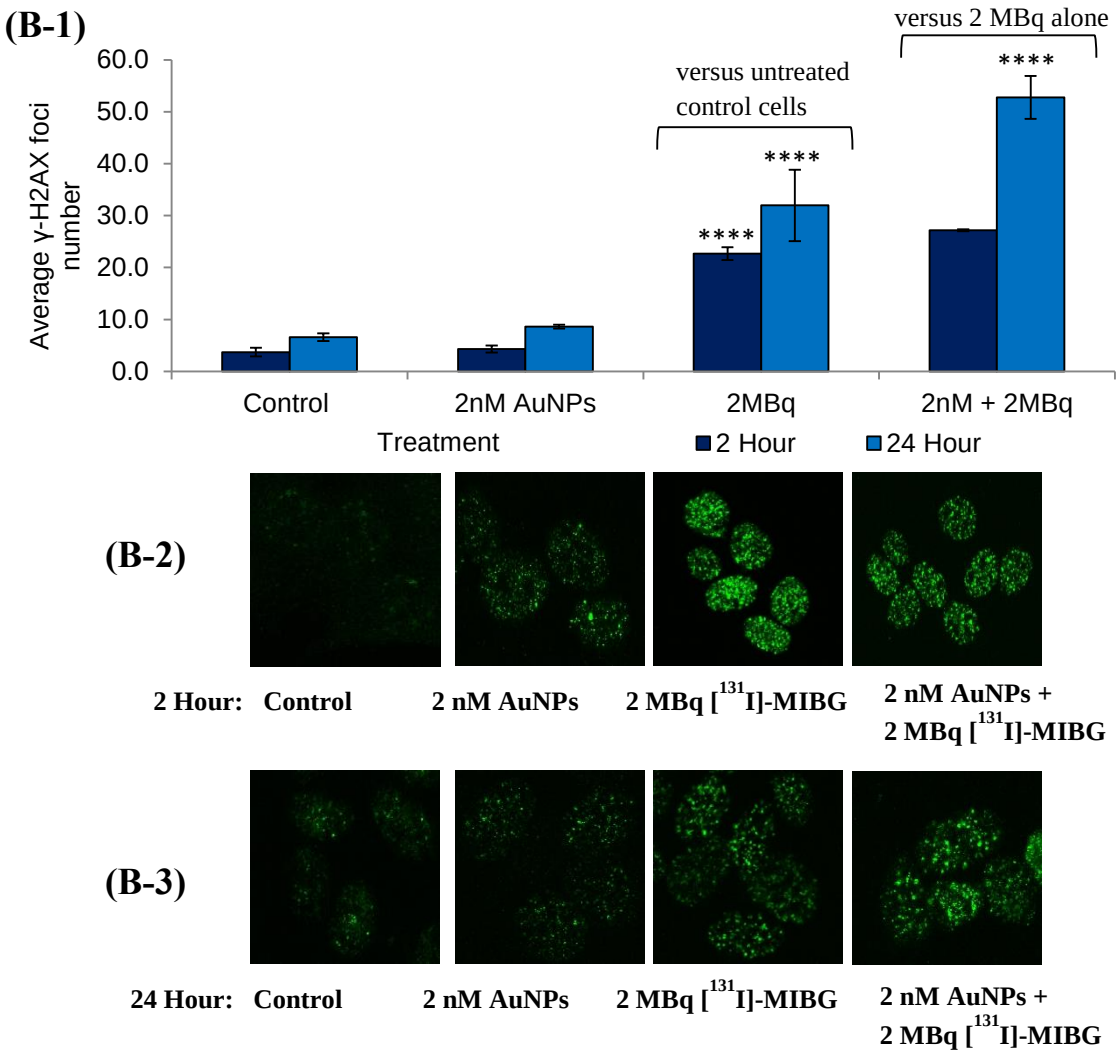

Figure 5-5: The effect of 2 nM AuNPs and 2 MBq [^{131}I]-MIBG alone, and in combination on the formation and resolution of γ-H2AX foci in UVW/NAT and SK-N-BE cells.

Cells were treated with 2 nM AuNPs for 24 hours and then exposed to 2 MBq [^{131}I]-MIBG for 2 hours. The number of γ-H2AX foci/cell was assessed at 2 and 24 hours after 2 MBq [^{131}I]-MIBG was removed using immunohistochemistry. Results presented are the mean number of γ-H2AX foci/cell (mean ± sd) of 3 independent experiments, unless otherwise stated, in UVW/NAT (A) and SK-N-BE (B) cells. Two-way ANOVA was used to determine if statistically significant changes in the number of γ-H2AX foci/cell resulted as an effect of AuNPs and 2 MBq [^{131}I]-MIBG exposure alone (compared to untreated control cells) or in combination (compared to 2 MBq [^{131}I]-MIBG alone). All tests were performed at the 95% C.I. Two (**) and four (****) symbols indicate $p<0.01$ and $p<0.0001$ respectively. Representative images of γ-H2AX foci/cell in each treatment group at 2 hours (A/B-2) and 24 hours (A/B-3) are presented.

In summary, the data demonstrated that the combination of AuNPs with [^{131}I]-MIBG resulted in a significant increase in the number of γ-H2AX foci/cell compared to [^{131}I]-MIBG alone, indicating that the presence of AuNPs increased the number of DNA DSBs. This was consistent with the clonogenic survival data which demonstrated that significant radiosensitisation was achieved in both UVW/NAT and SK-N-BE cells treated with AuNPs.

5.5 Discussion

This was the first study to provide experimental evidence of AuNP radiosensitisation in combination with ionising radiation in the form of ^{131}I conjugated to MIBG ([^{131}I]-MIBG). Results demonstrated that significant radiosensitisation was observed in the NAT transfected human glioma cell line, UVW/NAT, and the human neuroblastoma cell line, SK-N-BE with DEF_{50} values of 3.03 and 6.08, respectively. The observed DEF_{50} values were considerably higher than those achieved when AuNPs were combined with 225 kVp X-rays in UVW/NAT and SK-N-BE cells which were 1.12 and 0.93 respectively, as determined in the previous chapter. Furthermore the DEF_{50} values were also significantly higher those which have been reported in the majority of the literature when kVp and MV photon sources, and radionuclides such as ^{125}I were combined with AuNPs (Geng et al., 2011; Jain et al., 2011; Ngwa et al., 2013). Results of this present study also demonstrated that UVW/NAT cells were more sensitive to [^{131}I]-MIBG as a single agent than SK-N-BE cells, where the IC_{50} doses of [^{131}I]-MIBG were 2.80 MBq and 3.24 MBq in UVW/NAT and SK-N-BE cells respectively. This was consistent with the uptake of [^{131}I]-MIBG by each cell line which has been shown by McCluskey *et al*, (2005) to be 2-fold higher in UVW/NAT cells than SK-N-BE cells (McCluskey et al., 2005).

As discussed in section 1.6 the mechanisms by which AuNPs induce radiosensitisation have not been fully elucidated, however most studies suggest that the primary mechanism is due to physical interactions between the ionising radiation and AuNPs, with the greatest enhancement observed when the photoelectric effect dominates the ionisation process. Computational studies have therefore predicted that the greatest

radiation enhancement should be observed at lower kV photon energies as in this energy region the energy match between the radiation energy and the binding energy of Au electrons which range from 3-79 keV is highest (Figure 1-3) (Butterworth et al., 2012). Despite these predictions, several experimental studies have reported AuNP radiosensitisation with higher energy kVp beams and MV beams. However, in most studies where AuNP radiosensitisation has been investigated across a range of photon energies, the radiosensitisation decreased with an increase in photon energy. For example in a study by Chithrani *et al*, (2010), the DEF decreased from 1.66 to 1.18 when the photon energy was increased from 105 kVp to 662 keV and further decreased to 1.17 with 6 MV photons (Chithrani et al., 2010). Similarly, the study by Jain *et al,* (2011), reported a DEF of 1.41 when 1.9 nm AuNPs were combined with 160 kVp photons which decreased to 1.29 with 6 MV photons and further decreased to 1.16 with 15 MV photons. Despite the lower DEF values typically seen with higher energy beams compared to low kV beams, the observed DEF values are still greater than the predicted values, based on the simulated physical dose enhancement effects and the data therefore suggests that other biologically driven mechanisms besides photoelectric enhancement of dose are involved in AuNP radiosensitisation. This is supported by the data presented in the study by Sicard-Roselli *et al*, (2014) which proposed a mechanism of AuNP radiosensitisation as a result of oxidative stress. The study demonstrated a significant increase in ·OH production when aqueous samples containing AuNPs were irradiated. Based on this observation the authors proposed that radiolysis produced ROS, which then interacted with structured water layers at the AuNP-water interface where their excitation energy was used to produce subsequent ·OH, leading to a cascade of ·OH production The increased levels of ·OH species could contribute to the increase in the effective radiation dose that can be observed with MV radiation beams where the contribution from photoelectric absorption is likely to be low. (Carrasco et al., 2012; Sicard-Roselli et al., 2014)**.**

It is known however that the biological effect of ionising radiation on cells will be dependent on several factors, namely the dose rate of radiation, the energy of the radiation, the tissue penetration and the linear-energy transfer (LET) which is a measure of the energy transferred to a material as ionising radiation passes through it and therefore the effects of XBR and ^{131}I are likely to be very different.

The ^{131}I radioisotope conjugated to MIBG which was used in this study, decays primarily through the emission of β electrons at 606 keV and γ rays at 362 keV. As these energies greatly exceed the binding energy of electrons in Au, the probability of photoelectric ionisation of AuNPs and therefore subsequent enhancement in the delivered radiation dose through photoelectric absorption is low.

Despite this theoretical prediction, the DEF_{50} values in our study were significantly higher than that which were observed when AuNPs were combined with photons from a 225 kVp X-ray tube (chapter 4). Furthermore, the majority of other studies have reported DEF_{50} values in the region of 1-2 for AuNPs in combination with photon radiation sources ranging in energy from 6 kV to 15 MV (Table 1-1) (Chang et al., 2008; Coulter et al., 2012; Kong et al., 2008). In contrast to predictions based on the physical properties of the radiopharmaceutical decay (^{131}I), in this study it was hypothesised that an enhancement in the delivered radiation dose through photoelectric absorption may have contributed significantly to the radiosensitisation observed in our study.

In this study it was hypothesised that the long path range of 0.8 mm and half-life of ^{131}I of 8.02 days could contribute to the radiosensitisation observed. The emitted low LET β and γ radiation can travel through the cell population up to their maximum path range, equivalent to the diameter of a few cells, where they deposit energy along the decay track. Thus at some point in this traversal as the radiation decays the energy of the β and γ radiation will be within the optimum range to result in AuNP photoelectric absorption.

In the experimental set up used in this present study the NAT expressing tumour cells were incubated with [^{131}I]-MIBG for 2 hours, following which the cells were washed to remove any excess radiopharmaceutical which had not been taken up into the cells. Due to the long half-life of ^{131}I, the decay process continues for several days, compared to instantaneous XBR exposure where 2 Gy is administered in 52 seconds. Therefore, continuous ionisation of AuNPs from interaction with β and γ radiation until the emissions have fully decayed may occur. This could result in prolonged and substantial radiation dose enhancement. Additionally, the β and γ emissions from decay of ^{131}I will induce continuous production of ROS within the cells, which could then interact

with the AuNPs to generate further secondary electron and ·OH species production based on the mechanism proposed by Sicard-Roselli *et al*, (2014).

The radiosensitisation observed following treatment of cells with AuNPs in combination with [^{131}I]-MIBG was associated with a significant increase in the number of DNA DSBs, as determined by an increase in the number of γ-H2AX foci/cell compared to [^{131}I]-MIBG treatment alone at 2 and 24 hours after removal of [^{131}I]-MIBG. In the two cell lines examined the number of in γ-H2AX foci/cell increased by 22% and 66% in UVW/NAT and SK-N-BE cells respectively 24 hours after the removal of [^{131}I]-MIBG, compared to [^{131}I]-MIBG alone.

Twenty four hours after XBR treatment significant resolution of γ-H2AX foci/cell was observed. In contrast, following treatment with [^{131}I]-MIBG, γ-H2AX foci were either not resolved at 24 hours after removal of [^{131}I]-MIBG due to the presence of continued radiation from ^{131}I decay within cells, or γ-H2AX foci were repaired but this was not measurable due to the formation of new foci as a result of continual radioisotope decay. The exact mechanisms of the DNA damage and repair kinetics induced by the two radiation sources were not further interrogated in this present study.

The addition of AuNPs to cells treated with [^{131}I]-MIBG resulted in an increase in the number of γ-H2AX foci/cell, indicative of an increase in the DNA DSBs within the cell. The presence of AuNPs therefore increased the amount radiation induced DNA damage. This was in contrast to cells treated with a combination of XBR and AuNPs where radiosensitisation was primarily associated with a decrease in resolution of DNA DSBs, suggesting an increase in the complexity of DNA damage rather than an increased amount of DNA damage.

Surprisingly, the increase in DNA damage associated with the combination of AuNPs with [^{131}I]-MIBG in cells did not result in an increase in the arrest of cells throughout the cell cycle, compared to the effects of [^{131}I]-MIBG alone. This was in contrast to other studies which have investigated the combination of AuNPs with XBR and have reported an increase in cell cycle arrest which is associated with an increase in γ-H2AX foci (Roa et al., 2009). As this is the first reported study of the interrogation of the combination of AuNPs with [^{131}I]-MIBG, it is therefore difficult to compare the results

found in this study to other studies which have utilised either XBR or other radiopharmaceuticals in combination with AuNPs (Jain et al., 2011; Ngwa et al., 2013).

The results presented in this chapter provide initial *in vitro* experimental evidence demonstrating that significant radiosensitisation resulted from the combination of AuNPs with continuous low dose-rate, high keV energy β and γ radiation, using a targeted radionuclide, resulting in significantly higher DEF_{50} values than achieved when AuNPs were combined with rapid radiation from 225 kVp X-ray photons. These results motivate further investigations toward the development of AuNPs for clinical use in combination with radiopharmaceuticals.

Following on from this chapter the next aim of this study was to investigate the radiosensitising potential of HGNs as it was hypothesised that as a result of their superior physical properties, compared to solid AuNPs, HGNs would induce greater radiosensitisation in cells, compared to solid AuNPs and therefore deliver a greater radiation enhancement. The next chapter in this study aimed to characterise in house synthesised HGNs and establish their stability within cell growth medium and determine their uptake, localisation and interaction within a variety of cancer cell lines.

Chapter 6

Synthesis and Characterisation of Hollow Gold Nanoparticles (HGNs)

Chapter 6: Synthesis and Characterisation of Hollow Gold Nanoparticles (HGNs)

6.1 Introduction

The results presented in chapters 4 and 5 demonstrated the radiosensitisation potential of synthesised solid AuNPs in combination with X-ray and radioisotope radiation sources.

In addition to solid AuNPs, there have been limited reports on the radiosensitisation potential of HGNs (Chien Wen Huang, 2015). As discussed in section 1.7, compared to solid AuNPs, the literature has demonstrated that HGNs display both an increased capability for absorbing UV light as a result of the two surfaces present in HGNs, and a greater capacity to convert this absorbed light into sound waves (Gutrath et al., 2012). Additionally, it has been shown that the availability of two surfaces within HGNs results in an enhancement in the localised electromagnetic field at the nanoparticle surface, and in regions throughout the surrounding medium compared to solid AuNPs, which may induce an increase in the magnitude and dispersion of radiation dose enhancement throughout the cells (Jackson et al., 2003). Finally, the presence of pinholes on the surface of HGNs has been shown computationally to magnify and concentrate the electromagnetic field and result in localised hot spots of dose at the HGN surface (Hao et al., 2004).

Taking together the superior physical characteristics of HGNs, compared to solid AuNPs it is hypothesised in this study that the combination of HGNs with ionising radiation may provide a greater DEF than that which is achieved with solid AuNPs. The subsequent chapters of this thesis therefore aimed to determine the radiosensitisation potential of HGNs in combination with the 225 kVp X-ray photon and ^{131}I in the form of [^{131}I]-MIBG radiation sources which have been investigated in chapters 4 and 5.

However, before the radiosensitisation potential of HGNs could be assessed, their physical characteristics and interaction with several cancer cell lines were evaluated.

6.2 Aims

The aim of this chapter was to characterise HGNs synthesised via the sacrificial template method in collaboration with the Graham Lab (University of Strathclyde). The study aimed to first confirm the diameter and stability of the synthesised HGNs within cell growth medium. Following this the study aimed to measure the intracellular uptake, localisation and cytotoxicity of the synthesised HGNs in the human glioma cell line UVW/NAT, human neuroblastoma cell line SK-N-BE and human melanoma cell line A375.

6.3 Materials and Methods

6.3.1 Synthesis of hollow gold nanoparticles (HGNs)

All HGNs were synthesised in the Graham Lab (University of Strathclyde) by adaptation of previously reported methods utilising cobalt as a sacrificial template (Schwartzberg et al., 2006; Xie et al., 2013). All syntheses were carried out under inert conditions using a standard Schlenk line under argon to prevent premature oxidation of the cobalt nanoparticles. For a typical synthesis, 100 µL of 0.4 M cobalt chloride hexahydrate (99.99%, Fisher Scientific, Leicestershire, UK) and 550 µL of 0.1 M trisodium citrate dihydrate (>99% Sigma-Aldrich, Dorset, UK) were added into deionised water (10 0mL) and degassed several times (10 mins vacuum and 15 mins argon). 1 mL of 0.1 M sodium borohydride (99%, Fisher Scientific, Leicestershire, UK) was injected and the solution allowed to react for a further 20 mins under a constant argon flow until hydrogen evolution ceased, indicating complete hydrolysis of the reductant. The solution was then degassed (8 mins vacuum and 10 min argon) before 33 mL of 248 M chloroauric acid trihydrate (ACS reagent grade, Fischer Scientific, Leicestershire, UK) was injected. The reaction mixture was allowed to react for 10 mins under argon with vigorous stirring before being exposed to air where a colour change from brown to green was observed. Finally, 500 µL of 0.1 M trisodium citrate was added to stabilise the hollow gold nanoshell solution. HGNs were concentrated through centrifugation at 5000 rpm and the precipitate was re-dispersed in 2 mM trisodium citrate solution to give a final concentration of 3 µM. The protocol

employed synthesised citrate stabilised HGNs of approximately 56 nm diameter and this HGN size was employed in all subsequent studies.

6.3.2 Size and zeta potential measurement of synthesised HGNs

Following synthesis the diameter and zeta potential were measured by dynamic light scattering (DLS) as described in section 3.3.2. For HGN diameter measurements a standard solution (nanosphere tm) of 40 nm particles (Thermo Scientific, Loughborough, UK) was used to calibrate the instrument. All measurements were carried out in triplicate and results are presented as the mean particle size or zeta potential (mean ± sd) respectively of 3 independent experiments.

6.3.3 Stability of synthesised HGNs in cell culture medium

To ensure the synthesised HGNs would remain dispersed in solution and not aggregate when added to cell growth medium the stability of the HGNs was measured following incubation in growth medium by UV-Visible spectrophotometry as described in section 3.3.3.

6.3.4 Cells and culture conditions

The human glioblastoma cell line UVW/NAT, human neuroblastoma cell line SK-N-BE and human melanoma cell line A375 were employed in this study. All cells were cultured and maintained as detailed in sections 2.3.1 and 3.3.4.

6.3.5 Intracellular localisation of synthesised HGNs

To confirm uptake of HGNs within UVW/NAT, SK-N-BE and A375 cells and identify their intracellular location, transmission electron microscopy (TEM) was performed (Kumar et al., 2005; Selvakannan and Sastry, 2005) in collaboration with the

University of Glasgow as described in section 3.3.5. Each cell line was incubated with HGNs at a concentration of 5 nM for 24 hours.

6.3.6 Measurement of intracellular uptake of synthesised HGNs

Inductively coupled plasma-mass spectroscopy (ICP-MS) was used to assess the uptake of HGNs by measurement of the Au concentration within UVW/NAT, A375 and SK-N-BE cells following incubation with HGNs at either 0.1 nM or 5 nM for 2-24 hours and measurements performed as described in section 3.3.6 (Melancon et al., 2008).

6.3.7 Clonogenic survival assay

Clonogenic survival assays were used to determine the cytotoxicity of HGNs as a single agent in the concentration range from 0-10 nM. For assessment of UVW/NAT and A375 cell lines, clonogenic survival assays were performed as described in section 2.3.5. Due to the insufficient plating efficiency of SK-N-BE cells, soft agar clonogenic survival assays were performed as described in section 3.3.7.1. All results are presented as the mean cell survival fraction (mean ± sd) of 3 independent experiments unless otherwise stated.

6.3.8 Statistical Analysis

6.3.8.1 Analysis of variance (ANOVA)

All experiments were carried out 3 times, unless otherwise stated, with results reported as the (mean ± sd). Significant differences between the uptake of HGNs in the 3 cell lines investigated, and the cell survival following HGN incubation in each cell line were evaluated using two-way ANOVA with Bonferroni post-testing. All tests were performed using GraphPad Prism version 6.0.1 (CA.) at the 95% C.I where p values lower than 0.05 considered statistically different.

6.4 Results

6.4.1 Size and zeta potential measurement of synthesised HGNs

In this study, HGNs with an average diameter of 56 nm, a core size of 46 nm and a shell thickness of 10 nm were synthesised. Following synthesis the average diameter and zeta potential were measured to confirm successful synthesis of mono-dispersed HGNs and ensure their stability within suspension. The average diameter of in house synthesised HGNs used throughout the study was confirmed to be 51.63±6.90 nm and the zeta potential -38.40±1.60 mV, as shown in Table 6-1 and indicated that the synthesised HGNs were mono-dispersed and stable in the citrate suspension as the zeta potential was within ±30-40 mV, which was indicative of moderate stability (O'Brien et al., 1990).

Table 6-1: Average diameter and zeta potential of synthesised HGNs measured using dynamic light scattering (DLS).

Average HGN diameter (nm)	Average zeta potential (mV)
51.63 ± 6.90	-38.40 ± 1.60

6.4.2 Stability of in house synthesised HGNs within cell growth medium

The UV-visible absorption spectra of HGNs was assessed to determine the colloidal stability of the synthesised HGNs incubated within cell growth medium throughout the 24 hour cell incubation period to be used in subsequent experiments. The UV-visible absorption spectrum of HGNs at a concentration of 5 nM incubated within distilled water for 24 hours was used as a positive control for stability.

HGNs incubated in distilled water displayed an intense absorption peak at approximately 612 nm (Figure 6-1(A)). For HGNs incubated in cell growth medium without the addition of FCS, the UV-visible absorption spectrum showed no intense absorption peak at any wavelength between 400-800 nm at either 2 or 24 hours, indicating that in the absence of FCS, the HGNs aggregated almost immediately and

were no longer measurable (Figure 6-1(B)). In the presence of 10-50% FCS in the growth medium the HGNs remained stable across the time period assessed, as all samples demonstrated an absorption peak at ~625 nm at 2 hours incubation time and ~635 nm at 24 hours incubation time, independent of FCS concentration (Figure 6-1(C-E)). Compared to HGNs suspended in dH_2O however, the λ_{max} values increased for HGNs incubated in cell growth medium supplemented with FCS (Figure 6-1(F)). These data suggested that the synthesised HGNs were stable within the cell growth medium and were therefore used in all subsequent cell based experiments, utilising an incubation time of 24 hours and where the cell growth medium used was supplemented with 10% FCS under normal conditions.

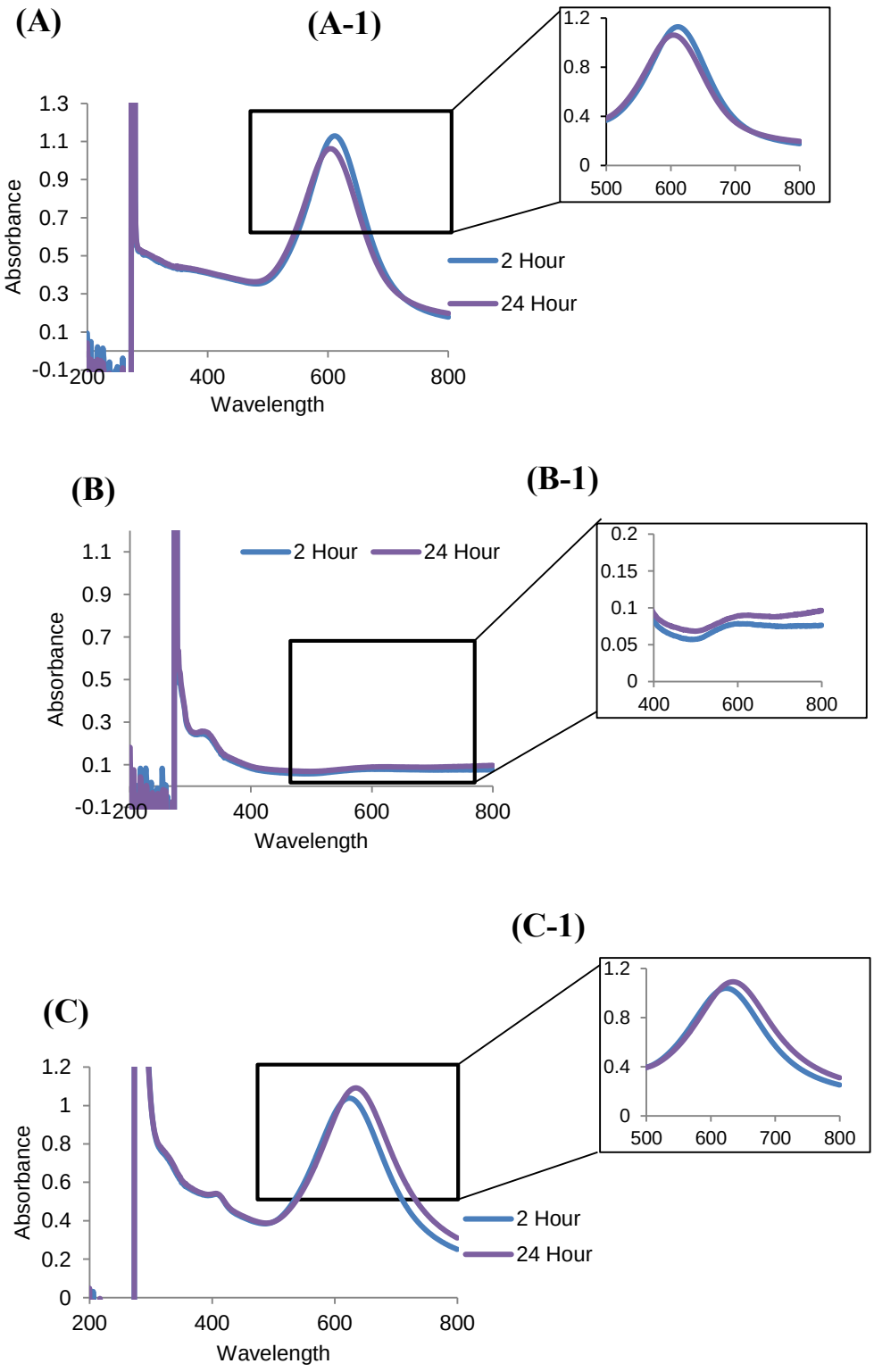

Figure 6-1 continued overleaf

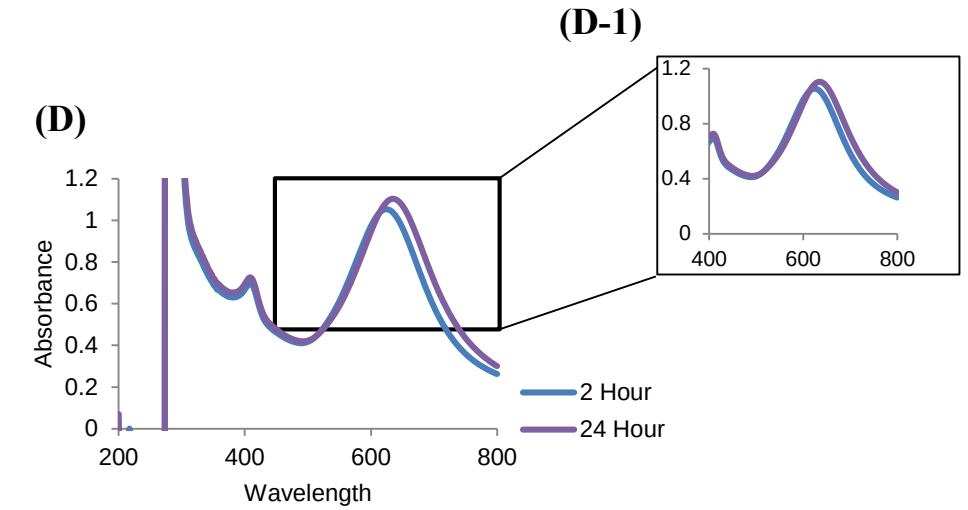

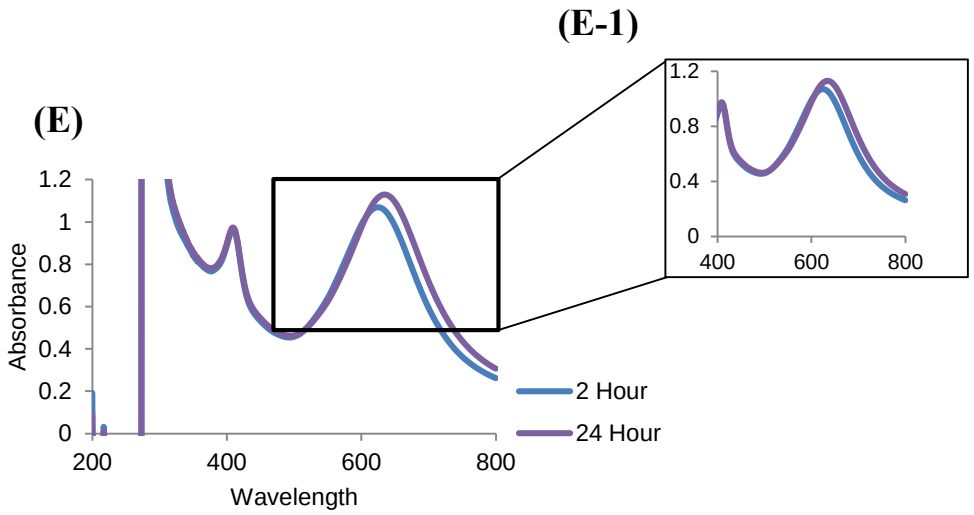

Figure 6-1 continued overleaf

(F)

Incubation Time	SPR Peak Wavelength (nm)			
	FCS Concentration			
	dH_2O Control	10%	25%	50%
2 Hour	612	623	625	625
24 Hour	604	635	635	635

Figure 6-1: The UV-visible absorption spectra of synthesised HGNs in cell growth medium with increasing FCS concentration from 0-50% following 2 and 24 hour incubation.

The UV-visible absorption spectra of synthesised HGNs at a concentration of 5 nM was measured in dH_2O (A) and cell growth medium either without FCS (B) or supplemented with 10% FCS (C), 25% FCS (D) or 50% FCS (E) following 2 and 24 hour incubation. All samples were incubated at 37^{o}C and 5% CO_2 atmosphere. The cell growth medium was supplemented with 5% of each of penicillin streptomyacin, L-glutamine and fungazone. The absorbance between 500-800 nm has been highlighted for all samples to allow clearer visualisation of the absorption peak at the wavelength of maximum absorption which occurs at approximately 612 nm for 50 nm HGNs. The wavelength of maximum absorption (λmax) of the HGNs under each culture condition is shown (G).

6.4.3 Intracellular localisation of synthesised HGNs in UVW/NAT, SK-N-BE and A375 cells

The intracellular localisation of synthesised HGNs in UVW/NAT, SK-N-BE and A375 cells was evaluated following 24 hour incubation with 5 nM HGNs by TEM in all 3 cell lines (Figure 6-2). Compared to the analysis solid AuNPs (Figure 3-2), HGNs within cells were much more difficult to detect, as anticipated due to the large hollow core and therefore much smaller electron density. The differences in electron density between the hollow core and Au shell are demonstrated in Figure 6-2(D). In each of the 3 cell lines small amounts of the HGNs localised within intracellular lysosomes, which was consistent with the localisation of solid AuNPs (section 3.4.3). However HGNs appeared less aggregated within lysosomes compared to solid AuNPs.

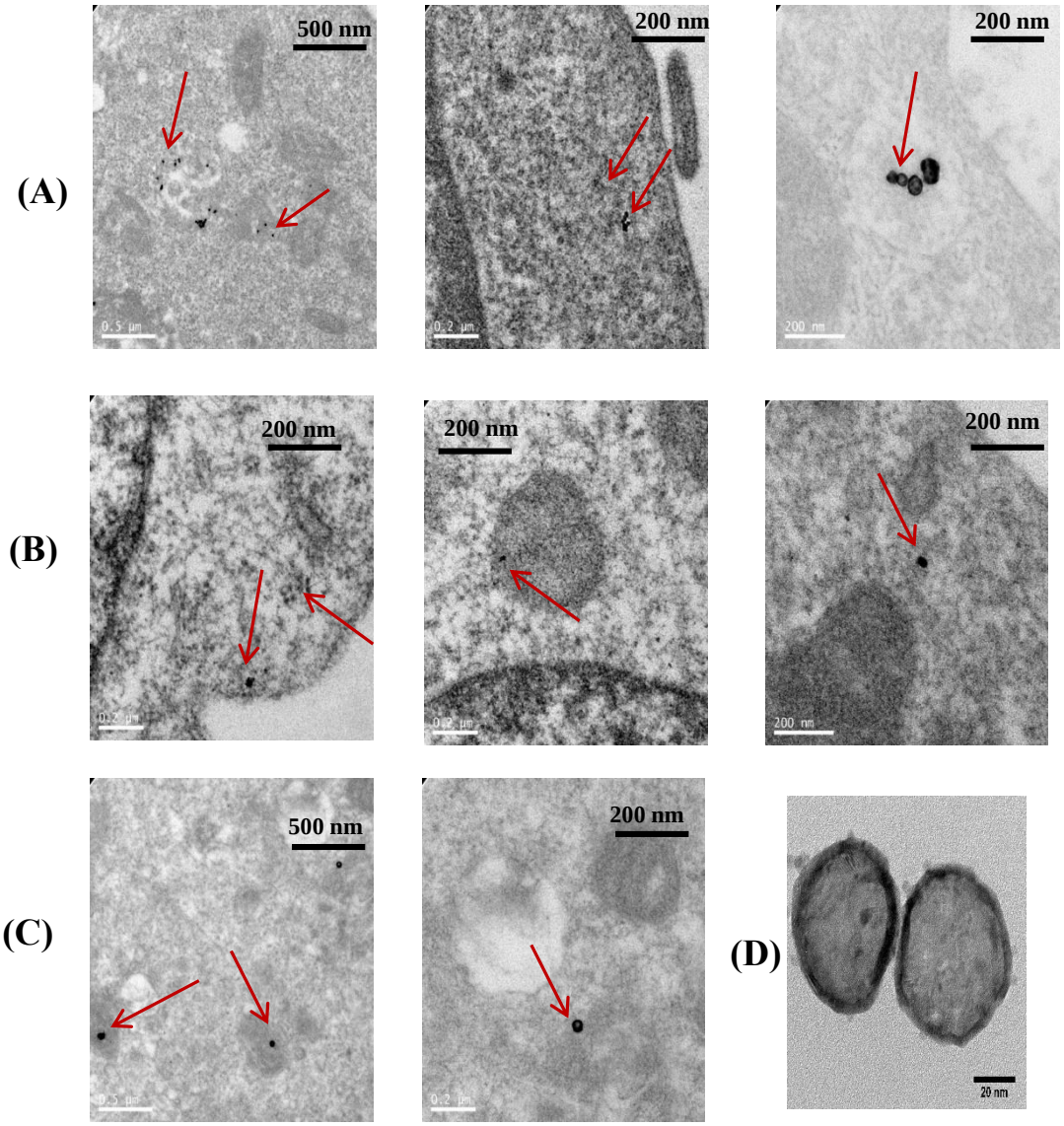

Figure 6-2: Intracellular localisation of HGNs in UVW/NAT, SK-N-BE and A375 cells evaluated by TEM.

UVW/NAT (A), SK-N-BE (B) and A375 (C) cells were incubated with 5 nM for 24 hours and processed for TEM imaging. TEM images are presented and demonstrate localisation of HGNs in the endosomes and lysosomes of cells indicated by the red arrows. Representative images for each cell line were selected. Scale bars are shown on each image. HGNs alone imaged to demonstrate differences in electron density between hollow core and Au shell (D)

6.4.4 Intracellular uptake of synthesised HGNs in UVW/NAT, SK-N-BE and A375 cells

ICP-MS was used to measure the intracellular Au content following incubation of UVW/NAT, SK-N-BE and A375 cells with HGNs at 0.1 nM and 5 nM for 2, 6 and 24 hours (Figure 6-3). The intracellular Au content measured following HGN incubation was in some cases close to the lower limit of detection for the ICP-mass spectrometer and consequentially the variability between experiments was high.

In all cell lines examined, the measured Au content within each sample increased with an increase in incubation time after exposure to 0.1 nM and 5 nM HGNs. Increasing the incubation time of samples from 2 to 24 hours in cells incubated with 5 nM HGNs resulted in a significant increase in the average Au content per cell (ng/L) from 0.007±0.003 ng/L to 0.021±0.01 ng/L ($p<0.05$) in UVW/NAT cells and from 0.009±0.007 ng/L to 0.018±0.01 ng/L ($p<0.0001$) in SK-N-BE cells. In A375 cells the Au content per cell increased from 0.001±0.0004 ng/L to 0.003±0.0005 ng/L however this increase was not statistically significant ($p>0.05$).

HGN concentration also influenced the uptake observed. In all cell lines the Au content was significantly greater following incubation with 5 nM HGNs than 0.1 nM. In UVW/NAT cells for example, following 24 hour incubation the Au content was 0.001±0.0008 ng/L in cells incubated with 0.1 nM HGNs, compared to 0.021±0.01 ng/L ($p<0.01$) with 5 nM HGNs. Likewise, in SK-N-BE cells, following 24 hour incubation the Au content was 0.0003±0.0004 ng/L in cells incubated with 0.1 nM AuNPs compared to 0.018±0.0003 ng/L ($p<0.001$) in cells incubated with 5 nM HGNs. Similarly, in A375 cells the Au content at 24 hour incubation was 0.002±0.001 ng/L following incubation with 0.1 nM HGNs compared to 0.005±0.004 ng/L ($p<0.05$) in cells incubated with 5 nM HGNs.

Furthermore, as was observed with solid AuNPs, the degree of HGN uptake differed significantly between the 3 cell lines examined. The highest uptake was found in UVW/NAT and SK-N-BE cells and the lowest in A375 cells. Following 24 hour incubation with 5 nM HGNs the measured Au content in UVW/NAT cells was to 0.021±0.01 ng/L compared to 0.018±0.0003 ng/L in SK-N-BE cells ($p<0.0001$) and 0.005±0.004 ng/L in A375 cells ($p<0.05$). Following exposure to 0.1 nM HGNs no

statistically significant differences in uptake were found in between the 3 cell lines examined at any timepoint investigated.

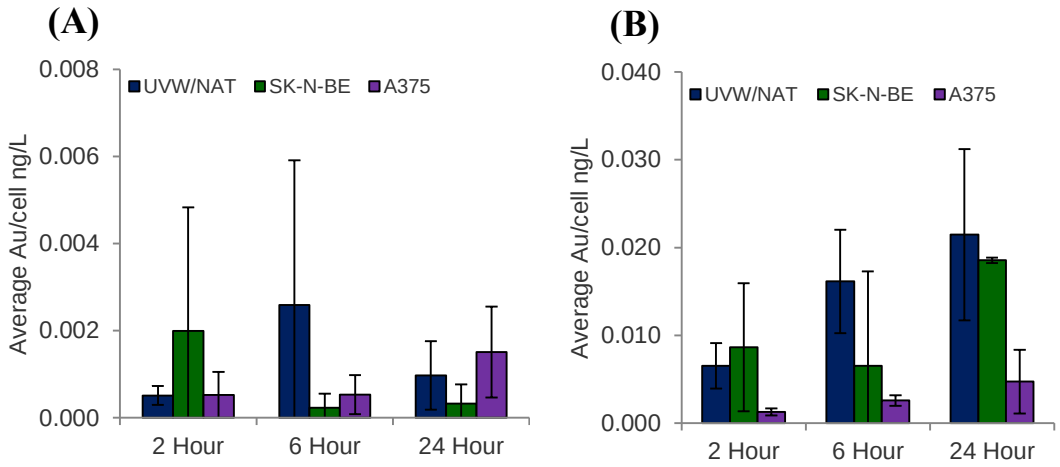

(C)

	UVW/NAT	SK-N-BE	A375
Incubation time (Hours)	5nM HGN concentration		
2 vs. 6	ns	ns	ns
2 vs. 24	*	****	ns
6 vs. 24	ns	****	ns
	0.1nM vs. 5nM HGN Concentration		
2 hour	ns	ns	ns
6 hour	**	ns	ns
24 Hour	****	***	*
	UVW/NAT vs A375	**UVW/NAT vs. SK-N-BE**	**A375 vs. SK-N-BE**
	5nM HGN Concentration		
2 hour	ns	ns	ns
6 hour	*	ns	ns
24 Hour	*	****	****

Figure 6-3: Intracellular uptake of synthesised HGNs in UVW/NAT, SK-N-BE and A375 cells measured by ICP-MS following 2, 6 or 24 hour incubation.

The mean Au content per cell was measured by ICP-MS in UVW/NAT, SK-N-BE and A375 cells incubated with HGNs at a concentration of 0.1 nM (A) or 5 nM (B). Results are displayed as the mean Au content per cell in ng/L (mean ± sd) of 3 independent experiments. Statistically significant differences in HGN uptake as an effect of HGN concentration, HGN incubation time and cell line were assessed using two-way ANOVA with Bonferroni post-tests (C). All statistical analysis was performed at the 95% C.I. One (*), two (**), three (***) and four (****) symbols indicate $p<0.05$, $p<0.01$, $p<0.001$ and $p<0.0001$ respectively and ns indicates no significance.

6.4.5 The cytotoxicity of synthesised HGNs within UVW/NAT, A375 and SK-N-BE cells

Clonogenic survival assays were performed to assess the cytotoxicity of the synthesised HGNs in UVW/NAT, SK-N-BE and A375 cells (Figure 6-4) following 24 hour incubation. In UVW/NAT and A375 cells, incubation with HGNs had no significant effect on the clonogenic survival of cells at any of the concentrations investigated, compared to untreated control cells, indicating that HGNs did not induce any significant toxicity in these 2 cell lines. In SK-N-BE cells however, incubation with HGNs reduced the clonogenic survival of the cells at the higher HGN concentrations of 7.5 nM and 10 nM. The clonogenic cell survival decreased to 0.78 ± 0.04 ($p<0.01$) and 0.79 ± 0.13 ($p<0.01$) following incubation with 7.5 nM and 10 nM HGNs compared to untreated control cells. Based on these data the HGN concentration range 0-5 nM was used in further combination studies.

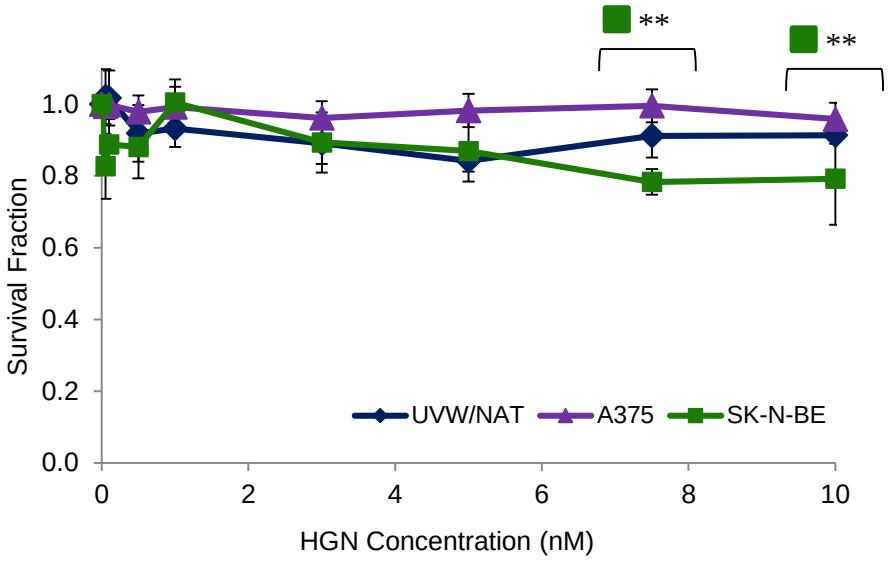

Figure 6-4: Clonogenic survival of UVW/NAT, A375 and SK-N-BE cells incubated with HGNs across the concentration range 0-10 nM for 24 hours.

Each cell line was incubated with HGNs across the concentration range 0-10 nM for 24 hours and cells plated for clonogenic survival assays. Results are presented as the mean survival fraction (mean ± sd), normalised to untreated control cells of 3 independent experiments. Two-way ANOVA with Bonferroni post-tests were performed to assess the effect of HGNs on the clonogenic survival in each cell line. All tests were performed at the 95% C.I. Two (**) symbols indicate $p<0.01$.

6.5 Discussion

The aim of this study was to initially evaluate the stability of in house synthesised HGNs within cell growth medium to ensure that the HGNs remained stable in solution and could be used in subsequent cell based experiments to evaluate their radiosensitisation potential. As was observed with solid AuNPs (Figure3-1), synthesised HGNs were stable following 24 hour incubation in MEM cell growth medium, provided the medium was supplemented with FCS (Figure 6-1). Results of this study demonstrated an increase in the SPR peak of HGNs which was consistent with the results of previous studies, and was indicative of an increase in HGN diameter as a result of the adsorption of serum proteins onto the surface of the HGNs (Chithrani et al., 2006). As discussed, the adsorption of serum proteins onto the surface of nanoparticles has been hypothesised in other studies as the mechanism underpinning the stability of the nanoparticles in cell growth medium, and the results of this present study are therefore consistent with this hypothesis.

As was demonstrated for solid AuNPs (section 3.4.3), HGNs also localised within intracellular lysosomes and endosomes (Figure 6-2), however compared to solid AuNPs, they appeared more dispersed throughout the lysosomes As a result of the hollow core within HGNs their overall electron density is much lower than that of solid AuNPs and it was therefore more difficult to visualise the HGNs within the cells by TEM analysis which is dependent on the degree of electron scatter from the sample material.

The ICP-MS results (Figure 6-3) demonstrated that the same patterns of nanoparticle uptake with respect to incubation time and nanoparticle concentration were observed following incubation of cells with HGNs as were seen with solid AuNPs. Firstly, the amount of internalised Au increased following an increase in both administered HGN concentration and HGN incubation time. As was observed with solid AuNPs, the greatest HGN uptake was observed in UVW/NAT cells and the lowest in A375 cells.

In an attempt to compare the uptake of solid AuNPs versus HGNs, the number of particles internalised by each cell line was calculated. In UVW/NAT cells the number of solid AuNPs internalised per cell following a 24 hour incubation were higher than the number of HGN taken up ($5.4x10^{\wedge 16}\pm1.2x10^{\wedge 16}$ vs. $3.9x10^{\wedge 16}\pm1.8x10^{\wedge 16}$). In SK-

N-BE and A375 cells however the number of solid and hollow particles per cell following a 24 hour incubation period were similar ($2.3x10^{\wedge16}\pm8.7x10^{\wedge15}$ vs. $2.3x10^{\wedge16}\pm4.7x10^{\wedge15}$ in SK-N-BE cells and $1.0x10^{\wedge16}\pm3.9x10^{\wedge15}$ vs. $9.2x10^{\wedge15}\pm6.0x10^{\wedge15}$ in A375 cells respectively). This suggested that the uptake of each type of nanoparticle was similar, however accurate conclusions regarding the uptake of each type of nanoparticle cannot be drawn as the nanoparticle concentration, diameter and surface chemistry were different between the solid AuNPs and the HGNs.

As discussed in section 1.6.5.2, whilst AuNPs were traditionally considered chemically inert, many studies have reported varying degrees of cytotoxicity in cells in response to solid AuNPs. HGNs have also been shown to induce some cytotoxicity in cells. For example the study by You *et al*, (2010), reported a 20% reduction in the cell survival of a breast cancer cell line following exposure to HGNs at a concentration of 2.5 μg/mL (You et al., 2010). In contrast this, Park *et al*, (2015), observed no toxicity in a lung cancer cell line following incubation with HGNs at a concentration of 1 mM (Park et al., 2015). In this present study, incubation of both UVW/NAT and A375 cells with HGNs as a single agent up to a concentration of 10 nM had no effect on their clonogenic survival (Figure 6-4). In SK-N-BE cells however, incubation of cells with the highest concentrations of HGNs resulted in a significant reduction in cell survival. Based on these observations the concentration range of HGNs from 0-5 nM was employed in subsequent experiments.

The results of this chapter demonstrated that the synthesised HGNs were stable in cell growth medium, localised within intracellular lysosomes and induced no reduction in cell survival fraction in any of the cell lines investigated up to a concentration of 5 nM. The aim of the subsequent chapters was to assess the radiosensitisation potential of HGNs in combination with kV X-ray photons and high energy β electrons from the decay of ^{131}I in the form of [^{131}I]-MIBG.

Chapter 7

Investigation of the radiosensitisation potential of HGNs in combination with External Beam Radiation (XBR)

Chapter 7: Investigation of the radiosensitisation potential of HGNs in combination with External Beam Radiation (XBR)

7.1 Introduction

Hollow gold nanoparticles (HGNs), as discussed in section 1.7 have been shown to demonstrate enhanced UV absorption properties which increase the electromagnetic field surrounding the HGN, compared to solid AuNPs (Gutrath et al., 2012; Jackson et al., 2003). The increased UV absorption, together with the greater surface area available in HGNs due to the hollow core should lead to increased photon absorption and subsequently a greater radiation dose enhancement within the target area following the combination of HGNs with ionising radiation, compared to solid AuNPs. However there are many additional considerations in attempting to directly compare the radiosensitising potential of different types of nanoparticles, such as the kinetics of uptake, nanoparticle diameter and surface chemistry. These variables make a direct comparison of the efficiency of HGNs and solid AuNPs as radiosensitisers extremely complex and out with the scope of this present study. The aims of this chapter was therefore to examine the radiosensitising potential of in house synthesised HGNs in combination with XBR.

The previous chapter demonstrated successful synthesis of HGNs and their stability in cell growth medium. Furthermore successful internalisation of the HGNs was demonstrated in each of the 3 cell lines investigated, although the degree of HGN uptake differed between the different cell lines. In each cell line, the HGNs localised within the cytoplasmic endosomes/lysosomes. In this chapter the radiosensitisation potential of the synthesised HGNs in combination with kVp X-ray XBR was assessed by evaluating the clonogenic cell survival following treatment of cells with HGNs alone and in combination with XBR, compared to XBR alone. This was followed by assessment of the effect of HGNs alone and in combination with XBR on the dynamics of DNA double stranded damage and repair, and the progression of cells through the cell cycle, compared to the effects of XBR alone.

7.2 Aims

The primary aim of this chapter was to evaluate the radiosensitisation potential of HGNs in combination with XBR by investigating the clonogenic cell survival of UVW/NAT, SK-N-BE and A375 cells incubated with HGNs prior to XBR exposure using clonogenic survival assays.

The subsequent aim of this study was to assess the effect of single and combination treatments on the progression of cells through the cell cycle and DNA double stranded damage and repair kinetics.

7.3 Materials and Methods

7.3.1 Cells and culture conditions

The human glioblastoma cell line UVW/NAT, human neuroblastoma cell line SK-N-BE and human melanoma cell line A375 were employed in this study. All cells were cultured and maintained as detailed in sections 2.3.1 and 3.3.4.

7.3.2 Synthesised hollow gold nanoparticles (HGNs)

All HGNs were synthesised in the Graham Lab (University of Strathclyde) by adaptation of previously reported methods (Schwartzberg et al., 2006; Xie et al., 2013) as detailed in section 6.3.1.

7.3.3 Treatment of cells with HGNs and XBR

The concentration range of synthesised HGNs employed in this study was 0-5 nM. All cells lines were incubated with HGNs for 24 hours as described in section 2.3.3.

All irradiation of cells with XBR was performed using a cell irradiation cabinet (XRAD 225) with a 225 kVp X-ray beam and a dose rate of 2.2 Gy/min and 13.00 mA current as described in section 2.3.3.

For all combination experiments cells were incubated with HGNs in the concentration range 0-5 nM for 24 hours and then exposed to XBR across the dose range 0-4 Gy.

7.3.4 Clonogenic survival assay

Clonogenic survival assays were used to assess the clonogenic survival of each cell line following exposure to HGNs alone and in combination with XBR. For assessment of UVW/NAT and A375 cells, clonogenic survival assays were performed as described in section 2.3.5 and in SK-N-BE cells as described in section 3.3.7.1. All results are presented as the average cell survival fraction (mean ± sd) of 3 independent experiments unless otherwise stated.

7.3.5 Cell cycle analysis

The progression of cells through the cell cycle was determined to assess whether XBR in combination with HGNs caused an abrogation to the normal cycling of cells. Cell cycle progression was assessed as described in section 4.3.7. Three independent experiments were carried out, unless otherwise stated and results presented as the percentage of cells in each phase of the cell cycle (mean ± sd).

7.3.6 γ-H2AX analysis by foci staining and confocal microscopy

The effect of XBR in combination with HGNs on the magnitude and dynamics of DNA DSBs was determined as described in section 4.3.8. Results are presented as the average number of γ-H2AX foci/cell (mean ± sd) of 3 independent experiments.

7.3.7 Caspase 3/7 apoptosis assays

Caspase 3 activity assays were performed to assess the effects of HGNs and XBR alone, and in combination, as described in section 4.3.9. Three independent

experiments were performed with results presented as the average fold increase in the fluorescence intensity of free AMC compared to control cells per sample (mean ± sd).

7.3.8 Statistical Analysis

7.3.8.1 Analysis of variance (ANOVA)

All experiments were carried out 3 times, unless otherwise stated, with results reported as the (mean ± sd). Clonogenic survival data are presented as the cell survival fraction normalised to untreated control cells for treatment with HGNs and XBR alone or normalised to HGN treatment alone for combination treatments. Cell cycle data is presented as the percentage of cells within each phase of the cell cycle and γ-H2AX data as the number of γ-H2AX foci/cell for each treatment group. Caspase 3 activity for each treatment group is presented as the fold change in activity compared to untreated control cells. Results were evaluated using two-way ANOVA with Bonferroni post-tests to determine if the effects of combination therapy on the clonogenic survival, progression and accumulation of cells throughout the cell cycle, formation of γ-H2AX foci and caspase activity were statistically significant compared to the effects of XBR alone. P-values lower than 0.05 were considered statistically different.

7.3.8.2 Linear quadratic analysis

To evaluate the radiosensitisation potential of HGNs in combination with XBR and determine if the intracellular presence of HGNs enhanced the clonogenic cell kill, the experimental clonogenic survival data for UVW/NAT, SK-N-BE and A375 cells exposed to XBR alone and in combination with HGNs was fitted to the linear quadratic model (equation 1) (Dale, 2004) using GraphPadPrism software, version 6.01, 2014 (CA) as described in section 2.3.6.2. The α and β values, IC_{50} and DEF at the 50% toxicity level were calculated for XBR alone and in combination with AuNPs for each cell line using equations 2 and 3 as described in sections 2.3.6.2.

7.4 Results

7.4.1 Determination of the radiosensitisation effect of HGNs in combination with XBR using the linear quadratic model

The effect of in house synthesised HGNs on the radiation induced cell kill in UVW/NAT, SK-N-BE and A375 cells was assessed using clonogenic survival assays. Cells were incubated with HGNs across the concentration range 0-5 nM for 24 hours prior to exposure to 0-4 Gy XBR and clonogenic survival assays were performed 24 hours after irradiation. The average clonogenic survival for cells treated with HGNs in combination with XBR was normalised to the effect of HGN alone. Two-way ANOVA with Bonferroni post-hoc testing for multiple comparisons was carried out for each cell line to determine if the clonogenic survival fractions observed for cells treated with HGNs in combination with XBR were significantly different from those observed following exposure to XBR alone. The clonogenic survival data for each cell line was then fitted to the linear quadratic model using GraphPad Prism software version 6.0.1.

7.4.1.1 The effect of HGNs in combination with XBR on clonogenic cell kill in UVW/NAT cells

In UVW/NAT cells, incubation with HGNs for 24 hours prior to XBR exposure resulted in a statistically significant decrease in clonogenic survival at all HGN concentrations in combination with 0.5 Gy and 1 Gy, and additionally the combination of 1 nM and 5 nM HGNs with 2 Gy, compared to radiation exposure alone (Figure 7-1(A-B)). Combination of HGNs at all concentrations with 4 Gy XBR resulted in no significant difference in clonogenic capacity, compared to 4 Gy alone. Combination of 5 nM HGNs with 0.5 Gy, 1 Gy, 2 Gy and 4 Gy resulted in cell survival fractions of 0.60±0.07, 0.49±0.06, 0.26±0.04 and 0.24±0.03, compared to 0.95±0.05 ($p<0.0001$), 0.81±0.04 ($p<0.0001$), 0.67±0.08 ($p<0.0001$) and 0.32±0.09 ($p>0.05$) for 0.5 Gy, 1 Gy, 2 Gy and 4 Gy alone.

The clonogenic survival data from Figure 7-1(A) was fitted to the linear quadratic model (Figure 7-1(C)) and values for α, β, IC_{50} and DEF_{50} calculated (Figure 7-1(D)). In UVW/NAT cells incubated with HGNs prior to XBR exposure a concentration

dependant decrease in the dose of XBR required to kill 50% of the cell population (IC_{50}) was observed with increasing HGN concentrations. The IC_{50} reduced from 2.89 Gy for XBR alone to 2.29 Gy, 1.71 Gy and 1.04 Gy in the presence of HGNs at 0.1 nM, 1 nM and 5 nM respectively, indicating that the presence of HGNs enhanced the efficacy of radiation in a concentration dependant manner. The calculated α coefficient values for the combination of HGNs with XBR increased proportionally with HGN concentration, compared to XBR. The calculated α values increased from 0.13 Gy^{-1}±0.02 for XBR alone to 0.37 Gy^{-1}±0.03, 0.52 Gy^{-1}±0.05 and 0.79 Gy^{-1}±0.02 in the presence of HGNs at 0.1 nM, 1 nM and 5 nM respectively, suggesting that the presence of HGNs resulted in a concentration dependant increase in toxicity at lower XBR doses, as discussed in section 2.3.6.2 (Barendsen, 1994). The DEFs calculated at the 50% toxicity level (DEF_{50}) were 1.26, 1.69 and 2.77 for XBR in combination with HGNs at 0.1 nM, 1 nM and 5 nM and demonstrated that the presence of HGNs resulted in a concentration dependant dose enhancement.

(A)

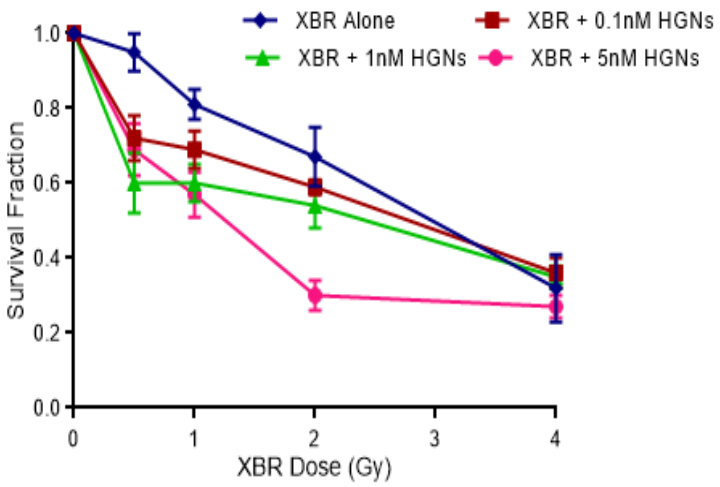

(B)

	0.1nM	1.0nM	5.0nM
0.5Gy	****	****	****
1.0Gy	**	****	****
2.0Gy	ns	***	****
4.0Gy	ns	ns	ns

Figure 7-1 continued overleaf

(C)

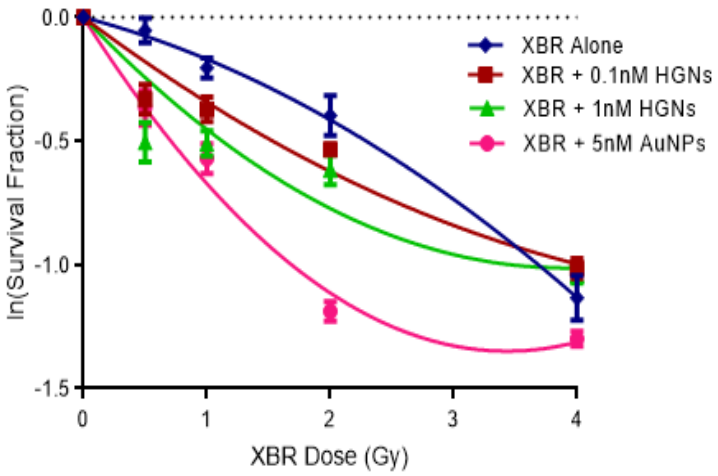

(D)

	0nM	**0.1nM**	**1.0nM**	**5.0nM**
α (Gy^{-1})	0.13±0.02	0.37±0.03	0.52±0.05	0.79±0.02
β (Gy^{-1})	0.04±0.005	-0.03±0.01	-0.07±0.01	-0.11±0.01
R^2	0.98	0.93	0.80	0.97
IC_{50} (Gy)	2.89	2.29	1.71	1.04
DEF_{50}	1.00	1.26	1.69	2.77

Figure 7-1: Clonogenic survival of UVW/NAT cells exposed to HGNs in combination with XBR.

UVW/NAT cells were incubated with HGNs from 0-5 nM for 24 hours. Following this cells were exposed to XBR from 0-4 Gy with clonogenic survival assays performed 24 hours after irradiation. Clonogenic survival results are presented as the mean survival fraction of treated cells (mean ± sd) normalised to HGN treatment alone, of 5 independent experiments (A). Statistically significant differences in the cell survival fraction for HGNs in combination with XBR, compared to XBR alone were assessed using two-way ANOVA with Bonferroni post-tests at 95% C.I. Two (**), three (***) and four (****) symbols indicate $p<0.01$, $p<0.001$ and $p<0.0001$ and ns indicates no significance respectively (B). Clonogenic survival data presented in (A) was fitted to the linear quadratic model using GraphPad Prism version 6.0.1 (C) and values calculated for the α and β coefficients and the IC_{50} and DEF_{50} for XBR in combination with HGNs at each HGN concentration (D).

7.4.1.2 The effect of HGNs in combination with XBR on clonogenic cell kill in SK-N-BE cells

In SK-N-BE cells, incubation with HGNs for 24 hours prior to XBR exposure resulted in a statistically significant decrease in clonogenic survival at all HGN concentrations in combination with 2 Gy and 4 Gy, and at 0.1 nM HGNs with 0.5 Gy and 1 Gy, and 5 nM HGNs with 1 Gy, compared to XBR exposure alone, (Figure 7-2(A-B)). The combination of HGNs at 5 nM with 0.5 Gy, 1 Gy, 2 Gy and 4 Gy resulted in cell survival fractions of 0.67±0.05, 0.50±0.07, 0.45±0.10 and 0.27±0.02 compared to 0.84±0.03, 0.77±0.01 ($p<0.0001$), 0.68±0.11 ($p<0.001$) and 0.48±0.08 ($p<0.001$) for 0.5 Gy, 1 Gy, 2 Gy and 4 Gy alone.

The clonogenic survival data from Figure 7-2(A) was fitted to the linear quadratic model (Figure 7-2(C)) and values for α, β, IC_{50} and DEF_{50} calculated (Figure 7-2(D)). In SK-N-BE cells, treatment with HGNs in combination with XBR resulted in a decrease in the dose of XBR required to kill 50% of the cell population (IC_{50}). The IC_{50} was 3.65 Gy for XBR alone and were 1.46 Gy, 1.96 Gy and 1.31 Gy in the presence of HGNs at 0.1 nM, 1 nM and 5 nM respectively, indicating that the presence of HGNs enhanced the efficacy of radiation, independently of the HGN concentration. The calculated α values for the combination of HGNs with XBR increased from 0.25 Gy^{-1}±0.02 for XBR alone to 0.59 Gy^{-1}±0.04, 0.36 Gy^{-1}±0.03 and 0.63 Gy^{-1}±0.04 in the presence of HGNs at 0.1 nM, 1 nM and 5 nM respectively, suggesting that the presence of HGNs resulted in an increase in toxicity at lower XBR doses, which was independent of HGN concentration. The DEFs calculated at the 50% toxicity level (DEF_{50}) were 2.51, 1.86 and 2.79 for XBR in combination with HGNs at 0.1 nM, 1 nM and 5 nM, and demonstrated that the presence of HGNs resulted in a radiation dose enhancement which was independent of HGN concentration.

(A)

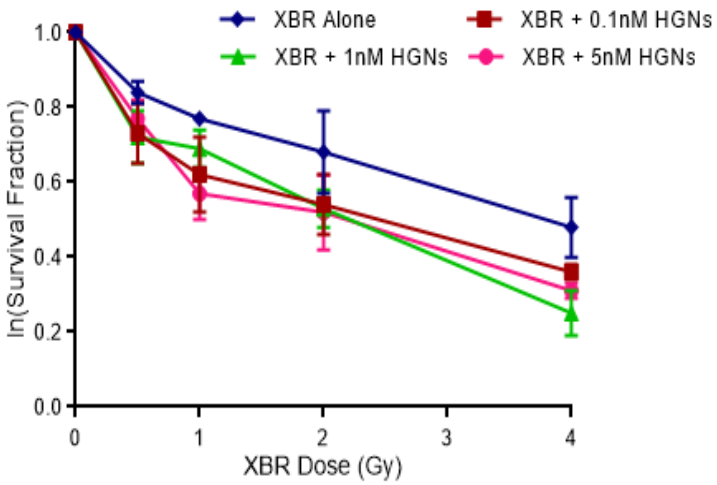

(B)

	0.1nM	1.0nM	5.0nM
0.5Gy	*	*	ns
1.0Gy	**	ns	****
2.0Gy	**	**	***
4.0Gy	*	****	***

Figure 7-2 continued overleaf

(C)

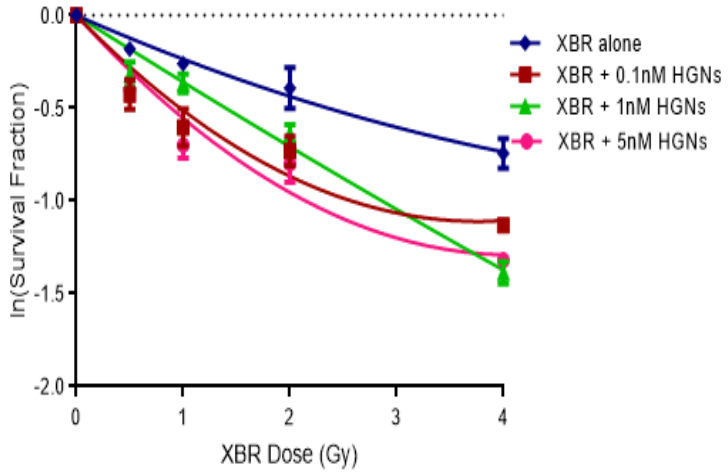

(D)

	0nM	0.1nM	1.0nM	5.0nM
α (Gy^{-1})	0.25±0.02	0.59±0.04	0.36±0.03	0.63±0.04
β (Gy^{-1})	0.02±0.02	-0.08±0.01	-0.01±0.008	-0.07±0.01
R^2	0.93	0.90	0.97	0.93
IC_{50} (Gy)	3.65	1.46	1.96	1.31
DEF_{50}	1.00	2.51	1.86	2.79

Figure 7-2: Clonogenic survival of SK-N-BE cells exposed to HGNs in combination with XBR.

SK-N-BE cells were incubated with HGNs from 0-5 nM for 24 hours. Following this cells were exposed to XBR from 0-4 Gy with clonogenic survival assays performed 24 hours after irradiation. Clonogenic survival results are presented as the mean survival fraction of treated cells (mean ± sd) normalised to HGN treatment alone, of 5 independent experiments (A). The statistical significance of the cell survival fractions for HGNs in combination with XBR, compared to XBR alone were assessed using two-way ANOVA with Bonferroni post-tests at 95% C.I. One (*), two (**), three (***) and four (****) symbols indicate $p<0.05$, $p<0.01$, $p<0.001$ and $p<0.0001$ and ns indicates no significance respectively (B). Clonogenic survival data presented in (A) was fitted to the linear quadratic model using GraphPad Prism version 6.0.1 (C) and values calculated for the α and β coefficients and the IC_{50} and DEF_{50} for XBR in combination with HGNs at each HGN concentration (D).

7.4.1.3 The effect of HGNs in combination with XBR on clonogenic cell kill in A375 cells

In A375 cells, due to time constraints, data was only obtained for HGNs at 0.1 nM and 5 nM in combination with 1 Gy and 2 Gy XBR. The combination of 5 nM HGNs and XBR resulted in a statistically significant decrease in clonogenic survival at all XBR doses, compared to XBR exposure alone (Figure 7-3(A-B)). Combination of HGNs at 5 nM with 1 Gy and 2 Gy resulted in cell survival fractions of 0.45±0.05 and 0.22±0.11 compared to 0.76±0.03 ($p<0.001$) and 0.53±0.05 ($p<0.001$) for 1 Gy and 2 Gy alone.

The clonogenic survival data from Figure 7-3(A) was fitted to the linear quadratic model (Figure 7-3(C)) and values for α, β, IC_{50} and DEF_{50} calculated (Figure 7-3(D)). In A375 cells, combination resulted in a concentration dependant decrease in the IC_{50} for XBR. The IC_{50} reduced from 2.15 Gy for XBR alone to 1.76 Gy and 0.89 Gy in the presence of HGNs at 0.1 nM and 5 nM respectively, indicating that the presence of HGNs enhanced the efficacy of radiation and that this enhancement increased with increasing HGN concentration. The calculated α values for the combination of HGNs with XBR increased from 0.24 Gy^{-1}±0.04 for XBR alone, to 0.46 Gy^{-1}±0.12 and 0.81 Gy^{-1}±0.07 in the presence of HGNs at 0.1 nM and 5 nM respectively suggesting that the presence of HGNs resulted in HGN concentration dependant increase in the toxicity at lower XBR doses. The DEFs calculated at the 50% toxicity level (DEF_{50}) were 1.22 and 2.42 for XBR in combination with HGNs at 0.1 nM and 5 nM, and demonstrated that the presence of HGNs resulted in a radiation dose enhancement which was greater at higher HGN concentrations.

(A)

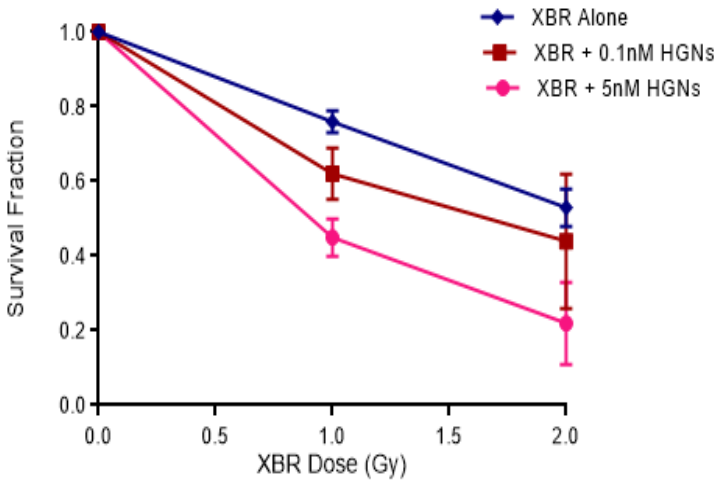

(B)

	0.1nM	5.0nM
1.0Gy	ns	***
2.0Gy	ns	***

Figure 7-3 continued overleaf

(C)

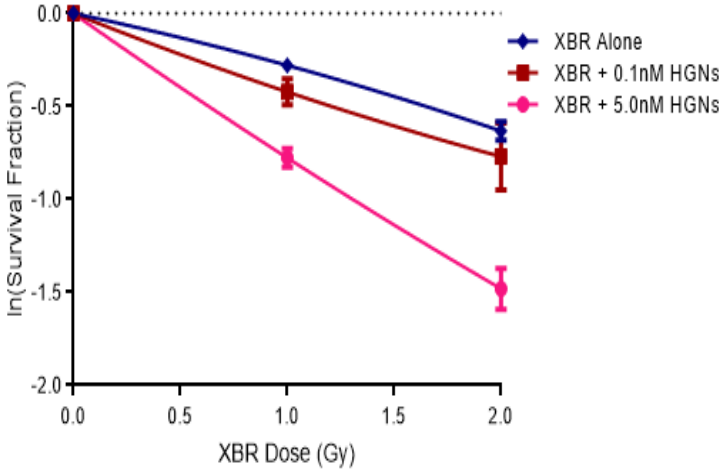

(D)

	0nM	0.1nM	5.0nM
α (Gy^{-1})	0.24±0.04	0.46±0.12	0.81±0.07
β (Gy^{-1})	0.04±0.02	-0.04±0.06	-0.03±0.04
R^2	0.99	0.92	0.99
IC_{50} (Gy)	2.15	1.76	0.89
DEF_{50}	1.00	1.22	2.42

Figure 7-3: Clonogenic survival of A375 cells exposed to HGNs in combination with XBR.

A375 cells were incubated with HGNs at 0.1 nM and 5 nM for 24 hours. Following this cells were exposed to XBR from 0-2 Gy with clonogenic survival assays performed 24 hours after irradiation. Clonogenic survival results are presented as the mean survival fraction of treated cells (mean ± sd) normalised to HGN treatment alone, of 3 independent experiments (A). The statistical significance of the cell survival fractions for HGNs in combination with XBR, compared to XBR alone was assessed using two-way ANOVA with Bonferroni post-tests at 95% C.I. Three (***) symbols indicate $p<0.001$ and ns indicates no significance respectively (B). Clonogenic survival data presented in (A) was fitted to the linear quadratic model using GraphPad Prism version 6.0.1 (C) and values calculated for the α and β coefficients and the IC_{50} and DEF_{50} for XBR in combination with HGNs at each HGN concentration (D).

In summary, the clonogenic survival data demonstrated that significant radiosensitisation was achieved from the combination of in house synthesised HGNs with XBR in all cell lines investigated, with DEF_{50} of 2.77, 2.79 and 2.42 with 5 nM HGNs in UVW/NAT, SK-N-BE and A375 cells respectively. The greatest degree of radiosensitisation was observed in UVW/NAT cells which demonstrated the highest uptake of HGNs and the lowest in A375 cells which had the lowest internalised HGN concentration.

The uptake of HGNs following 24 hour incubation with 5 nM, the IC_{50} for XBR and the DEF_{50} for 5 nM HGNs in each cell line is presented in Table 7-1 for each of the cell lines investigated to allow clear visualisation of the differences in dose enhancement between each of the cell lines, and the corresponding radiation sensitivity and intracellular Au content of the cell lines. Based on these data, the combination of 5 nM HGNs with 2 Gy XBR was used to determine if radiosensitisation was associated with changes in the progression of cells through the cell cycle, and changes in the dynamics of DNA double stranded breaks and apoptosis.

Table 7-1: Uptake of 5 nM HGNs, IC_{50} dose for XBR and DEF_{50} for 5 nM HGNs in UVW/NAT, SK-N-BE and A375 cells respectively.

	UVW/NAT	SK-N-BE	A375
5nM HGN uptake (ug/cell)	0.021±0.01	0.018±0.01	0.005±0.003
XBR IC_{50} (Gy)	2.89	3.65	2.15
DEF_{50} for 5nM HGNs + XBR	2.77	2.79	2.42

7.4.2 The effect of HGNs in combination with XBR on the cell cycle progression of UVW/NAT, SK-N-BE and A375 cells

The effect of 5 nM HGNs as a single agent and in combination with XBR at 2 Gy on the progression of each cell line through the cell cycle was determined at 2, 6 and 24 hours after treatment.

In each cell line investigated, treatment with 5 nM HGNs alone had no effect on the normal progression of cells through the cell cycle, compared to untreated control cells at any timepoint assessed ($p>0.05$) (Figure 7-4). This was consistent with the clonogenic survival data (Figure 6-4) which demonstrated no significant decrease in cell survival fraction in any of the cell lines following incubation with 5 nM HGNs.

In UVW/NAT cells, exposure to 2 Gy XBR alone resulted in a significant accumulation of cells within the G2/M phase of the cell cycle 24 hours post irradiation compared to untreated control cells (Figure 7-4(A)). The percentage of cells within G2/M increased from 31.4%±0.82 in untreated control cells to 41.8%±6.68 ($p<0.001$) in cells irradiated with 2 Gy XBR. At both 2 and 6 hours after irradiation treatment of UVW/NAT cells with 2 Gy XBR resulted in no significant accumulation of cells in G2/M compared to control cells ($p>0.05$).

In SK-N-BE cells, exposure to 2 Gy XBR alone resulted in an increase in the proportion of cells in G2/M at 6 and 24 hours post irradiation compared to untreated control cells, although the increase was not statistically significant at either time point (Figure 7-4(B)). The percentage of cells within G2/M increased from 47.1%±5.60 and 40.1%±4.80 in untreated control cells at 6 and 24 hours after irradiation to 59.9%±6.20 ($p>0.05$) and 52.8%±10.20 ($p>0.05$) at 6 and 24 hours after irradiation in cells irradiated with 2 Gy XBR.

In A375 cells, exposure to 2 Gy XBR alone resulted in a significant increase in the proportion of cells in G2/M at 6 hours post irradiation compared to untreated control cells (Figure 7-4(C)). The percentage of cells within G2/M increased from 22.4%±2.60 in untreated control cells to 33.1%±6.60 ($p<0.05$) in cells irradiated with 2 Gy XBR. At both 2 and 24 hours after irradiation treatment with 2 Gy XBR resulted in no increase in the proportion of cells in G2/M compared to control cells ($p>0.05$).

In each cell line investigated, treatment with 5 nM HGNs in combination with 2 Gy XBR did not significantly increase the percentage of cells in the G2/M phase of the cell cycle, compared to XBR alone at any timepoint measured (Figure 7-4).

In each case the proportion of cells in G1 decreased as the proportion of cells in G2/M increased and no significant changes to the proportion of cells in the S phase of the cell cycle was observed following any treatment in any of the cell lines or timepoints measured.

In summary, analysis of the progression of cells through the cell cycle demonstrated that the combination of HGNs at 5 nM with 2 Gy XBR did not result in a statistically significant increase in the proportion of cells which arrested in G2/M compared to XBR exposure alone in any of the cell lines investigated.

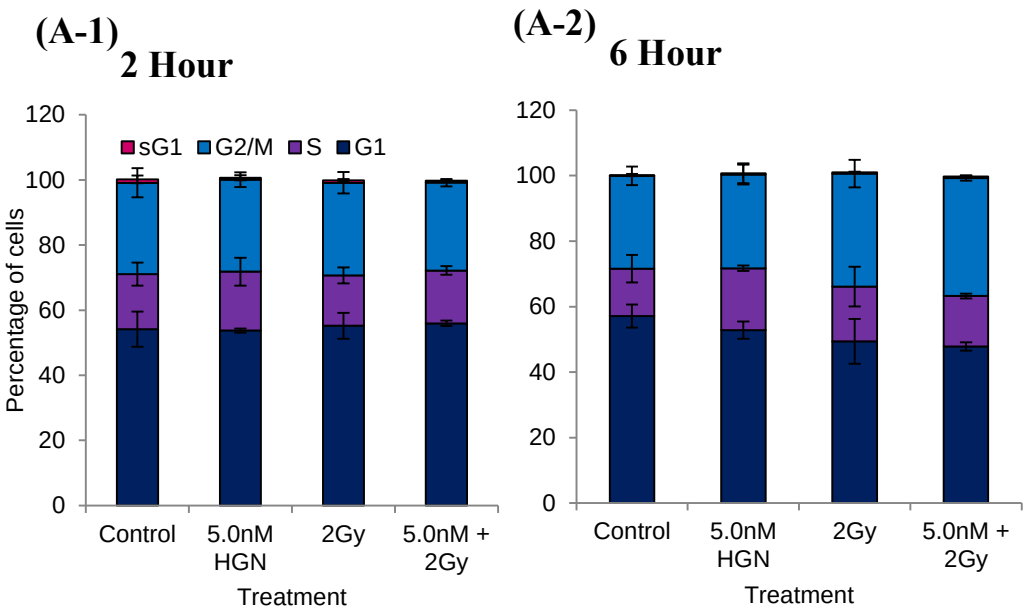

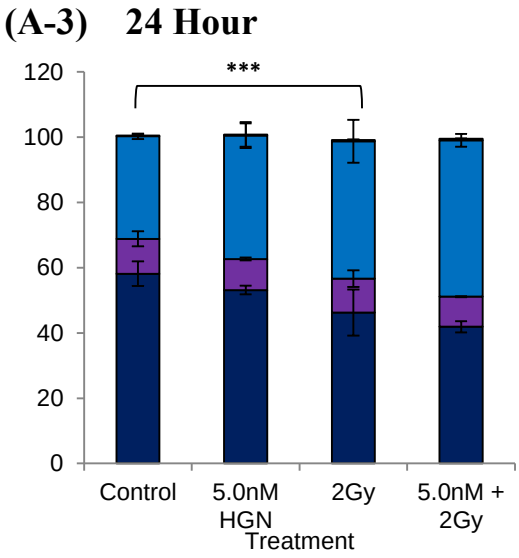

Figure 7-4 continued overleaf

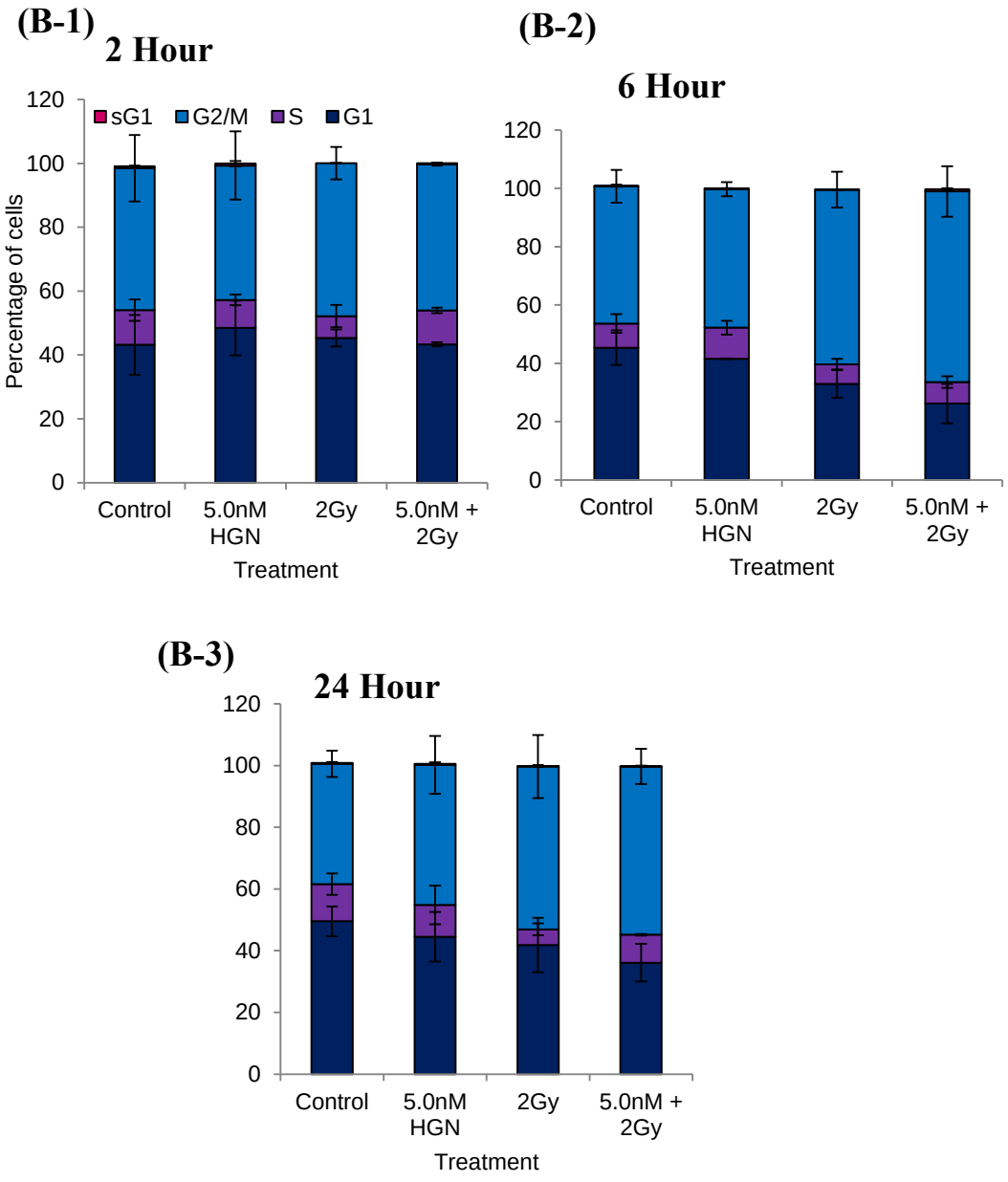

Figure 7-4 continued overleaf

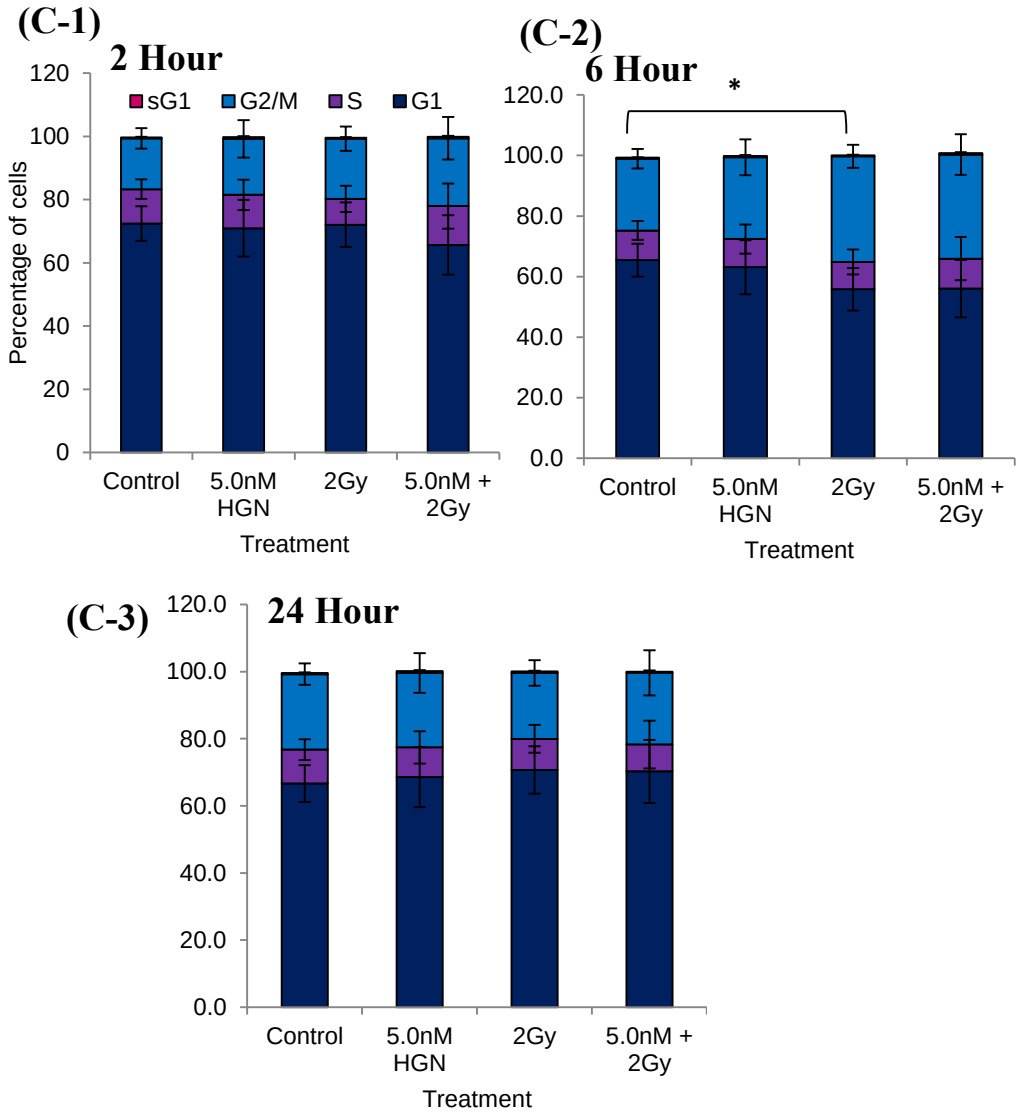

Figure 7-4: The effect of 5 nM HGNs and 2 Gy XBR, alone and in combination on the distribution of UVW/NAT, SK-N-BE and A375 cells throughout the cell cycle. UVW/NAT (A), SK-N-BE (B) and A375 (C) cells were incubated with HGNs at a concentration of 5 nM for 24 hours prior to 2 Gy XBR irradiation. The DNA content of the cells was labelled with PI and the cell cycle profiles obtained by FACS analysis at 2 (A-1, B-1, C-1), 6 (A-2, B-2, C-2) and 24 (A-3, B-3, C-3) hours after irradiation. The proportion of cells in G0/G1, S and G2/M were measured using BDCellDiva^{tm} Pro software. Two-way ANOVA was used to determine if statistically significant changes in the distribution of cells throughout the cell cycle resulted as an effect of HGN and XBR exposure alone (compared to untreated control cells) or in combination (compared to the effects of XBR alone). All tests were performed at the 95% C.I of 3 independent experiments, unless otherwise stated (A375 n=4). One (*) and three (***) symbols indicates $p<0.05$, $p<0.001$.

7.4.3 The effect of HGNs in combination with XBR on the magnitude and dynamics of DNA double strand break and repair in UVW/NAT, SK-N-BE and A375 cells

The average number of γ-H2AX foci/cell was measured in UVW/NAT, SK-N-BE and A375 cells following treatment with 5 nM HGNs and 2 Gy XBR alone and in combination at 2 and 24 hours after irradiation (Figure 7-5). Two-way ANOVA with Bonferroni post-hoc testing for multiple comparisons was used to assess the effect of XBR or HGNs as single treatments compared to untreated controls on the number of γ-H2AX foci/cell. The effect of HGNs in combination with XBR on the number of γ-H2AX foci/cell, was assessed compared to XBR treatment alone.

In each cell line, treatment of cells with 5 nM HGNs alone resulted in no significant increase in the formation γ-H2AX foci/cell, compared to untreated control cells at both of the timepoints investigated ($p>0.05$).

The effect of XBR exposure alone was investigated in each cell line in chapter 4, section 4.4.6 (Figure 4-6) where it was demonstrated that after exposure to 2 Gy XBR, the number of γ-H2AX foci/cell was significantly higher in irradiated cells, compared to untreated control cells at both 2 and 24 hours after irradiation in each cell line. As expected, the number of γ-H2AX foci/cell significantly decreased between 2 and 24 hours after irradiation in each cell line, reflecting the repair of DNA DSBs.

In UVW/NAT cells, at 2 hours after XBR exposure there was no significant difference in the number of γ-H2AX foci/cell in cells exposed to 2 Gy XBR alone and in combination with 5 nM HGNs (39 foci/cell±2.27vs.41 foci/cell±0.89), suggesting that combination treatment did not lead to an increase in the number of DNA DSBs. Between 2 and 24 hours after irradiation however, the number of γ-H2AX foci/cell had decreased by 56%±1.69 following 2 Gy alone, whereas in the presence of HGNs the number of γ-H2AX foci/cell had decreased by only 39%±2.71. The average number of γ-H2AX foci/cell was 17 foci/cell±1.69 in cells treated with 2 Gy alone compared to 25 foci/cell±2.71 for cells treated with 2 Gy XBR and HGNs. This indicated that the presence of HGNs in combination with XBR reduced the resolution of DNA DSBs, compared to XBR alone.

In SK-N-BE cells, as observed in UVW/NAT cells, there was no significant difference between the number of γ-H2AX foci/cell in cells treated with 5 nM HGNs and 2 Gy XBR, compared to 2 Gy alone 2 hours after irradiation (42 foci/cell±8.01 vs. 38 foci/cell±1.82, $p>0.05$). Again as in UVW/NAT cells, at 24 hours after irradiation a significant reduction in the resolution of γ-H2AX foci/cell was observed in cells exposed to XBR in combination with HGNs, compared to XBR alone. The number of γ-H2AX foci/cell had decreased by 63%±1.03 following 2 Gy alone, whereas in the presence of HGNs the number of γ-H2AX foci/cell had decreased by only 36%±3.88. The average number of γ-H2AX foci/cell was 15 foci/cell±0.78 in cells treated with 2 Gy alone compared to 22 foci/cell±2.55 for cells treated with 2 Gy XBR and HGNs. This indicated that as in UVW/NAT cells the presence of HGNs in combination with XBR reduced the resolution of DNA DSBs, compared to XBR alone.

As observed in the other two cell lines investigated, in A375 cells, there was no significant difference between the number of γ-H2AX foci/cell induced by the combination of HGNs and 2 Gy XBR, compared to 2 Gy alone at 2 hours after irradiation (35 foci/cell±1.95 vs. 32 foci/cell±3.98 $p>0.05$). However, again at 24 hours post irradiation, treatment with HGNs in combination with XBR had an effect on the resolution of γ-H2AX foci/cell, compared to XBR alone. In cells treated with 2 Gy alone the number of γ-H2AX foci/cell decreased by 57%±1.63, compared to 17%±4.55 in combination treated cells. The number of γ-H2AX foci/cell was 15 foci/cell±1.63 for cells treated with 2 Gy alone compared to 27 foci/cell±1.25 in cells exposed to HGNs in combination with XBR ($p<0.0001$).

Overall the data suggested that in each of the cell lines investigated the presence of HGNs reduced the resolution of DNA DSBs, compared to XBR alone.

(A-1)

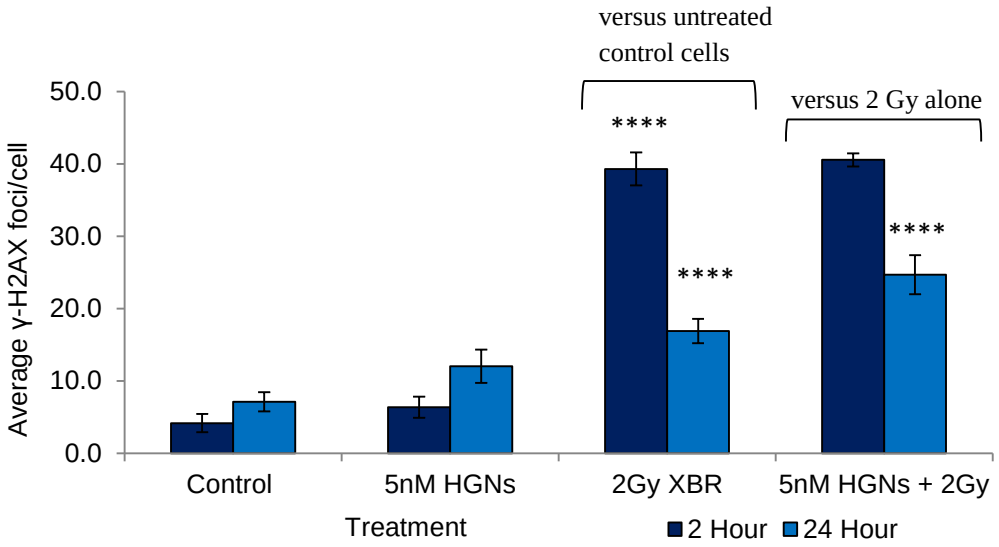

(A-2)

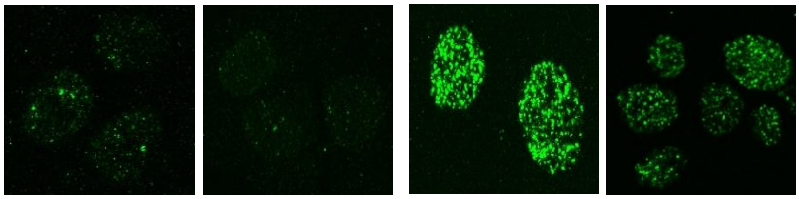

2 Hour: Control 5 nM HGNs 2 Gy XBR 5 nM HGNs + 2 Gy XBR

(A-3)

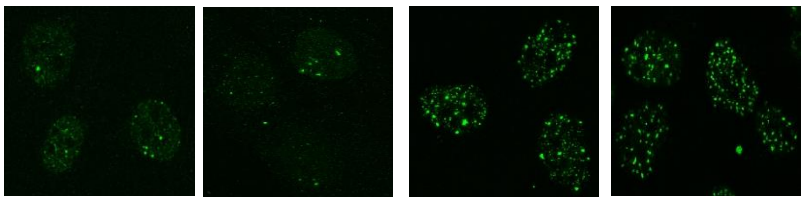

24 Hour: Control 5 nM HGNs 2 Gy XBR 5 nM HGNs + 2 Gy XBR

Figure 7-5 continued overleaf

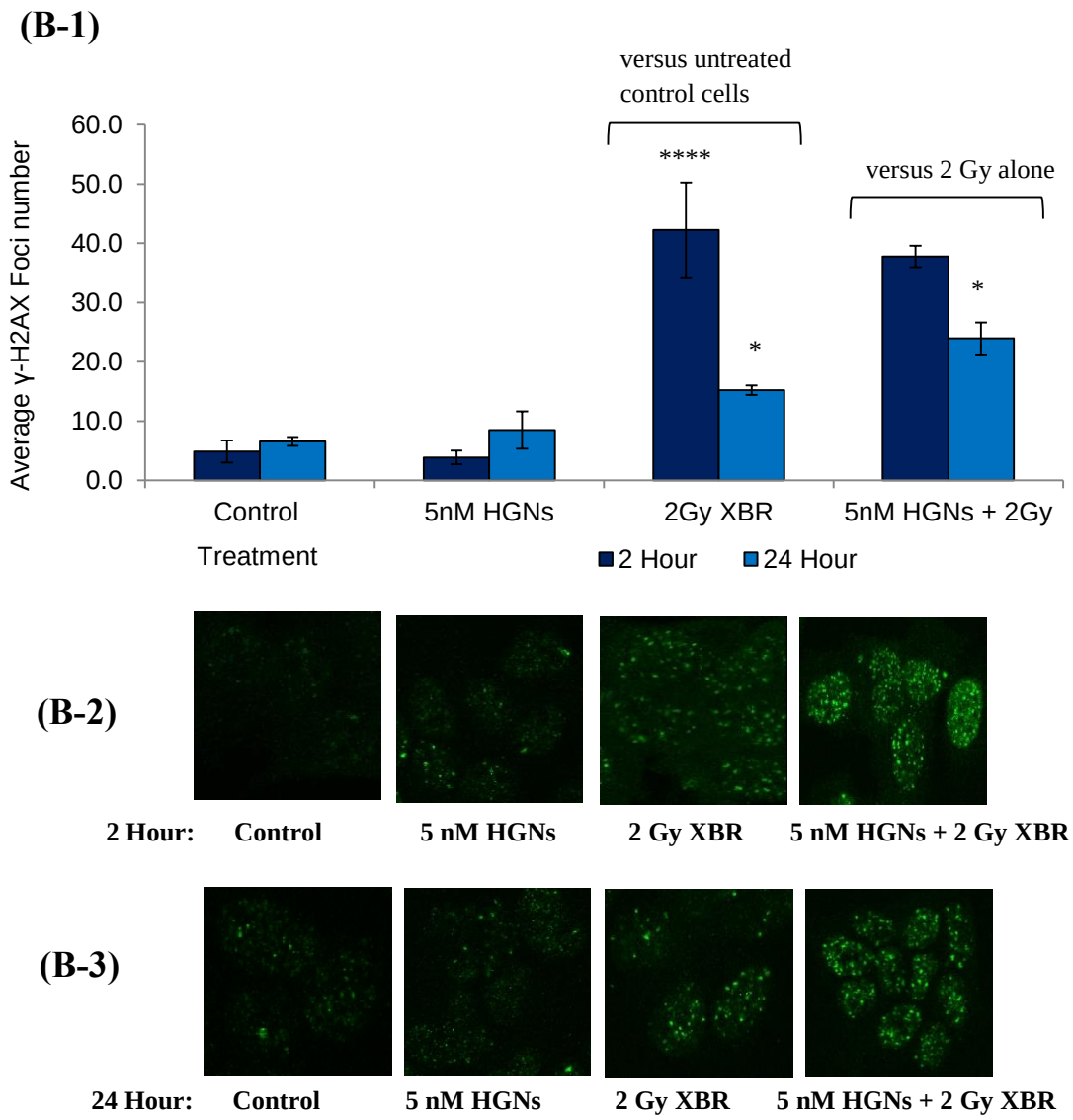

Figure 7-5 continued overleaf

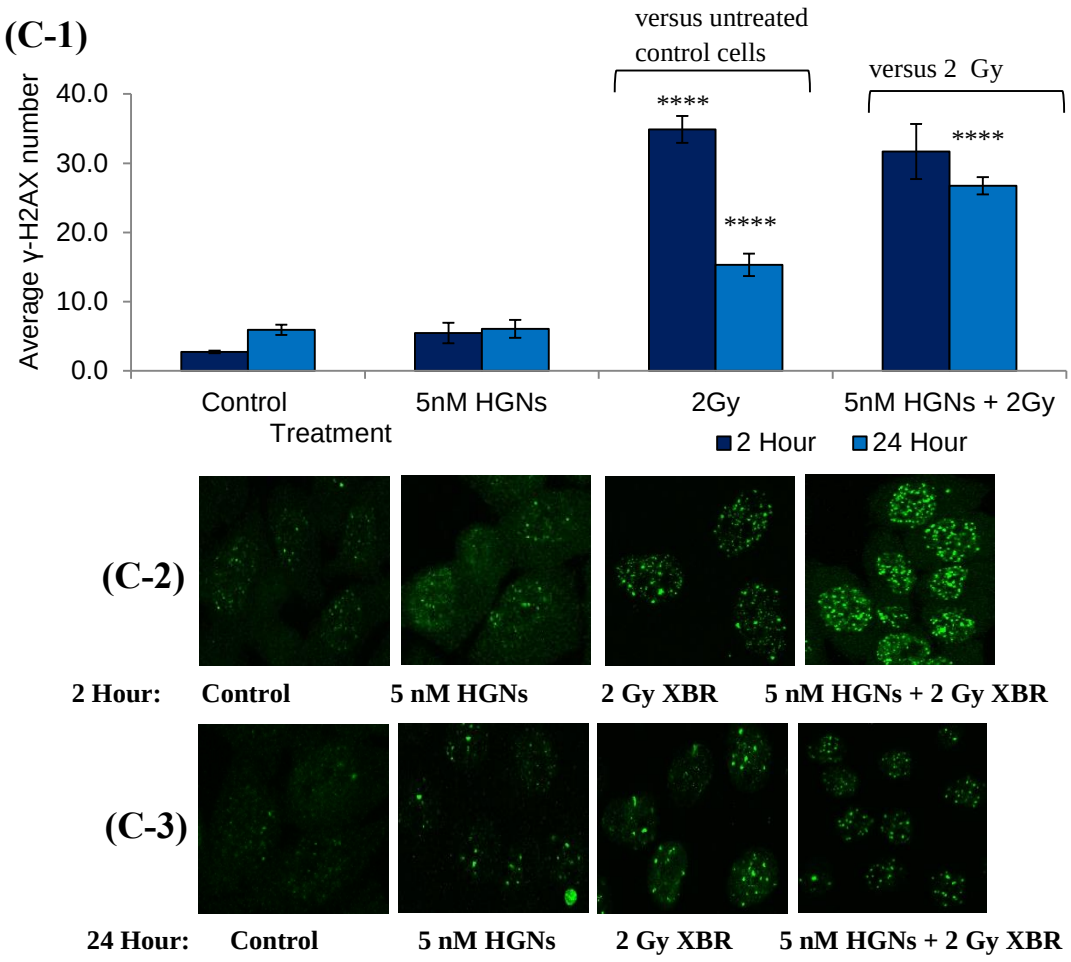

Figure 7-5: The effect of 5 nM HGNs and 2 Gy XBR alone and in combination on the formation and resolution of γ-H2AX foci in UVW/NAT, SK-N-BE and A375 cells.

Each cell line was treated with 5 nM HGNs for 24 hours prior to 2 Gy XBR exposure. The mean number of γ-H2AX foci/cell was assessed at 2 hour and 24 hour after irradiation using immunohistochemistry. Results presented are the mean number of γ-H2AX foci/cell (mean ± sd) of 3 independent experiments for HGNs and XBR alone and in combination in UVW/NAT (A), SK-N-BE (B) and A375 (C) cells respectively. Two-way ANOVA was used to determine if statistically significant changes in the number of γ-H2AX foci/cell resulted as an effect of 5 nM HGNs and 2 Gy alone (compared to untreated control cells) or in combination (compared to the effects of XBR alone). All tests were performed at the 95% C.I. One (*) and four (****) symbols indicate $p<0.05$ and $p<0.0001$ respectively. Representative images of γ-H2AX foci in each treatment group at 2 hours (A/B/C-2) and 24 hours (A/B/C-3) are presented.

7.4.4 The effect of XBR and HGNs alone and in combination on the activity of caspase 3 in UVW/NAT, SK-N-BE and A375 cells

Caspase 3 activity was used as a measure of apoptosis in response to treatment with HGNs and XBR alone and in combination in each cell line investigated (Figure 7-6). Two-way ANOVA with Bonferroni post-hoc testing for multiple comparisons was used to assess the effect of HGN treatment alone compared to untreated control cells on caspase 3 activity and in combination with XBR, compared to XBR alone.

In all cell lines investigated, exposure to HGNs alone at 0.1 nM, 1 nM and 5 nM for 6 or 24 hours induced no significant increase in caspase 3 activity compared to untreated control cells. Similarly, exposure to 2 Gy XBR alone induced no significant increase in caspase 3 activity at 6 or 24 hours after irradiation, compared to untreated control cells in any cell line. The combination of HGNs at 5 nM with 2 Gy XBR also had no effect on caspase 3 activity at 6 or 24 hours after irradiation, compared to XBR exposure alone in any of the cell lines examined. At 24 hours after irradiation the average fold-increase in caspase 3 activity in combination treated cells was 0.91±0.21 ($p>0.05$), 1.35±0.10 ($p>0.05$) and 1.01±0.06 ($p>0.05$) compared to 0.98±0.04, 1.22±0.03 and 1.00±0.04 for 2 Gy alone in UVW/NAT, SK-N-BE and A375 cells respectively. This suggested that the increased clonogenic cell kill observed from the combination of HGNs and XBR in all cell lines assessed was not a result of cell death by caspase mediated apoptosis.

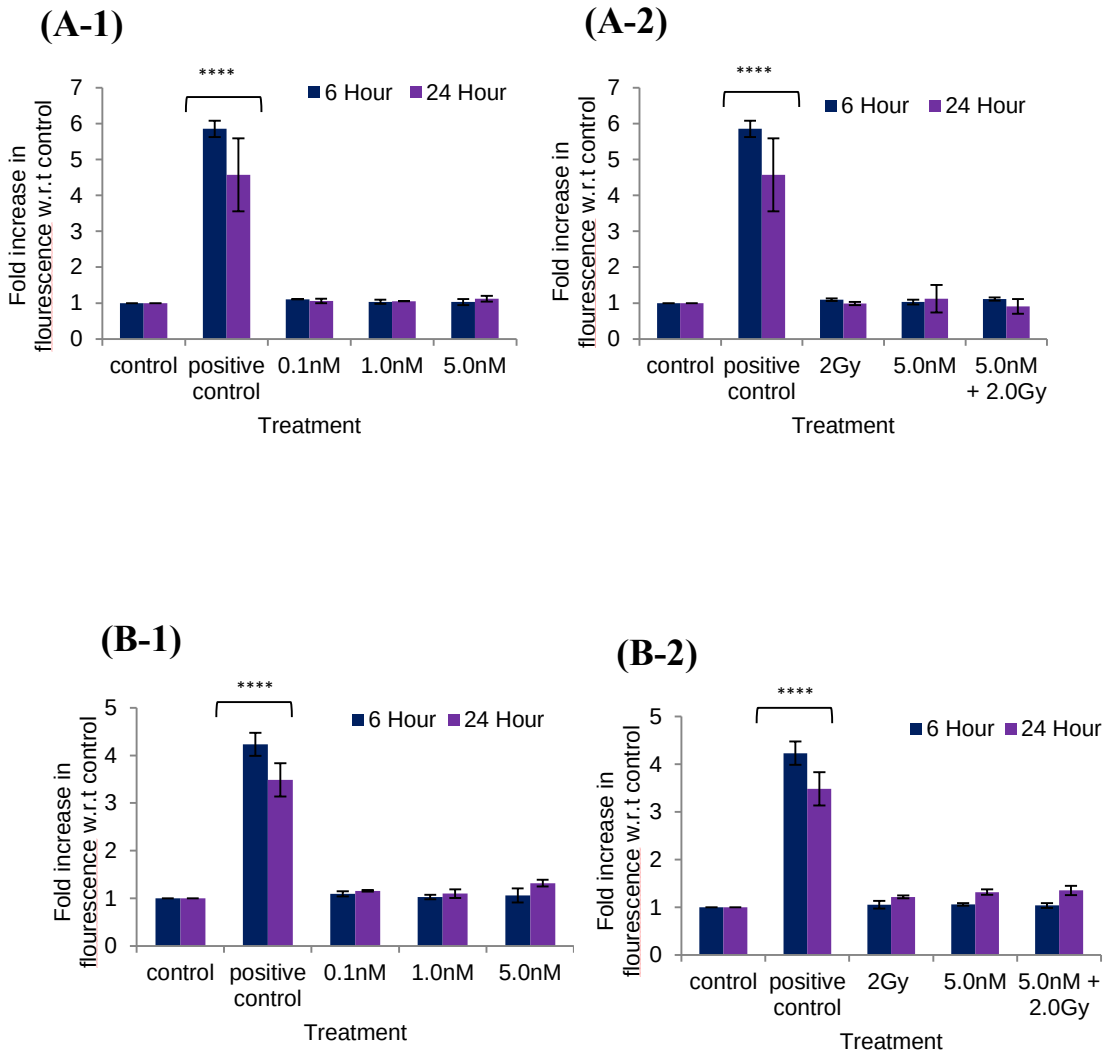

Figure 7-6 continued overleaf

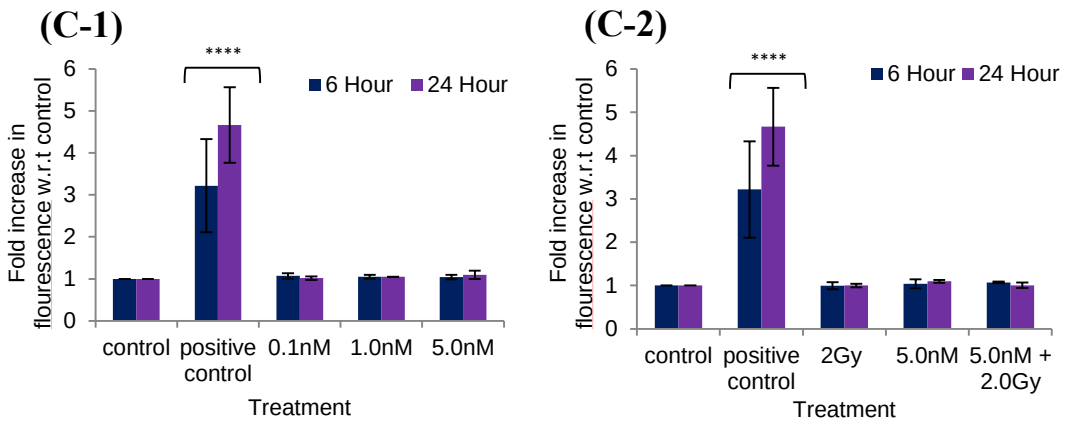

Figure 7-6: The effect of HGNs alone and in combination with XBR on the activity of caspase 3 measured in UVW/NAT, SK-N-BE and A375 cells.

Cells were exposed to 0-5 nM HGNs alone or to 5 nM HGNs in combination with 2 Gy XBR. The activity of caspase 3 was measured at 6 and 24 hours after irradiation in UVW/NAT (A), SK-N-BE (B) and A375 (C) cells. In all experiments Staurosporine (50µM) was used as a positive control for apoptosis associated with increased caspase 3 activity. The data is presented as the mean fold increase in fluorescence intensity (mean ± sd) of 3 independent experiments for HGNs alone (A-1, B-1, C-1), compared to untreated control cells and HGNs in combination with XBR (A-2, B-2 and C-2) compared to 2 Gy XBR alone for each cell line. Two-way ANOVA with Bonferroni post-hoc testing was used to determine if treatment with HGNs alone induced significant caspase 3 activity compared to untreated controls and to determine if the combination of HGNs with XBR induced significant caspase activity compared to XBR alone. All tests were performed at the 95% C.I. Four (****) symbols indicate $p<0.0001$.

7.5 Discussion

The aim of this study was to establish the radiosensitising potential of in house synthesised HGNs to 225 kVp x-irradiation. Statistically significant radiosensitisation was observed in all cell lines investigated when HGNs were combined with XBR. The DEF_{50} were 2.77, 2.79 and 2.42 in UVW/NAT, SK-N-BE and A375 cells respectively. The greatest dose enhancement factor was observed in UVW/NAT and SK-N-BE cells which also demonstrated the highest uptake of HGNs (section 6.4.4, Figure 6-3).

To date there have been very few published studies which investigate the effect of HGNs in combination with ionising radiation either *in vitro* or *in vivo*. However, based on studies which have evaluated the unique physical and optical properties of HGNs, it was hypothesised that they may radiosensitise cells to ionising radiation, and that the magnitude of radiosensitisation observed may be greater than with solid AuNPs (Gutrath et al., 2012; Hao et al., 2004; Jackson et al., 2003). This enhanced radiosensitisation potential is based on the presence of two exposed surfaces in HGNs which was shown by Gutrath *et al*, (2012) to allow increased absorption of light compared to solid AuNPs. In this study the absorption properties of solid AuNPs and HGNs were assessed by measuring their ability to absorb light from a NIR laser and convert this into sound waves. Results demonstrated that HGNs displayed significantly greater absorption of laser light compared to solid AuNPs, and a higher conversion efficacy for the conversion of light energy into sound waves (Gutrath et al., 2012). Although this study assessed the absorption and conversion of electromagnetic radiation, it was hypothesised that the greater absorption and conversion capacity of HGNs compared to solid AuNPs would be similar with ionising radiation.

Additionally, Jackson *et al*, (2003) demonstrated that HGNs displayed an enhanced electromagnetic field compared to solid AuNPs. This study used SERs to measure molecular scattering and excitation following interaction with laser light and showed a localised electromagnetic field at the HGN surface which was greater than observed for solid AuNPs (Jackson et al., 2003).

Furthermore, simulation studies have demonstrated that the electromagnetic field is enhanced 3-4 fold by the presence of nm sized pinholes on the HGN surface, compared to seamless HGNs (Hao et al., 2004). These investigated characteristics of HGNs

compared to solid AuNPs suggest that HGNs may absorb more radiation photons, and more effectively utilise these in the release of secondary electrons and therefore a greater radiation dose enhancement would be anticipated.

In this study the DEFs at the 50% cytotoxicity level when 5 nM HGNs were combined with 225 kVp XBR across the dose range from 0-4 Gy were 2.77, 2.79 and 2.42 in UVW/NAT, SK-N-BE and A375 cells respectively, compared to 1.12, 0.93 and 4.68 when 2 nM solid AuNPs were combined with XBR across the same dose range. In this study however, it was not possible to directly compare the radiosensitisation potential of the solid AuNPs used in chapter 4 and the HGNs used in this chapter due to the different physical characteristics between the two nanoparticles including the kinetics of nanoparticle uptake, nanoparticle diameter and concentration and the surface chemistry of the two nanoparticles.

However in an attempt to compare the uptake of solid AuNPs and HGNs in each cell line the number of particles per cell was calculated. In UVW/NAT cells the uptake of solid 20 nm AuNPs was higher than the uptake of 51 nm HGNs where the number of particles per cell following 24 hour incubation was $5.4x10^{\wedge16}\pm1.2x10^{\wedge16}$ vs. $3.9x10^{\wedge16}\pm1.8x10^{\wedge16}$ particles/cell. Comparatively, in SK-N-BE and A375 cells the number of intracellular particles following 24 hour incubation were similar for solid AuNPs and HGNs, $2.3x10^{\wedge16}\pm8.7x10^{\wedge15}$ vs. $2.3x10^{\wedge16}\pm4.7x10^{\wedge15}$ particles/cell in SK-N-BE cells and $1.0x10^{\wedge16}\pm3.9x10^{\wedge15}$ vs. $9.2x10^{\wedge15}\pm6.0x10^{\wedge15}$ particles/cell in A375 cells respectively which suggested that the level of uptake was not a differentiating factor in the observed dose enhancement.

In addition to the differences in administered concentration of the solid AuNPs and HGNs, their surface chemistry was also very different. Firstly the HGNs were considerably larger with an outer diameter of 51 nm, compared to 20 nm for the solid AuNPs; together with a core diameter of 46nm, the HGNs had a much greater overall surface area meaning a greater volume of free d electrons were available for ionisation. Additionally, the presence of pinholes on the surface of HGNs, which have been shown to enhance the electromagnetic field surrounding the nanoparticles, may increase the radiation dose enhancement localised at the surface of HGNs, compared to seamless solid AuNPs. Finally, whilst both solid AuNPs and HGNs are stabilised

using a citrate surface coating to prevent aggregation, due to the inherent instability of HGNs a greater volume of citrate was required for adequate stabilisation meaning more citrate was present when treating cells with HGNs compared to solid AuNPs. It was not possible to determine the exact effect of the citrate on the observed radiosensitisation without removing the citrate coating from the nanoparticles which would render them unstable and unusable. However as citrate can act as an antioxidant, and has been shown to reduce the formation of ROS it is possible that the presence of higher levels of citrate when treating with HGNs reduced the radiosensitisation observed to a greater extent than for solid AuNPs (Stefanie Klein, 2012).

As discussed in section 4.5, based on the suggested mechanisms of radiosensitisation it is most likely that the presence of HGNs enhances the effects of radiation with DNA via a free radical mediated mechanism which results in an increase in the complexity of DNA damage. In an experimental setting, this would most likely present as a reduction in DNA repair, rather than an increase in the number DNA DSBs observed. This was consistent with the results of this study where the combination of HGNs with XBR resulted in a decrease in the resolution of γ-H2AX foci/cell compared to the effects of XBR alone. The data was therefore indicative of a reduction in the efficiency of DNA damage repair and did not induce an increase in the absolute number of γ-H2AX foci/cell. The next aim of this study was to examine the radiosensitisation potential of HGNs in combination with ^{131}I in the form of [^{131}I]-MIBG.

Chapter 8

Investigation of the radiosensitisation potential of HGNs in combination with the radioisotope ^{131}I in the form of [^{131}I]-MIBG

Chapter 8: Investigation of the radiosensitisation potential of HGNs in combination with the radioisotope ^{131}I in the form of [^{131}I]-MIBG

8.1 Introduction

The results presented in chapter 7 demonstrated the ability of in house synthesised HGNs to induce significant radiosensitisation in combination with XBR, compared to XBR alone in each of the cell lines investigated. Additionally, the results presented in chapters 4 and 5 demonstrated that the radiosensitisation achieved by solid AuNPs in combination with kVp XBR was cell line specific, and was likely to be influenced substantially by a cell lines radiosensitivity. Significant radiosensitisation was achieved in combination with XBR within the radiosensitive human melanoma cell line A375, whereas little to no radiosensitisation was observed in either the human glioma cell line UVW/NAT, or the human neuroblastoma cell line SK-N-BE. In combination with the radioisotope ^{131}I however, solid AuNPs induced significant radiosensitisation in both UVW/NAT and SK-N-BE cells, which had demonstrated little to no radiosensitisation in combination with XBR. It was hypothesised that the long half-life together with the long path-length of the low LET β and γ emissions from ^{131}I resulted in continuous ionisation of the AuNPs present throughout the cells, as the β and γ emissions traversed through the cells with energies ranging anywhere between 0-600 keV.

Based on the superior radiosensitisation observed with solid AuNPs in combination with ^{131}I, compared to XBR, it was hypothesised that the radiosensitisation which could be achieved with HGNs in combination with ^{131}I would exceed the radiosensitisation observed in combination with 225 kVp XBR.

This study aimed to test this hypothesis and evaluate the radiosensitisation achieved using the in house synthesised HGNs in combination with ^{131}I in the form of [^{131}I]-MIBG. Radiosensitisation was evaluated by assessing the reduction in cell survival and establishing the effect of HGNs in combination with [^{131}I]-MIBG on the progression of cells through the cell cycle and the dynamics of DNA damage and repair.

8.2 Aims

The aims of this study were to assess the effect of HGNs in combination with [^{131}I]-MIBG on the cell survival, progression of cells through the cell cycle and the dynamics of DNA damage and repair, compared to the effect of [^{131}I]-MIBG alone in UVW/NAT and SK-N-BE cells

8.3 Materials and Methods

8.3.1 Cells and culture conditions

The human glioblastoma cell line UVW/NAT and human neuroblastoma cell line SK-N-BE were employed in this study. All cells were cultured and maintained as detailed in sections 2.3.1 and 3.3.4.

8.3.2 Synthesised hollow gold nanoparticles (HGNs)

All HGNs were synthesised in the Graham Lab (University of Strathclyde) by adaptation of previously reported methods (Schwartzberg et al., 2006; Xie et al., 2013) as detailed in section 6.3.1.

8.3.3 Treatment of cells with HGNs and [^{131}I]-MIBG

The concentration range of HGNs employed in this study was 0-5 nM. All cells lines were incubated with HGNs for 24 hours as described in section 2.3.3.

For treatment of cells with [^{131}I]-MIBG, cells were incubated with [^{131}I]-MIBG for 2 hours as this duration had been shown in previous studies to deliver maximal uptake (Armour et al., 1997). Following this, excess [^{131}I]-MIBG was removed by washing cells thrice with PBS and cells incubated for a further 24 hours in fresh cell growth medium.

For all combination experiments cells were incubated with HGNs in the concentration range 0-5 nM for 24 hours and then exposed to [^{131}I]-MIBG across the dose range 0-3 MBq.

8.3.4 Clonogenic survival assay

Clonogenic survival assays were used to assess the clonogenic survival in each cell following exposure to [^{131}I]-MIBG and HGNs alone and in combination. For the assessment of UVW/NAT cells and SK-N-BE cells, clonogenic survival assays were performed as described in section 2.3.5 and 3.3.7. All results are presented as the average cell survival fraction normalised with respect to untreated control cells for [^{131}I]-MIBG and HGN alone and to HGNs alone in all combination treatments (mean ± sd) of 3 independent experiments unless otherwise stated.

8.3.5 Cell cycle analysis

The progression of cells through the cell cycle was determined to assess whether [^{131}I]-MIBG alone, and in combination with HGNs caused an abrogation to the normal cycling of cells and was performed as described in section 4.3.7. Three independent experiments were carried out, unless otherwise stated and results presented as the percentage of cells in each phase of the cell cycle (mean ± sd).

8.3.6 γ-H2AX analysis by foci staining and confocal microscopy

The effect of [^{131}I]-MIBG alone and in combination with HGNs on the magnitude and dynamics of DNA DSBs was determined as described in section 4.3.8. Results are presented as the mean number of γ-H2AX foci/cell (mean ± sd) of 3 independent experiments.

8.3.7 Statistical Analysis

8.3.7.1 Analysis of variance (ANOVA)

All experiments were carried out 3 times unless otherwise stated, with all results reported as the (mean ± sd). Clonogenic survival data are presented as the cell survival fraction normalised to untreated control cells for treatment with HGNs and [^{131}I]-MIBG alone or normalised to HGN treatment alone for combination treatments. Cell cycle data is presented as the percentage of cells within each phase of the cell cycle and γ-H2AX data as the number of γ-H2AX foci/cell for each treatment group. Results were evaluated using two-way ANOVA with Bonferroni post-tests to determine if the effects of combination therapy on the clonogenic survival, progression and accumulation of cells throughout the cell cycle and formation of γ-H2AX foci/cell were statistically significant compared to the effects of [^{131}I]-MIBG alone. P-values lower than 0.05 were considered statistically different.

8.3.7.2 Linear quadratic analysis

To evaluate the radiosensitisation potential of HGNs in combination with [^{131}I]-MIBG, the experimental clonogenic survival data for UVW/NAT and SK-N-BE cells exposed to [^{131}I]-MIBG alone and in combination with HGNs was fitted to the linear quadratic model (equation 1) (Dale, 2004) using GraphPad Prism software, version 6.01, 2014 (CA) as described in section 2.3.6.2. The α and β values, IC_{50} and DEF at the 50% toxicity level were calculated for [^{131}I]-MIBG alone and in combination with AuNPs for each cell line using equations 2 and 3 as described in sections 2.3.6.2.

8.4 Results

8.4.1 Determination of the radiosensitisation effect of HGNs in combination with [^{131}I]-MIBG using the linear quadratic model

The effect of in house synthesised HGNs on the radiation induced cell kill in UVW/NAT and SK-N-BE cells was assessed using clonogenic survival assays. Cells were incubated with HGNs across the concentration range 0-5 nM for 24 hours prior

to irradiation with 0-3 MBq [^{131}I]-MIBG and clonogenic survival assays performed 24 hours after removal of [^{131}I]-MIBG. As in previous chapters the mean clonogenic survival for cells treated with HGNs in combination with [^{131}I]-MIBG was normalised with respect to the effect of HGNs alone. Two-way ANOVA with Bonferroni post-hoc testing for multiple comparisons was carried out for each cell line to determine if the clonogenic survival fractions observed for cells treated with HGNs in combination with [^{131}I]-MIBG were significantly different, compared to exposure to [^{131}I]-MIBG alone. The clonogenic survival data for each cell line was then fitted to the linear quadratic model using GraphPad Prism software version 6.0.1.

8.4.1.1 The effect of HGNs in combination with [^{131}I]-MIBG on the clonogenic cell kill in UVW/NAT cells

In UVW/NAT cells, incubation with HGNs for 24 hours prior to [^{131}I]-MIBG exposure resulted in a significant reduction in the cell survival, compared to cells exposed to [^{131}I]-MIBG alone at all HGN concentrations and [^{131}I]-MIBG doses (Figure 8-1). Combination of 5 nM HGNs with [^{131}I]-MIBG resulted in cell survival fractions of 0.42±0.01, 0.18±0.03 and 0.10±0.02 respectively, compared to 0.79±0.00 ($p<0.001$), 0.69±0.02 ($p<0.0001$) and 0.44±0.05 ($p<0.0001$) for [^{131}I]-MIBG alone at 1 MBq, 2 MBq and 3 MBq.

The clonogenic survival data from Figure 8-1 (A) was fitted to the linear quadratic model (Figure 8-1(C)) and values for α, β, IC_{50} and DEF_{50} calculated (Figure 8-1(D)). The presence of HGNs with [^{131}I]-MIBG resulted in a decrease in the dose of [^{131}I]-MIBG required to kill 50% of the cell population (IC_{50}). The IC_{50} decreased from 2.71 MBq for [^{131}I]-MIBG alone to 0.89 MBq, 0.82 MBq and 0.74 MBq with HGNs at 0.1 nM, 1 nM and 5 nM respectively, indicating that the presence of HGNs enhanced the efficiency of radiation, which increased with increasing HGN concentration. The calculated α values for the combination of HGNs at 0.1 nM, 1 nM and 5 nM with [^{131}I]-MIBG were 0.89 MBq^{-1}±0.17, 0.89 MBq^{-1}±0.18 and 0.98 MBq^{-1}±0.16 compared to 0.12 MBq^{-1}±0.04 for [^{131}I]-MIBG alone, suggesting that the presence of HGNs resulted in an increase in the toxicity at lower [^{131}I]-MIBG doses, as discussed in section 2.3.6.2 (Barendsen, 1994). The DEFs calculated at the 50% toxicity level

(DEF_{50}) were 3.05, 3.29 and 3.65 for [^{131}I]-MIBG in combination with HGNs at 0.1 nM, 1 nM and 5 nM respectively, indicating that the presence of HGNs resulted in an increase in toxicity, compared to [^{131}I]-MIBG alone.

(A)

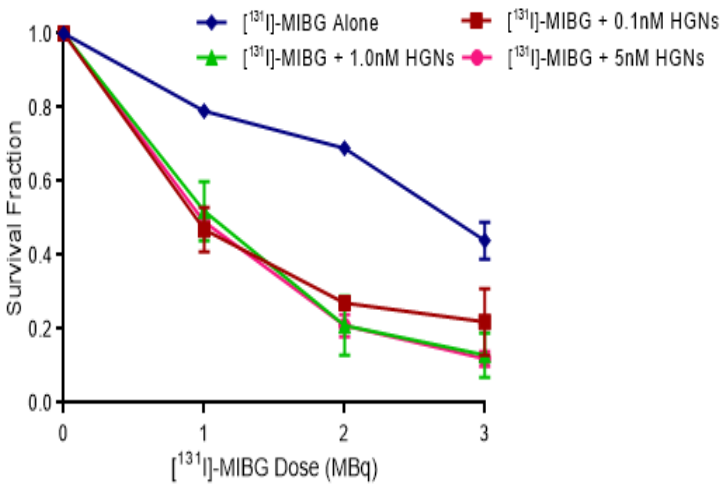

(B)

	0.1nM	1.0nM	5.0nM
1.0MBq	****	****	***
2.0MBq	****	****	****
3.0MBq	****	****	****

Figure 8-1 continued overleaf

(C)

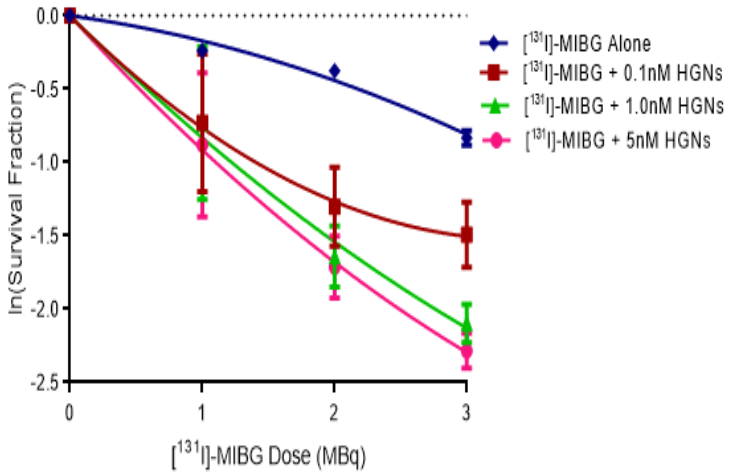

(D)

	0nM	**0.1nM**	**1.0nM**	**5.0nM**
α (Gy^{-1})	0.12±0.04	0.89±0.17	0.89±0.18	0.98±0.16
β (Gy^{-1})	0.04±0.01	-0.13±0.06	-0.06±0.07	-0.07±0.06
R^2	0.97	0.86	0.91	0.94
IC_{50} (MBq)	2.71	0.89	0.82	0.74
DEF_{50}	1.00	3.05	3.29	3.65

Figure 8-1: Clonogenic survival of UVW/NAT cells exposed to HGNs in combination with [^{131}I]-MIBG.

UVW/NAT cells were incubated with HGNs from 0-5 nM for 24 hours. Following this, cells were treated with [^{131}I]-MIBG from 0-3 MBq for 2 hours and clonogenic survival assays performed 24 hours after removal of [^{131}I]-MIBG. Clonogenic survival results are presented as the mean survival fraction (mean ± sd) of 3 independent experiments normalised to HGN alone treated cells (A). Statistically significance differences in the cell survival fraction for HGNs in combination with [^{131}I]-MIBG, compared to [^{131}I]-MIBG alone was assessed using two-way ANOVA with Bonferroni post-tests at 95% C.I. Three (***) and four (****) symbols indicate $p<0.001$ and $p<0.0001$ (B). Clonogenic survival data presented in (A) was fitted to the linear quadratic model using GraphPad Prism version 6.0.1 (C) and calculated values for the α and β coefficient and the IC_{50} and DEF_{50} for [^{131}I]-MIBG in combination with HGNs at each HGN concentration presented (D).

8.4.1.2 The effect of HGNs in combination with [^{131}I]-MIBG on the clonogenic cell kill in SK-N-BE cells

In SK-N-BE cells, incubation with HGNs for 24 hours prior to [^{131}I]-MIBG exposure resulted in a significant reduction in the cell survival, compared to cells exposed to [^{131}I]-MIBG alone at all HGN concentrations and [^{131}I]-MIBG doses (Figure 8-2). Combination of 5 nM HGNs with [^{131}I]-MIBG resulted in cell survival fractions of 0.36±0.02, 0.35±0.02 and 0.29±0.04 respectively, compared to 0.82±0.08 ($p<0.0001$), 0.72±0.08 ($p<0.0001$) and 0.61±0.09 ($p<0.0001$) for [^{131}I]-MIBG alone at 1 MBq, 2 MBq and 3 MBq.

The clonogenic survival data from Figure 8-2(A) was fitted to the linear quadratic model (Figure 8-2(C)) and values for α, β, IC_{50} and DEF_{50} calculated (Figure 8-2(D)). The presence of HGNs decreased the [^{131}I]-MIBG dose required to kill 50% of the cell population (IC_{50}). The IC_{50} decreased from 4.56 MBq for treatment with [^{131}I]-MIBG alone to 0.87 MBq, 0.76 MBq and 0.94 MBq in the presence of HGNs at 0.1 nM, 1 nM and 5 nM respectively indicating that the presence of HGNs reduced the IC_{50} of [^{131}I]-MIBG in a concentration independent manner. The calculated α values for the combination of HGNs at 0.1 nM, 1 nM and 5 nM with [^{131}I]-MIBG were 0.95 MBq^{-1}±0.10, 1.11 MBq^{-1}±0.11 and 0.91 MBq^{-1}±0.08 compared to 0.19 MBq^{-1}±0.03 for [^{131}I]-MIBG alone, suggesting that the presence of HGNs increased the toxicity at lower [^{131}I]-MIBG doses The DEFs calculated at the 50% toxicity level (DEF_{50}) were 5.26, 6.00 and 4.83 for [^{131}I]-MIBG in combination with HGNs at 0.1 nM, 1 nM and 5 nM respectively, indicating that the presence of HGNs enhanced the toxicity to [^{131}I]-MIBG alone, independent of the HGN concentration.

(A)

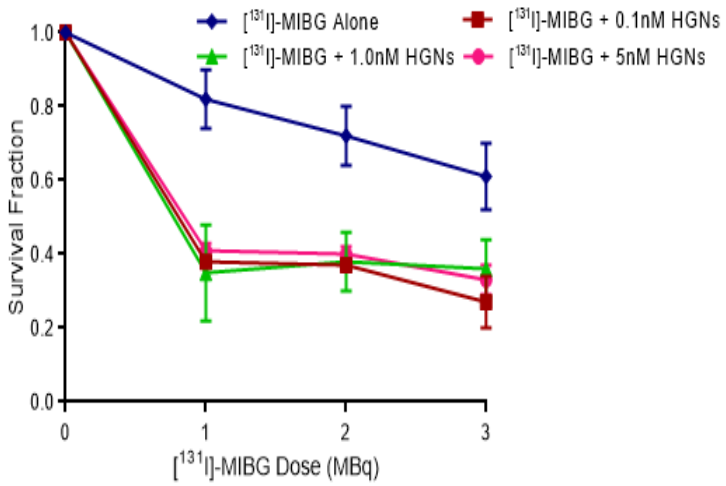

(B)

	0.1nM	1.0nM	5.0nM
1.0MBq	****	****	****
2.0MBq	****	****	****
3.0MBq	****	****	****

Figure 8-2 continued overleaf

(C)

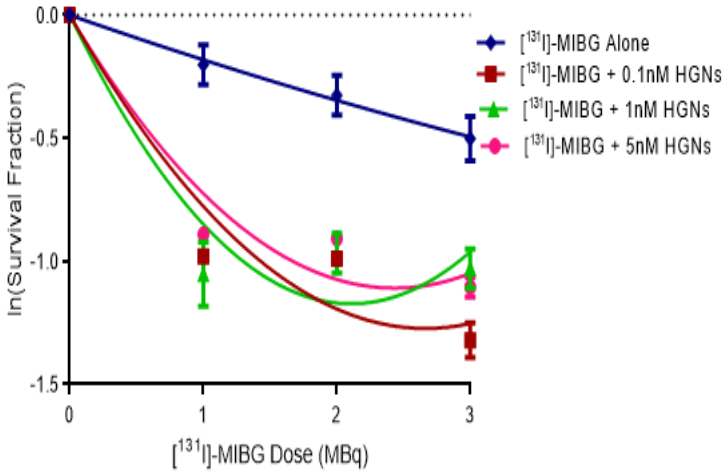

(D)

	0nM	0.1nM	1.0nM	5.0nM
α (Gy^{-1})	0.19±0.03	0.95±0.10	1.11±0.11	0.91±0.08
β (Gy^{-1})	-0.008±0.09	-0.17±0.04	-0.26±0.04	-0.18±0.03
R^2	0.90	0.91	0.87	0.92
IC_{50} (MBq)	4.56	0.87	0.76	0.94
DEF_{50}	1.00	5.26	6.00	4.83

Figure 8-2: Clonogenic survival of SK-N-BE cells exposed to HGNs in combination with [^{131}I]-MIBG.

SK-N-BE cells were incubated with HGNs from 0-5 nM for 24 hours. Following this, cells were treated with [^{131}I]-MIBG from 0-3 MBq for 2 hours and clonogenic survival assays performed 24 hours after removal of [^{131}I]-MIBG. Clonogenic survival results are presented as the mean survival fraction (mean ± sd) of 3 independent experiments normalised to HGN alone treated cells (A). Statistically significant differences in the cell survival fraction for HGNs in combination with [^{131}I]-MIBG, compared to [^{131}I]-MIBG alone was assessed using two-way ANOVA with Bonferroni post-tests at 95% C.I. Four (****) symbols indicate $p<0.0001$ (B). Clonogenic survival data presented in (A) was fitted to the linear quadratic model using GraphPad Prism version 6.0.1 (C) and calculated values for the α and β coefficient and the IC_{50} and DEF_{50} for [^{131}I]-MIBG in combination with HGNs at each HGN concentration presented (D).

In summary, the clonogenic survival data demonstrated that significant radiosensitisation was observed from the combination of HGNs with [^{131}I]-MIBG in both UVW/NAT and SK-N-BE cells. The magnitude of radiosensitisation differed in each cell line, where treatment with 5 nM HGNs in combination with [^{131}I]-MIBG in the dose range 0-3 MBq lead to a DEF_{50} in SK-N-BE cells of 4.83, compared to 3.65 in UVW/NAT cells.

The uptake of HGNs following 24 hour incubation with 5 nM, the IC_{50} for [^{131}I]-MIBG and the DEF_{50} for 5 nM HGNs in each cell line is presented in Table 8-1 to allow clear visualisation of the differences in dose enhancement between each of the cell lines, and the corresponding radiation sensitivity and intracellular Au content of the cell lines.

For subsequent studies assessing whether the radiosensitisation was associated with changes in the dynamics of DNA damage and repair and cell cycle progression a concentration of 5 nM HGNs in combination with 2 MBq [^{131}I]-MIBG was used.

Table 8-1: Uptake of 5 nM HGNs, IC_{50} dose for [^{131}I]-MIBG and DEF_{50} for 5 nM HGNs in UVW/NAT and SK-N-BE cells respectively.

	UVW/NAT	SK-N-BE
5nM HGN uptake (ng/cell)	0.021±0.01	0.018±0.01
[^{131}I]-MIBG IC_{50} (MBq)	2.71	4.56
DEF_{50} for 5nM HGNs + [^{131}I]-MIBG	3.65	4.83

8.4.2 The effect of HGNs in combination with [^{131}I]-MIBG on the cell cycle progression of UVW/NAT and SK-N-BE cells

The effect of 2 MBq [^{131}I]-MIBG alone and in combination with 5 nM HGNs on the progression of UVW/NAT and SK-N-BE cells through the cell cycle was determined at 2 and 24 hours after removal of [^{131}I]-MIBG.

Cell cycle data presented in chapter 7, section 7.4.2 demonstrated that exposure to 5 nM HGNs alone induced no effect on the normal progression of cells through the cell cycle, compared to untreated control cells at any time point in both UVW/NAT and SK-N-BE cells ($p>0.05$) (Figure 7-4). This was consistent with the results observed in this chapter.

Exposure of UVW/NAT cells to [^{131}I]-MIBG at 2 MBq resulted in a statistically significant accumulation of cells within the G2/M phase of the cell cycle, 24 hours after removal of [^{131}I]-MIBG, compared to untreated control cells (Figure 8-3(A)). The percentage of cells within G2/M increased from 33.9%±1.4 in control cells to 58.8%±4.1 ($p<0.0001$) in cells irradiated with 2 MBq [^{131}I]-MIBG. At 2 hours after removal of [^{131}I]-MIBG, exposure to 2 MBq [^{131}I]-MIBG induced no significant increase in the percentage of cells in G2/M compared to untreated control cells ($p>0.05$).

In SK-N-BE cells, exposure to 2 MBq [^{131}I]-MIBG alone also resulted in a statistically significant accumulation of cells within the G2/M phase of the cell cycle, 24 hours after removal of [^{131}I]-MIBG, compared to untreated control cells (Figure 8-3(B)). The percentage of cells within G2/M increased from 34.0%±4.4 in untreated control cells to 55.7%±1.1 ($p<0.01$) in cells irradiated with 2 MBq [^{131}I]-MIBG. No significant increase in the percentage of cells in G2/M following treatment with 2 MBq [^{131}I]-MIBG, compared to untreated control cells was observed 2 hours after removal of [^{131}I]-MIBG ($p>0.05$).

In both UVW/NAT and SK-N-BE cells, treatment with 5 nM HGNs in combination with 2 MBq [^{131}I]-MIBG resulted in no significant increase in the accumulation of cells within G2/M, compared to 2 MBq [^{131}I]-MIBG alone at any timepoint measured (Figure 8-3). In all of the experiments where an increase in the percentage of cells in

G2/M was observed this was associated with a decrease in the percentage of cells G1. Furthermore, no significant changes to the proportion of cells in the S phase of the cell cycle was observed following [^{131}I]-MIBG exposure alone or in combination with HGNs, compared to untreated control cells or cells exposed to [^{131}I]-MIBG alone.

In summary, combination of HGNs with [^{131}I]-MIBG resulted in no significant alterations to the proportion of cells in each stage of the cell cycle compared to [^{131}I]-MIBG alone in either UVW/NAT or SK-N-BE cells.

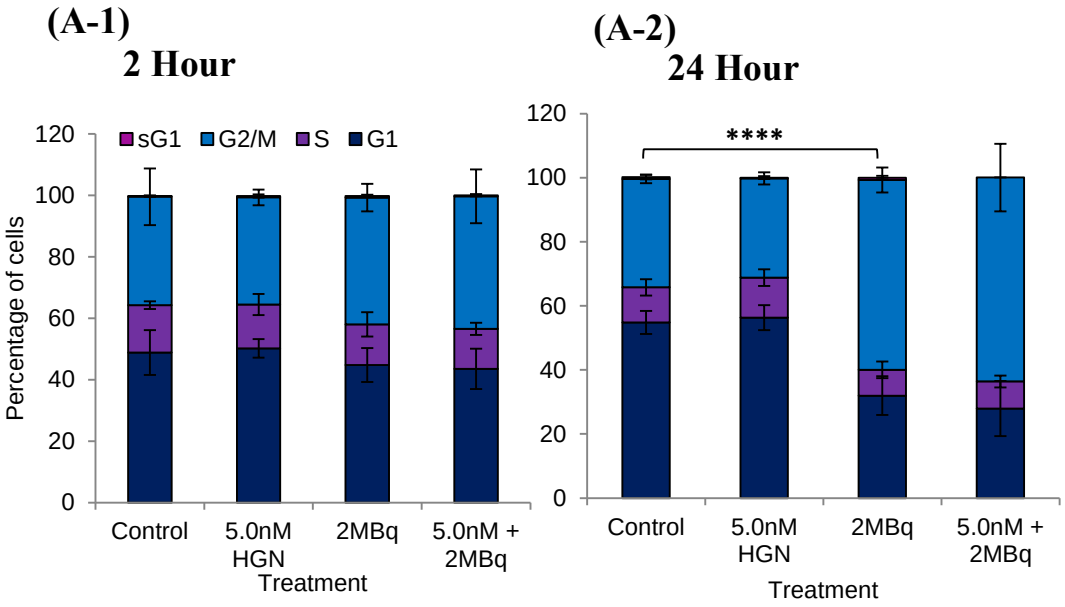

Figure 8-3 continued overleaf

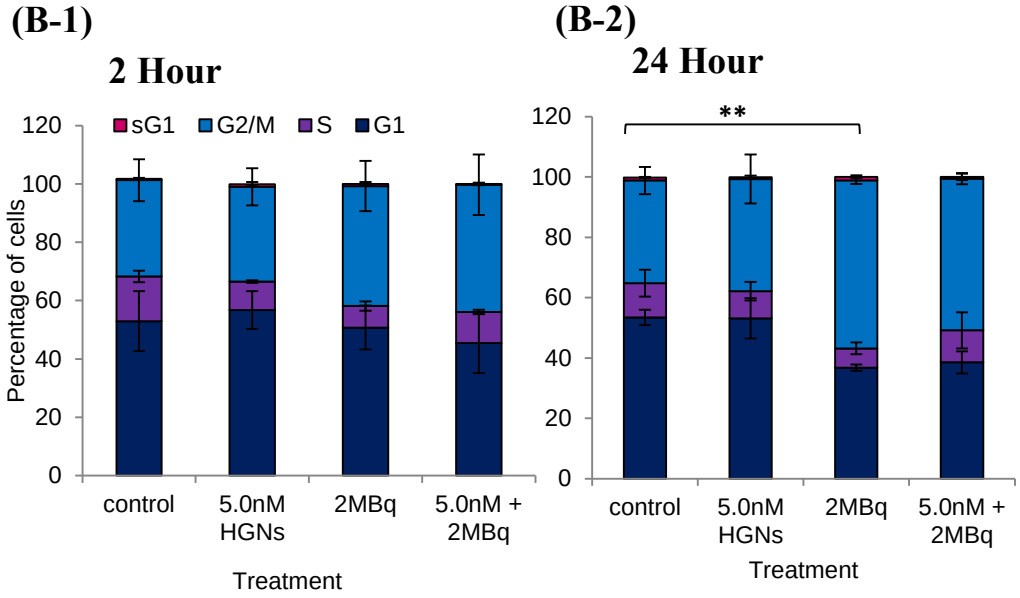

Figure 8-3: The effect of 2 MBq [^{131}I]-MIBG alone and in combination with 5 nM HGNs on the distribution of UVW/NAT and SK-N-BE cells throughout each phase of the cell cycle.

UVW/NAT (A) SK-N-BE (B) cells were incubated with HGNs at a concentration of 5 nM for 24 hours prior to treatment with 2 MBq [^{131}I]-MIBG. The DNA content of the cells was labelled with PI and the cell cycle profiles obtained by FACS analysis at 2 (A-1, B-1) and 24 (A-2, B-2) hours after removal of [^{131}I]-MIBG. The proportion of cells in G0/G1, S and G2/M was measured using BDCellDiva™ software. Two-way ANOVA was used to determine if statistically significant changes in the distribution of cells throughout the cell cycle resulted as an effect of HGN and [^{131}I]-MIBG treatment alone (compared to untreated control cells) or in combination (compared to the effects of [^{131}I]-MIBG alone). All tests were performed at the 95% C.I of 3 independent experiments unless otherwise stated (SK-N-BE n=4). Two (**) and four (****) symbols indicate $p<0.01$ and $p<0.0001$.

8.4.3 The effect of HGNs in combination with [^{131}I]-MIBG on the magnitude and dynamics of DNA double strand break and repair in UVW/NAT and SK-N-BE cells

The number of γ-H2AX foci/cell was determined in UVW/NAT and SK-N-BE cells following treatment with 2 MBq [^{131}I]-MIBG alone and in combination with 5 nM HGNs, at 2 and 24 hours after removal of [^{131}I]-MIBG (Figure 8-4).

In both cell lines two-way ANOVA with Bonferroni post-hoc testing for multiple comparisons was used to assess whether 5 nM HGNs or 2 MBq [^{131}I]-MIBG alone significantly increased the number of γ-H2AX foci/cell, compared to untreated controls, and whether treatment with 5 nM HGNs in combination with 2 MBq [^{131}I]-MIBG significantly increased the number of γ-H2AX foci/cell, compared to treatment with 2 MBq [^{131}I]-MIBG alone.

The results of chapter 7 (section 7.4.3) demonstrated that exposure of UVW/NAT and SK-N-BE cells to 5 nM HGNs alone resulted in no significant increase in the formation γ-H2AX foci compared to untreated control cells at any timepoint measured ($p>0.05$). This was confirmed in this chapter (Figure 8-4).

In UVW/NAT cells treated with 2 MBq [^{131}I]-MIBG alone the number of γ-H2AX foci/cell were higher at 2 hours after removal of [^{131}I]-MIBG, compared to untreated control cells although this was not statistically significant (Figure 8-4(A)). Between 2 and 24 hours after removal of [^{131}I]-MIBG the number of γ-H2AX foci/cell continued to increase by 252%, from 10 foci/cell±5.29 in untreated control cells to 59 foci/cell±4.29 ($p<0.0001$) in cells treated with 2 MBq [^{131}I]-MIBG at 24 hours after removal of [^{131}I]-MIBG.

Treatment of UVW/NAT cells with 5 nM HGNs in combination with 2 MBq [^{131}I]-MIBG significantly increased the number of γ-H2AX foci/cell at both 2 and 24 hours after removal of [^{131}I]-MIBG, compared to cells treated with 2 MBq [^{131}I]-MIBG alone. The number of γ-H2AX foci increased by 153% at 2 hours after removal of [^{131}I]-MIBG, from 17 foci/cell±0.56 in cells exposed to 2 MBq [^{131}I]-MIBG alone to 42 foci/cell±2.08 ($p<0.0001$) in combination treated cells. Similarly at 24 hours after removal of [^{131}I]-MIBG the number of γ-H2AX foci increased by 21%, from 59

foci/cell±4.29 in cells exposed to 2 MBq [^{131}I]-MIBG to 67 foci/cell±2.48 ($p<0.05$) in combination treated cells. These data suggested that the presence of HGNs in combination with [^{131}I]-MIBG increased the magnitude of DNA damage compared to [^{131}I]-MIBG alone.

In SK-N-BE cells, treatment with 2 MBq [^{131}I]-MIBG induced significant formation of γ-H2AX foci/cell both 2 and 24 hours after removal of [^{131}I]-MIBG, compared to untreated control cells (Figure 8-4(B)). The number of γ-H2AX foci/cell were 4 foci/cell±0.84 and 7 foci/cell±0.75 in untreated control cells at 2 and 24 hours after removal of [^{131}I]-MIBG, compared to 23 foci/cell±1.24 ($p<0.001$) and 32 foci/cell±6.88 ($p<0.0001$) in cells treated with 2 MBq [^{131}I]-MIBG.

Treatment of SK-N-BE cells with 5 nM HGNs in combination with 2 MBq [^{131}I]-MIBG, significantly increased the number of γ-H2AX foci/cell at 2 and 24 hours after removal of [^{131}I]-MIBG compared to cells treated with 2 MBq [^{131}I]-MIBG alone. The number of γ-H2AX foci increased by 52% at 2 hours after removal of [^{131}I]-MIBG, from 23 foci/cell±1.24 in cells exposed to 2 MBq [^{131}I]-MIBG alone to 35 foci/cell±4.99 ($p<0.01$) in combination treated cells. Similarly at 24 hours after removal of [^{131}I]-MIBG the number of γ-H2AX foci increased by 66%, from 32 foci/cell±6.88 in cells exposed to 2 MBq [^{131}I]-MIBG to 44 foci/cell±4.57 ($p<0.01$) in combination treated cells. The significant increase in γ-H2AX foci formation in the presence of HGNs compared to [^{131}I]-MIBG alone observed in these experiments suggested that the presence of HGNs increased the DNA damage, compared to [^{131}I]-MIBG alone.

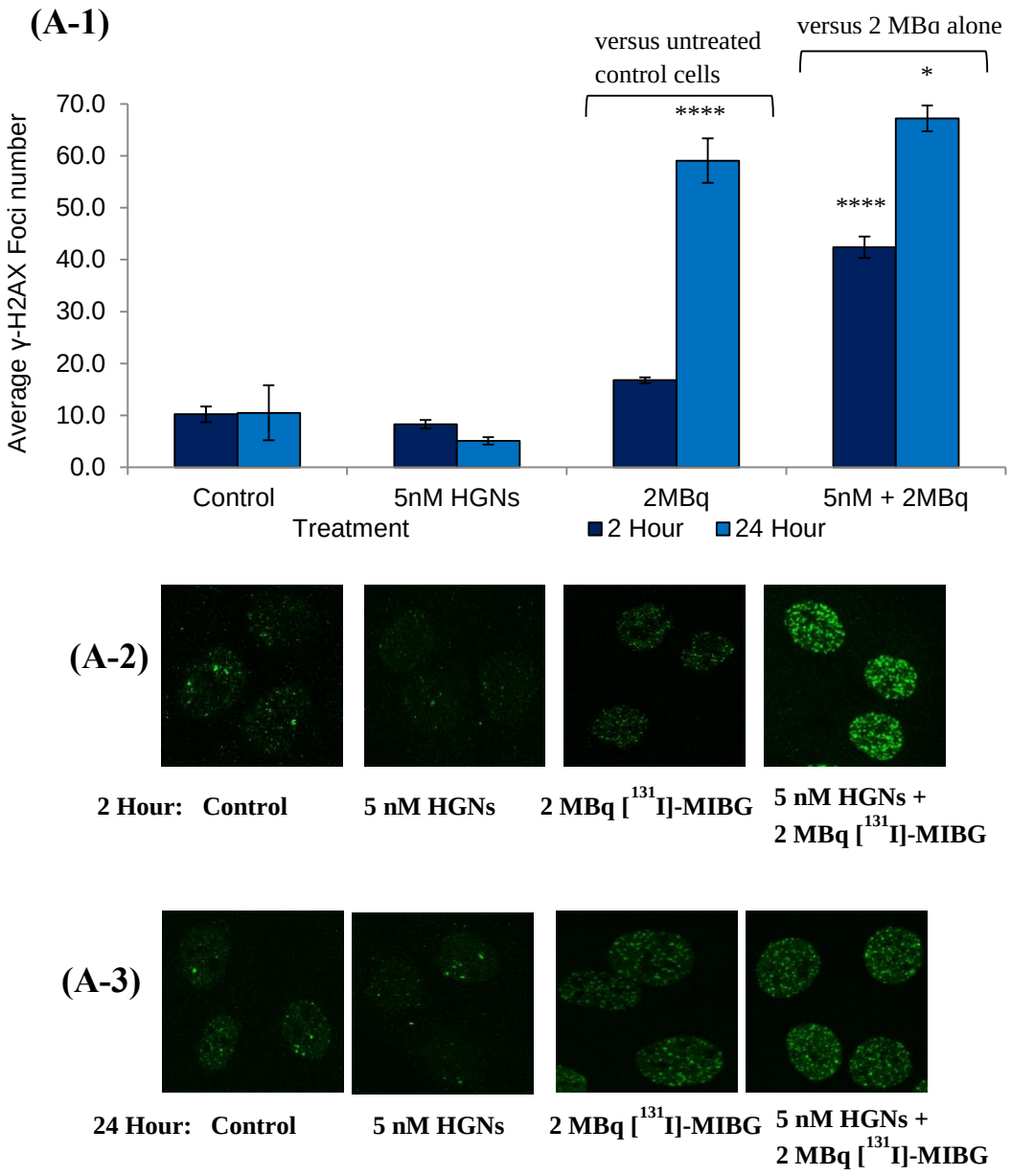

Figure 8-4 continued overleaf

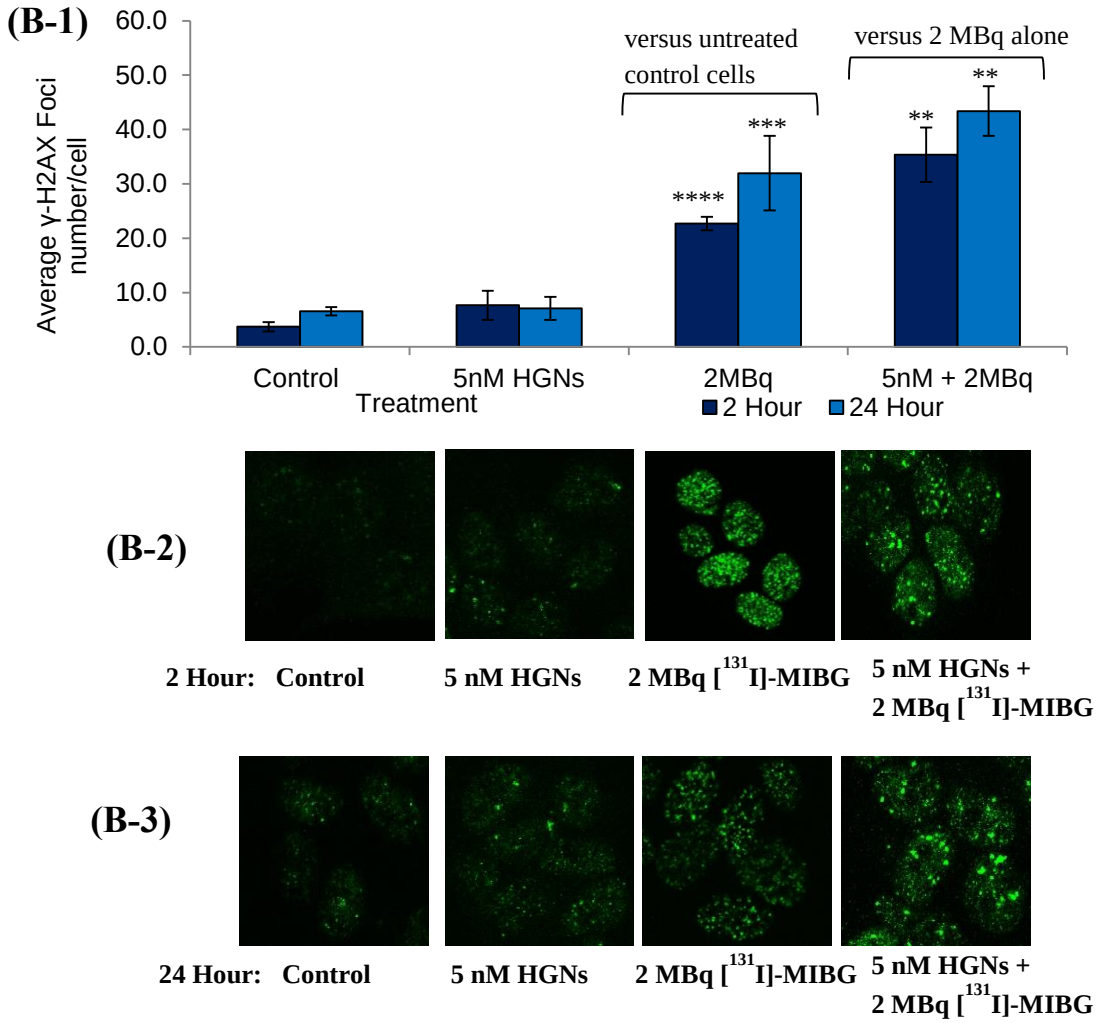

Figure 8-4: The effect of 2 MBq [^{131}I]-MIBG alone and in combination with 5 nM HGNs on the formation and resolution of γ-H2AX foci in UVW/NAT and SK-N-BE cells.

UVW/NAT and SK-N-BE cells were treated with 5 nM HGNs for 24 hours and then exposed to 2 MBq [^{131}I]-MIBG for 2 hours. The number of γ-H2AX foci/cell was assessed at 2 and 24 hours after [^{131}I]-MIBG was removed using immunohistochemistry. Results presented are the average number of γ-H2AX foci/cell (mean ± sd) of 3 independent experiments in UVW/NAT (A) and SK-N-BE (B) cells respectively. Two-way ANOVA was used to determine if statistically significant changes in the number of γ-H2AX foci/cell resulted as an effect of 5 nM HGNs and 2 MBq alone (compared to untreated control cells) or in combination (compared to the effects of [^{131}I]-MIBG alone). All tests were performed at the 95% C.I. One (*), two (**), three (***) and four (****) symbols indicate $p<0.05$, $p<0.01$, $p<0.001$ and $p<0.0001$ respectively. Representative images of γ-H2AX foci in each treatment group at 2 hours (A/B-2) and 24 hours (A/B-3) are presented.

In summary, the data demonstrated that the presence of HGNs at 5 nM in combination with 2 MBq [^{131}I]-MIBG resulted in a significant increase in the formation of γ-H2AX foci compared to 2 MBq alone at both 2 and 24 hours after [^{131}I]-MIBG exposure in UVW/NAT and SK-B-BE cells respectively. These observations were consistent with the clonogenic survival data presented in section 8.4.1 which demonstrated significant radiosensitisation by HGNs in both UVW/NAT and SK-N-BE cells to different extents.

8.5 Discussion

The aim of this study was to establish the radiosensitising potential of HGNs to ionising radiation in the form of ^{131}I from [^{131}I]-MIBG. This was the first study to provide experimental evidence of radiosensitisation by HGNs in combination with ionising radiation in the form of ^{131}I. The results of this study demonstrate that significant radiosensitisation was induced in both the human glioma cell line, UVW/NAT and the human neuroblastoma cell line, SK-N-BE with calculated DEF_{50} values of 3.65 and 4.83 for UVW/NAT and SK-N-BE cells respectively. As was observed with solid AuNPs, the DEF_{50} values were higher than those achieved when HGNs were combined with 225 kV X-rays in UVW/NAT and SK-N-BE cells which were 2.77 and 2.79 respectively (chapter 7, section 7.4.1), as determined in the previous chapter. The results of this chapter support the hypothesis outlined in section 1.7, that as a result of the substantial absorption ability, the efficiency of energy conversion and the availability of two surfaces in HGNs which could potentiate ionisations within HGNs and the generation of ROS, HGNs could act as successful radiosensitisers in combination with ionising radiation (Gutrath et al., 2012; Jackson et al., 2003).

Furthermore the higher DEF_{50} values achieved when HGNs were combined with [^{131}I]-MIBG compared to XBR were concurrent with the hypothesis previously presented (section 5.5) which predicted that a greater dose enhancement would result following the interaction of both solid AuNPs and HGNs with ^{131}I rather than XBR. The rationale behind this hypothesis was based on the continuous exposure to low LET emitted β

and γ emissions from ^{131}I as a result of the long half-life of ^{131}I, compared to the rapid irradiation by XBR. Furthermore, despite the energy of the β and γ emissions from ^{131}I not being optimal for photoelectric absorption by the nanoparticles it was hypothesised that due to the long path range of the low LET emissions, the β and γ radiation will travel through the cells losing energy as they traverse and thus at some point their energy will be within the optimum range to result in photoelectric ionisation of the HGNs.

The observed HGN radiosensitisation was associated with significantly higher number of DNA DSBs, reflected by the higher number of γ-H2AX foci/cell, compared to the number measured in cells treated with [^{131}I]-MIBG alone. The higher number of DNA DSBs was evident already 2 hours after removal of [^{131}I]-MIBG, where the number of γ-H2AX foci/cell was 153% and 52% greater in cells treated with HGNs in combination with [^{131}I]-MIBG, compared to [^{131}I]-MIBG alone in UVW/NAT and SK-N-BE cells respectively.

As with the previous investigations of solid AuNPs with both XBR and [^{131}I]-MIBG, and HGNs with XBR, the observed increase in DNA damage associated with the combination of HGNs and [^{131}I]-MIBG did not result in an increase in the arrest of cells throughout the cell cycle, compared to the effects of [^{131}I]-MIBG alone. However as this is the first study which has investigated the effects of HGNs in combination with ionising radiation in the form of ^{131}I it is not possible to compare the results found in this present study with any previous data.

In conclusion the results presented in this chapter provide initial *in vitro* evidence that significant radiosensitisation can be achieved from the combination of HGNs with continuous low dose-rate, high keV energy β and γ emissions from ^{131}I in the form of the targeted radiopharmaceutical [^{131}I]-MIBG.

Thus far in this study all of the work has been performed in 2D monolayer cells, however as detailed in section 1.8, many studies have demonstrated that the treatment outcome with both external beam and targeted radiotherapy based therapies can vary substantially between 2D cell studies and *in vitro* 3D cell models. In order to evaluate the radiosensitisation potential of both solid AuNPs and HGNs in combination with

XBR and [^{131}I]-MIBG in a 3D *in vitro* model, their effects alone and in combination on the growth kinetics of 3D multicellular spheroids were preliminarily assessed.

Chapter 9

Preliminary investigation of the radiosensitisation potential of solid AuNPs and HGNs in combination with XBR and [^{131}I]-MIBG in MTS models

Chapter 9: Preliminary investigation of the radiosensitisation potential of solid AuNPs and HGNs in combination with XBR and [^{131}I]-MIBG in MTS models

9.1 Introduction

The results presented in chapters 4, 5, 7 and 8 demonstrated that the combination of both solid AuNPs and HGNs with ionising radiation in the form of either XBR or [^{131}I]-MIBG, resulted in a radiosensitising effect and variable dose enhancement. The observed dose enhancement factor was dependent upon several factors namely; the radiation quality, the cancer cell line under investigation and its inherent sensitivity towards radiation and the type of nanoparticles investigated. Based on these results, both solid AuNPs and HGNs have demonstrated potential for future use in combination with radiation. Before progressing to preclinical studies however, this present study aimed to investigate if the radiosensitisation observed in 2D monolayer cultured cells could also be achieved in 3D multicellular tumour spheroid (MTS) models.

As discussed in section 1.8, tumour cells grown as 3D spheroids provide a more accurate representation of the morphology, physiology and heterogeneity of cell proliferation of *in vivo* micrometastases as they demonstrate nutrient and oxygen concentration gradients which are more representative of the *in vivo* scenario. Additionally, MTS models possess similar cell-cell interactions that are present in tumours thus giving a more realistic view of treatment outcomes. The use of MTS models with AuNPs and radiation therefore allows the effect of solid AuNPs and HGNs in combination with XBR and [^{131}I]-MIBG within a more representative 3D tumour model to be examined.

9.2 Aims

The primary aim of this chapter was to investigate the effect of solid AuNPs, HGNs, XBR and [^{131}I]-MIBG as single agents on the growth kinetics of UVW/NAT and SK-N-BE 3D spheroids. Following this, the impact of solid AuNPs and HGNs in

combination with XBR and [^{131}I]-MIBG on the growth kinetics of MTS models, compared to the effects of either radiation alone was examined using spheroid growth delay assays (Boyd et al., 2002; Gaze et al., 1992; Rae et al., 2013).

9.3 Materials and Methods

9.3.1 Cells and culture conditions

The NAT expressing human glioblastoma cell line, UVW/NAT and human neuroblastoma cell line SK-N-BE were employed in this study. All cells were cultured and maintained as detailed in sections 2.3.1 and 3.3.4.

9.3.2 Spheroid initiation and culture

MTS of UVW/NAT and SK-N-BE cells were cultured using the continuous agitation method (Boyd et al., 2002, 2001). In this method, $3x10^6$ cells derived from monolayer cells were seeded into a 750 mL sterile spinner flask (Sigma Aldrich, Dorset) containing 75 mL fresh cell growth medium and CO_2 and incubated at 37^{o}C on a magnetic spinner plate for approximately 4 days.

9.3.3 Synthesised AuNPs and HGNs

All solid AuNPs and HGNs were synthesised in the Graham Lab (University of Strathclyde) (Brown et al., 2010) as described in sections 3.3.1 and 6.3.1.

9.3.4 Treatment of MTS with AuNPs, HGNs, XBR and [^{131}I]-MIBG

Spheroids were split into treatments groups and the cell growth medium removed before replacing with fresh growth medium with or without AuNPs (2 nM), HGNs (5

nM) or [^{131}I]-MIBG. Following treatment samples were incubated for 24 hours at 37ºC on a continuous rocker to prevent spheroid agglomeration.

Irradiation of spheroids with XBR was performed using a cell irradiation cabinet (XRAD 225) with a 225 kVp X-ray beam and a dose rate of 2.2 Gy/min and 13.00 mA current as described in section 2.3.4. For all experiments examining the effect of XBR as a single agent cells were treated with XBR within a dose range from 0-4 Gy and in combination with AuNPs and HGNs XBR doses of 1 Gy and 2 Gy were employed.

Irradiation of spheroids with [^{131}I]-MIBG was performed as described in section 5.3.6. Briefly, spheroids were incubated with [^{131}I]-MIBG for 2 hours. Following this, excess [^{131}I]-MIBG was removed by washing spheroids thrice with PBS. The dose range of 0.1-2 MBq/mL was employed to assess the effect of [^{131}I]-MIBG alone and in combination experiments, spheroids were incubated with AuNPs or HGNs and then treated with 0.5 MBq/mL.

9.3.5 Spheroid volume measurement

Following treatment, spheroids were manually pipetted into individual wells of ultra-low attachment 96 well culture plates (VWR, West Sussex) containing 100 µL fresh cell growth medium. Spheroid images were captured twice per week at 4x magnification to monitor the spheroid growth for approximately 4 weeks. For each spheroid two orthogonal diameters, d_{max} and d_{min} (µm), were measured using image analysis software ImageJ version 1.48 and the spheroid volume, V (µm^3) calculated using equation 8 (Jensen et al., 2008);

$$V = 0.5 \times (d_{max} \times (d_{min})^2) \qquad \text{Equation 8}$$

The change in volume at each measurement point, (V/V_0) was calculated by dividing the calculated volume (V) at each timepoint, by the initial volume (V_0) to compare the change in volume between treatments.

9.3.6 Calculation of the growth delay (τ_x), doubling time (DT) and area under the curve (AUC) of spheroids

The kinetics of growth in UVW/NAT and SK-N-BE spheroids were measured following treatment using growth delay assays. A common method employed to assess the treatment induced growth delay of spheroids is by measurement of the time required for an x-fold increase in the spheroid volume (τ_x), demonstrated by Boyd *et al*, 2002 (Boyd et al., 2002). To measure the time required for a 2-fold increase in spheroid volume, (τ_2) which represents a measure of the growth delay following treatment, linear regression analysis of the logarithm of the fold increase in spheroid volume ($\log V/V_0$) with time (t), was performed using least squares method. The linear regression equation was then fitted to the exponential part of the spheroid growth curve to calculate values for the slope (b) and the y-intercept, (a) from the linear regression equation given by equation 9. The values of a and b were then used to calculate the τ_2 from day 0 using equation 10.

$\log V/V_0 = bt + a$ equation 9

$\tau_2 = (\log x - a) / b$ equation 10

Following calculation of τ_2, the time required for a 2-fold increase in spheroid volume within the exponential phase of the spheroid growth curve, defined as the doubling time (DT) which represents a measure of the growth rate following treatment was calculated using equation 11.

$DT = \log 2 / b$ equation 11

The area under the curve for $\log V/V_0$ versus time data (AUC_{log}) was then calculated by trapezoidal approximation using Excel to evaluate the change in overall spheroid growth following treatment.

9.3.7 Statistical Analysis

As the calculated values for τ_2, DT and AUC_{log} were not normally distributed non-parametric statistical analysis was performed. The Kruskal-Wallis test with post hoc

testing by Dunn's analysis of multiple comparisons, where p values below 0.05 were considered significant, was performed using GraphPad Prism, version 6.0.1 to determine if the effects of each different treatment alone, compared to untreated controls and for nanoparticles in combination with radiation, compared to the effects of radiation alone were significantly different.

9.4 Results

9.4.1 The effect of solid AuNPs and HGNs alone on the growth of UVW/NAT and SK-N-BE spheroids

9.4.1.1 The effect of solid AuNPs on the growth of UVW/NAT and SK-N-BE spheroids

The effect on the growth of UVW/NAT and SK-N-BE spheroids following 24 hour incubation with solid AuNPs at a concentration of 2 nM was assessed by evaluating changes in the growth delay (τ_2), doubling time (DT) and AUC_{log}, compared to untreated control spheroids.

In UVW/NAT spheroids, incubation with solid AuNPs at a concentration of 2 nM resulted in no significant differences in the growth of spheroids compared to untreated controls ($p>0.05$) (Figure 9-1(A)). The calculated values for spheroid growth delay (τ_2), DT and AUC_{log} for spheroids treated with 2 nM AuNPs were comparable to that of untreated control spheroids (Figure 9-1(A-3)), indicating that exposure of UVW/NAT spheroids to solid AuNPs had no effect on spheroid growth.

Similarly, in SK-N-BE spheroids, incubation with solid AuNPs at a concentration of 2 nM resulted in no significant change to the growth of spheroids compared to untreated controls ($p<0.05$). The calculated values for growth delay (τ_2), DT, and AUC_{log} were all comparable to those for untreated control spheroids (Figure 9-1(B-3)), indicating that exposure of SK-N-BE spheroids to solid AuNPs causes no deviation to normal spheroid growth compared to untreated control spheroids.

(A-1) **(A-2)**

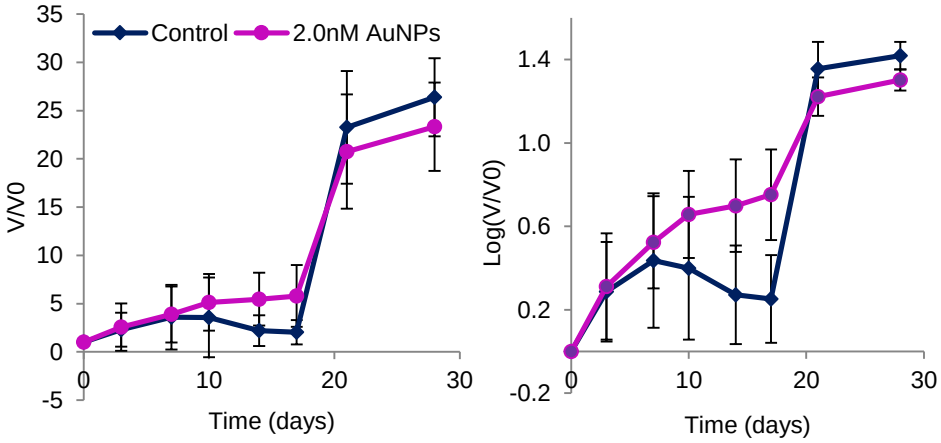

(A-3)

AuNP Concentration (nM)	τ_2	DT	AUC_{log}
0	10.50±2.09	9.09±1.55	8.70±3.02
2.0	6.20±0.39	9.38±0.75	7.20±0.42

Figure 9-1 continued overleaf

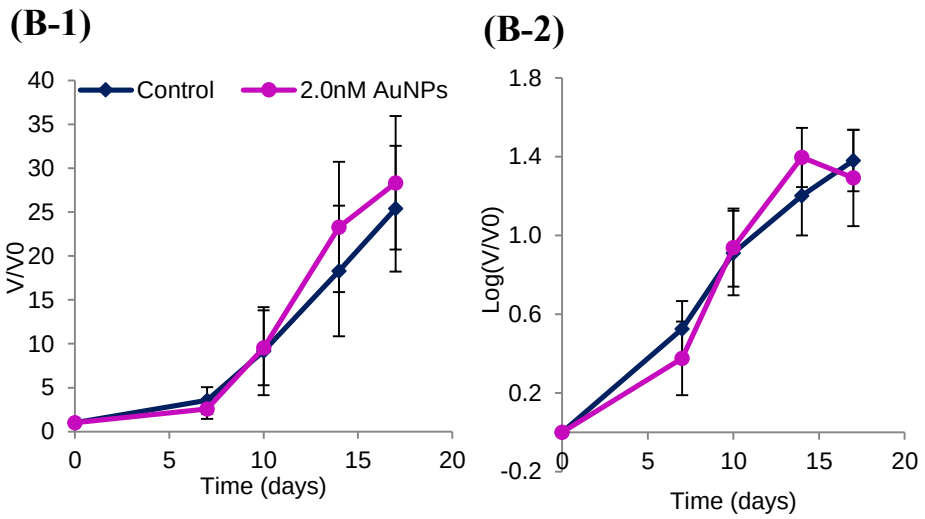

(B-3)

AuNP Concentration (nM)	τ_2	DT	AUC_{log}
0	2.86±0.41	4.09±0.53	11.00±0.65
2.0	1.59±0.83	3.73±0.45	14.04±0.83

Figure 9-1: The effect of solid AuNPs at a concentration of 2 nM on the growth of UVW/NAT and SK-N-BE spheroids.

UVW/NAT (A) and SK-N-BE (B) spheroids were incubated with solid AuNPs at a concentration of 2 nM for 24 hours with spheroids imaged twice per week for approximately 4 weeks. Spheroid volumes were calculated, and the average fold increase from initial volume (V/V0) (mean ± sd) is presented on a linear scale (A-1, B-1) and log scale (A-2, B-2). Additionally values for τ_2, DT and AUC_{log} were calculated (A-3, B-3) using GraphPad Prism v.6.0.1. Statistically significant differences in the median values of τ_2, DT and AUC_{log} compared to untreated control spheroids were determined by Kruskal-Wallis analysis with Dunn's post hoc testing for multiple comparisons.

9.4.1.2 The effect of HGNs on the growth of UVW/NAT and SK-N-BE spheroids

Incubation of UVW/NAT spheroids with HGNs at a concentration of 5 nM resulted in no significant change to the growth of spheroids, compared to untreated control spheroids (Figure 9-2(A)). No significant differences were found in the calculated values for growth delay (τ_2) and DT and AUC_{log}, compared to untreated control spheroids, indicating that the presence of HGNs resulted in no significant effect on the kinetics of spheroid growth.

Similarly, incubation of SK-N-BE spheroids with HGNs at 5 nM resulted in no significant changes in the growth of spheroids compared to untreated controls ($p>0.05$) (Figure 9-2(B)). The calculated values for growth delay (τ_2), DT and AUC_{log} were again all comparable to those for untreated control spheroids (Figure 9-2(B-3)), indicating that incubation of SK-N-BE spheroids with HGNs caused no change in the kinetics of spheroid growth compared to untreated control spheroids.

(A-1)

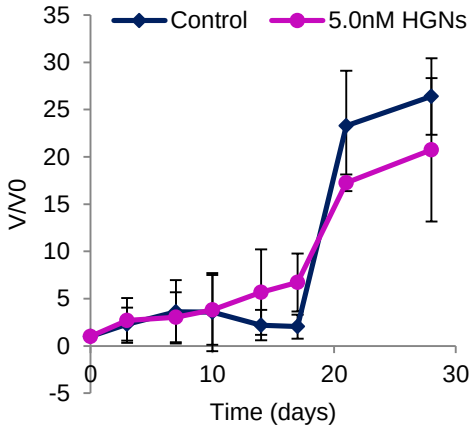

(A-2)

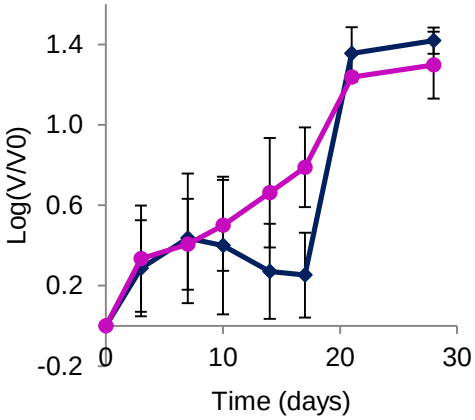

(A-3)

HGN Concentration (nM)	τ_2	DT	AUC_{log}
0	10.50±2.09	9.09±1.55	8.70±3.02
5.0	7.67±1.51	8.83±1.78	5.44±0.48

Figure 9-2 continued overleaf

(B-1) **(B-2)**

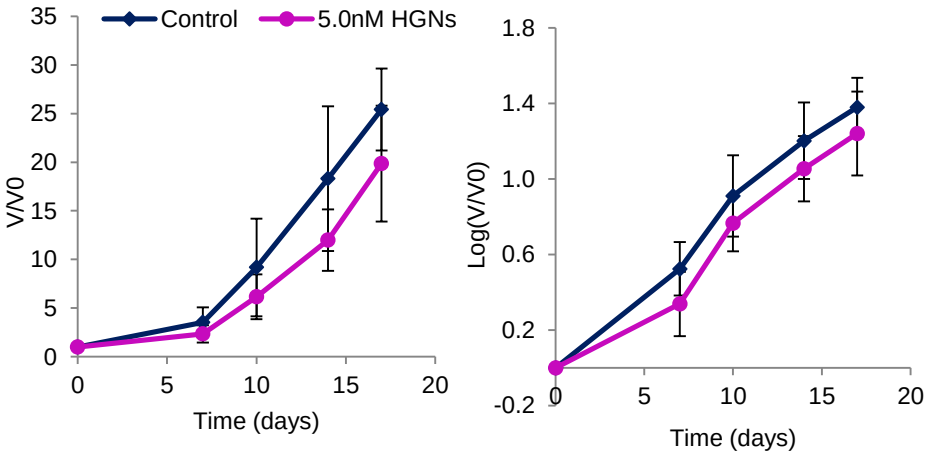

(B-3)

HGN Concentration (nM)	τ_2	DT	AUC_{log}
0	2.86±0.41	4.09±0.53	11.00±0.65
5.0	2.62±0.25	4.11±0.46	11.05±0.61

Figure 9-2: The effect of HGNs at a concentration of 5 nM on the growth of UVW/NAT and SK-N-BE spheroids.

UVW/NAT (A) and SK-N-BE (B) spheroids were incubated with HGNs at a concentration of 5 nM for 24 hours with spheroids imaged twice per week for approximately 4 weeks. Spheroid volumes were calculated, and the average fold increase from initial volume (V/V_0) (mean ± sd) is presented on a linear scale (A-1, B-1) and log scale (A-2, B-2). Additionally values for τ_2, DT and AUC_{log} were calculated (A-3, B-3) using GraphPad Prism v.6.0.1. Statistically significant differences in the median values of τ_2, DT and AUC_{log} compared to untreated control spheroids was determined by Kruskal-Wallis analysis with Dunn's post hoc testing for multiple comparisons.

9.4.2 The effect of XBR alone in UVW/NAT and SK-N-BE spheroids

Following assessment of the effect of solid AuNP and HGN incubation on the growth of UVW/NAT and SK-N-BE spheroids, the effect of XBR exposure alone was investigated. Both UVW/NAT and SK-N-BE spheroids were exposed to XBR across the dose range 0-4 Gy and statistically significant differences in the median values for τ_2, DT and AUC_{log} compared to untreated control spheroids were assessed by application of Kruskal-Wallis analysis with Dunn's post hoc testing for multiple comparisons.

In UVW/NAT spheroids, exposure to XBR from 0-2 Gy resulted in a dose dependent increase in τ_2 and DT compared to untreated control cells although the increase was not statistically significant ($p>0.05$) (Figure 9-3(A)). UVW/NAT spheroids exposed to 4 Gy XBR did not double in volume during the measurement period and therefore values for τ_2 and DT could not be calculated. The data therefore indicated that XBR exposure caused a dose dependant increase in the growth delay and a decrease in the growth rate of UVW/NAT spheroids. XBR exposure also resulted in a decrease in the calculated AUC_{log} values, compared to untreated control spheroids, where the calculated AUC_{log} decreased from 8.70±3.02 in untreated control spheroids to 1.88±0.31 following 4 Gy XBR exposure. Although the decrease in AUC_{log} at each XBR dose was not statistically significant, the data indicated that XBR exposure resulted in a dose dependant reduction in overall spheroid growth.

In SK-N-BE spheroids exposure to XBR from 0-4 Gy resulted in an increase in τ_2 and DT compared to untreated control cells, although this increase was not statistically significant ($p>0.05$) (Figure 9-5(B)). Exposure of SK-N-BE spheroids to 4 Gy XBR resulted in a significant decrease in the AUC where the calculated AUC_{log} value decreased from 11.00±0.65 in untreated control spheroids to 3.48±0.99 ($p<0.01$) following 4 Gy exposure. The data indicated that XBR exposure resulted in significant reduction in spheroid growth at XBR doses above 2 Gy, compared to untreated control spheroids.

(A-1) **(A-2)**

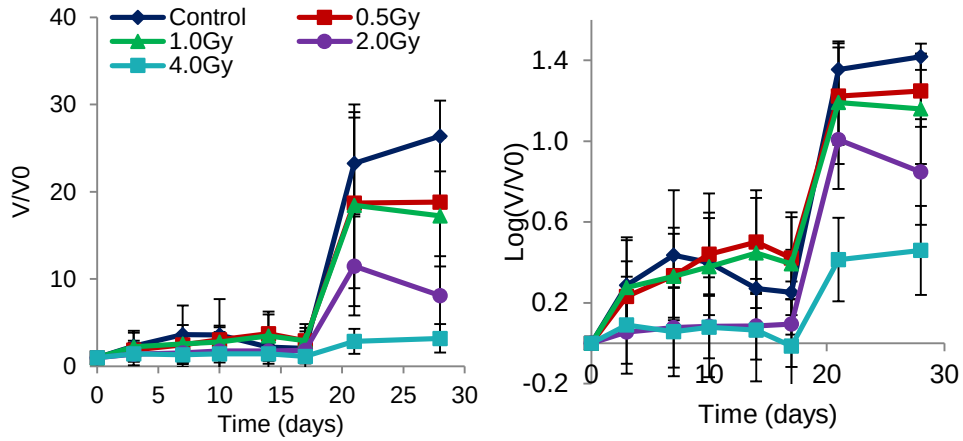

(A-3)

XBR Dose (Gy)	τ_2	DT	AUC_{log}
0	10.50±2.09	9.09±1.55	8.70±3.02
0.5	6.91±1.38	15.30±2.96	7.41±0.41
1.0	12.31±2.66	13.26±2.22	5.77±0.41
2.0	15.27±0.00	-----	4.64±0.37
4.0	-----	-----	1.88±0.31

Figure 9-3 continued overleaf

(B-1) **(B-2)**

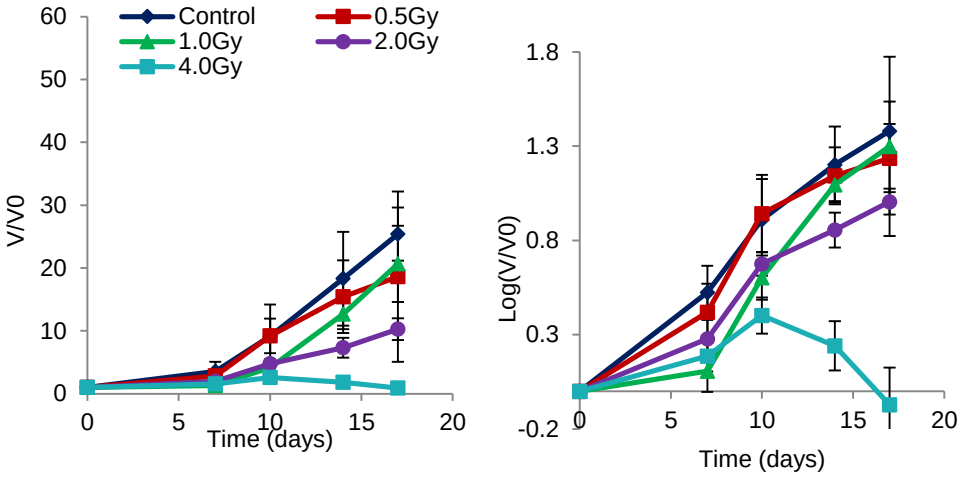

(B-3)

XBR Dose (Gy)	τ_2	DT	AUC_{log}
0	2.86±0.41	4.09±0.53	11.00±0.65
0.5	5.46±1.74	4.42±0.69	9.31±2.23
1.0	3.74±0.51	3.79±0.59	9.79±1.05
2.0	3.45±0.42	4.76±0.35	9.44±0.61
4.0	5.64±0.31	8.91±0.50	3.48±0.99**

Figure 9-3: The effect of XBR across the dose range 0-4 Gy on the growth of UVW/NAT and SK-N-BE spheroids.

UVW/NAT (A) and SK-N-BE (B) spheroids were exposed to XBR across the dose range 0-4 Gy with spheroids imaged twice per week for approximately 4 weeks. Spheroid volumes were calculated, and the average fold increase from initial volume (V/V_0) (mean ± sd) is presented on a linear scale (A-1, B-1) and log scale (A-2, B-2). Additionally values for τ_2, DT and AUC_{log} were calculated (A-3, B-3) using GraphPad Prism v.6.0.1. Statistically significant differences in the median values of τ_2, DT and AUC_{log} compared to untreated control spheroids was determined by Kruskal-Wallis analysis with Dunn's post hoc testing for multiple comparisons. Two (**) symbols indicate $p<0.01$.

9.4.3 The effect of solid AuNPs in combination with XBR in UVW/NAT and SK-N-BE spheroids

Following evaluation of the effect of solid AuNPs, HGNs and XBR alone on the growth of UVW/NAT and SK-N-BE spheroids, the effect of solid AuNPs at 2 nM in combination with XBR was examined to establish if the presence of solid AuNPs in combination with XBR had any significant effect on the kinetics of spheroid growth, compared to spheroids exposed to XBR alone.

The combination of 2 nM solid AuNPs with 1 Gy and 2 Gy XBR in UVW/NAT spheroids resulted in no significant change in the growth delay (τ_2), doubling time (DT) or overall growth of spheroids, compared to spheroids exposed to XBR alone ($p>0.05$) (Figure 9-4(A)). The calculated values for τ_2 and DT and AUC_{log} were comparable to those in spheroids exposed to XBR alone (Figure 9-4(A-5)), indicating that the combination of solid AuNPs with XBR did not significantly affect the kinetics of spheroid growth, compared to the effects of XBR exposure alone.

Similarly, in SK-N-BE spheroids, the combination of 2 nM solid AuNPs with 2 Gy resulted in no significant change in the growth delay (τ_2), doubling time (DT) and AUC, compared to 2 Gy XBR exposure alone ($p>0.05$), where the calculated values for τ_2, DT and AUC_{log} were comparable to those in spheroids exposed to XBR alone (Figure 9-4(B)), indicating, as in UVW/NAT spheroids that the combination of solid AuNPs with XBR did not significantly affect the kinetics of spheroid growth, compared to the effects of XBR exposure alone.

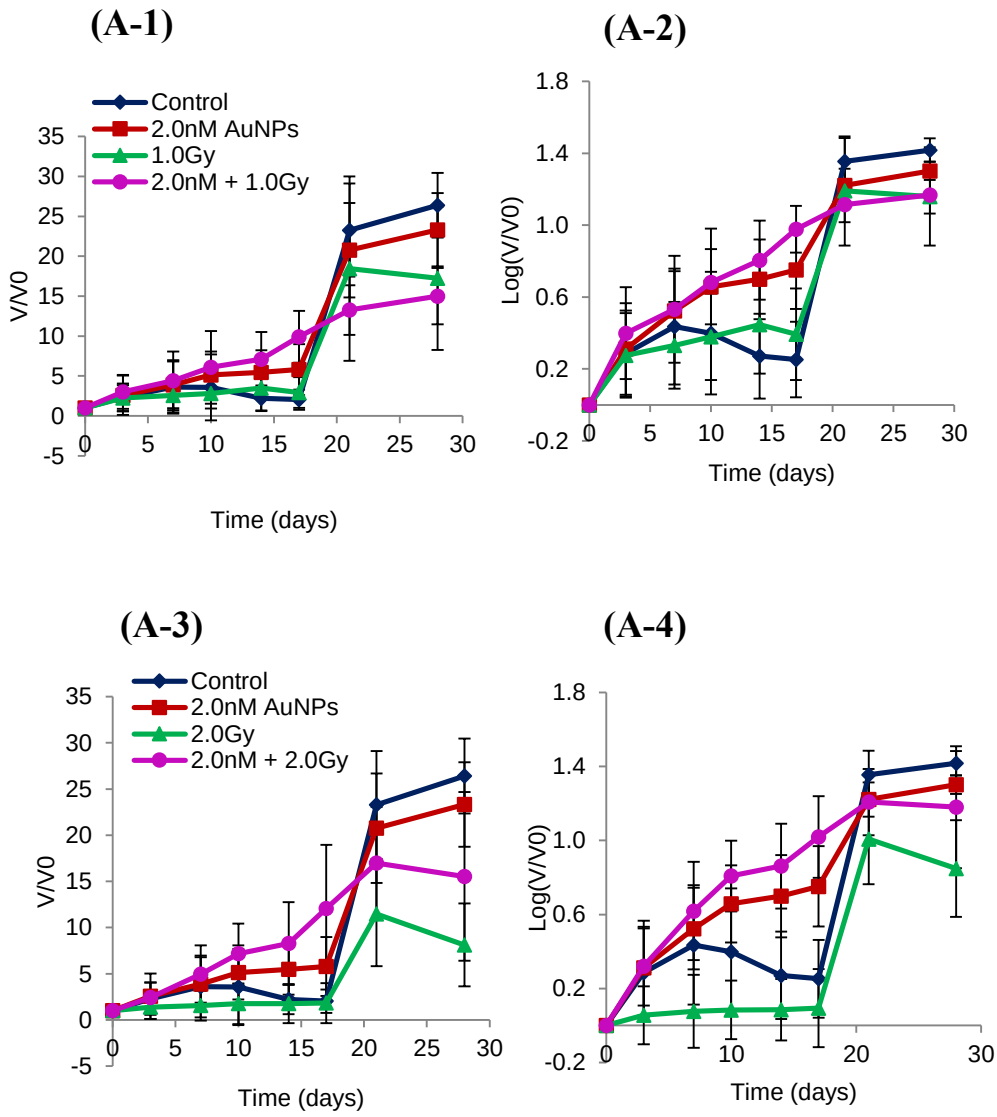

Figure 9-4 continued overleaf

(A-5)

	τ_2	DT	AUC_{log}
Control	10.50±2.09	9.09±1.55	8.70±3.02
2.0nM AuNPs	6.20±0.39	9.38±0.75	7.20±0.42
1Gy	12.31±2.66	13.26±2.22	5.77±0.41
2Gy	15.27±0.00	-----	4.64±0.37
2.0nM + 1Gy	5.48±1.02	11.43±1.12	5.51±0.47
2.0nM + 2Gy	5.82±0.94	8.69±1.14	4.69±0.72

Figure 9-4 continued overleaf

(B-1) **(B-2)**

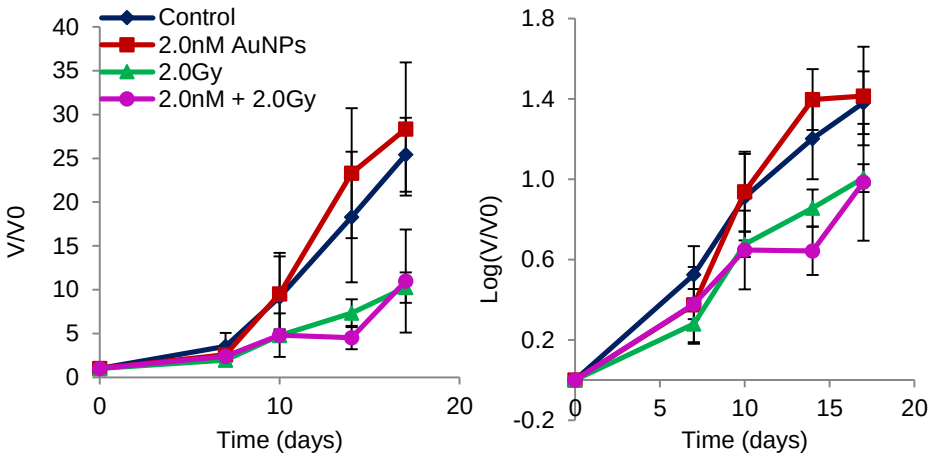

(B-3)

	τ_2	DT	AUC_{log}
Control	2.86±0.41	4.09±0.53	11.00±0.65
2.0nM AuNPs	1.59±0.83	3.73±0.45	14.04±0.83
2Gy	3.45±0.42	4.76±0.35	9.44±0.61
2.0nM + 2Gy	3.73±0.98	3.24±0.81	8.92±1.25

Figure 9-4: The effect of solid AuNPs in combination with XBR on the growth of UVW/NAT and SK-N-BE spheroids.

UVW/NAT (A) and SK-N-BE (B) spheroids were incubated with solid AuNPs at a concentration of 2 nM for 24 hours prior to exposure to XBR at 1 Gy and 2 Gy and spheroids imaged twice per week for approximately 4 weeks. Spheroid volumes were calculated, and the average fold increase from initial volume (V/V_0) (mean ± sd) is presented on a linear scale for 2 nM AuNPs + 1 Gy (A-1) and 2 nM AuNPs + 2 Gy (A-3, B-1) and a log scale for 2 nM AuNPs + 1 Gy (A-2) and 2 nM + 2 Gy (A-4, B-2). Additionally values for τ_2, DT and AUC_{log} were calculated (A-5, B-3) using GraphPad Prism v.6.0.1. Statistically significant differences in the median values of τ_2, DT and AUC_{log} compared to untreated control spheroids was determined by Kruskal-Wallis analysis with Dunn's post hoc testing for multiple comparisons.

9.4.4 The effect of HGNs in combination with XBR in UVW/NAT and SK-N-BE spheroids

The effect of HGNs at a concentration of 5 nM in combination with 1 Gy and 2 Gy XBR on the growth characteristics of UVW/NAT and SK-N-BE spheroids was also investigated (Figure 9-5).

In UVW/NAT spheroids treated with 5 nM HGNs in combination with XBR irradiation at 1 Gy and 2 Gy, no significant changes to the growth kinetics of spheroids, compared to treatment with XBR alone were observed (Figure 9-5(A)). The calculated growth delay (τ_2) and doubling time (DT) were lower, compared to spheroids exposed to XBR alone, although this difference was not statistically significant ($p>0.05$). The calculated values for the AUC_{log} for spheroids treated with HGNs and XBR were comparable to that of spheroids treated with XBR alone. The data indicated that the combination of XBR with 5 nM HGNs induced no significant changes in the growth rate and overall growth of UVW/NAT spheroids compared to XBR alone.

Similarly, in SK-N-BE spheroids, the combination of 5 nM HGNs with 1 Gy and 2 Gy XBR resulted in no significant alterations to the growth delay or growth rate of spheroids compared to XBR alone, where the calculated values for growth delay (τ_2) and doubling time (DT) were comparable to XBR exposure alone (Figure 9-5(B)). A decrease in the overall growth of SK-N-BE spheroids was observed following combination treatment, although the difference in the calculated values of AUC_{log} was not significant compared to exposure alone ($p>0.05$). The data indicated that the combination 5 nM HGNs with XBR induced a reduction in the growth of SK-N-BE spheroids compared to XBR alone, but this reduction was not statistically significant by the parameters of Kruskal-Wallis analysis.

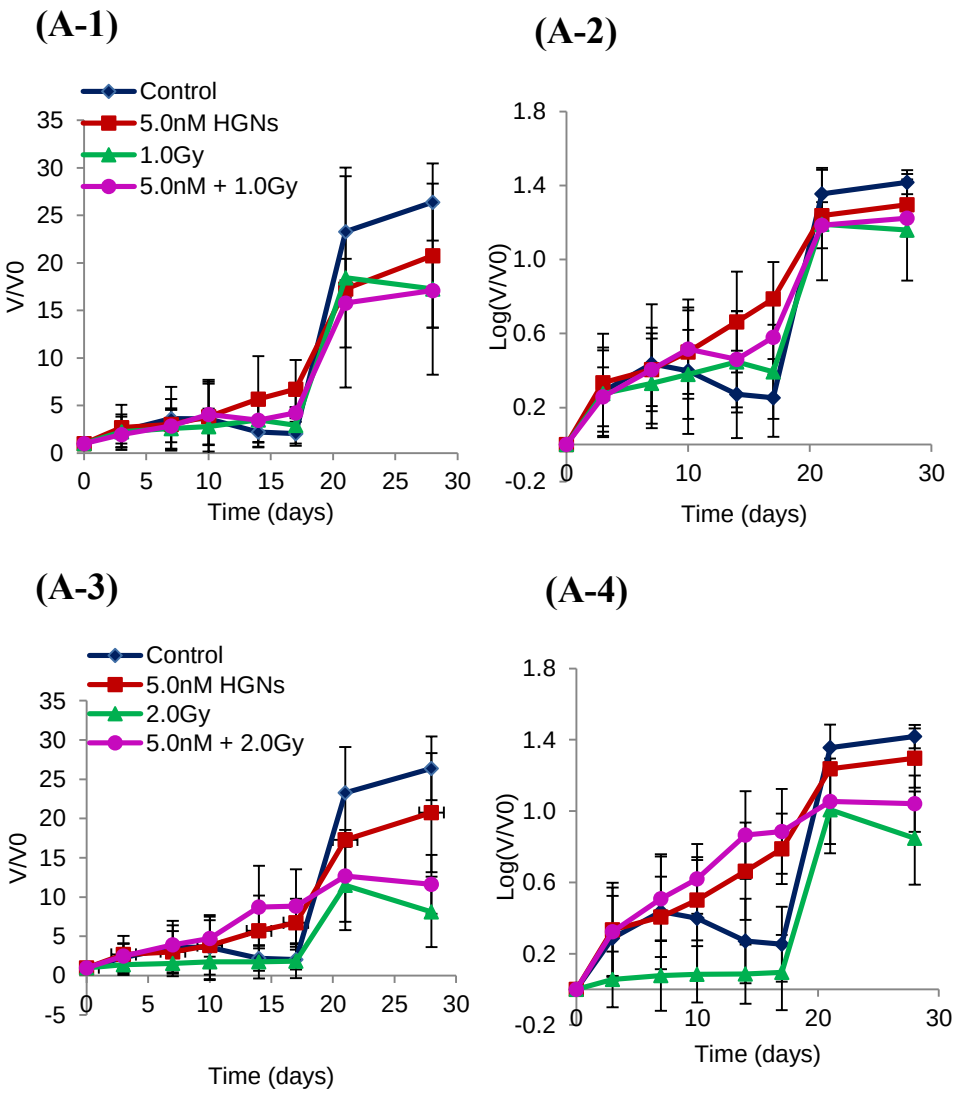

Figure 9-5 continued overleaf

(A-5)

	τ_2	DT	AUC_{log}
Control	10.50±2.09	9.09±1.55	8.70±3.02
5.0nM HGNs	7.67±1.51	8.83±1.78	5.44±0.48
1.0Gy	12.31±2.66	13.26±2.22	5.77±0.41
2Gy	15.27±0.00	-----	4.64±0.37
5.0nM + 1Gy	6.38±1.3	14.07±3.96	4.67±0.49
5.0nM + 2Gy	5.94±1.13	8.49±1.44	4.22±0.57

Figure 9-5 continued overleaf

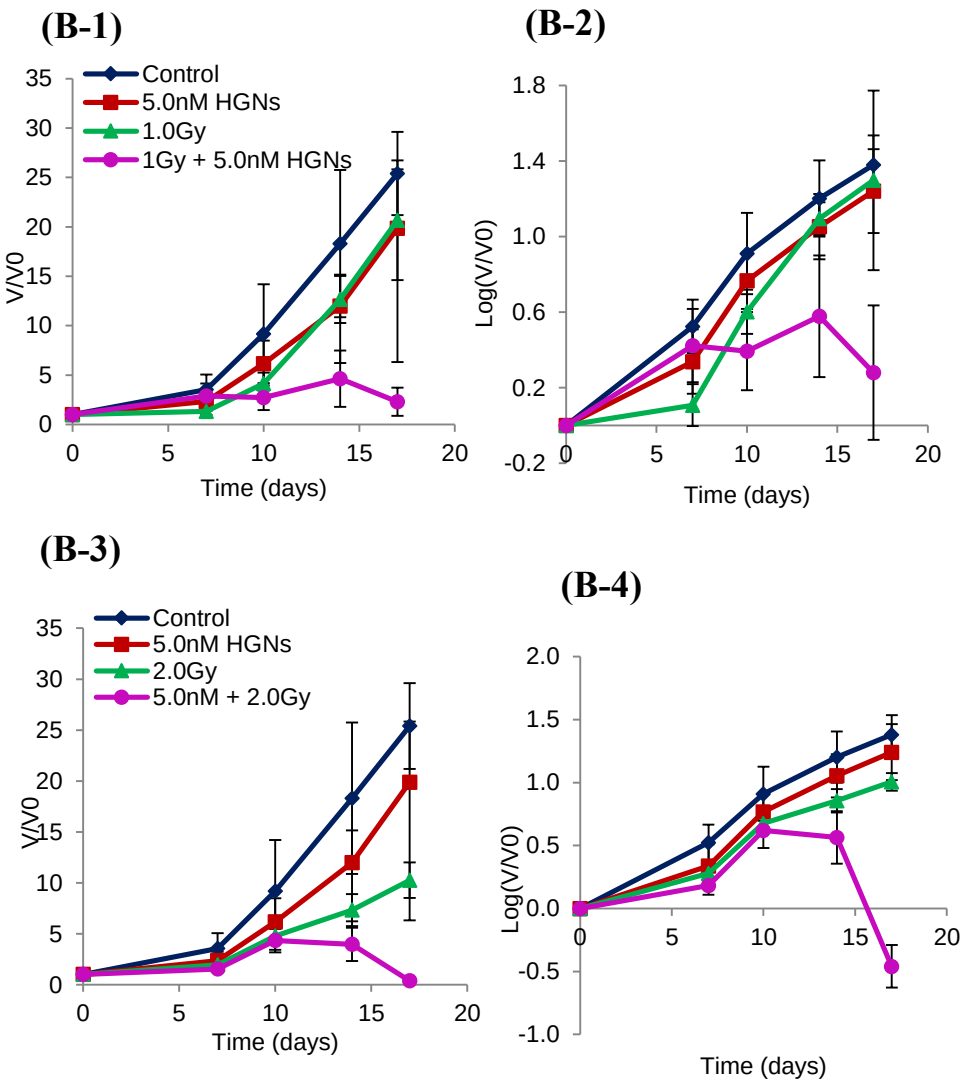

Figure 9-5 continued overleaf

(B-5)

	τ_2	DT	AUC_{log}
Control	2.86±0.41	4.09±0.53	11.00±0.65
5.0nM HGNs	2.62±0.25	4.11±0.46	11.05±0.61
1Gy	3.74±0.51	3.79±0.59	9.79±1.05
2Gy	3.45±0.42	4.76±0.35	9.44±0.61
5.0nM + 1Gy	5.68±2.12	5.36±1.62	6.15±1.04
5.0nM + 2Gy	3.91±1.24	4.10±1.38	2.61±2.36

Figure 9-5: The effect of HGNs in combination with XBR on the growth of UVW/NAT and SK-N-BE spheroids.

UVW/NAT (A) and SK-N-BE (B) spheroids were incubated with 5 nM HGNs for 24 hours prior to exposure to XBR at 1 Gy and 2 Gy and spheroids imaged twice per week for approximately 4 weeks. Spheroid volumes were calculated, and the average fold increase from initial volume (V/V_0) (mean ± sd) is presented on a linear scale for 5 nM HGNs + 1 Gy (A-1, B-1) and 5 nM HGNs + 2 Gy (A-3, B-3) and a log scale for 5 nM HGNs + 1 Gy (A-2, B-2) and 5 nM HGNs + 2 Gy (A-4, B-4). Additionally values for τ_2, DT and AUC_{log} were calculated (A-5, B-5) using GraphPad Prism v.6.0.1. Statistically significant differences in the median values of τ_2, DT and AUC_{log} compared to untreated control spheroids were determined by Kruskal-Wallis analysis with Dunn's post hoc testing for multiple comparisons.

9.4.5 The effect of solid AuNPs and HGNs in combination with [^{131}I]-MIBG on the growth of UVW/NAT spheroids

9.4.5.1 The effect of [^{131}I]-MIBG as a single agent on the growth of UVW/NAT spheroids

Following evaluation of the effect of XBR alone and in combination with solid AuNPs and HGNs on the growth characteristics of UVW/NAT and SK-N-BE spheroids, the effect of AuNPs and HGNs in combination with [^{131}I]-MIBG on the growth of spheroids was assessed. Due to time constraints in the end stages of this work, preliminary results in UVW/NAT spheroids only were achieved. The effect of [^{131}I]-MIBG alone across the dose range 0-2 MBq/mL is shown in Figure 9-6. Exposure of UVW/NAT spheroids to [^{131}I]-MIBG resulted in a dose dependant decrease in spheroid growth. Spheroids exposed to 0.1 MBq/mL demonstrated a decrease in the growth delay (τ_2) and an increase in the DT compared to untreated control spheroids, although this was not statistically significant ($p>0.05$). Spheroids exposed to [^{131}I]-MIBG at doses above 0.1 MBq/mL spheroids did not display a two-fold increase in volume during the measuring period and therefore values for τ_2 and DT could not be calculated.

[^{131}I]-MIBG exposure resulted in a significant dose dependant decrease in AUC in UVW/NAT spheroids where the calculated AUC_{log} values decreased from 8.30±0.28 in untreated control spheroids to 6.76±0.11, 4.35±0.49 ($p<0.05$), -1.21±0.92 and -4.26±3.19 ($p<0.01$) for spheroids exposed to 0.1 MBq/mL, 0.5 MBq/mL, 1 MBq/mL and 2 MBq/mL respectively. The data indicated that exposure of UVW/NAT spheroids to [^{131}I]-MIBG at doses above 0.1 MBq/mL resulted in significant reduction in the spheroid growth which was dose dependant compared to untreated control spheroids.

(A-1) **(A-2)**

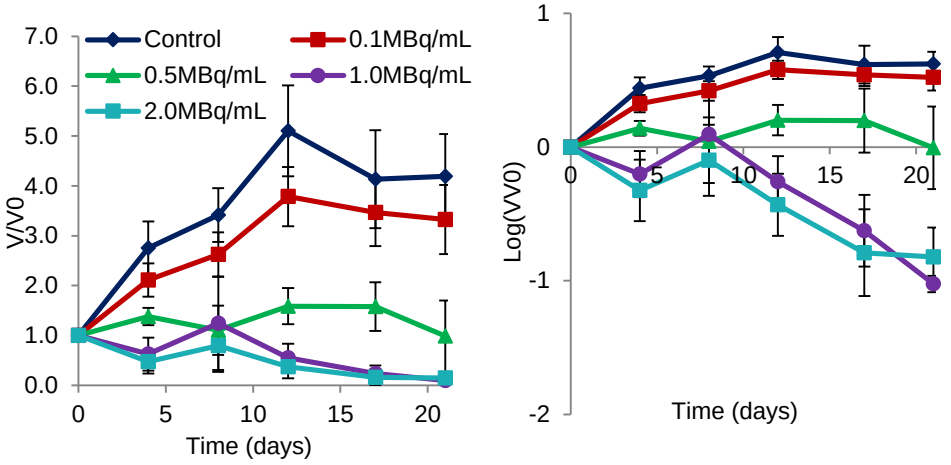

(A-3)

[^{131}I]-MIBG Dose (MBq/mL)	τ_2	DT	AUC_{log}
0	10.50±2.09	9.09±1.55	8.30±0.28
0.1	5.31±1.74	10.36±0.69	6.76±0.11
0.5	----	----	4.35±0.49*
1.0	----	----	-1.25±0.92
2.0	----	----	-4.26±3.19**

Figure 9-6: The effect of [^{131}I]-MIBG across the dose range 0-2 MBq/mL on the growth of UVW/NAT spheroids.

UVW/NAT spheroids were exposed to [^{131}I]-MIBG across the dose range 0-2 MBq/mL with spheroids imaged twice per week for approximately 4 weeks. Spheroid volumes were calculated, and the average fold increase from initial volume (V/V_0) (mean ± sd) is presented on a linear scale (A-1) and log scale (A-2). Additionally values for τ_2, DT and AUC_{log} were calculated (A-3). Statistically significant differences in the median values of τ_2, DT and AUC_{log} compared to untreated control spheroids were determined by Kruskal-Wallis analysis with Dunn's post hoc testing for multiple comparisons where one (*) and two symbols (**) indicate $p<0.05$ and $p<0.01$.

9.4.5.2 The effect of solid AuNPs in combination with [^{131}I]-MIBG on the growth of UVW/NAT spheroids

The effect of [^{131}I]-MIBG exposure in combination with solid AuNPs is shown in Figure 9-7. Due to time constraints the effect of [^{131}I]-MIBG alone across the dose range 0-2 MBq/mL was measured in tandem with the effect of [^{131}I]-MIBG in combination with solid AuNPs and HGNs. UVW/NAT spheroids were incubated with solid AuNPs at a concentration of 2 nM for 24 hours prior to [^{131}I]-MIBG exposure at 0.5 MBq/mL. As spheroids exposed to [^{131}I]-MIBG doses above 0.1 MBq/mL did not display a two-fold increase in volume, values for τ_2 and DT could not be calculated for 2 nM AuNPs in combination with 0.5 MBq/mL [^{131}I]-MIBG.

The presence of AuNPs at 2 nM in combination with [^{131}I]-MIBG resulted in a decrease in the AUC compared to the effects of 0.5 MBq/mL [^{131}I]-MIBG alone, although the decrease observed was not statistically significant ($p>0.05$). The data suggested that the combination of 2 nM AuNPs with [^{131}I]-MIBG in UVW/NAT spheroids may result in a decrease in spheroid growth compared to the effects of [^{131}I]-MIBG alone, however this was not significant by the parameters of Kruskal-Wallis analysis.

(A-1) **(A-2)**

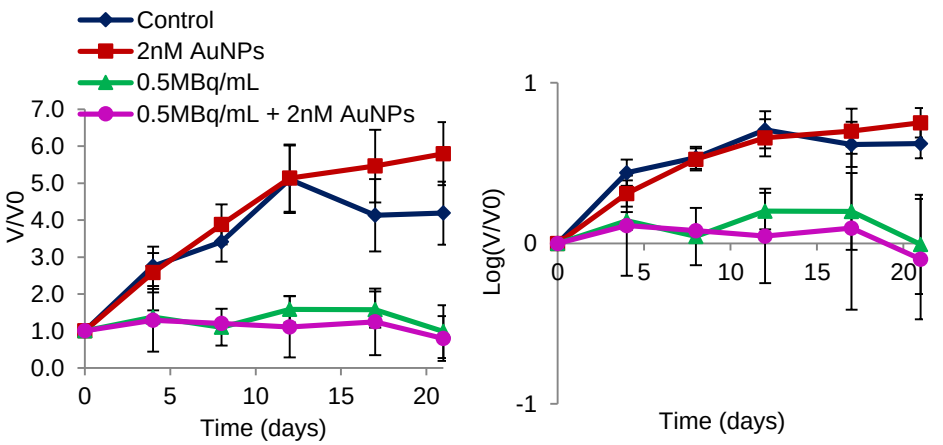

(A-3)

	τ_2	DT	AUC_{log}
Control	10.50±2.09	9.09±1.55	8.30±0.28
2nM AuNPs	1.59±0.83	3.73±0.45	14.04±0.83
0.5MBq/mL	----	----	4.35±0.49
2nM + 0.5MBq/mL	----	----	3.82±1.15

Figure 9-7: The effect of solid AuNPs in combination with [^{131}I]-MIBG on the growth of UVW/NAT spheroids.

UVW/NAT spheroids were incubated with AuNPs at 2 nM for 24 hours prior to exposure to [^{131}I]-MIBG at 0.5MBq/mL and spheroids imaged twice per week for approximately 4 weeks. Spheroid volumes were calculated, and the average fold increase from initial volume (V/V_0) (mean ± sd) is presented on a linear scale for 2 nM AuNPs + 0.5MBq/mL (A-1) and log scale for 2 nM AuNPs + 0.5MBq/mL (A-2). Additionally values for τ_2, DT and AUC_{log} were calculated where possible (A-3) using GraphPad Prism v.6.0.1. Statistically significant differences in the median values of τ_2, DT and AUC_{log} compared to untreated control spheroids were determined by Kruskal-Wallis analysis with Dunn's post hoc testing for multiple comparisons.

9.4.5.3 The effect of HGNs in combination with [^{131}I]-MIBG on the growth of UVW/NAT spheroids

The effect of [^{131}I]-MIBG in combination with HGNs was also investigated and UVW/NAT spheroids were incubated with HGNs at a concentration of 5 nM for 24 hours prior to [^{131}I]-MIBG exposure at 0.5 MBq/mL (Figure 9-8). Again as no two-fold increase in spheroid volume occurred in spheroids exposed to [^{131}I]-MIBG at doses above 0.1 MBq/mL, values for τ_2 and DT could not be calculated for spheroids treated with 5 nM HGNs in combination with 0.5 MBq/mL [^{131}I]-MIBG.

The presence of HGNs at 5 nM in combination with [^{131}I]-MIBG resulted in a decrease in the AUC compared to the effects of 0.5 MBq/mL [^{131}I]-MIBG alone although again the decrease observed was not statistically significant ($p>0.05$). The data suggested that, as with solid AuNPs, the combination of 5 nM HGNs with [^{131}I]-MIBG in UVW/NAT spheroids may result in a decrease in the growth of spheroids compared to the effects of [^{131}I]-MIBG alone, however this was not significant by the parameters of Kruskal-Wallis analysis.

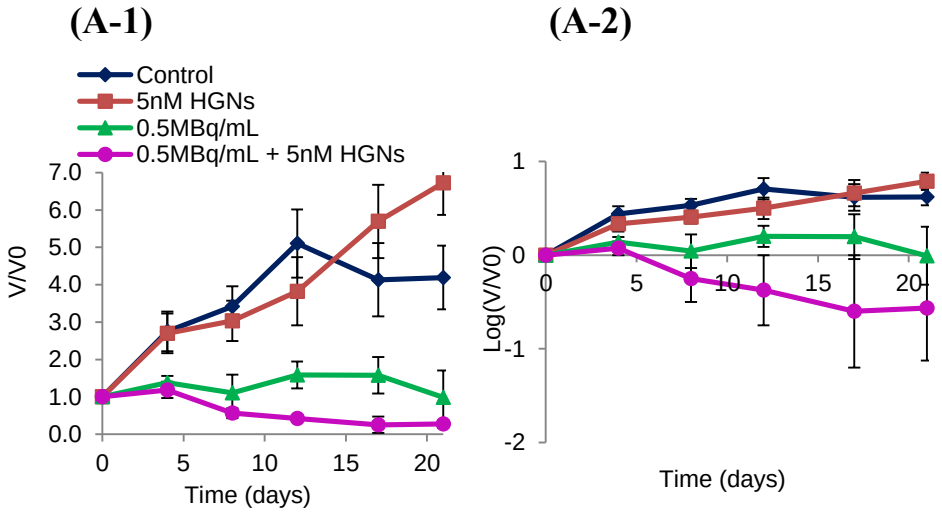

(A-3)

	τ_2	DT	AUC_{log}
Control	10.50±2.09	9.09±1.55	8.30±0.28
5nM HGNs	7.67±1.51	8.83±1.78	5.44±0.48
0.5MBq/mL	----	----	4.35±0.49
5nM + 0.5MBq/mL	----	----	-5.80

Figure 9-8: The effect of HGNs in combination with [^{131}I]-MIBG on the growth of UVW/NAT spheroids.

UVW/NAT spheroids were incubated with 5 nM HGNs for 24 hours prior to exposure to [^{131}I]-MIBG at 0.5 MBq/mL and spheroids imaged twice per week for approximately 4 weeks. Spheroid volumes were calculated, and the average fold increase from initial volume (V/V_0) (mean ± sd) is presented on a linear scale for 5 nM HGNs + 0.5 MBq/mL (A-1) and log scale (A-1). Additionally values for τ_2, DT and AUC_{log} were calculated where possible (A-3) using GraphPad Prism v.6.0.1. Statistically significant differences in the median values of τ_2, DT and AUC_{log} compared to untreated control spheroids were determined by Kruskal-Wallis analysis with Dunn's post hoc testing for multiple comparisons.

9.5 Discussion

The initial aim of this chapter was to investigate the effect of solid AuNPs, HGNs, XBR and [^{131}I]-MIBG as single agents on the growth kinetics of UVW/NAT and SK-N-BE spheroids. Following this, the effect on spheroid growth of solid AuNPs and HGNs in combination with XBR and [^{131}I]-MIBG was investigated, and compared to the effects of radiation alone. Results demonstrated that incubation of UVW/NAT and SK-N-BE spheroids with both solid AuNPs and HGNs did not significantly change the kinetics of spheroid growth. The calculated growth delay and growth rate together with the overall growth was comparable to that of untreated control spheroids. Exposure of spheroids to XBR and [^{131}I]-MIBG resulted in dose dependant decrease in overall spheroid growth, which was associated with an increase in the growth delay and decrease in growth rate. In combination with both solid AuNPs and HGNs, exposure of UVW/NAT and SK-N-BE spheroids to XBR induced no significant changes in the growth of spheroids, compared to XBR exposure alone. Similarly in combination with [^{131}I]-MIBG, the presence of AuNPs and HGNs induced no significant decrease in spheroid growth, compared to [^{131}I]-MIBG alone.

As discussed in section 1.8, multicellular tumour spheroid (MTS) models can be employed as a bridge between *in vitro* and *in vivo* studies to improve pre-clinical screening of the most promising new therapies as MTS provide a more accurate representation of the morphology and physiology of tumours. It is known that cells grown in 2D culture lack the essential cell-cell interactions and the extracellular matrix (ECM) found in tumours and MTS models. Additionally, 2D cultured cells do not demonstrate the diffusional gradients which are present in tumours and MTS models to control the transport of nutrients and oxygen into cells, and the removal of carbon dioxide and waste products out of cells, and regulate the cell pH. The diffusional gradients within spheroids lead to the formation of a layer of proliferating cells on the spheroid surface, under which lies hypoxic, quiescent cells and then finally necrotic cells residing in the centre of the spheroid (Figure 1-8) (Mehta et al., 2012). Compared to 2D cultured cells, MTS models can therefore provide a more accurate estimation of treatment outcome. As previously discussed in section 1.8, several studies have demonstrated that cells grown as 2D monolayers and as 3D MTS respond differently to radiation exposure by both XBR and radiopharmaceuticals. MTS display a greater

radioresistance towards XBR due to the lower oxygen concentration from the presence of hypoxic cells within the spheroid centre. In 2D monolayer cells oxygen is known to act as a potent radiosensitiser and is involved in indirect DNA damage through the production of hydroxyl radicals. Conversely, MTS have shown a greater sensitivity towards irradiation by radiopharmaceuticals such as [^{131}I]-MIBG as a result of the cross-fire of energy from radiopharmaceuticals targeting more cells within the 3D arrangement. This was demonstrated in the study by Boyd *et al*, (1999) in which treatment of UVW/NAT glioma cells with [^{131}I]-MIBG was twice effective when cells were grown as MTS compared to 2D monolayers (Boyd et al., 1999) This preliminary investigation using MTS models allowed evaluation of whether the results obtained in the previous chapters which investigated the effects of solid AuNPs, HGNs XBR and [^{131}I]-MIBG alone and in combination could be translated to 3D *in vitro* models.

Results of this present study demonstrated that XBR exposure from 0-4 Gy in UVW/NAT and SK-N-BE spheroids induced a dose dependant increase in growth delay (τ_2) and decrease in growth rate compared to untreated control spheroids (Figure 9-3). In this study the effect of XBR was evaluated by assessing the change in spheroid growth, compared to untreated control spheroids. Comparatively, in 2D monolayer cells the effect of XBR was measured by evaluating the change in clonogenic survival of XBR exposed cells, compared to untreated control cells. For this reason it was not possible to accurately compare the effects XBR in spheroids and 2D monolayer cells and determine if the hypothesis presented in previous studies, indicating that the efficacy of XBR will be less in 3D MTS is true of UVW/NAT and SK-N-BE spheroids. To further investigate this, clonogenic assays could be carried out using cells recovered from disaggregated spheroids following treatment.

Based on the literature it would be expected that the magnitude of any radiation dose enhancement observed in 2D monolayer cells from the combination of AuNPs with XBR would be lower following the same combination in MTS models due to the lower oxygen concentration. In our study the combination of solid AuNPs with XBR in both UVW/NAT and SK-N-BE spheroids induced no significant reduction in spheroid growth, compared to the effects of XBR alone which indicated that treatment with

solid AuNPs and XBR induced no significant radiosensitisation which was consistent with data obtained in 2D monolayer cell studies.

However, the combination of HGNs with XBR in UVW/NAT spheroids also resulted in no significant change to the growth characteristics, as no increase in the τ_2 and DT values, and no decrease in the AUC_{log} values were observed, compared to XBR alone (Figure 9-5(A)). The lack of radiosensitisation observed in UVW/NAT spheroids was in contrast to the results obtained for monolayer studies which demonstrated significant radiosensitisation (Figure 7-1). It is possible that the lower oxygen concentration within the spheroids as a result of the diffusional gradients diminished the radiosensitisation which is evident in monolayer cells. Additionally the uptake and localisation of the HGNs within the spheroid volume could affect the observed radiosensitisation; however due to time constraints the uptake and localisation of the particles was not measured. In contrast to this, SK-N-BE spheroids treated with HGNs in combination with XBR demonstrated a substantial decrease in spheroid growth compared to XBR alone, where the AUC_{log} value 9.44±0.61 following exposure to 2 Gy XBR alone compared to 2.61±2.36 in combination with HGNs. The data indicated that combination of HGNs with 2 Gy XBR in SK-N-BE spheroids reduced the overall growth of spheroids however, due to the small data set the variability of results was very high and the decrease in spheroid survival observed was not statistically significant by non-parametric testing, compared to XBR alone.

The data demonstrated that a greater reduction in growth was seen in SK-N-BE spheroids with HGNs, compared to UVW/NAT spheroids, despite displaying SK-N-BE spheroids displaying a greater radioresistance towards XBR alone. The average initial volume of UVW/NAT spheroids was $1.7x10^7 \mu m^3$ compared to only $4.9x10^6$ μm^3 in SK-N-BE spheroids. Previous studies, such as that performed by West *et al*, (1989) have demonstrated that smaller spheroids are more susceptible to XBR exposure, as the proportion of hypoxic cells will be lower and there will therefore be a greater oxygen concentration allowing more indirect DNA damage (West, 1989). Additionally, the uptake of HGNs by UVW/NAT and SK-N-BE spheroids may be different, and it is possible that due to the smaller initial volume of SK-N-BE spheroids the HGNs could have penetrated further throughout the spheroid volume and thus

induce a greater radiosensitising effect. As discussed however due to the time constraints at the latter stage of this study and the uptake and distribution of nanoparticles in the spheroids was not measured.

The hypothesis and data in previous literature indicated that treatment of spheroids with radiopharmaceuticals such as [^{131}I]-MIBG would have a greater effect than in monolayer cells due to the more effective cross-fire reactions throughout the 3D spheroid structure. Due to time constraints the effect of [^{131}I]-MIBG alone and in combination with solid AuNPs and HGNs was investigated in UVW/NAT spheroids only. Exposure of UVW/NAT spheroids to [^{131}I]-MIBG alone at doses above 0.1 MBq/mL resulted in almost sterilisation of spheroids and a two-fold increase in spheroid volume was not observed following treatment of spheroids with [^{131}I]-MIBG doses above 0.1 MBq/mL. Analysis of the AUC_{log} values however demonstrated a significant dose dependant decrease in UVW/NAT spheroid growth, where the calculated AUC_{log} values were 4.35±0.49 ($p<0.01$) and -1.25±0.92 for UVW/NAT spheroids exposed to 0.5 MBq/mL and 1.0 MBq/mL. The effect of [^{131}I]-MIBG was therefore greater in MTS models compared to 2D monolayer cells, however again to accurately compare the survival fraction clonogenic assay studies could be performed using disaggregated spheroids. This was consistent with previous study performed by Boyd *et al*, (1999) which demonstrated greater efficacy of [^{131}I]-MIBG in spheroids compared to monolayers (Boyd et al., 1999). Based on this therefore, it was expected that in combination with solid AuNPs and HGNs, greater radiosensitisation than observed in monolayer cells could be achieved.

In combination with solid AuNPs the spheroid growth (AUC_{log}) decreased from 4.35±0.49 following exposure to 0.5 MBq/mL alone to 3.82±1.15 in combination with 2 nM solid AuNPs. This was not statistically significant compared to [^{131}I]-MIBG alone by non-parametric testing ($p>0.05$) and was much lower than expected.

Similarly, the combination of [^{131}I]-MIBG with HGNs resulted in a decrease in AUC_{log} from 4.35±0.49 following treatment with 0.5 MBq/mL alone to -5.80 in the presence of 5 nM HGNs; however this decrease was not significant by non-parametric testing. The radiation enhancement observed when HGNs were combined with [^{131}I]-MIBG

was greater than with solid AuNPs, which was consistent with the results presented in previous chapters from the combination with both XBR and [^{131}I]-MIBG.

The surprising lack of significant radiosensitisation by solid AuNPs and HGNs observed in spheroid models following the combination of [^{131}I]-MIBG may be due to the uptake of nanoparticles and subsequent penetration throughout the spheroid mass which is possibly considerably lower in spheroids than monolayer cells across the same incubation time. Additionally the doses of [^{131}I]-MIBG employed in this preliminary study with the exception of 0.1 MBq/mL caused significant reduction in spheroid growth, preventing spheroids achieving a two-fold increase in spheroid volume across the entire measurement period. It is therefore possible that the damage caused to spheroids exposed to 0.5 MBq/mL [^{131}I]-MIBG was too extensive and therefore the presence of solid AuNPs or HGNs could offer no further decrease in spheroid growth.

The results of this preliminary study demonstrate that MTS models of both UVW/NAT and SK-N-BE cells can be used to assess the effects of XBR, [^{131}I]-MIBG, solid AuNPs and HGNs alone and in combination to determine the potential radiosensitisation offered by AuNPs and HGNs by assessing the spheroid growth kinetics. Compared to the behaviour of monolayer cells, spheroids display a much greater variation in their response to treatment which can be influenced based on their initial volume at time of treatment and the integrity of the outer proliferative cells. In addition to this, in this study only a small dataset was investigated due to time constraints and as a result of this there was a high degree of variation present throughout the results in this chapter. Therefore, whilst reductions in spheroid growth were observed, the results were not statistically significant by non-parametric analysis and therefore no accurate conclusions can be drawn regarding the potential effects of either solid AuNPs or HGNs in combination with XBR or [^{131}I]-MIBG. In continuation of this work a much larger sample set of spheroids should be analysed for each treatment group to obtain a more accurate representation of the treatment outcome. Analysis of a larger sample set would allow the results for individual spheroids to be separated and grouped according the initial spheroid volume which would reduce the variability within the results. Additionally, on continuation of this project, the

measurement time for the experiment could be extended which may allow a larger differential between treated groups and the respective controls to develop. This may increase the statistical significance of results where a decrease in spheroid growth is observed but is not significant by non-parametric testing. Furthermore, if the radiosensitisation offered by solid AuNPs and HGNs within spheroids were to be further investigated it would be imperative to measure the uptake and spheroid penetration of each type of nanoparticle. The degree of AuNP and HGN uptake relative to monolayer cells across the same incubation time frame must be assessed along with the effect that initial spheroid volume and the presence of diffusional gradients within spheroids have on the uptake. Little work has been done to date to compare the uptake within monolayer cells and spheroids, or to investigate the effect that the diffusional gradients present within spheroids above approximately 200 μm. It is likely however, that as nanoparticle uptake is governed by endocytosis that these gradients and the corresponding spheroid volume will play a significant role in governing the degree of nanoparticle uptake and their subsequent penetration throughout the spheroid volume. The location of AuNPs within spheroids will likely directly impact the efficacy of their combination with radiation and the resulting radiosensitisation achieved. AuNPs which can distribute throughout the entire spheroid will likely result in a much greater reduction in spheroid survival through direct targeting of the hypoxic cells in the spheroid centre.

The results of this preliminary investigation with MTS models are encouraging but extremely preliminary and inconclusive at this stage due to the time constraints of the project which meant that only a small sample set per treatment group could be analysed. Completion of the suggested further work would provide a much greater understanding of the uptake and penetration of AuNPs and HGNs in spheroids. Following this, it is clear that [^{131}I]-MIBG was more effective in MTS models than monolayer cells and therefore assessment of lower [^{131}I]-MIBG doses in combination with AuNPs and HGNs would allow greater visualisation of the potential radiosensitising effects. Finally, due to the higher variability associated with the growth of spheroids, which can be influenced by their initial diameter upon treatment, which dictates the relative concentrations of necrotic, hypoxic and proliferating cells,

substantially more replicates should be performed when utilising MTS models, compared to 2D monolayer cell cultures.

Chapter 10

Summary of Results and Future Work

Chapter 10: Summary of Results & Future Work

10.1 Introduction: Gold nanoparticles as radiosensitisers

The aims of this study were to establish the radiosensitising potential of solid AuNPs and HGNs in combination with ionising radiation in the form of both low kV XBR, and high kV radiation from ^{131}I as part of the targeted radiopharmaceutical [^{131}I]-MIBG. To date this is the first report to provide experimental data of both solid AuNPs and HGNs combined with the targeted radiopharmaceutical [^{131}I]-MIBG.

Previous studies which have investigated the radiosensitising potential of solid AuNPs have reported conflicting results. For example the study by Yasui *et* al, (2014) reported a radiation dose enhancement factor (DEF) of 1.51 following the combination of 106 nm PEGylated AuNPs with 200 kVp X-rays within murine squamous carcinoma SCCVII cells (Yasui et al., 2014). Similarly, Kong *et* al, (2008) reported a DEF of 1.63 with 15 nM glucose functionalised AuNPs in combination with 200 kVp X-rays in breast cancer derived MCF7 cells (Kong et al., 2008). In combination with high kV or MV radiation sources however, the dose enhancement observed in previous studies is minimal, and in each case where a comparison between observed radiosensitisation utilising kV and MV radiation sources has been done, the DEFs have been less with MV sources. For example in the study by Jain *et al*, (2011) the DEF within breast cancer MDA-MB-231 cells for 1.9 nm AuNPs reduced from 1.41with 160 kVp X-rays, to 1.29 with 6 MV photons, and further reduced to 1.16 with 15 MV photons (Jain et al., 2011). The results of previous studies suggest that substantial further work is necessary to fully understand the mechanisms which govern the differences in radiosensitisation observed.

Results of the previous work investigating the radiosensitisation by solid AuNPs with ionising radiation are consistent with the proposed physical mechanism of radiosensitisation by AuNPs, discussed in section 1.6.1. It is rationalised that due to the difference in the mass absorption coefficients between AuNPs and soft tissue, when the incident radiation energy is close to the absorption energies in each electron shell of AuNPs (3-79 keV), photoelectric ionisation of AuNPs will dominate and lead to a large dose deposition of secondary electrons in the vicinity around the AuNPs. At

radiation energies which lie outside the absorption range of AuNPs however, no photoelectric ionisation will occur and Compton scattering will dominate the ionisation processes leading to very little dose enhancement from the presence of AuNPs (Butterworth et al., 2012). Recent research has proposed that additional physical mechanisms may contribute to the greater than predicted radiosensitisation observed in some studies. These mechanisms include the presence of photoelectric ionisation by small amounts of lower energy photons and electrons which are scattered from the incident high kV or MV radiation beam (McMahon et ,al., 2011). Furthermore it has been proposed that ·OH species produced by the interaction of radiation with intracellular water can interact directly with the water-nanoparticle layers to generate substantial amounts of ·OH species to contribute to more complex DNA damage (Sicard-Roselli et al., 2014).

10.2 Summary of the results of this study

10.2.1 Solid gold nanoparticles in combination with XBR

This study demonstrated that the radiosensitisation achieved in UVW/NAT, SK-N-BE and A375 cell lines when solid AuNPs were combined with 225 kVp XBR was variable and likely influenced by the cell lines inherent sensitivity to radiation and their response to AuNPs as a single agent. The IC_{50} values measured for UVW/NAT, SK-N-BE and A375 cells were 2.85 Gy, 3.40 Gy and 1.79 Gy respectively, which were consistent with the variation in the DEFs measured at the 50% toxicity level for AuNPs with XBR which were 1.12, 0.93 and 4.68 UVW/NAT, SK-N-BE and A375 respectively. Additionally, A375 cells were the only cell line to demonstrate a significant concentration dependent reduction in clonogenic survival following treatment with AuNPs alone. The cell line specific radiosensitisation by solid AuNPs observed was consistent with the results observed in other studies. For example, the study by Jain *et al*, (2011) demonstrated that the combination of 1.9 nm AuNPs with 160 kVp X-rays resulted in DEFs of 0.92, 1.05 and 1.41 in DU145, L132 and MDA-MB-231 cells respectively. The study also demonstrated that MDA-MB-231 cells were the most sensitive to XBR exposure alone, and that significant reduction in cell

survival following incubation with AuNPs was observed in MDA-MB-231 cells only which was consistent with the results of this present study (Jain et al., 2011).

Results of this present study demonstrated that the observed radiosensitisation from solid AuNPs with XBR did not correspond to an increase in the formation of DNA DSBs, but was associated with a decrease in the resolution of γ-H2AX foci, indicative of a reduction in the repair of DNA DSBs, compared to XBR alone. These results were consistent with the data presented in the study by Taggart *et al*, (2014) which reported that the number of 53BP1 foci in MDA-MB-231and DU145 cells following treatment with 1.9nm AuNPs in combination with 2 Gy XBR were significantly higher 24 hours post irradiation, compared to 2 Gy XBR alone (Taggart et al., 2014).

10.2.2 Solid gold nanoparticles in combination with [^{131}I]-MIBG

Following evaluation of the radiosensitisation potential of solid AuNPs in combination with 225 kVp XBR, their ability to radiosensitise cells to high keV β and γ emissions from ^{131}I in the form of the targeted radiopharmaceutical [^{131}I]-MIBG was evaluated in the NAT expressing cell lines UVW/NAT and SK-N-BE. Results of this study demonstrated significant radiosensitisation in both cell lines with calculated DEF_{50} values of 3.03 and 6.08 in UVW/NAT and SK-N-BE cells respectively. The observed DEFs were much greater than those achieved with XBR, and exceeded any DEF_{50} value reported previously in the literature following combination of AuNPs with both kV and MV X-rays radiation. Results also demonstrated that the significant radiosensitisation observed following the combination of solid AuNPs with [^{131}I]-MIBG was associated with a significant increase in the formation of γ-H2AX foci, compared to [^{131}I]-MIBG alone indicating that in combination with [^{131}I]-MIBG, the radiosensitisation was associated with an increase in DNA DSBs. Due to the presence of continual radiation from ^{131}I decay within cells which have internalised [^{131}I]-MIBG, no resolution of γ-H2AX foci was observed between 2 and 24 hours after removal of [^{131}I]-MIBG. It is therefore not possible to comment on the effect of AuNPs on the repair of [^{131}I]-MIBG induced DNA, however it conceivable that the presence of AuNPs reduced the repair of DNA DSBs, as was observed with XBR, however due

to the formation of new foci as a result of continual radioisotope decay the repair was not detected. The exact mechanisms of the DNA damage and repair kinetics induced by the two radiation sources were not further interrogated in this present study.

The energy of β electrons and γ rays produced through decay of ^{131}I are 606 keV and 362 keV respectively. As these energies greatly exceed the binding energy of electrons in Au, the probability of photoelectric ionisation of AuNPs by the emissions of ^{131}I is low, and based on the predictions of dose enhancement by AuNPs detailed in previous studies no dose enhancement through photoelectric absorption was predicted. Despite these predictions however, significant radiosensitisation was observed, where the observed DEFs not only exceeded those observed when AuNPs were combined with XBR, but were also substantially greater than any DEFs which have been previously reported for AuNPs in combination with either kV or MV radiation sources.

It can be hypothesised therefore, that as the emitted low LET β and γ radiation travel through the cell population up to their maximum path range, which is equivalent to the diameter of a few cells, they will deposit energy along the decay track. Therefore, at some point in this traversal, the energy of the β and γ radiation will be within the optimum range to result in photoelectric absorption within the nanoparticles. Furthermore, as half-life of the β and γ radiation is 8.02 days the much longer exposure of nanoparticles to radiation compared to the rapid exposure with XBR, where 2 Gy is delivered in 52 seconds, could contribute to a greater magnitude of nanoparticle ionisation and subsequent dose enhancement. Additionally, it was suggested that the β and γ emissions from decay of ^{131}I could induce prolonged production of ROS within the cells, which could then interact with the AuNPs to generate further secondary electron and $^{\cdot}$OH species production based on the mechanism proposed by Sicard-Roselli *et al*, (2014).

10.2.3 Hollow gold nanoparticles in combination with XBR

Following on from the investigation of solid AuNPs in combination with XBR and [^{131}I]-MIBG, this study examined the radiosensitising potential of HGNs with both radiation qualities. Previous work with HGNs has focused their use in photoablation

therapy (PTA); however literature has demonstrated that they have superior physical properties, compared to solid AuNPs. As discussed in section 1.7, previous studies have established that due to the availability of two exposed surfaces HGNs demonstrate increased absorption, and a higher energy conversion capability compared to solid AuNPs (Gutrath et al., 2012). Additionally, HGNs have demonstrated an enhanced electromagnetic field surrounding the particles, which is increased by the presence of pinholes on the HGN surface (Hao et al., 2004; Jackson et al., 2003). Despite the clear advantages over solid AuNPs, to date very little research has been performed to investigate their potential as radiosensitisers.

Results of this study demonstrated for the first time that the combination of HGNs with XBR resulted in significant radiosensitisation in each of the cell lines investigated, with DEFs at the 50% cytotoxicity level of 2.77, 2.49 and 2.42 were observed in UVW/NAT, SK-N-BE and A375 cells respectively. Comparing the physical properties of solid and hollow nanoparticles, under identical conditions it could be hypothesised that in combination with ionising radiation, HGNs should induce a greater dose enhancement. In this study however it was not possible to directly compare the radiosensitisation achieved with each radiation quality in combination with both solid AuNPs and HGNs. Whilst the calculated DEF_{50} values were greater following the combination of HGNs with XBR compared to solid AuNPs, it was not possible to conclude that this was a result of superior radiosensitising potential of HGNs due to the differences in physical characteristics between the two nanoparticles. In this study the nanoparticle diameter, administered concentration and the kinetics of nanoparticle uptake were variable factors. Furthermore, due to the differences in the surface chemistry between solid AuNPs and HGNs it would be not be possible to achieve identical conditions and therefore flawed directly compare the effects of each nanoparticle type following combination with radiation. Due to the hollow core HGNs will always have a larger overall surface area even if the nanoparticle diameter was the same. Additionally, the presence of pinholes on the surface of HGNs has been shown to enhance the electromagnetic field surrounding the nanoparticles. The use of seamless HGNs would therefore likely reduce the dose enhancement observed. Finally, whilst both solid AuNPs and HGNs were stabilised using citrate, a greater volume of citrate was required for adequate stabilisation of HGNs. Removal of excess

citrate in order to match the citrate concentration of solid and hollow nanoparticles would likely result in instability of the HGNs, preventing their use. For this reasons the aim of this present study was only to investigate the radiosensitising potential of HGNs due to the lack of previous work in this area, and their positive physical properties.

The significant radiosensitisation observed following the combination of HGNs with XBR was associated with a decrease in the resolution of γ-H2AX foci as was observed with solid AuNPs.

10.2.4 Hollow gold nanoparticles in combination with [^{131}I]-MIBG

In combination with [^{131}I]-MIBG, HGNs induced significant radiosensitisation in both UVW/NAT and SK-N-BE cells where the observed DEFs of 3.65 and 4.83 were achieved in UVW/NAT and SK-N-BE cells respectively. As with solid AuNPs the observed DEFs when HGNs were combined with ^{131}I were greater than achieved with HGNs in combination with XBR. The radiosensitisation from the combination of HGNs with [^{131}I]-MIBG was associated with a significant increase in the formation of γ-H2AX foci, compared to [^{131}I]-MIBG treatment alone. As with solid AuNPs, at 24 hours after removal of [^{131}I]-MIBG no resolution of γ-H2AX foci was observed, likely due to the formation of new foci.

Again the observed radiosensitisation was hypothesised to be a result of the traversal of low LET β and γ emissions from ^{131}I through the cells where they could interact with HGNs via photoelectric absorption upon loss of sufficient energy to bring their energy into the optimum range for AuNP absorption.

10.2.5 Assessment of the effect of solid AuNPs, HGNs, XBR and [^{131}I]-MIBG on the growth of MTS

Following evaluation of the radiosensitisation potential of solid AuNPs and HGNs in combination with XBR and [^{131}I]-MIBG *in vitro,* utilising 2D monolayer cell cultures,

the effects of each agent alone and in combination on the growth of 3D MTS was examined. As discussed in section 1.8, 3D MTS models can be used to provide a more accurate representation of the morphology, physiology and heterogeneity of cell proliferation of *in vivo* micrometastases. Data presented in previous studies has demonstrated that MTS display a greater radioresistance towards XBR as a result of the lower oxygen concentration from the presence of hypoxic cells within the spheroid centre. Comparatively, studies such as that by Boyd *et al*, (1999) have demonstrated that MTS have a greater sensitivity towards irradiation by radiopharmaceuticals such as [^{131}I]-MIBG, as the cross-fire effect from radiopharmaceuticals is much more effective within the 3D cell arrangement (Boyd et al., 1999) The aim of this preliminary investigation using MTS models was to evaluate whether the results obtained in the previous chapters which investigated the effects of solid AuNPs, HGNs XBR and [^{131}I]-MIBG alone and in combination could be translated to 3D *in vitro* models.

Results of this preliminary study demonstrated that treatment of UVW/NAT and SK-N-BE spheroids with solid AuNPs and HGNs resulted in no significant changes in spheroid growth, whilst treatment with XBR and [^{131}I]-MIBG resulted in a dose dependant decrease in spheroid growth and survival which was consistent with the results in previous studies (Boyd et al., 2002, 1999; Gaze et al., 1992). However, surprisingly, treatment of spheroids with solid AuNPs and HGNs in combination with XBR and [^{131}I]-MIBG induced no significant changes in the growth of spheroids, compared to radiation exposure alone.

10.3 Future work arising from the results of this study

10.3.1 Further investigation of the interaction of solid and hollow AuNPs with XBR

Based on the results of solid AuNPs and HGNs in combination with XBR summarised in sections 10.2.1 and 10.2.3, it was hypothesised that the interaction of AuNPs with XBR caused an increase in the complexity of DNA damage, likely due to the production of ROS which could contribute to both the formation of more DNA SSBs, and the conversion of these DNA SSBs into more complex damage. In order to confirm

this hypothesis the intracellular ROS concentration could be measured using fluorescent DCFH-DA assays to determine if the presence of nanoparticles in combination with radiation significantly increased the ROS concentration (Aranda et al., 2013). Additionally, as it is hypothesised that the radiosensitisation results through a ROS mediated mechanism, ROS scavengers could be used to remove the ROS species generated following radiation exposure in the presence and absence of AuNPs. Analysis of the effect of diminished ROS on the clonogenic survival and DNA damage and repair in the presence and absence of AuNPs, compared to the results in this study would indicate whether ROS affected the observed radiosensitisation and the effect on DNA damage and repair (Kim et al., 2005). Furthermore, the results suggest that the complexity of DNA damage is increasing, and the literature suggesting that this is likely through a free radical mechanism which would contribute to DNA SSBs. An important future investigation would therefore be to assess the dynamics of DNA SSBs using techniques such as, comet assays to determine if the magnitude and complexity of DNA damage via SSBs increased in the presence of AuNPs (Azqueta et al., 2014). Finally, results of this study demonstrated that the reduction in cell survival observed following the combination of AuNPs and HGNs with XBR was not via apoptosis by caspase 3 mediated mechanisms. Therefore, subsequent studies to examine other cell death pathways could be carried out, such as analysis caspase 3 independent apoptosis using Tunel assays, or measurement of apoptotic and necrotic cell death using dual-staining with propidium iodide and acridine orange (Bai et al., 2015; Qutob and Ng, 2001).

10.3.2 Further investigation of the interaction of solid and hollow AuNPs with [^{131}I]-MIBG

Based on the results of solid AuNPs and HGNs in combination with [^{131}I]-MIBG it was hypothesised that the decay of the low LET β and γ emissions to within the optimum energy range for AuNP absorption, together with the extended radiation exposure with [^{131}I]-MIBG resulted in the observed radiosensitisation and biological effect. Ideally, in order to fully investigate the hypothesis presented, the decay characteristics of ^{131}I would have to be established, where the energy of the β and γ emissions can be measured at different points throughout the decay, in order to confirm

that they reside at some point in the optimum range for photoelectric absorption by AuNPs However, due to the complex nature of this investigation this would not be feasible. In order to investigate areas of the hypothesis further, ROS studies utilising fluorescent DCFH-DA and ROS scavenger assays could be performed as discussed previously in section 10.3.1. As the probability of photoelectric ionisation dominating will be greater when the difference in the energy of the incident radiation and the electron binding energies of Au electrons is low, one option to investigate this would be to conjugate MIBG with radioisotopes which decay with energies closer to the electron binding energies such as ^{125}I which decays by emission of γ rays of 35 keV. However, as the half-life and tissue penetration of ^{125}I is different from ^{131}I, direct comparison between the effects of [^{125}I]-MIBG and [^{131}I]-MIBG would not be possible, as it would be difficult to conclude that any observed effects were due to differences in the decay energy and not another parameter such as the radioisotope path length. Another investigation which could be carried out to explore the influence of the prolonged radiation exposure with [^{131}I]-MIBG compared to XBR would be to reduce the dose rate of the XBR from 2.20 Gy/min to deliver the same radiation dose over a longer time (eg. 0.22 Gy/min or 0.022 Gy/min). Comparison of these results to those achieved with AuNPs in combination with XBR which was delivered at 2.20 Gy/min as this study could determine if increased exposure to XBR influenced the degree of radiosensitisation, and corresponding biological effect observed. The radiosensitisation observed when solid AuNPs and HGNs were combined with XBR was associated with a decrease in DNA repair, measured through a reduction in the resolution of γ-H2AX foci. Due to the presence of continued radiation from ^{131}I decay within cells however, no resolution of γ-H2AX foci was observed between 2 and 24 hours after removal of [^{131}I]-MIBG. In order to further investigate the effect of solid AuNPs and HGNs in combination with [^{131}I]-MIBG on the repair of [^{131}I]-MIBG induced DNA damage a longer time frame following removal of [^{131}I]-MIBG could be examined to determine when resolution of foci following removal of [^{131}I]-MIBG is measurable and therefore determine the effect of both solid AuNPs and HGNs on the repair of DNA damage.

As this study is the first to present experimental data demonstrating successful radiosensitisation of cells to [^{131}I]-MIBG it is not possible to corroborate the results

observed with previous studies. The results however are extremely encouraging as they demonstrate that despite the poor energy match between the β and γ emissions from ^{131}I and the electrons within Au; significant radiation dose enhancement is possible with high keV radiation, allowing the use of AuNPs as radiosensitisers to be considered more clinically relevant following optimisation of an appropriate AuNP formulation.

10.3.3 Cell cycle results and future work

Following the combination of both solid AuNPs and HGNs with XBR and [^{131}I]-MIBG, no significant changes in the progression of cells through the cell cycle were observed, compared to the effects of radiation alone. The mechanism of radiosensitisation by AuNPs suggests that the presence of AuNPs will increase the complexity of radiation induced damage, and not necessarily increase the number of damaged cells. It could therefore be expected that the proportion of cells arresting in G2/M following exposure to radiation in the presence and absence of nanoparticles to be the same. This could be further examined using western blot analysis of cyclins associated with cell cycle progression to determine the effect of radiation exposure with and without nanoparticles on normal cell progression and determine if cell cycle arrest was activated (Cabrera et al., 2015).

10.3.4 Future work for the investigation of MTS models

Compared to the behaviour of monolayer cells, spheroids demonstrate greater variation in their response to treatment which can be influenced based on their initial volume at time of treatment. Additionally, due to time constraints only a small dataset was investigated in this preliminary study, and as a result of this there was a high degree of variation present throughout the results in this chapter. Whilst reductions in spheroid growth and survival were observed, the results were not statistically significant by non-parametric analysis. In continuation of this work a much larger sample set of spheroids should be analysed for each treatment group and would allow

the results to be separated and grouped according the initial spheroid volume which would reduce the variability within the results. Additionally, on continuation of this project, the measurement time for the experiment could be extended which may allow a larger differential between treated groups and the respective controls to develop. This may increase the statistical significance of results where a decrease in spheroid growth is observed but is not significant by non-parametric testing. Furthermore, if the radiation enhancement offered by solid AuNPs and HGNs within spheroids were to be further investigated it would be imperative to measure the degree of nanoparticle uptake within spheroids and the effect that initial spheroid volume and the presence of diffusional gradients within spheroids have on the uptake. This could be done by disaggregating spheroids and performing ICP-MS analysis, as was carried out in chapters 3 and 6 of this study to measure the uptake of solid AuNPs and HGNs in monolayer cells.

It would also be important to establish the location of nanoparticles within spheroids as this could directly impact the efficacy of their combination with radiation. Previous studies have demonstrated that the AuNP diameter can influence their penetration within spheroids, where smaller AuNPs can penetrate further through the spheroid volume. For example, the study by Huang *et al,* (2012) found 2 nm and 6 nm AuNPs distributed completely through spheroids (Huang et al., 2012). Whereas, AuNPs>100nm were seen to localise around the peripheral edge of MTS with limited uptake throughout the spheroids (Huo et al., 2013). Based on this information, a range of nanoparticle diameters could be investigated in order to optimise their uptake and penetration in spheroids to achieve the highest possible dose enhancement in combination with radiation. The location of nanoparticles throughout spheroids could be assessed by sequential sectioning of wax embedded spheroids and imaging the sections using either dark field microscopy or transmission electron microscopy (TEM) (Rosman et al., 2012). Imaging of spheroids following different nanoparticle incubation times, and at different times following removal of excess nanoparticles would allow the degree of nanoparticle retention to be evaluated.

Finally, the results of this preliminary study showed that [^{131}I]-MIBG was more effective in MTS models than monolayer cells, which was consistent with the results

of previous studies (Boyd et al., 1999). However, due to time constraints appropriate optimisation of the doses of [^{131}I]-MIBG to be used in combination with solid AuNPs and HGNs could not be performed. Therefore in continuation of this study a wider range of lower [^{131}I]-MIBG doses in combination with AuNPs and HGNs should be evaluated to allow greater visualisation of the potential radiosensitising effects.

In 2D monolayer studies radiosensitisation was evaluated by measuring the reduction in clonogenic cell survival compared to radiation alone. Therefore, in order to compare the effects of combination treatments in spheroids to the results in 2D monolayer cultures more effectively, clonogenic assays could be carried out using cells from disaggregated spheroids following treatment (Mikhail et al., 2013).

10.3.5 Additional future work and final conclusions

In conclusion, this study is the first to provide experimental evidence of radiosensitisation by solid AuNPs and HGNs in combination with [^{131}I]-MIBG, where the observed DEF_{50} values were considerably greater than the values calculated for the combination with XBR, and compared to any dose enhancement factors previously reported in literature. The use of low kV XBR is limited clinically to the treatment of superficial skin tumours due to the short tissue penetration of kV photons and therefore the successful radiosensitisation achieved with high kV radiation is encouraging as it demonstrates the success of nanoparticles as radiosensitisers with clinically relevant radiation.

Despite the use of radiotherapy in the treatment of approximately 50% of cancer patients, as a result of the heterogeneous nature of cancer the optimal use of radiotherapy will be through combination strategies and targeted therapies, in order to deliver the radiation specifically to cancerous cells and alleviate dose reducing limitations. Therefore the successful radiosensitisation of solid AuNPs and HGNs in combination with the targeted radiopharmaceutical [^{131}I]-MIBG is supportive of the advancement of targeted radiotherapy. As this is the first study to provide experimental evidence of successful radiosensitisation of cells to a targeted radiopharmaceutical, it demonstrates substantial potential for the future use of AuNPs as radiosensitisers in

clinically relevant radiotherapy scenarios. These results are particularly promising, as the radiosensitisation was not predicted based on the previous theoretical calculations of the radiation energies needed for optimal interaction with AuNPs via photoelectric ionisation. Therefore, these results highlight that other biological mechanisms must be involved in the observed radiosensitisation, in addition to the proposed physical mechanism.

Much more work is still required before this work can be translated into an *in vivo* setting. The results of studies investigating AuNPs as radiosensitisers are still extremely variable and show dependence on a number of factors including the radiation energy, the cell lines investigated and the AuNP diameter and functionalisation. In this study solid AuNPs with a diameter of 21 nM and HGNs with a diameter of 51 nM were investigated and the diameters of the nanoparticles were kept constant throughout the study. Further work could include assessment a range of nanoparticle diameters in order to optimise the uptake, cytotoxicity and radiosensitisation in each cell line which previous studies have shown can all be affected by changes in nanoparticle diameter (Chithrani et al., 2006; Pan et al., 2007).

Before any *in vivo* studies can be considered successful, functionalisation of the nanoparticles with molecules such as, PEG must be achieved in order to reduce their clearance from the RES and enhance the circulation time which is a major limitation associated with bare nanoparticles (Niidome et al., 2006). The ability to easily functionalise the surface of nanoparticles dramatically expands the scope of future work available. For example, functionalisation of AuNPs with targeting moieties, such as aptamers and monoclonal antibodies has been shown to increase the uptake selectively within cells expressing the corresponding surface target. This has been demonstrated in the recent study by Malik *et al*, (2015) which reported successful functionalisation of 5 nM HGNs with a cytotoxic DNA aptamer which is selective to the nucleolin protein present on the surface of cancer cells. Treatment of cells with the HGN conjugates resulted in selective uptake within cancer cells and increased cytotoxic effects both *in vitro* and *in vivo*, compared to the aptamer alone (Malik et al., 2015).

In an attempt to increase the lethality of the damage induced by the secondary electrons produced by AuNPs, nuclear targeting of the AuNPs could be investigated. Nuclear targeting of AuNPs through the functionalisation with an argine-glycine-aspartic acid peptide (RGD) and subsequent functionalisation with a nuclear localisation signal (NLS) has been reported previously by Kang *et al*, (2010). Results of the study reported increased DNA DSB formation and cytokinesis arrest to disrupt cell division following treatment of cancer cells with functionalised 30 nm AuNPs (Kang et al., 2010).

Whilst an increase in cytotoxicity was observed in the study by Kang *et al*, (2009), the therapeutic gain could be increased further by the administration of radiotherapy in the form of XBR, or a targeted radiopharmaceutical such as [^{131}I]-MIBG, following cell incubation with nuclear targeting AuNPs as the secondary electrons produced through AuNP ionisation would be localised in the vicinity of the nucleus and could potentially cause direct DNA damage.

Finally, in an attempt to advance this work further towards the development of targeted therapies conjugation of radioisotopes to the surface of nanoparticles could be investigated. This would combine the use of nanoparticles as a delivery vehicle through exploitation of the EPR effect, with their radiosensitising capability to develop a novel therapy which could deliver radiation directly to the cancer cells and subsequently enhance the radiation efficacy. Successful conjugation of radioisotopes to AuNPs has been demonstrated in the study by Su *et al*, (2015) which reported a therapeutic benefit in NCI-H446 tumour bearing mice treated with 21 nM AuNPs functionalised with cyclic Arg-Gly-Asp integrated with ^{125}I. Results of the study demonstrated acute apoptosis in mice 2 days post treatment and long-term volume reduction of tumours, compared to treatment with ^{125}I alone and non-targeted AuNPs in combination with ^{125}I respectively (Su et al., 2015).

The necessary future studies demonstrate that extensive work is still required in order to optimise AuNPs for clinical use. However, the results of this study with respect to the significant radiosensitisation potential of solid and hollow AuNPs in combination with the targeted radiopharmaceutical [^{131}I]-MIBG are encouraging for the future development and continued improvement of targeted radiotherapies.

Bibliography

Alkilany, A.M., Murphy, C.J., 2010a. Toxicity and cellular uptake of gold nanoparticles: what we have learned so far? J. Nanoparticle Res. 12, 2313–2333. doi:10.1007/s11051-010-9911-8

Alkilany, A.M., Murphy, C.J., 2010b. Toxicity and cellular uptake of gold nanoparticles: what we have learned so far? J. Nanoparticle Res. 12, 2313–2333. doi:10.1007/s11051-010-9911-8

Aranda, A., Sequedo, L., Tolosa, L., Quintas, G., Burello, E., Castell, J.V., Gombau, L., 2013. Dichloro-dihydro-fluorescein diacetate (DCFH-DA) assay: A quantitative method for oxidative stress assessment of nanoparticle-treated cells. Toxicol. In Vitro 27, 954–963. doi:10.1016/j.tiv.2013.01.016

Armour, A., Cunningham, S.H., Gaze, M.N., Wheldon, T.E., Mairs, R.J., 1997. The effect of cisplatin pretreatment on the accumulation of MIBG by neuroblastoma cells in vitro. Br. J. Cancer 75, 470–476.

Azqueta, A., Slyskova, J., Langie, S.A.S., O'Neill Gaivão, I., Collins, A., 2014. Comet assay to measure DNA repair: approach and applications. Front. Genet. 5. doi:10.3389/fgene.2014.00288

Bai, X., Kinney, W.H., Su, W.-L., Bai, A., Ovrutsky, A.R., Honda, J.R., Netea, M.G., Henao-Tamayo, M., Ordway, D.J., Dinarello, C.A., Chan, E.D., 2015. Caspase-3-independent apoptotic pathways contribute to interleukin-32γ-mediated control of Mycobacterium tuberculosis infection in THP-1 cells. BMC Microbiol. 15. doi:10.1186/s12866-015-0366-z

Banáth, J.P., MacPhail, S.H., Olive, P.L., 2004. Radiation Sensitivity, H2AX Phosphorylation, and Kinetics of Repair of DNA Strand Breaks in Irradiated Cervical Cancer Cell Lines. Cancer Res. 64, 7144–7149. doi:10.1158/0008-5472.CAN-04-1433

Barendsen, G.W., 1994. The Relationships between RBE and LET for Different Types of Lethal Damage in Mammalian Cells: Biophysical and Molecular Mechanisms. Radiat. Res. 139, 257–270. doi:10.2307/3578823

Baskar, R., Lee, K.A., Yeo, R., Yeoh, K.-W., 2012. Cancer and Radiation Therapy: Current Advances and Future Directions. Int. J. Med. Sci. 9, 193–199. doi:10.7150/ijms.3635

Biedler, J.L., Roffler-Tarlov, S., Schachner, M., Freedman, L.S., 1978. Multiple Neurotransmitter Synthesis by Human Neuroblastoma Cell Lines and Clones. Cancer Res. 38, 3751–3757.

Boyd, M., Cunningham, S.H., Brown, M.M., Mairs, R.J., Wheldon, T.E., 1999a. Noradrenaline transporter gene transfer for radiation cell kill by 131I meta-iodobenzylguanidine. Gene Ther. 6, 1147–1152. doi:10.1038/sj.gt.3300905

Boyd, M., Cunningham, S.H., Brown, M.M., Mairs, R.J., Wheldon, T.E., 1999b. Noradrenaline transporter gene transfer for radiation cell kill by 131I meta-iodobenzylguanidine. Gene Ther. 6, 1147–1152. doi:10.1038/sj.gt.3300905

Boyd, M., Mairs, R.J., Mairs, S.C., Wilson, L., Livingstone, A., Cunningham, S.H., Brown, M.M., Quigg, M., Keith, W.N., 2001. Expression in UVW glioma cells of the noradrenaline transporter gene, driven by the telomerase RNA promoter, induces active uptake of [131I]MIBG and clonogenic cell kill. Oncogene 20, 7804–7808. doi:10.1038/sj.onc.1204955

Boyd, M., Mairs, S.C., Stevenson, K., Livingstone, A., Clark, A.M., Ross, S.C., Mairs, R.J., 2002. Transfectant mosaic spheroids: a new model for evaluation of tumour cell killing in targeted radiotherapy and experimental gene therapy. J. Gene Med. 4, 567–576. doi:10.1002/jgm.293

Brenner, D.J., 2008. Point: The linear-quadratic model is an appropriate methodology for determining iso-effective doses at large doses per fraction. Semin. Radiat. Oncol. 18, 234–239. doi:10.1016/j.semradonc.2008.04.004

Brenner DJ, Shuryak I, Jozsef G, DeWyngaert KJ, Formenti SC, 2014. RIsk and risk reduction of major coronary events associated with contemporary breast radiotherapy. JAMA Intern. Med. 174, 158–160. doi:10.1001/jamainternmed.2013.11790

Brown, S.D., Nativo, P., Smith, J.-A., Stirling, D., Edwards, P.R., Venugopal, B., Flint, D.J., Plumb, J.A., Graham, D., Wheate, N.J., 2010. Gold Nanoparticles for the Improved Anticancer Drug Delivery of the Active Component of Oxaliplatin. J. Am. Chem. Soc. 132, 4678–4684. doi:10.1021/ja908117a

Bucci, M.K., Bevan, A., Roach, M., 2005. Advances in Radiation Therapy: Conventional to 3D, to IMRT, to 4D, and Beyond. CA. Cancer J. Clin. 55, 117–134. doi:10.3322/canjclin.55.2.117

Butterworth, K.T., McMahon, S.J., Currell, F.J., Prise, K.M., 2012. Physical basis and biological mechanisms of gold nanoparticle radiosensitization. Nanoscale 4, 4830–4838. doi:10.1039/C2NR31227A

Butterworth, K.T., McMahon, S.J., Taggart, L.E., Prise, K.M., 2013. Radiosensitization by gold nanoparticles: effective at megavoltage energies and potential role of oxidative stress. Transl. Cancer Res. 2, 269–279.

Cabrera, M., Gomez, N., Remes Lenicov, F., Echeverría, E., Shayo, C., Moglioni, A., Fernández, N., Davio, C., 2015. G2/M Cell Cycle Arrest and Tumor Selective Apoptosis of Acute Leukemia Cells by a Promising Benzophenone Thiosemicarbazone Compound. PloS One 10, e0136878. doi:10.1371/journal.pone.0136878

Caffo, O., 2001. Radiosensitization with chemotherapeutic agents. Lung Cancer 34, 81–90. doi:10.1016/S0169-5002(01)00382-8

Candelaria, M., Garcia-Arias, A., Cetina, L., Dueñas-Gonzalez, A., 2006. Radiosensitizers in cervical cancer. Cisplatin and beyond. Radiat. Oncol. 1, 15. doi:10.1186/1748-717X-1-15

Carrasco, J., Hodgson, A., Michaelides, A., 2012. A molecular perspective of water at metal interfaces. Nat. Mater. 11, 667–674. doi:10.1038/nmat3354

Cassidy, J., Bissett, D., OBE, R.A.J.S., Payne, M., Morris-Stiff, G., 2015. Oxford Handbook of Oncology. OUP Oxford.

Chamarthy, M.R., Williams, S.C., Moadel, R.M., 2011. Radioimmunotherapy of Non-Hodgkin's Lymphoma: From the "Magic Bullets" to "Radioactive Magic Bullets." Yale J. Biol. Med. 84, 391–407.

Chang, M.-Y., Shiau, A.-L., Chen, Y.-H., Chang, C.-J., Chen, H.H.-W., Wu, C.-L., 2008. Increased apoptotic potential and dose-enhancing effect of gold nanoparticles in combination with single-dose clinical electron beams on tumor-bearing mice. Cancer Sci. 99, 1479–1484. doi:10.1111/j.1349-7006.2008.00827.x

Chattopadhyay, N., Cai, Z., Kwon, Y.L., Lechtman, E., Pignol, J.-P., Reilly, R.M., 2013. Molecularly targeted gold nanoparticles enhance the radiation response of breast cancer cells and tumor xenografts to X-radiation. Breast Cancer Res. Treat. 137, 81–91. doi:10.1007/s10549-012-2338-4

Chattopadhyay, N., Cai, Z., Pignol, J.-P., Keller, B., Lechtman, E., Bendayan, R., Reilly, R.M., 2010. Design and Characterization of HER-2-Targeted Gold Nanoparticles for Enhanced X-radiation Treatment of Locally Advanced Breast Cancer. Mol. Pharm. 7, 2194–2206. doi:10.1021/mp100207t

Chen, S.-Y.C., Hung, P.J., Lee, P.J., 2011. Microfluidic array for three-dimensional perfusion culture of human mammary epithelial cells. Biomed. Microdevices 13, 753–758. doi:10.1007/s10544-011-9545-3

Cherry, P., Duxbury, A., 2009. Practical Radiotherapy: Physics and Equipment. John Wiley & Sons.
Chien Wen Huang, V.K., 2015. Hollow Gold Nanoparticals as Biocompatible Radiosensitizer: An In Vitro Proof of Concept Study. J. Nano Res. 32, 106–112. doi:10.4028/www.scientific.net/JNanoR.32.106
Chithrani, B.D., Chan, W.C.W., 2007. Elucidating the Mechanism of Cellular Uptake and Removal of Protein-Coated Gold Nanoparticles of Different Sizes and Shapes. Nano Lett. 7, 1542–1550. doi:10.1021/nl070363y
Chithrani, B.D., Ghazani, A.A., Chan, W.C.W., 2006. Determining the Size and Shape Dependence of Gold Nanoparticle Uptake into Mammalian Cells. Nano Lett. 6, 662–668. doi:10.1021/nl052396o
Chithrani, D.B., Jelveh, S., Jalali, F., van Prooijen, M., Allen, C., Bristow, R.G., Hill, R.P., Jaffray, D.A., 2010. Gold Nanoparticles as Radiation Sensitizers in Cancer Therapy. Radiat. Res. 173, 719–728. doi:10.1667/RR1984.1
Cho, S.H., 2005a. Estimation of tumour dose enhancement due to gold nanoparticles during typical radiation treatments: a preliminary Monte Carlo study. Phys. Med. Biol. 50, N163–173. doi:10.1088/0031-9155/50/15/N01
Cho, S.H., 2005b. Estimation of tumour dose enhancement due to gold nanoparticles during typical radiation treatments: a preliminary Monte Carlo study. Phys. Med. Biol. 50, N163. doi:10.1088/0031-9155/50/15/N01
Cho, S.H., Jones, B.L., Krishnan, S., 2009. The dosimetric feasibility of gold nanoparticle-aided radiation therapy (GNRT) via brachytherapy using low-energy gamma-/x-ray sources. Phys. Med. Biol. 54, 4889–4905. doi:10.1088/0031-9155/54/16/004
Connor, E.E., Mwamuka, J., Gole, A., Murphy, C.J., Wyatt, M.D., 2005. Gold Nanoparticles Are Taken Up by Human Cells but Do Not Cause Acute Cytotoxicity. Small 1, 325–327. doi:10.1002/smll.200400093
Coradeghini, R., Gioria, S., García, C.P., Nativo, P., Franchini, F., Gilliland, D., Ponti, J., Rossi, F., 2013. Size-dependent toxicity and cell interaction mechanisms of gold nanoparticles on mouse fibroblasts. Toxicol. Lett. 217, 205–216. doi:10.1016/j.toxlet.2012.11.022
Coulter, J.A., Hyland, W.B., Nicol, J., Currell, F.J., 2013. Radiosensitising nanoparticles as novel cancer therapeutics--pipe dream or realistic prospect? Clin. Oncol. R. Coll. Radiol. G. B. 25, 593–603. doi:10.1016/j.clon.2013.06.011
Coulter, J.A., Jain, S., Butterworth, K.T., Taggart, L.E., Dickson, G.R., McMahon, S.J., Hyland, W.B., Muir, M.F., Trainor, C., Hounsell, A.R., O'Sullivan, J.M., Schettino, G., Currell, F.J., Hirst, D.G., Prise, K.M., 2012. Cell type-dependent uptake, localization, and cytotoxicity of 1.9 nm gold nanoparticles. Int. J. Nanomedicine 7, 2673–2685. doi:10.2147/IJN.S31751
Craig, G.E., Brown, S.D., Lamprou, D.A., Graham, D., Wheate, N.J., 2012. Cisplatin-Tethered Gold Nanoparticles That Exhibit Enhanced Reproducibility, Drug Loading, and Stability: a Step Closer to Pharmaceutical Approval? Inorg. Chem. 51, 3490–3497. doi:10.1021/ic202197g
CS_KF_ALLCANCERS [WWW Document], n.d. URL http://publications.cancerresearchuk.org/publicationformat/formatfactsheet/keyfactsall.html (accessed 7.4.15).
CS_REPORT_MORTALITY [WWW Document], n.d. URL http://publications.cancerresearchuk.org/publicationformat/formatstats/mortality.html (accessed 7.4.15).
CS_REPORT_TOP10INCMORT [WWW Document], n.d. URL http://publications.cancerresearchuk.org/cancerstats/statsincidence/reporttop10incmort.html (accessed 7.4.15).

Dale, R., 2004. Use of the linear-quadratic radiobiological model for quantifying kidney response in targeted radiotherapy. Cancer Biother. Radiopharm. 19, 363–370. doi:10.1089/1084978041425070

Deitch, A.D., Law, H., White, R. deVere, 1982. A stable propidium iodide staining procedure for flow cytometry. J. Histochem. Cytochem. 30, 967–972. doi:10.1177/30.9.6182188

De Jong, W.H., Hagens, W.I., Krystek, P., Burger, M.C., Sips, A.J.A.M., Geertsma, R.E., 2008. Particle size-dependent organ distribution of gold nanoparticles after intravenous administration. Biomaterials 29, 1912–1919. doi:10.1016/j.biomaterials.2007.12.037

Dreaden, E.C., Alkilany, A.M., Huang, X., Murphy, C.J., El-Sayed, M.A., 2012. The golden age: gold nanoparticles for biomedicine. Chem. Soc. Rev. 41, 2740–2779. doi:10.1039/C1CS15237H

DuBois, S.G., Allen, S., Bent, M., Hilton, J.F., Hollinger, F., Hawkins, R., Courtier, J., Mosse, Y.P., Matthay, K.K., 2015. Phase I/II study of 131I-MIBG with vincristine and 5 days of irinotecan for advanced neuroblastoma. Br. J. Cancer. doi:10.1038/bjc.2015.12

Ersahin, D., Doddamane, I., Cheng, D., 2011. Targeted Radionuclide Therapy. Cancers 3, 3838–3855. doi:10.3390/cancers3043838

Eustis, S., El-Sayed, M.A., 2006. Why gold nanoparticles are more precious than pretty gold: Noble metal surface plasmon resonance and its enhancement of the radiative and nonradiative properties of nanocrystals of different shapes. Chem. Soc. Rev. 35, 209. doi:10.1039/b514191e

Faraday, M., 1857. The Bakerian Lecture: Experimental Relations of Gold (and Other Metals) to Light. Philos. Trans. R. Soc. Lond. 147, 145–181. doi:10.1098/rstl.1857.0011

Frens, G., 1973. Controlled Nucleation for the Regulation of the Particle Size in Monodisperse Gold Suspensions. Nature 241, 20–22. doi:10.1038/10.1038/physci241020a0

Gao, H., Shi, W., Freund, L.B., 2005. Mechanics of receptor-mediated endocytosis. Proc. Natl. Acad. Sci. U. S. A. 102, 9469–9474. doi:10.1073/pnas.0503879102

Gaze, M.N., Chang, Y.-C. 'ing, Flux, G.D., Mairs, R.J., Saran, F.H., Meller, S.T., 2005. Feasibility of dosimetry-based high-dose 131I-meta-iodobenzylguanidine with topotecan as a radiosensitizer in children with metastatic neuroblastoma. Cancer Biother. Radiopharm. 20, 195–199. doi:10.1089/cbr.2005.20.195

Gaze, M.N., Mairs, R.J., Boyack, S.M., Wheldon, T.E., Barrett, A., 1992a. 131I-meta-iodobenzylguanidine therapy in neuroblastoma spheroids of different sizes. Br. J. Cancer 66, 1048–1052.

Gaze, M.N., Mairs, R.J., Boyack, S.M., Wheldon, T.E., Barrett, A., 1992b. 131I-meta-iodobenzylguanidine therapy in neuroblastoma spheroids of different sizes. Br. J. Cancer 66, 1048–1052.

Geng, F., Song, K., Xing, J.Z., Yuan, C., Yan, S., Yang, Q., Chen, J., Kong, B., 2011a. Thio-glucose bound gold nanoparticles enhance radio-cytotoxic targeting of ovarian cancer. Nanotechnology 22, 285101. doi:10.1088/0957-4484/22/28/285101

Geng, F., Song, K., Xing, J.Z., Yuan, C., Yan, S., Yang, Q., Chen, J., Kong, B., 2011b. Thio-glucose bound gold nanoparticles enhance radio-cytotoxic targeting of ovarian cancer. Nanotechnology 22, 285101. doi:10.1088/0957-4484/22/28/285101

Geng, F., Song, K., Xing, J.Z., Yuan, C., Yan, S., Yang, Q., Chen, J., Kong, B., 2011c. Thio-glucose bound gold nanoparticles enhance radio-cytotoxic targeting of ovarian cancer. Nanotechnology 22, 285101. doi:10.1088/0957-4484/22/28/285101

Giard, D.J., Aaronson, S.A., Todaro, G.J., Arnstein, P., Kersey, J.H., Dosik, H., Parks, W.P., 1973. In Vitro Cultivation of Human Tumors: Establishment of Cell Lines Derived

From a Series of Solid Tumors. J. Natl. Cancer Inst. 51, 1417–1423. doi:10.1093/jnci/51.5.1417
Goldberg, Z., Lehnert, B., 2002. Radiation-induced effects in unirradiated cells: A review and implications in cancer. Int. J. Oncol. doi:10.3892/ijo.21.2.337
Goldsmith, S.J., 2010. Radioimmunotherapy of Lymphoma: Bexxar and Zevalin. Semin. Nucl. Med. 40, 122–135. doi:10.1053/j.semnuclmed.2009.11.002
Gosens, I., Post, J.A., Fonteyne, L.J. de la, Jansen, E.H., Geus, J.W., Cassee, F.R., Jong, W.H. de, 2010. Impact of agglomeration state of nano- and submicron sized gold particles on pulmonary inflammation. Part. Fibre Toxicol. 7, 37. doi:10.1186/1743-8977-7-37
Gutrath, B.S., Beckmann, M.F., Buchkremer, A., Eckert, T., Timper, J., Leifert, A., Richtering, W., Schmitz, G., Simon, U., 2012a. Size-dependent multispectral photoacoustic response of solid and hollow gold nanoparticles. Nanotechnology 23, 225707. doi:10.1088/0957-4484/23/22/225707
Gutrath, B.S., Beckmann, M.F., Buchkremer, A., Eckert, T., Timper, J., Leifert, A., Richtering, W., Schmitz, G., Simon, U., 2012b. Size-dependent multispectral photoacoustic response of solid and hollow gold nanoparticles. Nanotechnology 23, 225707. doi:10.1088/0957-4484/23/22/225707
Hainfeld, J.F., Slatkin, D.N., Smilowitz, H.M., 2004. The use of gold nanoparticles to enhance radiotherapy in mice. Phys. Med. Biol. 49, N309. doi:10.1088/0031-9155/49/18/N03
Hall, E.J., Giaccia, A.J., 2006. Radiobiology for the Radiologist. Lippincott Williams & Wilkins.
Hamoudeh, M., Kamleh, M.A., Diab, R., Fessi, H., 2008a. Radionuclides delivery systems for nuclear imaging and radiotherapy of cancer. Adv. Drug Deliv. Rev., Delivery Systems for the Targeted Radiotherapy of Cancer 60, 1329–1346. doi:10.1016/j.addr.2008.04.013
Hamoudeh, M., Kamleh, M.A., Diab, R., Fessi, H., 2008b. Radionuclides delivery systems for nuclear imaging and radiotherapy of cancer. Adv. Drug Deliv. Rev. 60, 1329–1346. doi:10.1016/j.addr.2008.04.013
Hao, E., Li, S., Bailey, R.C., Zou, S., Schatz, G.C., Hupp, J.T., 2004a. Optical Properties of Metal Nanoshells. J. Phys. Chem. B 108, 1224–1229. doi:10.1021/jp036301n
Hao, E., Schatz, G.C., Hupp, J.T., 2004b. Synthesis and Optical Properties of Anisotropic Metal Nanoparticles. J. Fluoresc. 14, 331–341. doi:10.1023/B:JOFL.0000031815.71450.74
Harrap, K.R., Hill, B.T., 1969. The selectivity of action of alkylating agents and drug resistance. I. Biochemical changes occurring in sensitive and resistant strains of the Yoshida ascites sarcoma following chemotherapy. Br. J. Cancer 23, 210–226.
Harrison, L.B., Chadha, M., Hill, R.J., Hu, K., Shasha, D., 2002. Impact of tumor hypoxia and anemia on radiation therapy outcomes. The Oncologist 7, 492–508.
Hauck, T.S., Ghazani, A.A., Chan, W.C.W., 2008. Assessing the Effect of Surface Chemistry on Gold Nanorod Uptake, Toxicity, and Gene Expression in Mammalian Cells. Small 4, 153–159. doi:10.1002/smll.200700217
Haycock, J.W., 2011. 3D cell culture: a review of current approaches and techniques. Methods Mol. Biol. Clifton NJ 695, 1–15. doi:10.1007/978-1-60761-984-0_1
Higgins, G.S., O'Cathail, S.M., Muschel, R.J., McKenna, W.G., 2015. Drug radiotherapy combinations: Review of previous failures and reasons for future optimism. Cancer Treat. Rev. 41, 105–113. doi:10.1016/j.ctrv.2014.12.012
Hirschhaeuser, F., Menne, H., Dittfeld, C., West, J., Mueller-Klieser, W., Kunz-Schughart, L.A., 2010. Multicellular tumor spheroids: an underestimated tool is catching up again. J. Biotechnol. 148, 3–15. doi:10.1016/j.jbiotec.2010.01.012

Hoefnagel, C.A., Voûte, P.A., De Kraker, J., Valdés Olmos, R.A., 1991. [131I]metaiodobenzylguanidine therapy after conventional therapy for neuroblastoma. J. Nucl. Biol. Med. Turin Italy 1991 35, 202–206.

Huang, K., Ma, H., Liu, J., Huo, S., Kumar, A., Wei, T., Zhang, X., Jin, S., Gan, Y., Wang, P.C., He, S., Zhang, X., Liang, X.-J., 2012. Size-Dependent Localization and Penetration of Ultrasmall Gold Nanoparticles in Cancer Cells, Multicellular Spheroids, and Tumors in Vivo. ACS Nano 6, 4483–4493. doi:10.1021/nn301282m

Huang, X., Jain, P.K., El-Sayed, I.H., El-Sayed, M.A., 2007. Gold nanoparticles: interesting optical properties and recent applications in cancer diagnostics and therapy. Nanomed. 2, 681–693. doi:10.2217/17435889.2.5.681

Huo, S., Ma, H., Huang, K., Liu, J., Wei, T., Jin, S., Zhang, J., He, S., Liang, X.-J., 2013. Superior penetration and retention behavior of 50 nm gold nanoparticles in tumors. Cancer Res. 73, 319–330. doi:10.1158/0008-5472.CAN-12-2071

Iyer, A.K., Khaled, G., Fang, J., Maeda, H., 2006. Exploiting the enhanced permeability and retention effect for tumor targeting. Drug Discov. Today 11, 812–818. doi:10.1016/j.drudis.2006.07.005

Jackson, J.B., Westcott, S.L., Hirsch, L.R., West, J.L., Halas, N.J., 2003. Controlling the surface enhanced Raman effect via the nanoshell geometry. Appl. Phys. Lett. 82, 257–259. doi:10.1063/1.1534916

Jain, S., Coulter, J.A., Hounsell, A.R., Butterworth, K.T., McMahon, S.J., Hyland, W.B., Muir, M.F., Dickson, G.R., Prise, K.M., Currell, F.J., O'Sullivan, J.M., Hirst, D.G., 2011a. Cell-specific radiosensitization by gold nanoparticles at megavoltage radiation energies. Int. J. Radiat. Oncol. Biol. Phys. 79, 531–539. doi:10.1016/j.ijrobp.2010.08.044

Jain, S., Coulter, J.A., Hounsell, A.R., Butterworth, K.T., McMahon, S.J., Hyland, W.B., Muir, M.F., Dickson, G.R., Prise, K.M., Currell, F.J., O'Sullivan, J.M., Hirst, D.G., 2011b. Cell-specific radiosensitization by gold nanoparticles at megavoltage radiation energies. Int. J. Radiat. Oncol. Biol. Phys. 79, 531–539. doi:10.1016/j.ijrobp.2010.08.044

Janssen, H.L., Haustermans, K.M., Balm, A.J., Begg, A.C., 2005. Hypoxia in head and neck cancer: How much, how important? Head Neck 27, 622–638. doi:10.1002/hed.20223

Jayakumar, S., Kunwar, A., Sandur, S.K., Pandey, B.N., Chaubey, R.C., 2014. Differential response of DU145 and PC3 prostate cancer cells to ionizing radiation: role of reactive oxygen species, GSH and Nrf2 in radiosensitivity. Biochim. Biophys. Acta 1840, 485–494. doi:10.1016/j.bbagen.2013.10.006

Jensen, M.M., Jørgensen, J.T., Binderup, T., Kjær, A., 2008. Tumor volume in subcutaneous mouse xenografts measured by microCT is more accurate and reproducible than determined by 18F-FDG-microPET or external caliper. BMC Med. Imaging 8, 16. doi:10.1186/1471-2342-8-16

Jiang, W., Kim, B.Y.S., Rutka, J.T., Chan, W.C.W., 2008. Nanoparticle-mediated cellular response is size-dependent. Nat. Immunol. 3, 145–150. doi:10.1038/nnano.2008.30

Joshi, P., Chakraborti, S., Ramirez-Vick, J.E., Ansari, Z.A., Shanker, V., Chakrabarti, P., Singh, S.P., 2012. The anticancer activity of chloroquine-gold nanoparticles against MCF-7 breast cancer cells. Colloids Surf. B Biointerfaces 95, 195–200. doi:10.1016/j.colsurfb.2012.02.039

Kang, B., Mackey, M.A., El-Sayed, M.A., 2010. Nuclear targeting of gold nanoparticles in cancer cells induces DNA damage, causing cytokinesis arrest and apoptosis. J. Am. Chem. Soc. 132, 1517–1519. doi:10.1021/ja9102698

Kao, H.-W., Lin, Y.-Y., Chen, C.-C., Chi, K.-H., Tien, D.-C., Hsia, C.-C., Lin, M.-H., Wang, H.-E., 2013. Evaluation of EGFR-targeted radioimmuno-gold-nanoparticles as a theranostic agent in a tumor animal model. Bioorg. Med. Chem. Lett. 23, 3180–3185. doi:10.1016/j.bmcl.2013.04.002

Kartalou, M., Essigmann, J.M., 2001. Mechanisms of resistance to cisplatin. Mutat. Res. 478, 23–43.
Kassis, A.I., Adelstein, S.J., 2005. Radiobiologic principles in radionuclide therapy. J. Nucl. Med. Off. Publ. Soc. Nucl. Med. 46 Suppl 1, 4S–12S.
Kayano, D., Kinuya, S., 2015. Iodine-131 Metaiodobenzylguanidine Therapy for Neuroblastoma: Reports So Far and Future Perspective. Sci. World J. 2015, e189135. doi:10.1155/2015/189135
Kelly, K.L., Coronado, E., Zhao, L.L., Schatz, G.C., 2002. The Optical Properties of Metal Nanoparticles: The Influence of Size, Shape, and Dielectric Environment. J. Phys. Chem. B 107, 668–677. doi:10.1021/jp026731y
Kim, J.-K., Seo, S.-J., Kim, H.-T., Kim, K.-H., Chung, M.-H., Kim, K.-R., Ye, S.-J., 2012. Enhanced proton treatment in mouse tumors through proton irradiated nanoradiator effects on metallic nanoparticles. Phys. Med. Biol. 57, 8309. doi:10.1088/0031-9155/57/24/8309
Kim, J.-K., Seo, S.-J., Kim, K.-H., Kim, T.-J., Chung, M.-H., Kim, K.-R., Yang, T.-K., 2010. Therapeutic application of metallic nanoparticles combined with particle-induced x-ray emission effect. Nanotechnology 21, 425102. doi:10.1088/0957-4484/21/42/425102
Kimling, J., Maier, M., Okenve, B., Kotaidis, V., Ballot, H., Plech, A., 2006. Turkevich Method for Gold Nanoparticle Synthesis Revisited. J. Phys. Chem. B 110, 15700–15707. doi:10.1021/jp061667w
Kim, S.J., Kim, M.S., Lee, J.W., Lee, C.H., Yoo, H., Shin, S.H., Park, M.J., Lee, S.H., 2005. Dihydroartemisinin enhances radiosensitivity of human glioma cells in vitro. J. Cancer Res. Clin. Oncol. 132, 129–135. doi:10.1007/s00432-005-0052-x
Kohara, H., Tabata, M., Kiura, K., Ueoka, H., Kawata, K., Chikamori, M., Aoe, K., Chikamori, K., Matsushita, A., Harada, M., 2002. Synergistic Effects of Topoisomerase I Inhibitor, 7-ethyl-10-hydroxycamptothecin, and Irradiation in a Cisplatin-resistant Human Small Cell Lung Cancer Cell Line. Clin. Cancer Res. 8, 287–292.
Kong, T., Zeng, J., Wang, X., Yang, X., Yang, J., McQuarrie, S., McEwan, A., Roa, W., Chen, J., Xing, J.Z., 2008. Enhancement of radiation cytotoxicity in breast-cancer cells by localized attachment of gold nanoparticles. Small Weinh. Bergstr. Ger. 4, 1537–1543. doi:10.1002/smll.200700794
Kubetzko, F.B.B., Paolo, C. di, Maag, C., Meier, R., Schäfer, B.W., Betts, D.R., Stahel, R.A., Himmelmann, A., 2004. The PAX5 oncogene is expressed in N-type neuroblastoma cells and increases tumorigenicity of a S-type cell line. Carcinogenesis 25, 1839–1846. doi:10.1093/carcin/bgh190
Kumar, R., Maitra, A.N., Patanjali, P.K., Sharma, P., 2005. Hollow gold nanoparticles encapsulating horseradish peroxidase. Biomaterials 26, 6743–6753. doi:10.1016/j.biomaterials.2005.04.045
Kurudirek, M., 2014. Effective atomic numbers and electron densities of some human tissues and dosimetric materials for mean energies of various radiation sources relevant to radiotherapy and medical applications. Radiat. Phys. Chem. 102, 139–146. doi:10.1016/j.radphyschem.2014.04.033
Lee, J., Lilly, G.D., Doty, R.C., Podsiadlo, P., Kotov, N.A., 2009. In vitro toxicity testing of nanoparticles in 3D cell culture. Small Weinh. Bergstr. Ger. 5, 1213–1221. doi:10.1002/smll.200801788
Libutti, S.K., Paciotti, G.F., Byrnes, A.A., Alexander, H.R., Gannon, W.E., Walker, M., Seidel, G.D., Yuldasheva, N., Tamarkin, L., 2010. Phase I and pharmacokinetic studies of CYT-6091, a novel PEGylated colloidal gold-rhTNF nanomedicine. Clin. Cancer Res. Off. J. Am. Assoc. Cancer Res. 16, 6139–6149. doi:10.1158/1078-0432.CCR-10-0978

Li, J., Gupta, S., Li, C., 2013. Research perspectives: gold nanoparticles in cancer theranostics. Quant. Imaging Med. Surg. 3, 284–291. doi:10.3978/j.issn.2223-4292.2013.12.02

Link, S., El-Sayed, M.A., 1999. Spectral Properties and Relaxation Dynamics of Surface Plasmon Electronic Oscillations in Gold and Silver Nanodots and Nanorods. J. Phys. Chem. B 103, 8410–8426. doi:10.1021/jp9917648

Lin, Y., McMahon, S.J., Scarpelli, M., Paganetti, H., Schuemann, J., 2014. Comparing gold nano-particle enhanced radiotherapy with protons, megavoltage photons and kilovoltage photons: a Monte Carlo simulation. Phys. Med. Biol. 59, 7675–7689. doi:10.1088/0031-9155/59/24/7675

Liou, G.-Y., Storz, P., 2010. Reactive oxygen species in cancer. Free Radic. Res. 44. doi:10.3109/10715761003667554

Li, Q., Chow, A.B., Mattingly, R.R., 2010. Three-Dimensional Overlay Culture Models of Human Breast Cancer Reveal a Critical Sensitivity to Mitogen-Activated Protein Kinase Kinase Inhibitors. J. Pharmacol. Exp. Ther. 332, 821–828. doi:10.1124/jpet.109.160390

Liu, C.-J., Wang, C.-H., Chen, S.-T., Chen, H.-H., Leng, W.-H., Chien, C.-C., Wang, C.-L., Kempson, I.M., Hwu, Y., Lai, T.-C., Hsiao, M., Yang, C.-S., Chen, Y.-J., Margaritondo, G., 2010. Enhancement of cell radiation sensitivity by pegylated gold nanoparticles. Phys. Med. Biol. 55, 931–945. doi:10.1088/0031-9155/55/4/002

Liu, T., Kempson, I., Jonge, M. de, Howard, D.L., Thierry, B., 2014. Quantitative synchrotron X-ray fluorescence study of the penetration of transferrin-conjugated gold nanoparticles inside model tumour tissues. Nanoscale 6, 9774–9782. doi:10.1039/C4NR02100B

Liu, Z., Wu, Y., Guo, Z., Liu, Y., Shen, Y., Zhou, P., Lu, X., 2014. Effects of Internalized Gold Nanoparticles with Respect to Cytotoxicity and Invasion Activity in Lung Cancer Cells. PLoS ONE 9. doi:10.1371/journal.pone.0099175

Longo, D.L., Harrison, T.., 2012. Harrison's principles of internal medicine. McGraw-Hill Medical, New York, N.Y., [etc.].

Maeda, H., Fang, J., Inutsuka, T., Kitamoto, Y., 2003. Vascular permeability enhancement in solid tumor: various factors, mechanisms involved and its implications. Int. Immunopharmacol. 3, 319–328. doi:10.1016/S1567-5769(02)00271-0

Maeda, H., Wu, J., Sawa, T., Matsumura, Y., Hori, K., 2000. Tumor vascular permeability and the EPR effect in macromolecular therapeutics: a review. J. Controlled Release 65, 271–284. doi:10.1016/S0168-3659(99)00248-5

Mairs, R.J., Livingstone, A., Gaze, M.N., Wheldon, T.E., Barrett, A., 1994. Prediction of accumulation of 131I-labelled meta-iodobenzylguanidine in neuroblastoma cell lines by means of reverse transcription and polymerase chain reaction. Br. J. Cancer 70, 97–101.

Maity, A., McKenna, W.G., Muschel, R.J., 1995. Evidence for post-transcriptional regulation of cyclin B1 mRNA in the cell cycle and following irradiation in HeLa cells. EMBO J. 14, 603–609.

Majewski, W., Wesolowska, I., Urbanczyk, H., Hawrylewicz, L., Schwierczok, B., Miszczyk, L., 2009. Dose Distribution in Bladder and Surrounding Normal Tissues in Relation to Bladder Volume in Conformal Radiotherapy for Bladder Cancer. Int. J. Radiat. Oncol. 75, 1371–1378. doi:10.1016/j.ijrobp.2009.01.005

Maleki, M.S., Moradi, O., Tahmasebi, S., n.d. Adsorption of albumin by gold nanoparticles: Equilibrium and thermodynamics studies. Arab. J. Chem. doi:10.1016/j.arabjc.2012.10.009

Malik, M.T., O'Toole, M.G., Casson, L.K., Thomas, S.D., Bardi, G.T., Reyes-Reyes, E.M., Ng, C.K., Kang, K.A., Bates, P.J., 2015. AS1411-conjugated gold nanospheres and their potential for breast cancer therapy. Oncotarget 6, 22270–22281. doi:10.18632/oncotarget.4207

Manke, A., Wang, L., Rojanasakul, Y., 2013. Mechanisms of Nanoparticle-Induced Oxidative Stress and Toxicity. BioMed Res. Int. 2013, e942916. doi:10.1155/2013/942916

Mastrangelo, S., Rufini, V., Ruggiero, A., Di Giannatale, A., Riccardi, R., 2011. Treatment of advanced neuroblastoma in children over 1 year of age: The critical role of 131I-metaiodobenzylguanidine combined with chemotherapy in a rapid induction regimen. Pediatr. Blood Cancer 56, 1032–1040. doi:10.1002/pbc.22986

Mastrangelo, S., Tornesello, A., Diociaiuti, L., Pession, A., Prete, A., Rufini, V., Troncone, L., Mastrangelo, R., 2001. Treatment of advanced neuroblastoma: feasibility and therapeutic potential of a novel approach combining 131-I-MIBG and multiple drug chemotherapy. Br. J. Cancer 84, 460–464. doi:10.1054/bjoc.2000.1645

McCluskey, A.G., Boyd, M., Gaze, M.N., Mairs, R.J., 2005. [131I]MIBG and topotecan: A rationale for combination therapy for neuroblastoma. Cancer Lett. 228, 221–227. doi:10.1016/j.canlet.2004.11.062

McCluskey, A.G., Boyd, M., Pimlott, S.L., Babich, J.W., Gaze, M.N., Mairs, R.J., 2008. Experimental treatment of neuroblastoma using [131I]meta-iodobenzylguanidine and topotecan in combination. Br. J. Radiol. 81, S28–S35. doi:10.1259/bjr/27723093

McCluskey, A.G., Mairs, R.J., Sorensen, A., Robson, T., McCarthy, H.O., Pimlott, S.L., Babich, J.W., Champion, S., Boyd, M., 2013. Gamma irradiation and targeted radionuclides enhance the expression of the noradrenaline transporter transgene controlled by the radio-inducible p21(WAF1/CIP1) promoter. Radiat. Res. 179, 282–292. doi:10.1667/RR3030.1

McCluskey, A.G., Mairs, R.J., Tesson, M., Pimlott, S.L., Babich, J.W., Gaze, M.N., Champion, S., Boyd, M., 2012. Inhibition of Poly(ADP-Ribose) Polymerase Enhances the Toxicity of 131I-Metaiodobenzylguanidine/Topotecan Combination Therapy to Cells and Xenografts That Express the Noradrenaline Transporter. J. Nucl. Med. 53, 1146–1154. doi:10.2967/jnumed.111.095943

McMahon, S.J., Hyland, W.B., Muir, M.F., Coulter, J.A., Jain, S., Butterworth, K.T., Schettino, G., Dickson, G.R., Hounsell, A.R., O'Sullivan, J.M., Prise, K.M., Hirst, D.G., Currell, F.J., 2011a. Nanodosimetric effects of gold nanoparticles in megavoltage radiation therapy. Radiother. Oncol. J. Eur. Soc. Ther. Radiol. Oncol. 100, 412–416. doi:10.1016/j.radonc.2011.08.026

McMahon, S.J., Hyland, W.B., Muir, M.F., Coulter, J.A., Jain, S., Butterworth, K.T., Schettino, G., Dickson, G.R., Hounsell, A.R., O'Sullivan, J.M., Prise, K.M., Hirst, D.G., Currell, F.J., 2011b. Biological consequences of nanoscale energy deposition near irradiated heavy atom nanoparticles. Sci. Rep. 1. doi:10.1038/srep00018

McMahon, S.J., Hyland, W.B., Muir, M.F., Coulter, J.A., Jain, S., Butterworth, K.T., Schettino, G., Dickson, G.R., Hounsell, A.R., O'Sullivan, J.M., Prise, K.M., Hirst, D.G., Currell, F.J., 2011c. Nanodosimetric effects of gold nanoparticles in megavoltage radiation therapy. Radiother. Oncol. J. Eur. Soc. Ther. Radiol. Oncol. 100, 412–416. doi:10.1016/j.radonc.2011.08.026

Mehta, G., Hsiao, A.Y., Ingram, M., Luker, G.D., Takayama, S., 2012. Opportunities and challenges for use of tumor spheroids as models to test drug delivery and efficacy. J. Controlled Release, Drug Delivery and Cancer: Today's Challenges, Tomorrow's Directions. 164, 192–204. doi:10.1016/j.jconrel.2012.04.045

Melancon, M.P., Lu, W., Yang, Z., Zhang, R., Cheng, Z., Elliot, A.M., Stafford, J., Olson, T., Zhang, J.Z., Li, C., 2008. In vitro and in vivo targeting of hollow gold nanoshells directed at epidermal growth factor receptor for photothermal ablation therapy. Mol. Cancer Ther. 7, 1730–1739. doi:10.1158/1535-7163.MCT-08-0016

Mesbahi, A., 2010. A review on gold nanoparticles radiosensitization effect in radiation therapy of cancer. Rep. Pract. Oncol. Radiother. 15, 176–180. doi:10.1016/j.rpor.2010.09.001

Meyers, J.D., Cheng, Y., Broome, A.-M., Agnes, R.S., Schluchter, M.D., Margevicius, S., Wang, X., Kenney, M.E., Burda, C., Basilion, J.P., 2014. Peptide-Targeted Gold Nanoparticles for Photodynamic Therapy of Brain Cancer. Part. Part. Syst. Charact. n/a–n/a. doi:10.1002/ppsc.201400119

Mikhail, A.S., Eetezadi, S., Allen, C., 2013. Multicellular tumor spheroids for evaluation of cytotoxicity and tumor growth inhibitory effects of nanomedicines in vitro: a comparison of docetaxel-loaded block copolymer micelles and Taxotere®. PloS One 8, e62630. doi:10.1371/journal.pone.0062630

Mironava, T., Hadjiargyrou, M., Simon, M., Rafailovich, M.H., 2014. Gold nanoparticles cellular toxicity and recovery: adipose Derived Stromal cells. Nanotoxicology 8, 189–201. doi:10.3109/17435390.2013.769128

Missailidis, S. (Ed.), 2007. The Cancer Clock, 1 edition. ed. Wiley-Blackwell, Chichester, West Sussex, England ; Hoboken, NJ.

Morais, T., Soares, M.E., Duarte, J.A., Soares, L., Maia, S., Gomes, P., Pereira, E., Fraga, S., Carmo, H., Bastos, M. de L., 2012. Effect of surface coating on the biodistribution profile of gold nanoparticles in the rat. Eur. J. Pharm. Biopharm. Off. J. Arbeitsgemeinschaft Für Pharm. Verfahrenstechnik EV 80, 185–193. doi:10.1016/j.ejpb.2011.09.005

Moudi, M., Go, R., Yien, C.Y.S., Nazre, M., 2013. Vinca Alkaloids. Int. J. Prev. Med. 4, 1231–1235.

Mueller, S., Bhargava, S., Molinaro, A.M., Yang, X., Kolkowitz, I., Olow, A., Wehmeijer, N., Orbach, S., Chen, J., Matthay, K.K., Haas-Kogan, D.A., 2013. Poly (ADP-Ribose) polymerase inhibitor MK-4827 together with radiation as a novel therapy for metastatic neuroblastoma. Anticancer Res. 33, 755–762.

Nagata, Y., 2014. Recent advances in radiation oncology. Int. J. Clin. Oncol. 19, 563–563. doi:10.1007/s10147-014-0720-4

Nestor, M.V., 2010. Targeted radionuclide therapy in head and neck cancer. Head Neck 32, 666–678. doi:10.1002/hed.21243

Ng, Q.K.T., Olariu, C.I., Yaffee, M., Taelman, V.F., Marincek, N., Krause, T., Meier, L., Walter, M.A., 2014. Indium-111 labeled gold nanoparticles for in-vivo molecular targeting. Biomaterials 35, 7050–7057. doi:10.1016/j.biomaterials.2014.04.098

Ngwa, W., Korideck, H., Kassis, A.I., Kumar, R., Sridhar, S., Makrigiorgos, G.M., Cormack, R.A., 2013. In vitro radiosensitization by gold nanoparticles during continuous low-dose-rate gamma irradiation with I-125 brachytherapy seeds. Nanomedicine Nanotechnol. Biol. Med. 9, 25–27. doi:10.1016/j.nano.2012.09.001

Nicolas, G., Giovacchini, G., Müller-Brand, J., Forrer, F., 2011. Targeted Radiotherapy with Radiolabeled Somatostatin Analogs. Endocrinol. Metab. Clin. North Am. 40, 187–204. doi:10.1016/j.ecl.2010.12.006

Niidome, T., Yamagata, M., Okamoto, Y., Akiyama, Y., Takahashi, H., Kawano, T., Katayama, Y., Niidome, Y., 2006. PEG-modified gold nanorods with a stealth character for in vivo applications. J. Control. Release Off. J. Control. Release Soc. 114, 343–347. doi:10.1016/j.jconrel.2006.06.017

O'Brien, R.W., Midmore, B.R., Lamb, A., Hunter, R.J., 1990. Electroacoustic studies of moderately concentrated colloidal suspensions. Faraday Discuss. Chem. Soc. 90, 301–312. doi:10.1039/DC9909000301

Pan-Bartneck, Y., Jahnen-Dechent, W., 2010. Assessing the toxicity of gold nanoparticles in vitro and in vivo 23.11.2010.

Pan, Y., Leifert, A., Ruau, D., Neuss, S., Bornemann, J., Schmid, G., Brandau, W., Simon, U., Jahnen-Dechent, W., 2009. Gold Nanoparticles of Diameter 1.4 nm Trigger Necrosis by Oxidative Stress and Mitochondrial Damage. Small 5, 2067–2076. doi:10.1002/smll.200900466

Pan, Y., Neuss, S., Leifert, A., Fischler, M., Wen, F., Simon, U., Schmid, G., Brandau, W., Jahnen-Dechent, W., 2007. Size-dependent cytotoxicity of gold nanoparticles. Small Weinh. Bergstr. Ger. 3, 1941–1949. doi:10.1002/smll.200700378

Park, J., Park, J., Ju, E.J., Park, S.S., Choi, J., Lee, J.H., Lee, K.J., Shin, S.H., Ko, E.J., Park, I., Kim, C., Hwang, J.J., Lee, J.S., Song, S.Y., Jeong, S.-Y., Choi, E.K., 2015. Multifunctional hollow gold nanoparticles designed for triple combination therapy and CT imaging. J. Controlled Release 207, 77–85. doi:10.1016/j.jconrel.2015.04.007

Patra, H.K., Banerjee, S., Chaudhuri, U., Lahiri, P., Dasgupta, A.K., 2007. Cell selective response to gold nanoparticles. Nanomedicine Nanotechnol. Biol. Med. 3, 111–119. doi:10.1016/j.nano.2007.03.005

P. Franken, N.A., Hovingh, S., Oei, A., Cobussen, P., J. Bergs, J.W., van, C., Rodermond, H., Stalpers, L., Kok, P., W., G., Crezee, J., 2012. Radiosensitization with Hyperthermia and Chemotherapeutic Agents: Effects on Linear-Quadratic Parameters of Radiation Cell Survival Curves, in: Nenoi, M. (Ed.), Current Topics in Ionizing Radiation Research. InTech.

Pollack, A., Ciancio, G., 1990. Chapter 3 Cell Cycle Phase-Specific Analysis of Cell Viability Using Hoechst 33342 and Propidium Iodide after Ethanol Preservation, in: Crissman, Z.D. and H.A. (Ed.), Methods in Cell Biology, Flow Cytometry. Academic Press, pp. 19–24.

Pories, S.E., Zurakowski, D., Roy, R., Lamb, C.C., Raza, S., Exarhopoulos, A., Scheib, R.G., Schumer, S., Lenahan, C., Borges, V., Louis, G.W., Anand, A., Isakovich, N., Hirshfield-Bartek, J., Wewer, U., Lotz, M.M., Moses, M.A., 2008. Urinary metalloproteinases: noninvasive biomarkers for breast cancer risk assessment. Cancer Epidemiol. Biomark. Prev. Publ. Am. Assoc. Cancer Res. Cosponsored Am. Soc. Prev. Oncol. 17, 1034–1042. doi:10.1158/1055-9965.EPI-07-0365

Prabhakar, U., Maeda, H., Jain, R.K., Sevick-Muraca, E.M., Zamboni, W., Farokhzad, O.C., Barry, S.T., Gabizon, A., Grodzinski, P., Blakey, D.C., 2013. Challenges and Key Considerations of the Enhanced Permeability and Retention Effect for Nanomedicine Drug Delivery in Oncology. Cancer Res. 73, 2412–2417. doi:10.1158/0008-5472.CAN-12-4561

Qutob, S.S., Ng, C.E., 2001. Comparison of apoptotic, necrotic and clonogenic cell death and inhibition of cell growth following camptothecin and X-radiation treatment in a human melanoma and a human fibroblast cell line. Cancer Chemother. Pharmacol. 49, 167–175. doi:10.1007/s00280-001-0403-5

Rae, C., Tesson, M., Babich, J.W., Boyd, M., Mairs, R.J., 2013a. Radiosensitization of noradrenaline transporter-expressing tumour cells by proteasome inhibitors and the role of reactive oxygen species. EJNMMI Res. 3, 73. doi:10.1186/2191-219X-3-73

Rae, C., Tesson, M., Babich, J.W., Boyd, M., Sorensen, A., Mairs, R.J., 2013b. The role of copper in disulfiram-induced toxicity and radiosensitization of cancer cells. J. Nucl. Med. Off. Publ. Soc. Nucl. Med. 54, 953–960. doi:10.2967/jnumed.112.113324

Regulla, D.F., Hieber, L.B., Seidenbusch, M., 1998. Physical and biological interface dose effects in tissue due to X-ray-induced release of secondary radiation from metallic gold surfaces. Radiat. Res. 150, 92–100.

Riley, P.A., 1994. Free Radicals in Biology: Oxidative Stress and the Effects of Ionizing Radiation. Int. J. Radiat. Biol. 65, 27–33. doi:10.1080/09553009414550041

Roa, W., Zhang, X., Guo, L., Shaw, A., Hu, X., Xiong, Y., Gulavita, S., Patel, S., Sun, X., Chen, J., Moore, R., Xing, J.Z., 2009. Gold nanoparticle sensitize radiotherapy of prostate cancer cells by regulation of the cell cycle. Nanotechnology 20, 375101. doi:10.1088/0957-4484/20/37/375101

Roeske, J.C., Nunez, L., Hoggarth, M., Labay, E., Weichselbaum, R.R., 2007. Characterization of the theorectical radiation dose enhancement from nanoparticles. Technol. Cancer Res. Treat. 6, 395–401.

Rosman, C., Pierrat, S., Henkel, A., Tarantola, M., Schneider, D., Sunnick, E., Janshoff, A., Sönnichsen, C., 2012. A New Approach to Assess Gold Nanoparticle Uptake by Mammalian Cells: Combining Optical Dark-Field and Transmission Electron Microscopy. Small 8, 3683–3690. doi:10.1002/smll.201200853
Rowinsky, E., 2003. The Vinca Alkaloids.
Saptarshi, S.R., Duschl, A., Lopata, A.L., 2013. Interaction of nanoparticles with proteins: relation to bio-reactivity of the nanoparticle. J. Nanobiotechnology 11, 26. doi:10.1186/1477-3155-11-26
Savic, V., Sanborn, K.B., Orange, J.S., Bassing, C.H., 2009. Chipping Away at γ-H2AX Foci. Cell Cycle Georget. Tex 8, 3285–3290.
Schwartzberg, A.M., Olson, T.Y., Talley, C.E., Zhang, J.Z., 2006. Synthesis, characterization, and tunable optical properties of hollow gold nanospheres. J. Phys. Chem. B 110, 19935–19944. doi:10.1021/jp062136a
Selim, M.E., Hendi, A.A., 2012. Gold nanoparticles induce apoptosis in MCF-7 human breast cancer cells. Asian Pac. J. Cancer Prev. APJCP 13, 1617–1620.
Selvakannan, P., Sastry, M., 2005. Hollow gold and platinum nanoparticles by a transmetallation reaction in an organic solution. Chem. Commun. 1684–1686. doi:10.1039/B418566H
Shang, L., Nienhaus, K., Nienhaus, G.U., 2014. Engineered nanoparticles interacting with cells: size matters. J. Nanobiotechnology 12, 5. doi:10.1186/1477-3155-12-5
Sharkey, R.M., Goldenberg, D.M., 2005. Perspectives on cancer therapy with radiolabeled monoclonal antibodies. J. Nucl. Med. Off. Publ. Soc. Nucl. Med. 46 Suppl 1, 115S–27S.
Short, S.C., Martindale, C., Bourne, S., Brand, G., Woodcock, M., Johnston, P., 2007. DNA repair after irradiation in glioma cells and normal human astrocytes. Neuro-Oncol. 9, 404–411. doi:10.1215/15228517-2007-030
Shukla, R., Bansal, V., Chaudhary, M., Basu, A., Bhonde, R.R., Sastry, M., 2005. Biocompatibility of Gold Nanoparticles and Their Endocytotic Fate Inside the Cellular Compartment: A Microscopic Overview. Langmuir 21, 10644–10654. doi:10.1021/la0513712
Sicard-Roselli, C., Brun, E., Gilles, M., Baldacchino, G., Kelsey, C., McQuaid, H., Polin, C., Wardlow, N., Currell, F., 2014. A new mechanism for hydroxyl radical production in irradiated nanoparticle solutions. Small Weinh. Bergstr. Ger. 10, 3338–3346. doi:10.1002/smll.201400110
Singh, V.P., Badiger, N.M., 2014. Effective atomic numbers of some tissue substitutes by different methods: A comparative study. J. Med. Phys. Assoc. Med. Phys. India 39, 24–31. doi:10.4103/0971-6203.125489
Söderstjerna, E., Bauer, P., Cedervall, T., Abdshill, H., Johansson, F., Johansson, U.E., 2014. Silver and Gold Nanoparticles Exposure to In Vitro Cultured Retina – Studies on Nanoparticle Internalization, Apoptosis, Oxidative Stress, Glial- and Microglial Activity. PLoS ONE 9, e105359. doi:10.1371/journal.pone.0105359
Stefanie Klein, A.S., 2012. Superparamagnetic iron oxide nanoparticles as radiosensitizer via enhanced reactive oxygen species formation. Biochem. Biophys. Res. Commun. 425, 393–7. doi:10.1016/j.bbrc.2012.07.108
Stockham, A.L., Balagamwala, E.H., Macklis, R., Wilkinson, A., Singh, A.D., 2014. Principles of Radiation Therapy, in: Singh, A.D., Damato, B. (Eds.), Clinical Ophthalmic Oncology. Springer Berlin Heidelberg, pp. 89–98.
Strojan, P., Vermorken, J.B., Beitler, J.J., Saba, N.F., Haigentz, M., Bossi, P., Worden, F.P., Langendijk, J.A., Eisbruch, A., Mendenhall, W.M., Lee, A.W.M., Harrison, L.B., Bradford, C.R., Smee, R., Silver, C.E., Rinaldo, A., Ferlito, A., 2015. Cumulative cisplatin dose in concurrent chemoradiotherapy for head and neck cancer: A systematic review. Head Neck n/a–n/a. doi:10.1002/hed.24026

Su, N., Dang, Y., Liang, G., Liu, G., 2015. Iodine-125-labeled cRGD-gold nanoparticles as tumor-targeted radiosensitizer and imaging agent. Nanoscale Res. Lett. 10, 1–9. doi:10.1186/s11671-015-0864-9

Sun, Y., Xia, Y., 2002. Increased Sensitivity of Surface Plasmon Resonance of Gold Nanoshells Compared to That of Gold Solid Colloids in Response to Environmental Changes. Anal. Chem. 74, 5297–5305. doi:10.1021/ac0258352

Su, X.-Y., Liu, P.-D., Wu, H., Gu, N., 2014. Enhancement of radiosensitization by metal-based nanoparticles in cancer radiation therapy. Cancer Biol. Med. 11, 86–91. doi:10.7497/j.issn.2095-3941.2014.02.003

Taggart, L.E., McMahon, S.J., Currell, F.J., Prise, K.M., Butterworth, K.T., 2014. The role of mitochondrial function in gold nanoparticle mediated radiosensitisation. Cancer Nanotechnol. 5. doi:10.1186/s12645-014-0005-7

Terentyuk, G.S., Maslyakova, G.N., Suleymanova, L.V., Khlebtsov, B.N., Kogan, B.Y., Akchurin, G.G., Shantrocha, A.V., Maksimova, I.L., Khlebtsov, N.G., Tuchin, V.V., 2009. Circulation and distribution of gold nanoparticles and induced alterations of tissue morphology at intravenous particle delivery. J. Biophotonics 2, 292–302. doi:10.1002/jbio.200910005

T, K., U, F., J, T., P, R., R, H., D, N., 1990. Treatment of neuroblastoma with [131I]metaiodobenzylguanidine: long-term results in 25 patients. J. Nucl. Biol. Med. Turin Italy 1991 35, 216–219.

Tribius, S., Bergelt, C., 2011. Intensity-modulated radiotherapy versus conventional and 3D conformal radiotherapy in patients with head and neck cancer: Is there a worthwhile quality of life gain? Cancer Treat. Rev. 37, 511–519. doi:10.1016/j.ctrv.2011.01.004

Turkevich, J., Stevenson, P.C., Hillier, J., 1953. The Formation of Colloidal Gold. J. Phys. Chem. 57, 670–673. doi:10.1021/j150508a015

Turkevich, J., Stevenson, P.C., Hillier, J., 1951. A study of the nucleation and growth processes in the synthesis of colloidal gold. Discuss. Faraday Soc. 11, 55–75. doi:10.1039/DF9511100055

Wardman, P., 2007. Chemical Radiosensitizers for Use in Radiotherapy. Clin. Oncol. 19, 397–417. doi:10.1016/j.clon.2007.03.010

Weinberg, R.A., 2006. The Biology of Cancer, 1 Pck Pap/ edition. ed. Garland Science, New York.

West, C.M., 1989. Size-dependent resistance of human tumour spheroids to photodynamic treatment. Br. J. Cancer 59, 510–514.

Wheate, N.J., Walker, S., Craig, G.E., Oun, R., 2010. The status of platinum anticancer drugs in the clinic and in clinical trials. Dalton Trans. Camb. Engl. 2003 39, 8113–8127. doi:10.1039/c0dt00292e

Wichmann, M.W., Beukes, E., Esufali, S.T., Plaumann, L., Maddern, G., 2013. Five-year results of surgical colorectal cancer treatment in rural Australia. ANZ J. Surg. 83, 112–117. doi:10.1111/ans.12065

Wiogo, H.T.R., Lim, M., Bulmus, V., Yun, J., Amal, R., 2010. Stabilization of Magnetic Iron Oxide Nanoparticles in Biological Media by Fetal Bovine Serum (FBS). Langmuir 27, 843–850. doi:10.1021/la104278m

Worden, F., 2014. Treatment strategies for radioactive iodine-refractory differentiated thyroid cancer. Ther. Adv. Med. Oncol. 6, 267–279. doi:10.1177/1758834014548188

Xie, H., Larmour, I.A., Chen, Y.-C., Wark, A.W., Tileli, V., McComb, D.W., Faulds, K., Graham, D., 2013. Synthesis and NIR optical properties of hollow gold nanospheres with LSPR greater than one micrometer. Nanoscale 5, 765–771. doi:10.1039/c2nr33187j

Yasui, H., Takeuchi, R., Nagane, M., Meike, S., Nakamura, Y., Yamamori, T., Ikenaka, Y., Kon, Y., Murotani, H., Oishi, M., Nagasaki, Y., Inanami, O., 2014. Radiosensitization of tumor cells through endoplasmic reticulum stress induced by

PEGylated nanogel containing gold nanoparticles. Cancer Lett. 347, 151–158. doi:10.1016/j.canlet.2014.02.005
You, J., Zhang, G., Li, C., 2010. Exceptionally High Payload of Doxorubicin in Hollow Gold Nanospheres for Near-Infrared Light-Triggered Drug Release. ACS Nano 4, 1033–1041. doi:10.1021/nn901181c
Zarnegar, R., Brunaud, L., Kanauchi, H., Wong, M., Fung, M., Ginzinger, D., Duh, Q.-Y., Clark, O.H., 2002. Increasing the effectiveness of radioactive iodine therapy in the treatment of thyroid cancer using Trichostatin A, a histone deacetylase inhibitor. Surgery 132, 984–990. doi:10.1067/msy.2002.128690

Appendix

Conference posters presented

1. ***"Expanding the use of Gold Nanoparticles to enhance Radiotherapy"***

Association for radiation research conference, Brunel University, London, 24th-27th June 2012

2. ***"The Golden Age of Cancer"***

University of Strathclyde Research Day, University of Strathclyde, Glasgow, May 2013

3. ***"Expanding the use of Gold Nanoparticles to enhance Radiotherapy"***

40th Annual Meeting of the European Radiation Research (ERR) and Association for Radiation Research (ARR), Dublin Castle, Dublin, 1st-5th September 2013